



저작자표시-비영리-변경금지 2.0 대한민국

이용자는 아래의 조건을 따르는 경우에 한하여 자유롭게

- 이 저작물을 복제, 배포, 전송, 전시, 공연 및 방송할 수 있습니다.

다음과 같은 조건을 따라야 합니다:



저작자표시. 귀하는 원저작자를 표시하여야 합니다.



비영리. 귀하는 이 저작물을 영리 목적으로 이용할 수 없습니다.



변경금지. 귀하는 이 저작물을 개작, 변형 또는 가공할 수 없습니다.

- 귀하는, 이 저작물의 재이용이나 배포의 경우, 이 저작물에 적용된 이용허락조건을 명확하게 나타내어야 합니다.
- 저작권자로부터 별도의 허가를 받으면 이러한 조건들은 적용되지 않습니다.

저작권법에 따른 이용자의 권리는 위의 내용에 의하여 영향을 받지 않습니다.

이것은 [이용허락규약\(Legal Code\)](#)을 이해하기 쉽게 요약한 것입니다.

[Disclaimer](#)

이학박사 학위논문

**Catalytic Asymmetric Synthesis
and Stereospecific Transformation
of Alkylboron Compounds**

알킬붕소화합물의

촉매적 비대칭 합성 및 입체특이적 변환

2023 년 8 월

서울대학교 대학원

화학부 유기화학 전공

노 병 도

알킬붕소화합물의
촉매적 비대칭 합성 및 입체특이적 변환

지도교수 이 홍 근

이 논문을 이학박사 학위논문으로 제출함
2023 년 8 월

서울대학교 대학원
화학부 유기화학 전공
노 병 도

노병도의 이학박사 학위논문을 인준함
2023 년 8 월

위 원 장 _____ 이 철 범 _____ (인)

부위원장 _____ 이 홍 근 _____ (인)

위 원 _____ 김 병 문 _____ (인)

위 원 _____ 이 윤 호 _____ (인)

위 원 _____ 장 원 준 _____ (인)

Catalytic Asymmetric Synthesis and Stereospecific Transformation of Alkylboron Compounds

Abstract

The development of novel strategies for new carbon-carbon bond formation is central to organic chemistry. Over decades, transition-metal-catalyzed cross-coupling has served as a versatile protocol for enabling efficient access to complex molecules. Among them, the Suzuki-Miyaura cross-coupling reaction has been regarded as the most attractive toolkit owing to the numerous advantages of organoboron compounds, which are used as nucleophiles in Suzuki cross-coupling, over other types of organometallic reagents. These advantages include their less toxic nature, safety for the environment, and easier preparation and application under milder reaction conditions.

As such, synthetic organic communities have required more efficient methods for the synthesis of organoboron compounds. At the same time, significant attempts have been made to broaden the utility of organoboron compounds as useful synthetic handles. Despite the advancement of these approaches, the majority of them are mainly limited to C(sp²)-based organoboron reagents. Therefore, the extension of these protocols to the efficient use of C(sp³)-

hybridized alkylboron would provide facile access to previously inaccessible chemical space.

In this context, our efforts to develop more effective strategies for the synthesis and functionalization of alkylboron compounds are presented in this dissertation. Chapter 1 provides a brief introduction to the importance of the synthesis and transformation of C(sp³)-based organoboron compounds. Then, in Chapter 2, we mainly discuss the use of *gem*-diborylalkanes for the synthesis of alkylboron species, highlighting the relevant seminal work and recent advances. Chapter 3 describes our development of the asymmetric conjugate addition of *gem*-diborylalkanes to α,β -unsaturated enones, which enabled the construction of complexity-added chiral alkylboron compounds.

In Chapter 4, we next focus on the stereospecific functionalization of alkylboron compounds, specifically the stereospecific Suzuki-Miyaura cross-coupling of enantioenriched C(sp³)-based organoboron compounds. Then, we describe our recent contribution to the development of stereospecific acylative Suzuki-Miyaura cross-coupling, exhibiting highly efficient stereochemical transfer, in Chapter 5.

Keyword: organoboron, alkylboron compounds, asymmetric catalysis, stereoselective synthesis, stereospecific cross-coupling, enantioenriched carbonyls, copper, palladium

Student Number: 2018-28460

TABLE OF CONTENTS

Abstract.....	i
Table of Contents	iii
List of Tables.....	vi
List of Figures.....	viii
List of Schemes.....	x
Contributions	xiii
Abstract in Koreans	394

Chapter 1: Outline of the Dissertation

1.1. Introduction.....	2
1.2. References.....	4

Chapter 2: Utilization of *gem*-Diborylalkanes in Asymmetric catalysis

2.1. Introduction.....	6
2.2. Deprotonative Activation of <i>gem</i> -Diborylalkanes	8
2.2.1. Substrate-controlled Stereoselective Strategies	8
2.2.2. Catalyst-controlled Stereoselective Strategies	14
2.3. Deborylative Activation of <i>gem</i> -Diborylalkanes	15
2.3.1. Stereoselective Suzuki-Miyaura Cross-Coupling	15
2.3.2. Stereoselective 1,2-addition Reactions	19
2.3.3. Stereoselective 1,4-addition Reactions	23
2.3.4. Stereoselective Allylic Substitution Reactions.....	25
2.3.5. Utility of Allylic <i>gem</i> -Diborylalkanes.....	28
2.4. References.....	32

Chapter 3: Asymmetric Conjugated Addition of *gem*-Diborylalkanes to α,β -Unsaturated Enones

3.1. Introduction.....	36
3.2. Results and Discussion	39
3.2.1. Optimization of the Protocol.....	39
3.2.2. Applicability of the Protocol.....	43

3.2.3. NMR Investigations	48
3.2.4. Proposed Mechanism	56
3.3. Conclusion	58
3.4. References.....	59
3.5. Experimental Section	63
3.5.1. General Information.....	63
3.5.2. General Procedure for Preparation of Enones.....	65
3.5.3. Evaluation on Reaction Conditions.....	66
3.5.4. General Procedure for Enantioselective Conjugate Addition.....	73
3.5.5. General Procedure for Further Derivatizations	114
3.5.6. ³¹ P and ¹¹ B NMR studies.....	123
3.5.7. Preliminary Mass Spectroscopic Data (HRMS)	136
3.5.8. References in Experimental Section	142

Chapter 4: Stereospecific Transformation of Enantioenriched Alkylboron

4.1. Introduction.....	144
4.2. Stereospecific Suzuki-Miyaura Cross-Coupling (SSMC) reactions	146
4.2.1. SSMC reactions with primary alkylboron.....	146
4.2.2. SSMC reactions with benzylic alkylboron.....	149
4.2.3. SSMC reactions with allylic/propargylic alkylboron	154
4.2.4. SSMC reactions with activated secondary alkylboron.....	160
4.2.5. SSMC reactions with unactivated secondary alkylboron.....	170
4.3. References.....	174

Chapter 5: Stereospecific Acylative Suzuki-Miyaura Cross-Coupling Reaction

5.1. Introduction.....	179
5.2. Results and Discussion	183
5.2.1. Optimization of the Protocol.....	183
5.2.2. Applicability of the Protocol.....	189
5.2.3. DFT Computed Reaction Mechanism.....	198
5.2.4. Mechanistic Investigations.....	201
5.3. Conclusion	204
5.4. References.....	205
5.5. Experimental Section	213

5.5.1. General Information.....	213
5.5.2. Optimization in Details	215
5.5.3. Procedure for the Preparation of Acid chlorides and Borates	223
5.5.4. Procedure for the Preparation of Optimal Ligand L1	272
5.5.5. General Procedure for Pd-Catalyzed Stereospecific Couplings.....	274
5.5.6. Determination of the Yields, Optical Rotations and ee Values	275
5.5.7. Synthetic Applications	360
5.5.8. Mechanistic Investigations.....	373
5.5.9. Assignment of Absolute Configuration.....	380
5.5.10. References in Experimental Section	382
5.6. Computational Section.....	385
5.6.1. Complete Authorship of Gaussian 16	385
5.6.2. General Computational Procedure	386
5.6.3. Ligand Comparison.....	387
5.6.4. Effect of KCl Coordination and Distortion-Interaction Analysis.....	390
5.6.5. Inversion and Retention Paths to Transmetalation.....	391
5.6.6. Ion Coordination	392
5.6.7. References in Computational Section	393

List of Tables

Chapter 3

Table 3.1. Evaluation of the supporting ligands.....
Table 3.2. Evaluation of the additives.....
Table 3.3. Enantioselective conjugate addition 1,1-diborylmethane to α,β -unsaturated enones
Table S3.1. Screening of metal and base
Table S3.2. Screening of ligands.....
Table S3.3. Screening of chiral ligands.....
Table S3.4. Screening of additives.....

Chapter 5

Table 5.1. Initial investigation for the development of acylative Suzuki coupling using unactivated secondary trifluoroborates
Table 5.2. Evaluation of the supporting ligands.....
Table 5.3. Evaluation of chiral secondary benzylic trifluoroborates
Table 5.4. Evaluation of acid chlorides.....
Table 5.5. Further evaluation of reaction parameters for sterically encumbered trifluoroborates.....
Table 5.6. Further evaluation of reaction parameters for aliphatic acid chlorides
Table 5.7. Evaluation of carbamoyl chlorides and transformation of chiral

Weinreb amide as versatile intermediate	
Table 5.7. Functionalization of complex commercial pharmaceuticals	
Table S5.1. Effect of Pd source as precatalyst on the reactions	
Table S5.2. Effect of loading of Pd-precatalyst and Pd to L1 ratio on the reactions.....	
Table S5.3. Effect of solvent identity and the concentration of (<i>S</i>)- 2b on the reactions.....	
Table S5.4. Effect of additives on the reactions.....	
Table S5.5. Effect of electrophilic coupling partners on the reactions	
Table S5.6. Effect of nucleophilic coupling partners on the reactions.....	
Table S5.7. Reaction profile over time	
Table S5.8. Ligand evaluation.....	
Table S5.9. Aryl and alkyl acid chlorides 1a–1u and carbamoyl chlorides 1aa–1af	
Table S5.10. Enantioenriched trifluoroborate salts 2a–2p	
Table S5.11. Comparison of value of the optical rotation.....	
Table S5.12. Control experiments with <i>18-crown-6</i>	
Table S5.13. Control experiments to compare the coordinating effect of crown ether	
Table S5.14. Crystal data and structure refinement for (<i>R</i>)- 3jb	

List of Figures

Chapter 3

Figure 3.1. ^{31}P NMR spectra (162 MHz, THF- d_8 , rt) of the reaction mixture.....

Figure 3.2. Monitoring of ligand decomposition over time by ^{31}P NMR spectroscopies.....

Figure 3.3. Monitoring the reaction mixture by ^{11}B NMR

Figure 3.4. Plausible mechanistic scenario

Figure S3.1. ^{31}P NMR spectra (162 MHz, THF- d_8 , rt) of the reaction mixture

Figure S3.2. ^{31}P NMR spectra (162 MHz, THF- d_8 , rt) of the reaction mixture in the presence of Li(acac).....

Figure S3.3. ^{31}P NMR spectra (162 MHz, THF- d_8 , rt) of the reaction mixture in the absence of Li(acac).....

Figure S3.4. ^{11}B NMR spectra (128 MHz, THF- d_8 , rt) of the reaction mixture

Figure S3.5. ^{11}B NMR spectra (128 MHz, THF- d_8 , rt) of the reaction mixture

Figure S3.6. ^{11}B NMR spectra (128 MHz, THF- d_8 , rt) of the reaction mixture

Chapter 5

Figure 5.1. Stereospecific transformation utilizing chiral boronates and current synthetic strategies for access chiral carbonyl groups

Figure 5.2. Significance of chiral carbonyl compounds and inspiring works

Figure 5.3. DFT computed reaction coordinate diagram (Top, A); Transmetalation transition structures, energies in kcal/mol, distances in Å (Bottom, B).....

Figure 5.4. Mechanistic investigations

Figure S5.1. A. DFT computed reaction coordinate diagram of APhos, PPh₃, and PMe₃ bis-oxidative addition and transmetalation steps, B. Mono-oxidative addition route to transmutation, C. DFT computed oxidative addition transition states, D. Isomerization and ligand dissociation (energies in kcal/mol, distances in Å)

Figure S5.2. Transmetalation transition structures based on the presence (Top, A) or absence of KCl (Bottom, B).....

Figure S5.3. Paths leading to inversion and retention TS.....

Figure S5.4. Model system analysis of possible ion coordination in solution

List of Schemes

Chapter 2

Scheme 1.1. Outline of the dissertation	
Scheme 2.1. Functionalization of <i>gem</i> -diborylalkanes	
Scheme 2.2. Pioneering discovery of lithiated <i>gem</i> -diborylalkanes	
Scheme 2.3. Ring-opening reactions of chiral epoxides	
Scheme 2.4. Sequential ring-opening and cyclization with chiral epoxides...	
Scheme 2.5. Diastereoselective addition to chiral aldimines	
Scheme 2.6. Iridium-catalyzed asymmetric allylic substitution	
Scheme 2.7. Pioneering discovery of deborylative functionalization.....	
Scheme 2.8. Asymmetric Suzuki-Miyaura cross-coupling	
Scheme 2.9. Initial discovery of stereoselective 1,2-addition.....	
Scheme 2.10. Stereoselective 1,2-addition to various carbonyl compounds ..	
Scheme 2.11. Stereoselective conjugate addition of <i>gem</i> -diborylalkanes.....	
Scheme 2.12. Stereoselective allylic substitution reactions.....	
Scheme 2.13. Recent advances in asymmetric allylic substitution.....	
Scheme 2.14. Reactivity of Allylic <i>gem</i> -diborylalkanes	
Scheme 2.15. Asymmetric addition reactions of allylic <i>gem</i> -diborylalkanes ..	
Scheme 2.16. Recent advances in asymmetric addition of allylic <i>gem</i> - diborylalkanes.....	

Chapter 3

- Scheme 3.1.** Stereoselective reactions with 1,1-diborylalkanes
- Scheme 3.2.** Evaluation of electrophilic coupling partners.....
- Scheme 3.3.** Evaluations of sterically encumbered substrates.....
- Scheme 3.4.** Competitive 1,2-addition pathway with alkyl-substituted enones
.....
- Scheme 3.5.** Transformation of the chiral products **3a**
- Scheme 3.6.** Viability of Li(acac) as a better activator than LiOt-Bu.....
- Scheme 3.7.** Possibility of Li(acac) sequestering borate by-products
- Scheme S3.1.** Versatility of the reaction
- Scheme S3.2.** Quantitative analysis of the side product

Chapter 4

- Scheme 4.1.** Stereospecific Suzuki-Miyaura coupling
- Scheme 4.2.** Stereochemical courses of transmetalation in Stereospecific Suzuki-Miyaura coupling
- Scheme 4.3.** Stereochemical course of primary alkylboronates
- Scheme 4.4.** Stereospecific Suzuki reaction with enantioenriched benzylic boronates.....
- Scheme 4.5.** Utilization of stereo-enriched diarylboronates.
- Scheme 4.6.** Early discovery of stereoinvertive cross-coupling
- Scheme 4.7.** Coupling with enantioenriched allylic- and propargylic boronate

Scheme 4.8. Coupling with enantioenriched cyclic allylic boronate.....	
Scheme 4.9. Synthesis quaternary carbon and sequential reactions utilizing enantioenriched allylic boronate	
Scheme 4.10. Suzuki coupling with carbonyl-substituted enantioenriched boronates.....	
Scheme 4.11. β -Hydroxyl-directed Suzuki reactions.....	
Scheme 4.12. Suzuki reactions of α -alkoxy-substituted enantioenriched boronate	
Scheme 4.13. Suzuki reactions of enantioenriched 1,1-diboronates.....	
Scheme 4.14. Pioneering discovery for Suzuki-coupling of enantioenriched unactivated secondary.....	
Scheme 4.15. Suzuki cross-coupling of enantioenriched unactivated secondary	

Chapter 5

Scheme 5.1. Early results of Pd-catalyzed acylative Suzuki-Miyaura cross-coupling with benzylic trifluoroborates.....	
Scheme 5.2. Preparation of enantioenriched benzylic trifluoroborates	
Scheme 5.3. ^1H NMR investigations of crude reaction mixtures	
Scheme S5.1. ^1H NMR analysis of crude mixture for control experiment with [Pd]-A as catalyst.....	

Contributions

Portions of this dissertation have been adapted from the following published articles co-written by the authors and are reproduced with permission.

Chapter 3 has been adapted with permission from:

Kim, C.‡; **Roh, B.**‡; Lee, H. G*. *Chem. Sci.* **2021**, *12*, 3668–3673.

‡These authors contributed equally to this work.

Chapter 3 was adapted from a manuscript written by C.K., B.R. and H.G.L. The following individuals directly contributed to the data presented: Changhee Kim, Byeongdo Roh and Prof. Hong Geun Lee. Conceptualization: C.K., H.G.L., Project administration and supervision: H.G.L., Synthetic experiments: C.K., B.R., Mechanistic studies: C.K., B.R., Writing: C.K., B.R., H.G.L.

Chapter 5 has been adapted with permission from:

Roh, B.; Farah, A. O.; Kim, B.; Feoktistova, T.; Moeller, F.; Kim, K. D.; Cheong, P. H.-Y.*; Lee, H. G.* *J. Am. Chem. Soc.* **2023**, *145*, 7075–7083.

Chapter 5 was adapted from a manuscript written by B.R., A.O.F., B.K., T.F., F.M., K.D.K., P.H.-Y.C. and H.G.L. The following individuals directly contributed to the data presented: Byeongdo Roh, Abdikani Omar Farah, Beomsu Kim, Taisiia Feoktistova, Finn Moeller, Kyeong Do Kim, Prof. Paul Ha-Yeon Cheong, and Prof. Hong Geun Lee. Conceptualization: B.R., Project administration and supervision: P.H.-Y.C., H.G.L., Synthetic experiments: B.R., B.K., F.M., K.D.K., Mechanistic studies: B.R., Computational analysis: A.O.F., T.F., Writing: B.R., A.O.F., P.H.-Y.C. H.G.L

CHAPTER 1

Outline of the Dissertation

1.1. Introduction

The development of novel methods for efficient construction of new carbon-carbon bonds is undoubtedly central to synthetic organic chemistry, enabling facile access to complicated chemical structures. Over recent decades, organoboron chemistry has evolved to become one of the most feasible protocols in this context due to the unusual properties of organoboron reagents, such as their non-toxic nature and excellent functional group tolerance (Scheme 1.1A).¹ As such, their representative transformation, which is Suzuki-Miyaura cross-coupling, has also been considered an indispensable strategy for the synthesis of diverse and complex molecules due to its operational simplicity and wide applicability.²

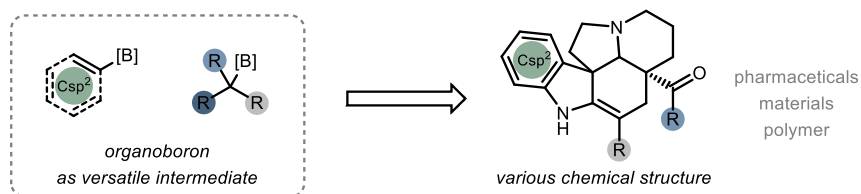
Since the award of the 2010 Nobel Prize in palladium-catalyzed cross-coupling reactions, significant progress in the development of the synthesis and applications of organoboron compounds has been widely disclosed.³ However, most approaches have been limited to the use of C(sp²)-based organoboron reagents because alkylboron compounds have relatively lower reactivities, and also evoke various side reactions such as β -hydride elimination derived from metal-alkyl intermediates. Thus, the chemical structures we could access were constrained by this circumstance.

After recent efforts devoted to the synthesis and applications of C(sp³)-based organometallic reagents, alkylboron compounds have played a critical role in allowing facile access to three-dimensional chemical space that were

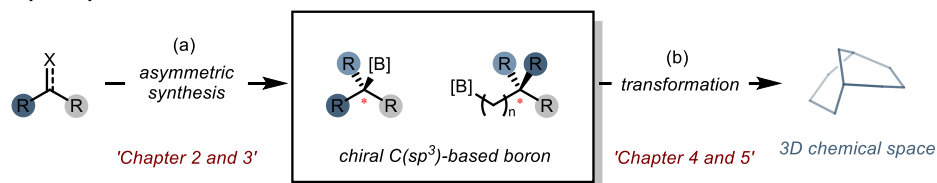
previously difficult to access (Scheme 1.1B).⁴ Importantly, after the pioneering discovery of asymmetric hydroboration developed by Brown in 1961,⁵ chiral organoboronates bearing stereogenic centers are considered highly useful synthetic handles that have been widely utilized as key intermediates for the construction of diverse chiral molecules (Scheme 1.1B. a).⁶ In fact, the chiral boronates can be transferred to potentially all types of functional groups through the developed protocols, such as hydrogen (via protodeborylation), alcohol (via oxidation), amines (via amination), halogen (via halogenation), and carbon-based functional groups (via either cross-coupling or addition reactions) (Scheme 1.1B. b).⁷

In this context, the development of efficient preparation and transformation methods for chiral organoboronates is of utmost importance. In the following Chapter, our efforts and contributions to expanding the applicability of those protocols are introduced.

A. organoboron in synthetic chemistry



B. Utility of alkylboron



Scheme 1.1. Outline of the dissertation

1.2. References

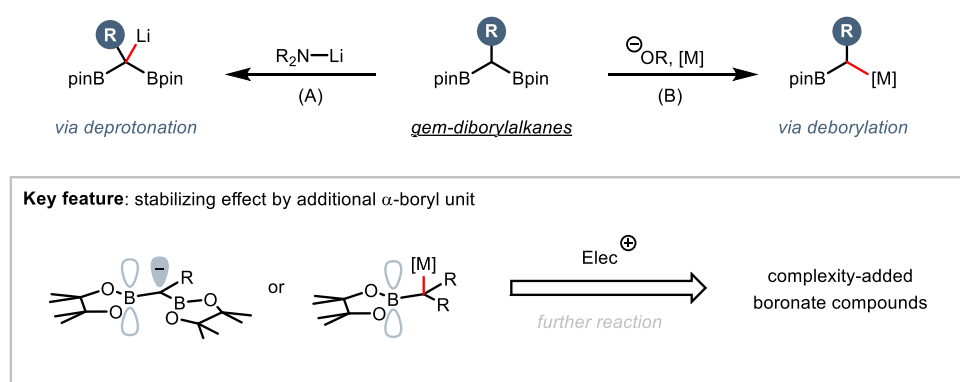
- (1) (a) Defrancesco, H.; Dudley, J.; Coca, A. *ACS Symp. Ser.* **2016**, *1236*, 1.
(b) Fyfe, J. W. B.; Watson, A. J. B. *Chem.* **2017**, *3*, 31.
- (2) (a) Miyaura, N.; Suzuki, A. *Chem. Rev.* **1995**, *95*, 2457. (b) Maluenda, I.; Navarro, O. *Molecules* **2015**, *20*, 7528. (c) Lennox, A. J. J.; Lloyd-Jones, G. C. *Chem. Soc. Rev.* **2014**, *43*, 412.
- (3) (a) Johansson Seechurn, C. C. C.; Kitching, M. O.; Colacot, T. J.; Snieckus, V. *Angew. Chem., Int. Ed.* **2012**, *51*, 5062. (b) Beletskaya, I. P.; Alonso, F.; Tyurin, V. *Coord. Chem. Rev.* **2019**, *385*, 137.
- (4) El-Maiss, J.; Mohy El Dine, T.; Lu, C.-S.; Karame, I.; Kanj, A.; Polychronopoulou, K.; Shaya, J. *Catalysts* **2020**, *10*, 296.
- (5) (a) Brown, H. C.; Zweifel, G. *J. Am. Chem. Soc.* **1961**, *83*, 486. (b) Zweifel, G.; Brown, H. C. *J. Am. Chem. Soc.* **1964**, *86*, 393. (c) Brown, H. C.; Desai, M. C.; Jadhav, P. K. *J. Org. Chem.* **1982**, *47*, 5065.
- (6) Hu, J.; Ferger, M.; Shi, Z.; Marder, T. B. *Chem. Soc. Rev.* **2021**, *50*, 13129.
- (7) Sandford, C.; Aggarwal, V. K. *Chem. Commun.* **2017**, *53*, 5481.
- (8) (a) Kim, C.; Roh, B.; Lee, H. G. *Chem. Sci.* **2021**, *12*, 3668. (b) Roh, B.; Farah, A. O.; Kim, B.; Feoktistova, T.; Moeller, F.; Kim, K. D.; Cheong, P. H.-Y.; Lee, H. G. *J. Am. Chem. Soc.* **2023**, *145*, 7075.

CHAPTER 2

Utilization of *gem*-Diborylalkanes in Asymmetric Catalysis

2.1. Introduction

In recent decades, geminal 1,1-diborylalkanes have attracted significant interest as versatile compounds in the synthetic organic chemistry (Scheme 2.1).¹ Compared to the generally utilized mono-borylated compounds, they have distinct features derived from additional boron unit that is present at α -position. The vacant empty orbital of the remaining boron atom can stabilize anion at adjacent carbon center.



Scheme 2.1. Functionalization of *gem*-diborylalkanes

As such, hydrogen atoms existing in α -position of *gem*-diborylalkane have highly acidic properties exhibiting enough lower pK_a resulting in being easily deprotonated with common amide bases (Scheme 2.1A). The intermediate formed at this time, *gem*-diboryl carbanion, can also react with electrophiles. Even after the functionalization of one boron unit, the other boron part still remains (Scheme 2.1B). This intermediate, called α -boryl carbanion, is a reactive nucleophilic species, participating in further

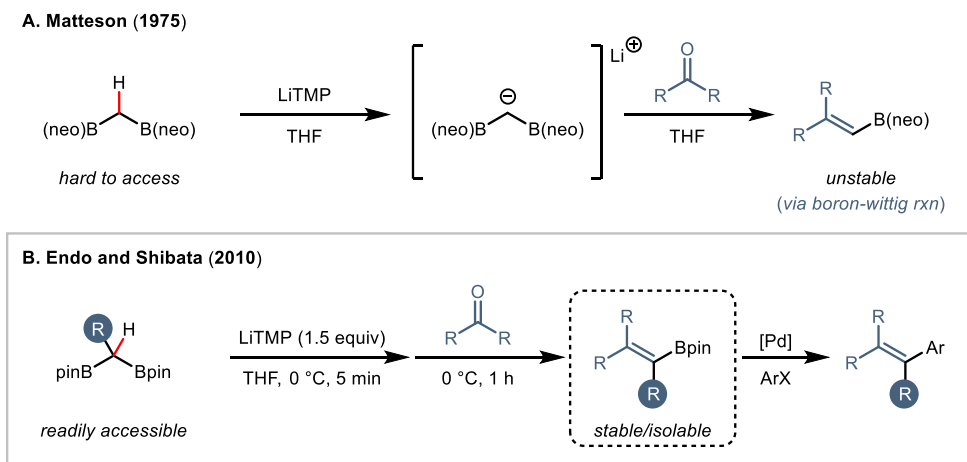
transformation with various electrophiles.

The resulting products generated from above-mentioned two of functionalization modes still have one another boron group and it enables further transformation. Because of these unique properties, the protocols utilizing *gem*-diborylalkanes have become one of the most powerful strategies to access densely substituted complex molecules. Concurrently, based on unprecedented properties of *gem*-diborylalkanes, tremendous efforts have been devoted to extending these approaches to catalytic asymmetric methods. In this context, this chapter will describe the development and recent advances of the strategies employing geminal 1,1-diborylalkanes, particularly in asymmetric catalysis will be discussed.

2.2. Deprotonative Activation of *gem*-Diborylalkanes

2.2.1. Substrate-controlled Stereoselective Strategies

As mentioned above, one of the representative properties *gem*-diborylalkanes is the increased acidity of the hydrogen atoms existing in α -position, which enables to be easily deprotonated with common amide bases such as LiTMP or LDA (Scheme 2.1A). The formed *gem*-diboryl carbanion have been further reacted with various electrophiles such as alkyl halide and carbonyl derivatives, affording the corresponding complexity-added borylated compounds.



Scheme 2.2. Pioneering discovery of lithiated *gem*-diborylalkanes

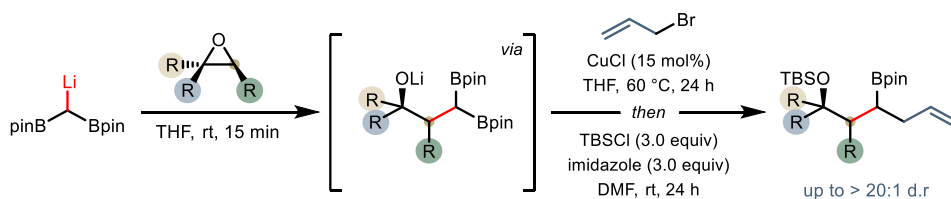
In 1975, Matteson and co-workers first reported the pioneering work demonstrating that germinal 1,1-diboryl carbanion can be used as reactive nucleophilic species (Scheme 2.2A).² After that, Matteson group disclosed the 1,1-diborylalkanes can be deprotonated with bulky amide bases affording

germinal 1,1-diboryl carbanion as intermediate, subsequently undergoing nucleophilic reactions with alkyl halide or carbonyls compounds.³ However, the synthetic methods for access to glycol-derived 1,1-diborylalkanes which are used in these protocol were not straightforward and vinyl intermediate formed during the reaction was also not stable. These limitations have suppressed the potential to expand this unique reactivity.

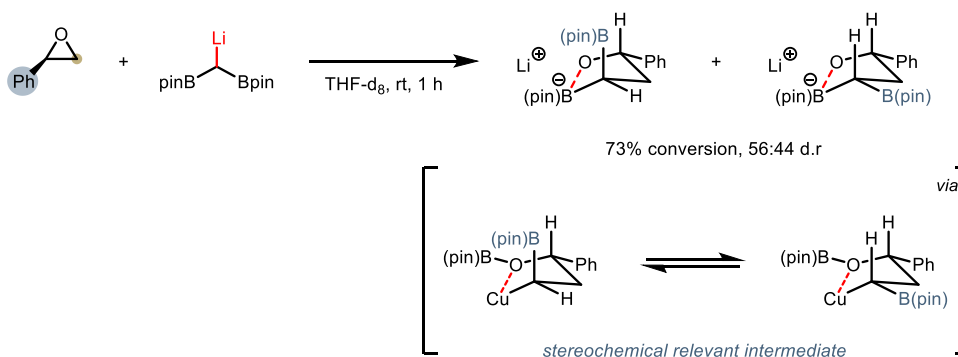
In 2010, based on the pioneering discoveries, Endo and Shibata reported a more general and practical method utilizing readily accessible and more stable pinacol-based *gem*-diborylalkanes, opening the door for extending the deprotonative strategies of *gem*-diborylalkanes (Scheme 2.2B).⁴

With the beginning of these initial discoveries, α -Diboryl lithium species have been widely utilized in stereoselective transformations. In 2017, Meek group disclosed a stereoselective addition of α -diboryl lithium species generated during the reaction process to optically pure epoxides (Scheme 2.3A).⁵ The corresponding β -hydroxyl diboron intermediates were employed in subsequent copper-catalyzed allylic substitution enabling the formation of optically pure boronates compounds. Through monitoring the ring opening process by ^1H NMR spectrum, the authors proposed that five-membered cyclic boronate intermediates play a key role in determining the diastereoselectivity (Scheme 2.3B).

A. Meek (2017)



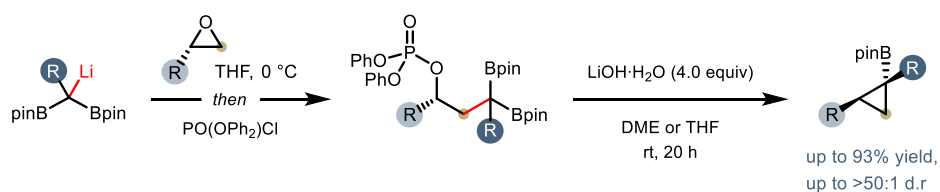
B. Key features



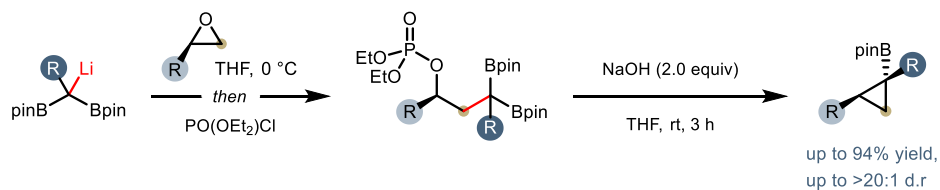
Scheme 2.3. Ring-opening reactions of chiral epoxides

Recently, Hong⁶ and Cho⁷ group independently reported the tandem strategies of deprotonative addition and deborylative cyclization from chiral epoxide and *gem*-diborylalkanes (Scheme 2.4A, B). This nucleophilic addition of α -lithiated diboryl species to enantioenriched epoxide enabled the formation of leaving group-containing 1,1-diborylalkanes. Under the similar reaction conditions, the subsequent deborylative stereospecific cyclization in the presence of alkoxide base furnished enantioenriched cyclopropylboronates.

A. Hong (2023)

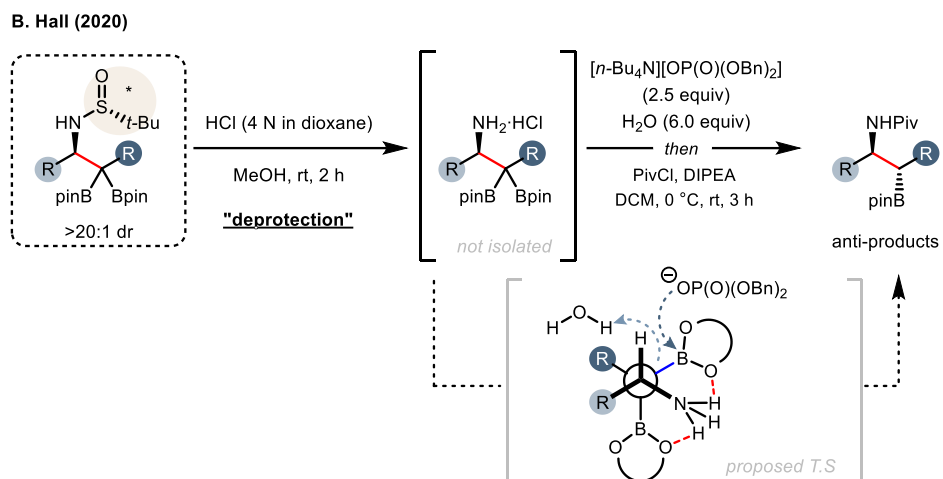
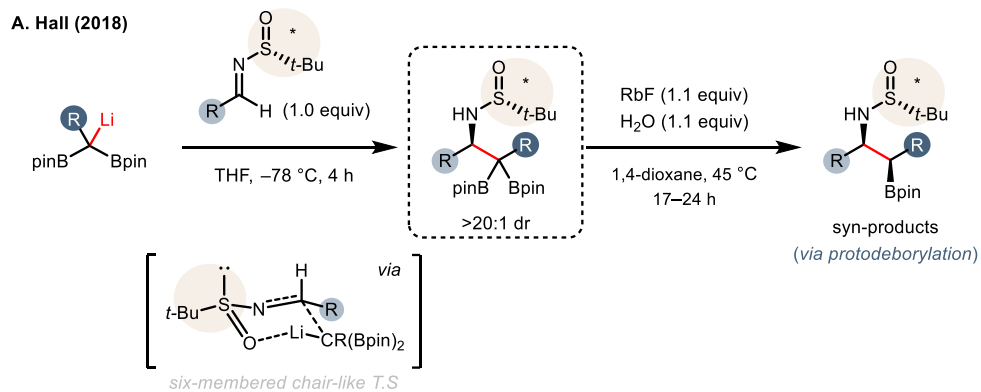


B. Cho (2023)



Scheme 2.4. Sequential ring-opening and cyclization with chiral epoxides

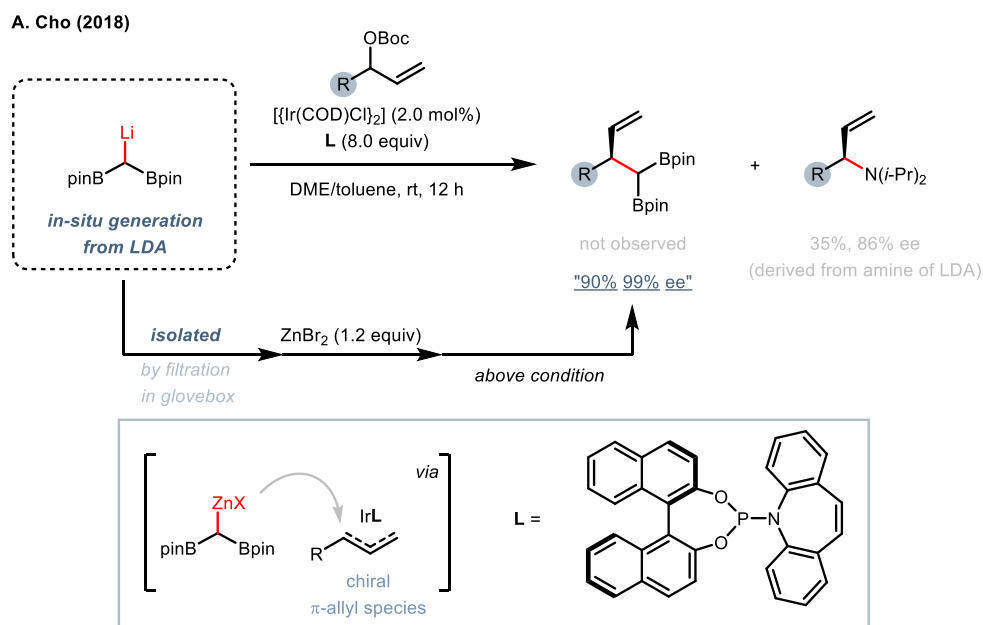
Next, Hall and co-workers developed the diastereoselective strategy using 1,1-diborylalkanes and Ellman auxiliary-containing aldimine providing α,β -disubstituted β -aminoalkylboronates (Scheme 2.5A).⁸ The 1,1-diborylalkanes initially was deprotonated and the generated α -diboryl lithium species was subjected to the 1,2-addition with optically pure aldimine affording β -sulfinimido *gem*-diborylalkanes in high yield with high diastereoselectivity. The stereochemical outcome was rationalized by suggesting the involvement of the six-membered chair-like transition structure. The further protodeborylation based on Aggarwal's method⁹ enabled the formation of the corresponding β -aminoalkylboronates. Recent in 2020, Hall group developed the stereodivergent approach enabling access to both syn and anti diastereomers of the products (Scheme 2.5B).¹⁰ Surprisingly, by switching the order of protodeborylation and desulfinylation sequence, anti-products were observed as major diastereomer. Under modified conditions, desulfinylated intermediate was employed in the following diastereoselective protodeborylation process, delivering anti-product as major isomer. Based on mechanistic investigations, the authors proposed that anti-selective protodeborylation proceeds via the formation of rotameric transition state featuring two hydrogen bonding between ammonium cation and boronic acid pinacol ester units. The proposed transition state enables the coordination of the phosphate anion to boron, undergoing a concomitant stereoretentive protonation at the least sterically hindered position.



Scheme 2.5. Diastereoselective addition to chiral aldimines

2.2.2. Catalyst-controlled Stereoselective Strategies

Unlike the aforementioned substrate-controlled strategies, the catalyst-controlled asymmetric strategy was only recently developed by Cho group in 2018 (Scheme 2.6).¹¹ The authors demonstrated the general method enabling the isolation of α -diboryl lithium species for applications to iridium-catalyzed asymmetric allylic alkylation reaction. In the preliminary results, the chiral amines were formed presumably due to the reaction with potential amine nucleophile derived from LDA. Notably, in the presence of additional zinc halides, the desired products were formed in high yield with excellent stereoselectivity, indicating that α -diboryl zinc species in-situ generated under the reaction conditions participated in the reactions. These results showed that the use of isolated lithiated species is crucial.



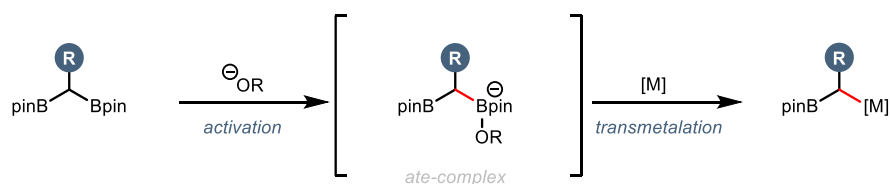
Scheme 2.6. Iridium-catalyzed asymmetric allylic substitution

2.3. Deborylative Activation of *gem*-Diborylalkanes

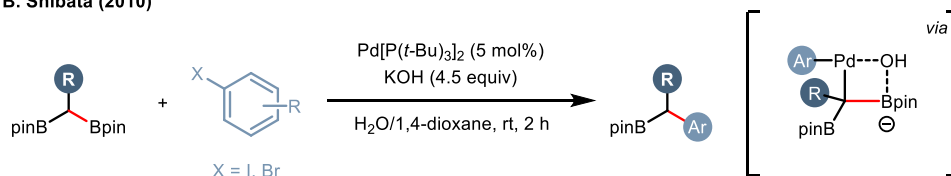
2.3.1. Stereoselective Suzuki-Miyaura Cross-Coupling

In the presence of either alkoxide or hydroxide base, 1,1-diborylalkanes could be activated through monodeborylation, affording α -boryl anion intermediate (Scheme 2.1).¹ In general, the deborylative transformations proceeds with the addition of a transition metal such as copper and palladium. The strong alkoxide base initially coordinate to boron center forming reactive ate-complex and it undergoes transmetalation with either copper or palladium. (Scheme 2.7A). Subsequently, the corresponding α -boryl organometallic species have participated in diverse transformations such as cross-coupling, addition reactions.

A. Deborylative functionalization of 1,1-diborylalkanes with alkoxide bases



B. Shibata (2010)



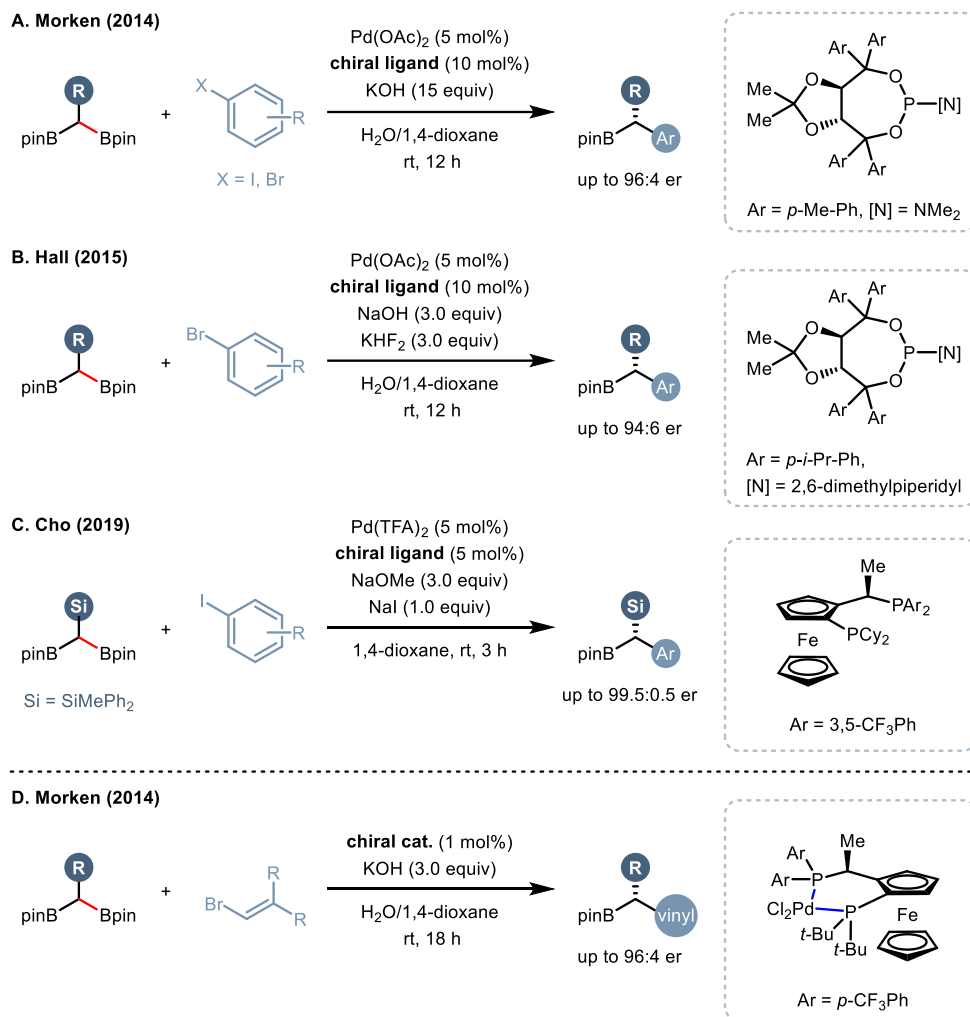
Scheme 2.7. Pioneering discovery of deborylative functionalization

In 2010, Shibata and co-workers disclosed that *gem*-diborylalkanes can be utilized as competent coupling partner in Suzuki-Miyaura cross-coupling reaction with aryl bromide (Scheme 2.7B).¹² Under the mild reaction conditions such as room temperature, the desired coupling products were formed efficiently. It was found that the use of strong alkoxide or hydroxide base is crucial promoting the cross-coupling reaction of 1,1-diborylalkanes. In addition, high chemoselectivity was observed using aryl bromide bearing primary alkylboronic ester, showing the selectively formation of coupling products.

After the pioneering discovery developed by Shibata, the reactivity of *gem*-diborylalkanes in cross-coupling have been extended to asymmetric approaches. In 2014, Morken and coworkers independently reported asymmetric Suzuki-Miyaura cross-coupling reaction of *gem*-diborylalkanes with aryl halides under the palladium-based catalytic system (Scheme 2.8A).¹³ In the presence of the chiral monodentate phosphoramidite ligands, the reaction efficiently proceeded affording the chiral coupling product with high yield and enantioselectivity. In addition, the applicability of the protocol was examined by successful synthesis of key intermediate for access to (*R*)-tolterodine. In the proposed mechanism, the authors suggested that the reaction might occur through the intermediacy of hydroxide palladium intermediates in the presence of hydroxide which is accord with previous work (Scheme 2.7B). As such, this intermediate undergoes transmetalation

which is considered as the stereoselective-determining and subsequent reductive elimination, affording the chiral products.

A year later, in 2015, Hall group also independently described a catalytic enantioselective Suzuki-Miyaura cross-coupling reaction of *gem*-diborylalkanes (Scheme 2.8B).¹⁴ This approach also worked with chiral phosphoramidite-type ligands under palladium catalysis, furnishing optically enriched secondary benzylic boronic esters with great stereoselectivity. Later, Morcken group extended the aforementioned reaction conditions to the stereoselective Suzuki-Miyaura cross-coupling of 1,1-diborylalkanes with vinyl bromides, highlighting the synthesis of chiral allylic boronates (Scheme 2.8D).¹⁵ The utilization of Josiphos-type ligands was crucial for the best performance of the protocol, showing excellent yield and great stereoselectivity. In 2019, Cho and co-workers demonstrated palladium-catalyzed enantiotopic-group selective cross-coupling of *gem*-diborylsilane with aryl iodides, affording chiral benzylic 1,1-silyl boronates esters (Scheme 2.8C).¹⁶ The authors discovered that the chiral Josiphos-type ligand-based palladium catalytic system promote the efficiency of the reactivity and enantioselectivity.

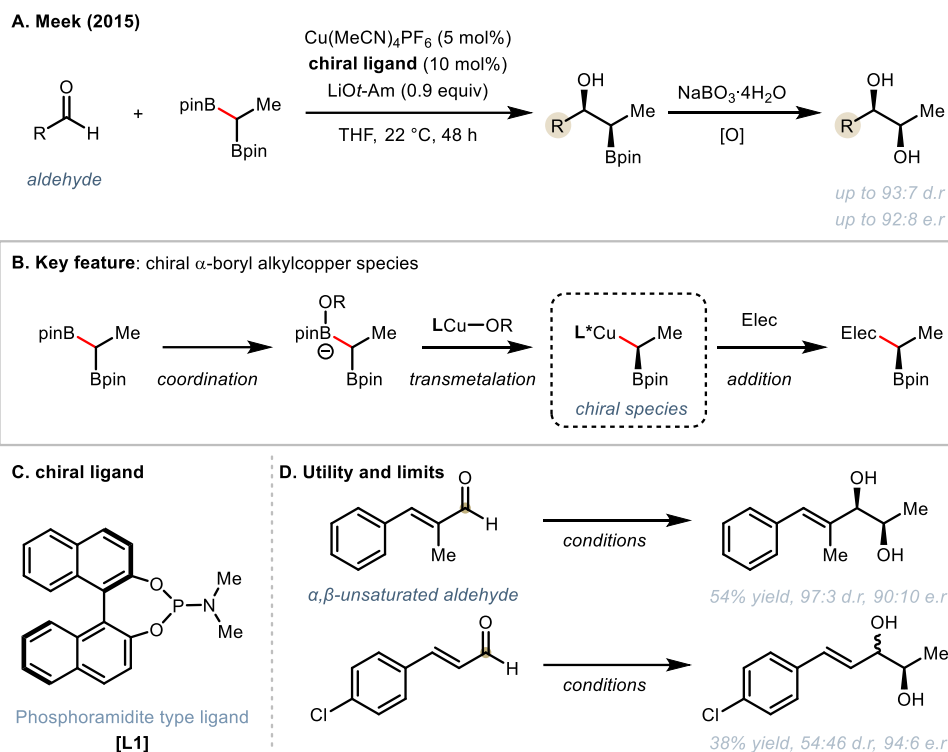


Scheme 2.8. Asymmetric Suzuki-Miyaura cross-coupling

2.3.2. Stereoselective 1,2-addition Reactions

The above-mentioned reactions enabled the direct cross-coupling reaction of *gem*-diborylalkanes under palladium catalysis for the construction of chiral boronates. However, these approaches were only limited to the use of aryl- and vinyl halides as coupling partners. The utilization of other types of transition-metal catalysts can be another option for the synthesis of diverse chiral structures. Among them, copper-based catalytic reactions have been most widely applied for asymmetric functionalization of *gem*-diborylalkanes.

In 2015, Meek and coworkers unveiled the potential reactivity of copper-based catalyst enabling applications to asymmetric transformation of *gem*-diborylalkanes (Scheme 2.9A).¹⁷ The key feature of this copper-based protocol is the generation of chiral copper-alkyl species from the 1,1-diborylalkanes and copper alkoxide (Scheme 2.9B). This nucleophilic species was subjected to the stereoselective 1,2-addition reaction with aldehyde followed by oxidation to furnish the resulting chiral 1,2-diol. The phosphoramidite-type ligand showed best performance for the reaction (Scheme 2.9C). In addition, the α,β -unsaturated aldehyde also reacted to give the chiral 1,2-diol in high enantio- and diastereo-selectivity, except for the sterically unhindered cinnamaldehyde (Scheme 2.9D).



Scheme 2.9. Initial discovery of stereoselective 1,2-addition

A year later in 2016, Meek group described a similar copper-catalyzed enantioselective 1,2-addition of 1,1-diborylalkanes, the scope of which they extended to α -keto esters (Scheme 2.10A).¹⁸ In this work, the chiral copper complex derived from phosphoramidite ligand has emerged as the optimal system. The proposed working process features the transmetalation between a copper alkoxide and 1,1-diborylalkanes followed by stereoselective 1,2-addition. Lastly, the reaction with alkoxide regenerated chiral copper-complex.

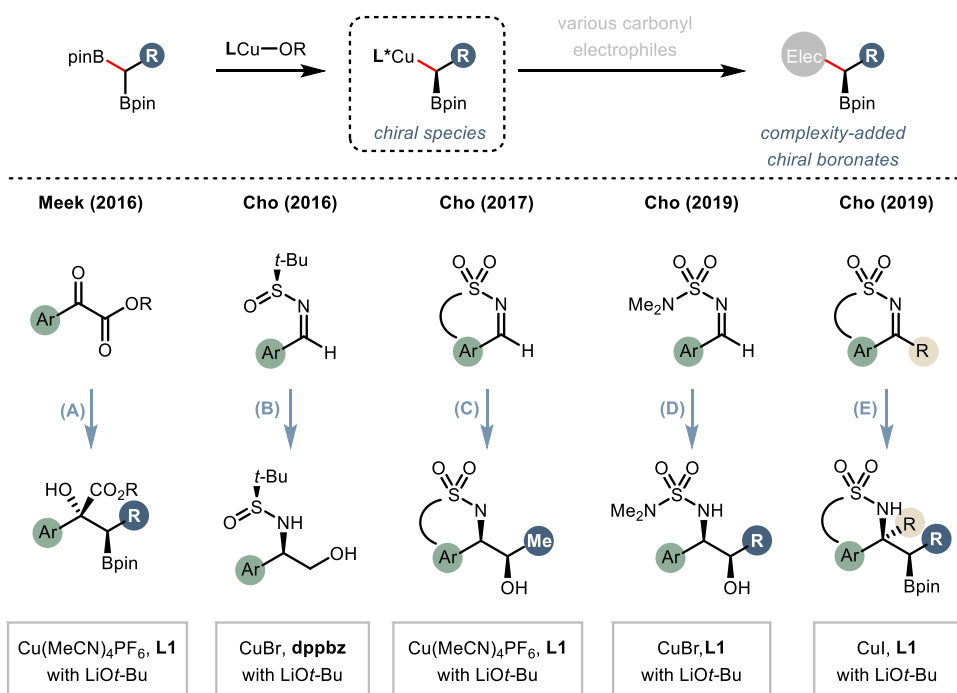
Additionally, the development of copper-catalyzed stereoselective addition reaction using 1,1-diborylalkane as pronucleophile was extended to the use of aldimine and ketimines for preparation of β -amino boronates. In 2016, Cho and co-workers reported the diastereoselective addition of 1,1-diborylmethane utilizing chiral auxiliary-based aldimines (Scheme 2.10B).¹⁹ The sequence of addition and oxidation afforded chiral β -amino alcohol. The observed high diastereoselectivity was proposed by describing that the reaction proceeded via a chairlike six-membered cyclic transition state, in which the boron unit of copper alkyl species was coordinated to the oxygen atom of the sulfinyl moiety.

A year later, Cho and co-workers developed the copper-catalyzed enantioselective 1,2-addition reaction with cyclic aldimine, affording chiral β -amino alcohol in excellent stereoselectivity (Scheme 2.10C).²⁰ After that, in 2019, the same group described the improved and scalable method for their previous 1,2-addition protocol, enabling the utilization of acyclic arylaldimine (Scheme 2.10D).²¹ In this reaction, it was found that the use of *N,N*-dimethyl sulfamoyl-protected acyclic arylaldimines were crucial for improving the diastereo- and enantioselectivity. The developed protocol proceeded successfully in 10 mmol scale showing the synthetic utility.

In addition, Cho group extended their protocol to the sterically more encumbered cyclic ketimines and α -imino ester (Scheme 2.10E).²² The combination of copper salt, lithium alkoxide and phosphoramidite ligand

enabled the formation of the desired addition product in excellent yield and stereoselectivity. More recently, copper-catalyzed enantioselective 1,2-addition to isatins was also established by Chen and Xiao, affording the chiral 3-hydroxyoxindoles.²³

Generally accepted mechanism

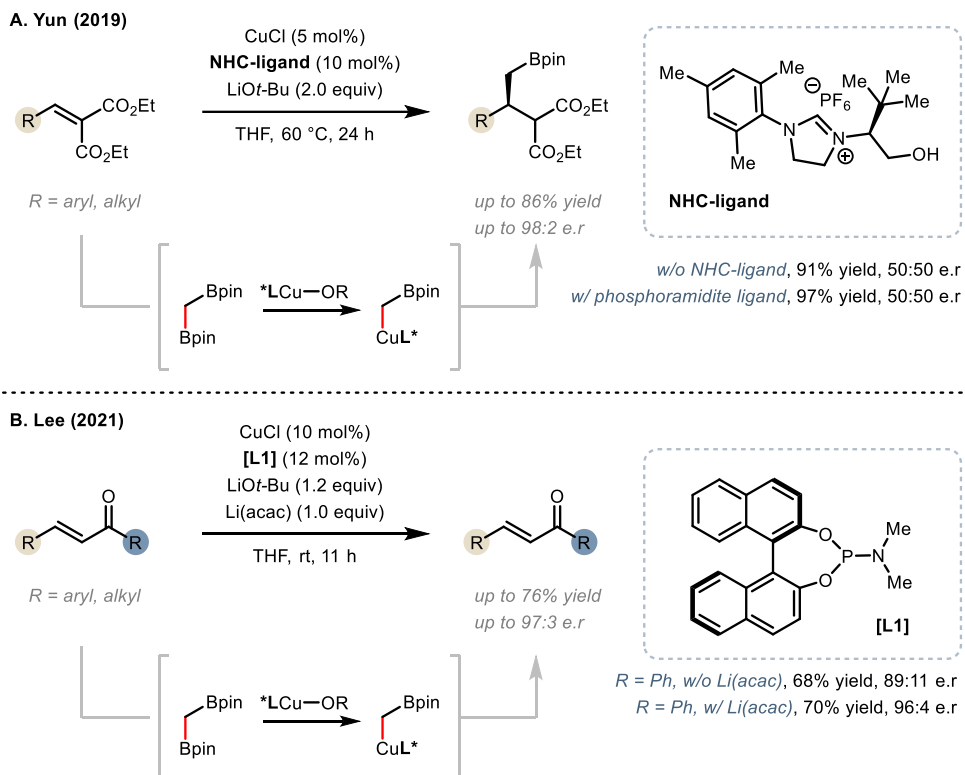


Scheme 2.10. Stereoselective 1,2-addition to various carbonyl compounds

2.3.3. Stereoselective 1,4-addition Reactions

In addition to 1,2-addition of *gem*-diborylalkanes, asymmetric conjugate addition reactions were also developed. In 2019, Yun and Jang first disclosed the enantioselective conjugate addition reaction of 1,1-diborylalkanes with α,β -unsaturated diester (Scheme 2.11A).²⁴ In the absence of the additional ligand, the stereochemical information was not introduced to the product despite the observation of high reactivity. Even with the phosphoramidite-type ligand which has been exhibited the efficiency in 1,2-addition reactions, the product was only formed as a racemate form, implying the facile background reaction impeded the stereoinduction process. Notably, the authors utilized chiral NHC-ligated copper complex which can coordinate tightly to copper and enabled the formation of the desired 1,4-addition product with excellent enantioselectivity. Moreover, the high diastereoselectivity was observed using optically pure α,β -unsaturated diester as electrophiles, showing the synthetic utility.

Shortly later, Lee and co-workers reported stereoselective conjugate addition of 1,1-diborylalkanes to enones (Scheme 2.11B).²⁵ Various α,β -unsaturated enone substrates were tolerated in this protocol, affording the chiral boronic ester with good yield and enantioselectivity despite the decreased reactivity with alkyl-substituted enones. However, the efficiency of the reaction could be conserved in a larger-scale reaction, demonstrating the robustness of the reaction.

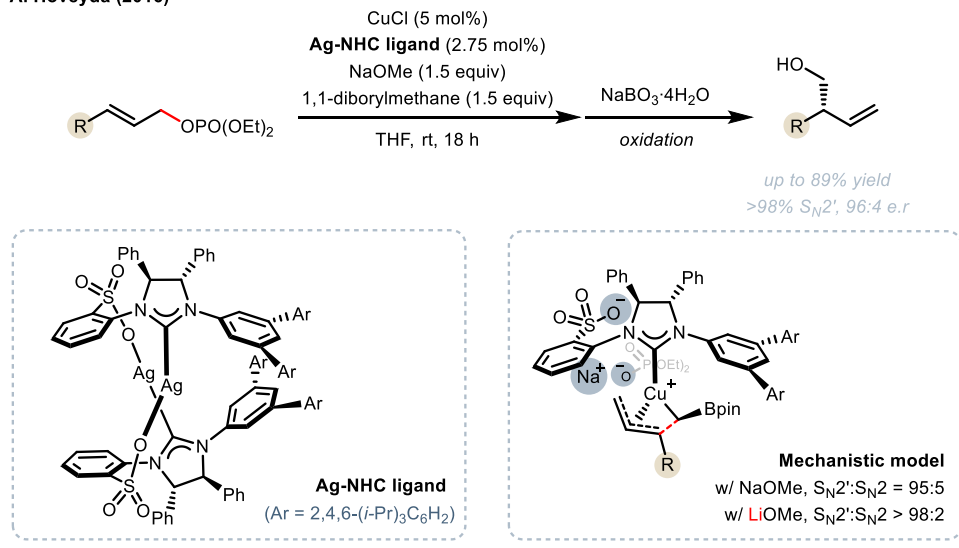


Scheme 2.11. Stereoselective conjugate addition of *gem*-diborylalkanes

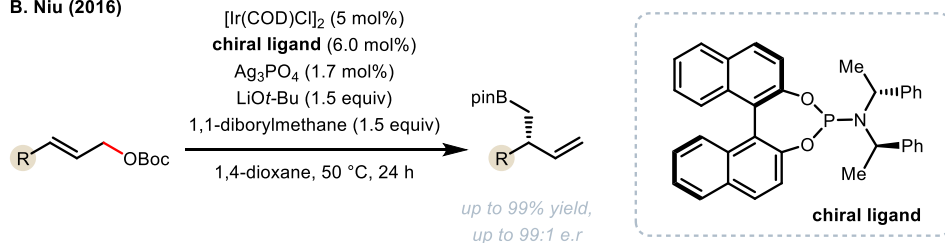
2.3.4. Stereoselective Allylic Substitution Reactions

In 2016, Hoveyda and co-workers applied the reactivity of *gem*-diborylalkanes to asymmetric allylic substitution reaction with allylic phosphates as electrophilic partners (Scheme 2.12A).²⁶ In the presence of NHC-copper complex, the desired chiral homoallylic boronates was predominantly formed via S_N2' reaction pathway. The distinct feature of this protocol was the utilization of the sulfonate-containing chiral NHC ligand. The authors proposed that the formation of non-covalent interaction between sodium cation and phosphate unit enhanced the transition structure more well-defined, facilitating the S_N2' pathway. In fact, in the presence of the more Lewis acidic lithium salt, the increased regioselectivity was observed, supporting their rationale. In same year, Niu group reported the iridium-catalyzed asymmetric allylic substitution reaction between 1,1-diborylalkane and allylic carbonates. The authors proposed that the initial formation of chiral copper or silver-based alkyl species undergoes subsequently stereoselective allylic substitution reactions (Scheme 2.12B).²⁷

A. Hoveyda (2016)



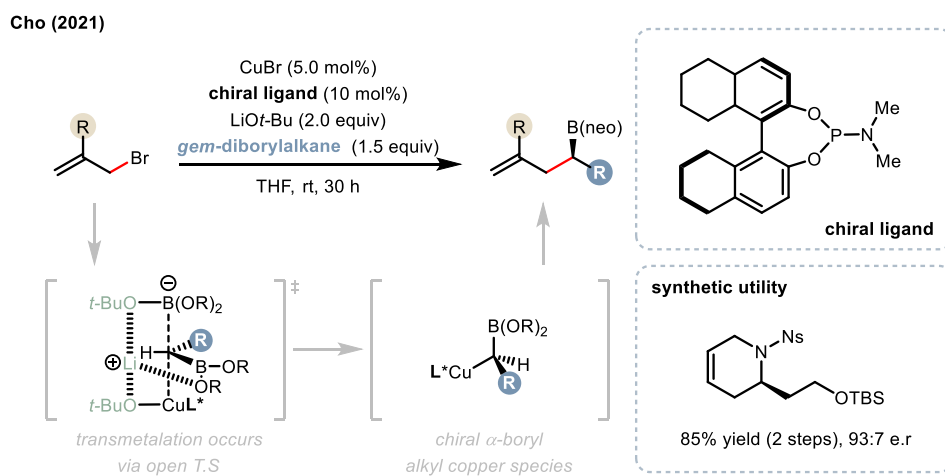
B. Niu (2016)



Scheme 2.12. Stereoselective allylic substitution reactions

Recent in 2021, Cho and colleagues developed an enantiotopic-group-selective allylation reaction with various allyl bromide, enabling the formation of enantioenriched homoallylic boronates (Scheme 2.13).²⁸ It was found that the BINOL-derived phosphoramidite ligand proved to be most effective for this strategy. The authors performed quantum mechanical calculations based on density functional theory. Based on the computational investigations, the plausible mechanism was proposed, suggesting that the reaction begins with the formation of chiral ligand-supported copper-alkoxide

complex. Noteworthy is the subsequent transmetalation that occurs via a lithium tert-butoxide-assisted open transition state. The further synthetic utility of the products was evaluated by the synthesis of the core structure of piperidine alkaloids.

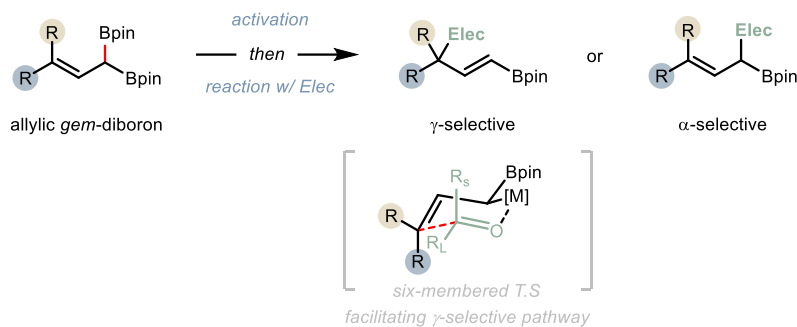


Scheme 2.13. Recent advances in asymmetric allylic substitution

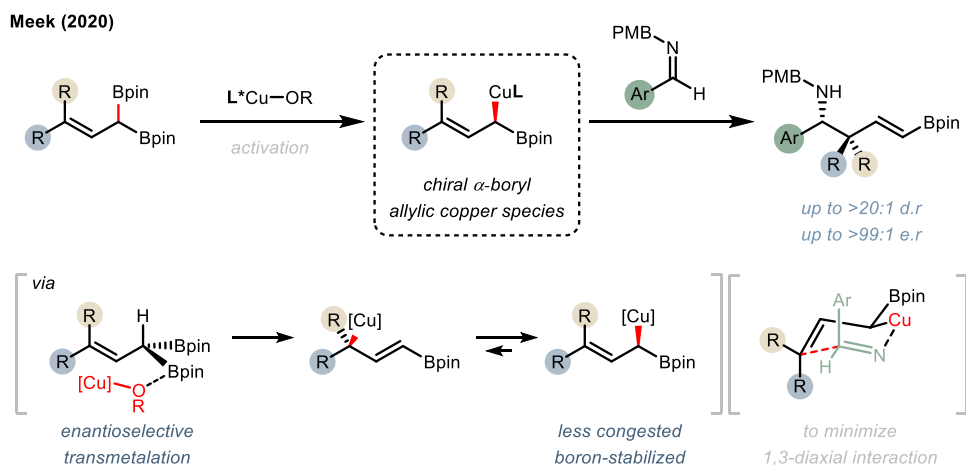
2.3.5. Utility of Allylic *gem*-Diborylalkanes

Along with the generally available aliphatic 1,1-diborylalkanes, allylic 1,1-diborylalkanes have been also recently utilized in the asymmetric version of various transformation. Compared to the aliphatic *gem*-diborylalkanes, they usually participated in the transformation via a six-membered cyclic transition state, facilitating the predominant formation of γ -selective addition product (Scheme 2.14). The representative examples of asymmetric reaction utilizing allylic diborylalkanes were recently developed by Meek group. Meek and colleagues disclosed the potential reactivity of allylic 1,1-diborylalkanes by applying them to the asymmetric 1,2-addition,²⁹⁻³¹ nucleophilic substitution reactions³² and conjugate addition.³³

The reactivity of allylic 1,1-diborylalkanes



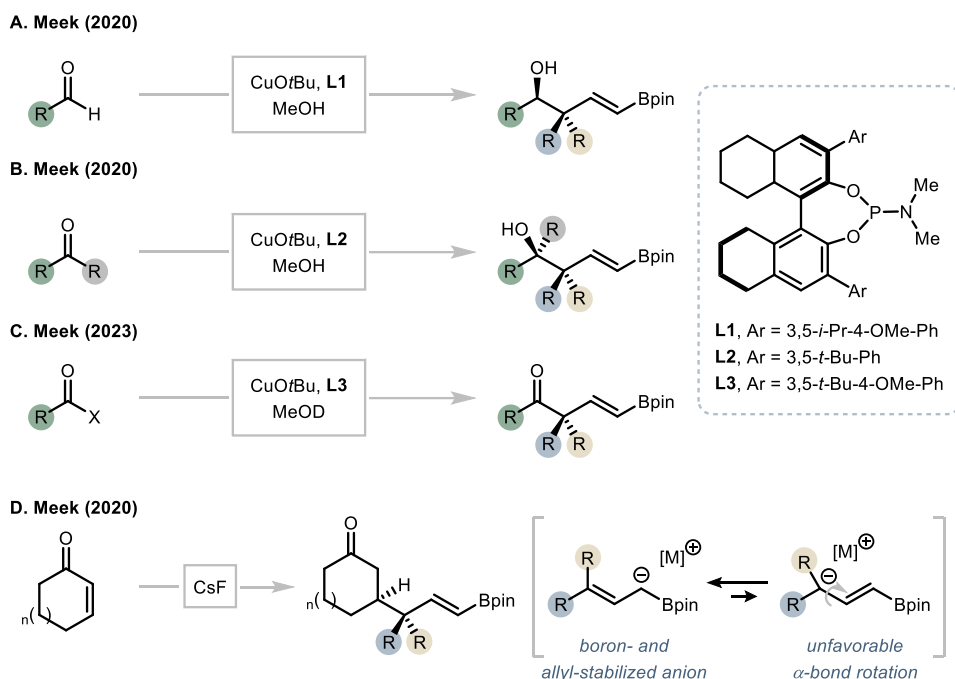
Scheme 2.14. Reactivity of Allylic *gem*-diborylalkanes



Scheme 2.15. Asymmetric addition reactions of allylic *gem*-diborylalkanes

The reaction between allylic *gem*-diboronate ester and protected-aldimine afforded chiral homoallylic amines bearing quaternary stereogenic centers in high stereoselectivity (Scheme 2.15).²⁹ This transformation was accomplished by the monodentate phosphoramidate ligand-based catalytic copper system. Notably, it was found that the formation of both E- and Z-product from different allylic boronates was observed. These results indicated that the reactions occur with enantioselective transmetalation process, followed by copper-allyl addition to aldimine. The plausible mechanism starts with the generation of enantioenriched allylic copper species from copper alkoxide and allylic boronates. Facile isomerization to sterically less encumbered and α -boryl-assisted more stable allylic copper species participated in stereoselective 1,2-addition. At this time, the remaining boron unit was positioned in the equatorial position to minimize additional 1,3-diaxial interactions. The synthetic utility was further displayed by the

synthesis of densely substituted chiral pyrrolidines. Meek and co-workers further expanded the usefulness of the aforementioned strategy with ketone³⁰ and aldehyde³¹ under the slightly modified reaction conditions, enabling access to complexity-added chiral alcohol bearing α -quaternary carbon center (Scheme 2.16A, B). Recent in 2023, Meek reported the enantioselective nucleophilic substitution of allylic gem-diborylalkane with activated acyl surrogates (Scheme 2.16C).³² This strategy enabled facile access to chiral ketones and α -keto esters having α -quaternary carbon center.



Scheme 2.16. Recent advances in asymmetric addition of allylic gem-diborylalkanes

In addition, same group developed the diastereoselective synthesis of γ -quaternary carbon center-containing ketones through α -boron stabilized allylic nucleophiles from allylic *gem*-diborylalkanes (Scheme 2.16D).³³ The choice of cesium fluoride as activator was critical for improvement of reactivity due to its less basicity to avoid competitive deprotonation. The proposed mechanism begins with the initiation by cesium fluoride, generating the corresponding boron enolate. Also, the authors suggested that the E/Z isomerization of the cesium allylic anion intermediate can be minimized due to unfavorable α -bond rotation.

2.4. References

- (1) For reviews, see: (a) Wu, C.; Wang, J. *Tetrahedron Lett.* **2018**, *59*, 2128.
(b) Nallagonda, R.; Padala, K.; Masarwa, A. *Org. Biomol. Chem.* **2018**, *16*, 1050. (c) Zhang, C.; Hu, W.; Morken, J. P. *ACS Catal.* **2021**, *11*, 10660.
(d) Lee, Y.; Han, S.; Cho, S. H. *Acc. Chem. Res.* **2021**, *54*, 3917. (e) Paul, S.; Das, K. K.; Aich, D.; Manna, S.; Panda, S. *Org. Chem. Front.* **2022**, *9*, 838.
- (2) Matteson, D. S.; Moody, R. J.; Jesthi, P. K. *J. Am. Chem. Soc.* **1975**, *97*, 5608.
- (3) (a) Matteson, D. S.; Jesthi, P. K. *J. Organomet. Chem.* **1976**, *110*, 25. (b) Matteson, D. S.; Moody, R. J. *J. Am. Chem. Soc.* **1977**, *99*, 3196. (c) Matteson, D. S.; Moody, R. J. *Organometallics* **1982**, *1*, 20.
- (4) Endo, K.; Hirokami, M.; Shibata, T. *J. Org. Chem.* **2010**, *75*, 3469.
- (5) Murray, S. A.; Liang, M. Z.; Meek, S. J. *J. Am. Chem. Soc.* **2017**, *139*, 14061.
- (6) Chen, X. Y.; Gao, F. C.; Ning, P. F.; Wei, Y.; Hong, K. *Angew. Chem., Int. Ed.* **2023**, *62*, e202302638.
- (7) Kim, G.; Kim, M.; Ryu, C.; Choi, J.; Cho, S. H. *Org. Lett.* **2023**, *25*, 4130.
- (8) Li, X.; Hall, D. G. *Angew. Chem., Int. Ed.* **2018**, *57*, 10304.
- (9) Nave, S.; Sonawane, R. P.; Elford, T. G.; Aggarwal, V. K. *J. Am. Chem.*

Soc. **2010**, *132*, 17096.

(10) Li, X.; Hall, D. G. *J. Am. Chem. Soc.* **2020**, *142*, 9063.

(11) Lee, Y.; Park, J.; Cho, S. H. *Angew. Chem. Int. Ed.* **2018**, *57*, 12930.

(12) Endo, K.; Ohkubo, T.; Hirokami M.; Shibata, T. *J. Am. Chem. Soc.* **2010**, *132*, 11033.

(13) Sun, C.; Potter, B.; Morken, J. P. *J. Am. Chem. Soc.* **2014**, *136*, 6534.

(14) Sun, H. Y.; Kubota, K.; Hall, D. G. *Chem. - Eur. J.* **2015**, *21*, 19186.

(15) Potter, B.; Szymaniak, A. A.; Edelstein, E. K.; Morken, J. P. *J. Am. Chem. Soc.* **2014**, *136*, 17918.

(16) Kim, J.; Cho, S. H. *ACS Catal.* **2019**, *9*, 230.

(17) Joannou, M. V.; Moyer, B. S.; Meek, S. J. *J. Am. Chem. Soc.* **2015**, *137*, 6176.

(18) Murray, S. A.; Green, J. C.; Tailor, S. B.; Meek, S. J. *Angew. Chem., Int. Ed.* **2016**, *55*, 9065.

(19) Park, J.; Lee, Y.; Kim, J.; Cho, S. H. *Org. Lett.* **2016**, *18*, 1210.

(20) Kim, J.; Ko, K.; Cho, S. H. *Angew. Chem., Int. Ed.* **2017**, *56*, 11584.

(21) Kim, J.; Hwang, C.; Kim, Y.; Cho, S. H. *Org. Process Res. Dev.* **2019**, *23*, 1663.

(22) Kim, J.; Shin, M.; Cho, S. H. *ACS Catal.* **2019**, *9*, 8503.

- (23) Zhou, Y.; Xiong, T.; Zhou, L. Y.; Li, H. Y.; Xiao, Y. C.; Chen, F. E. *Org. Lett.* **2022**, *24*, 791.
- (24) Jang, W. J.; Yun, J. *Angew. Chem., Int. Ed.* **2019**, *58*, 18131.
- (25) Kim, C.; Roh, B.; Lee, H. G. *Chem. Sci.* **2021**, *12*, 3668.
- (26) Shi, Y.; Hoveyda, A. H. *Angew. Chem., Int. Ed.* **2016**, *55*, 3455.
- (27) Zhan, M.; Li, R. Z.; Mou, Z. D.; Cao, C. G.; Liu, J.; Chen, Y. W.; Niu, D. W. *ACS Catal.* **2016**, *6*, 3381.
- (28) Kim, M.; Park, B.; Shin, M.; Kim, S.; Kim, J.; Baik, M.; Cho, S. H. *J. Am. Chem. Soc.* **2021**, *143*, 1069.
- (29) Green, J. C.; Zanghi, J. M.; Meek, S. J. *J. Am. Chem. Soc.* **2020**, *142*, 1704.
- (30) Zanghi, J. M.; Meek, S. J. *Angew. Chem., Int. Ed.* **2020**, *59*, 8451.
- (31) Wheatley, E.; Zanghi, J. M.; Meek, S. J. *Org. Lett.* **2020**, *22*, 9269.
- (32) Wheatley, E.; Zanghi, J. M.; Mason, M. M.; Meek, S. J. *Angew. Chem., Int. Ed.* **2023**, *62*, e202215855.
- (33) Liang, M. Z.; Meek, S. J. *J. Am. Chem. Soc.* **2020**, *142*, 9925.

CHAPTER 3

Asymmetric Conjugated Addition of *gem*-Diborylalkanes to α,β -unsaturated enones

This chapter has been adapted with permission from:

Kim, C.[‡]; **Roh, B.**[‡]; Lee, H. G*. *Chem. Sci.* **2021**, *12*, 3668–3673.

© 2021 The Royal Society of Chemistry

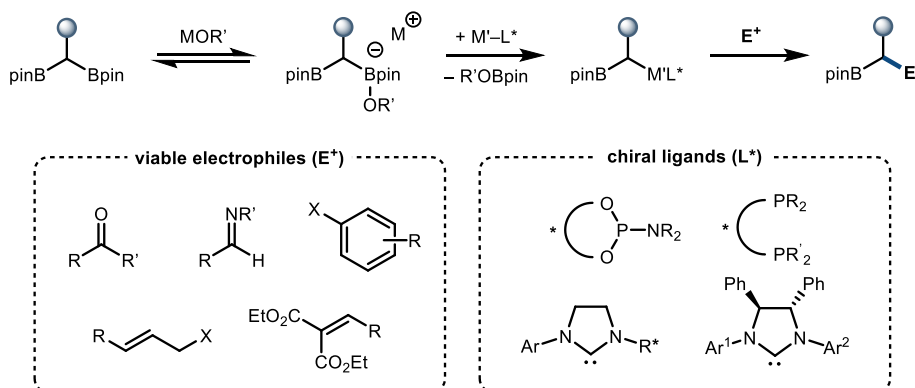
3.1. Introduction

As previously stated in Chapter 2, 1,1-diborylalkanes have been widely utilized as versatile intermediate for construction of value and complexity-added chiral boronates in various asymmetric methods. The deborylative process, which is one of two activation modes for 1,1-diborylalkanes are initiated by the activation of a C–B bond through the action of oxygen-based nucleophiles (Scheme 3.1A). Subsequent transmetalation to the transition metal catalyst, such as Pd, Cu, or Ir, generates an organometallic species that can react with a variety of electrophilic counterparts, enabling the formation of stereochemically enriched alkylboronate products, a class of compounds that can be diversely functionalized.

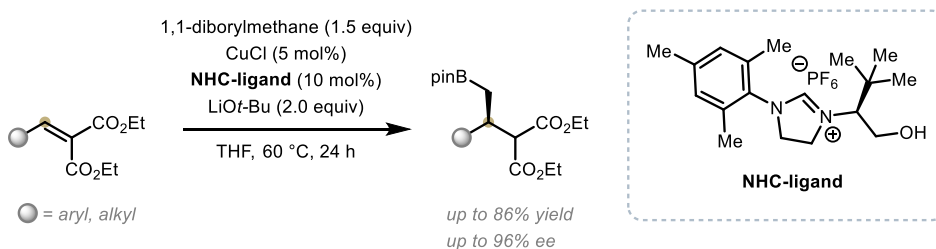
Despite the recent advancement, the reactivity of 1,1-diborylalkanes have been mostly limited to nucleophilic addition to carbonyl functional groups. At this point, our focus was to extend the unique properties of 1,1-diborylalkanes to asymmetric version of 1,4-addition reactions, enabling the synthesis of diverse and valuable chiral alkylboronates. While exploring the optimal conditions for the asymmetric conjugate addition of *gem*-diborylalkanes, Yun and Jang presented pioneering work that is the first example of 1,4-addition of 1,1-diborylmethanes, resulting in an addition product with excellent yield and stereoselectivity (Scheme 3.1B).¹ Of note, they utilized a well-designed chiral NHC ligand, impeding the undesirable background reactions. Under the presented novel protocol, various α,β -

unsaturated diesters participated in the reaction, providing the desired chiral boronates, but a monoester was unreactive, not enabling the formation of the products.

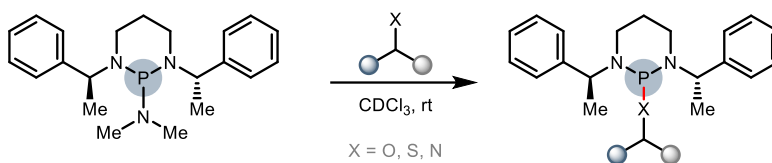
A. Deborylative activation of 1,1-diborylalkanes



B. Pioneering work - asymmetric conjugate addition (Yun and Jang)



C. Vulnerability of phosphoramidite ligand with various nucleophiles (Feringa)



Scheme 3.1. Stereoselective reactions with 1,1-diborylalkanes

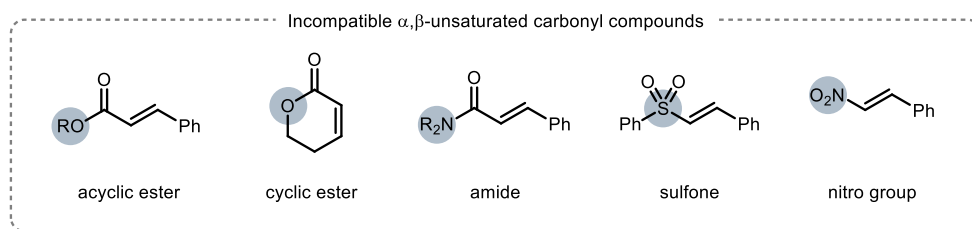
We then envisioned the possibility of expanding to less reactive α,β -unsaturated enones and then, herein, we disclosed the underdeveloped Cu-catalysed conjugate addition with 1,1-diborylmethane to an α,β -unsaturated

ketone substrate. Notably, the reaction conditions revealed insufficient reactivities in reactions involving 1,1-diborylalkanes using transition metal-phosphoramidite complexes. In fact, over the course of the reaction, the involvement of chiral ligands, including bidentate phosphines,² N-heterocyclic carbenes,^{1,3} and most commonly phosphoramidites,^{4a-4c} have been played a critical role in terms of stereochemical induction. However, in view of the documented susceptibility of phosphoramidite ligands to hydroxide or alkoxide nucleophiles,⁵ it has been recognized that an undesirable ligand degradation pathway may be involved in reactions with phosphoramidite supporting ligands, especially if the reaction outcome is suboptimal (Scheme 3.1C). Based on these observations, we conducted a more in-depth examination of the degradation pathway of the phosphoramidate by utilizing heteroatom-based NMR spectroscopy, and evaluated the feasibility of the reactions.

3.2. Results and Discussion

3.2.1. Optimization of the Protocol

A variety of α,β -unsaturated carbonyl groups were tested for asymmetric conjugate addition of 1,1-diborylalkanes. Most of the α,β -unsaturated carbonyl groups – such as α,β -unsaturated monoester, amide and cyclic enones – were not reactive and only acyclic α,β -unsaturated enones were compatible with the reaction conditions (Scheme 3.2).



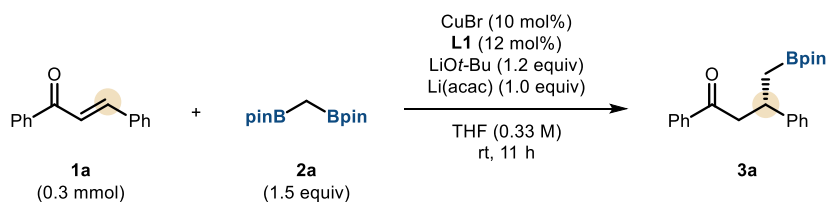
Scheme 3.2. Evaluation of electrophilic coupling partners

In this context, the catalyst system was initially investigated using trans-chalcone as the model substrate with various chiral ligands (Table 3.1). The stereoselective conjugate addition reaction were conducted with 1,1-diborylmethane as pronucleophile by employing a Cu(I) source, a chiral supporting ligand, and LiOt-Bu which triggers C–B bond cleavage. Among the evaluated chiral ligands, those with a phosphoramidite backbone exhibited the highest reactivity, with concomitant formation of the boron-Wittig product, which accounts for the remainder of the reactivity (Table 3.1, entries 2–6). (*S*)-MonoPhos (**L1**) showed the most promising results in terms of product formation and stereinduction, although not reaching synthetically

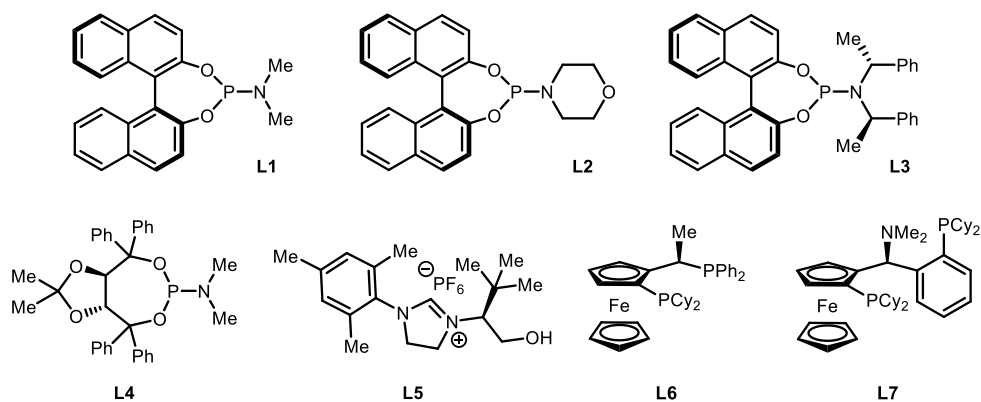
ideal level (Table 3.1, entry 2). Other catalytic systems based on different chiral ligands exhibited lower conversion levels (Table 3.1, entries 7–9) and/or underwent competitive boron-Wittig reactions.⁶ The approach of using a large excess of ligand, which is commonly employed to enhance ligand ligation, did not significantly improve reactivity to a practically useful level (Table 3.1, entry 3).

During the exploration for more reactive conditions, the addition of Li(acac) to the reaction mixture proved to be highly beneficial, resulting in improved product formation and enantiomeric excess (Table 3.2, entry 1).⁷ Further investigations with different catalyst loadings revealed that the optimal performance was achieved at a catalyst loading of 10 mol%. (Table 3.2, entries 2–3). However, the use of other lithium salts, acetylacetonate derivatives, or Lewis acidic entities did not show similarly effective results (Table 3.2, entries 4–12).⁸ The best catalytic system was ultimately determined to be the (*S*)-MonoPhos-based catalytic protocol with the Li(acac) additive.

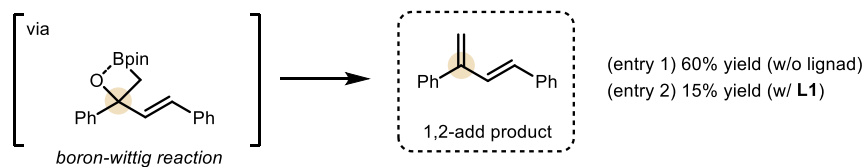
Table 3.1. Evaluation of the supporting ligands



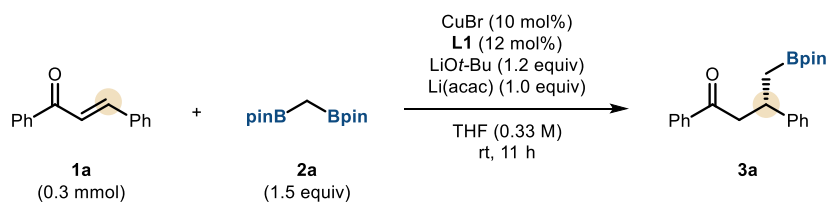
entry ^a	ligand	additive	conversion	yield (%) ^b	ee (%) ^c
1	-	-	>99	20	-
2	L1 (12 mol%)	-	>99	63	76
3	L1 (24 mol%)	-	>99	68	79
4	L2	-	>99	40	55
5	L3	-	74	19	6
6	L4	-	98	40	4
7	L5	-	<5	<5	-
8	L6	-	28	<5	-
9	L7	-	29	<5	-



----- Commonly observed undesirable 1,2-addition product -----



^a**Reaction conditions:** CuBr (10 mol%), ligand (12 mol%), LiOt-Bu (1.2 equiv), additive (1.0 equiv), **2a** (1.5 equiv), and **1a** (0.3 mmol, 0.33 M) in THF (0.9 mL). ^bDetermined by GC analysis with *n*-dodecane as an internal standard. ^cDetermined by HPLC analysis.

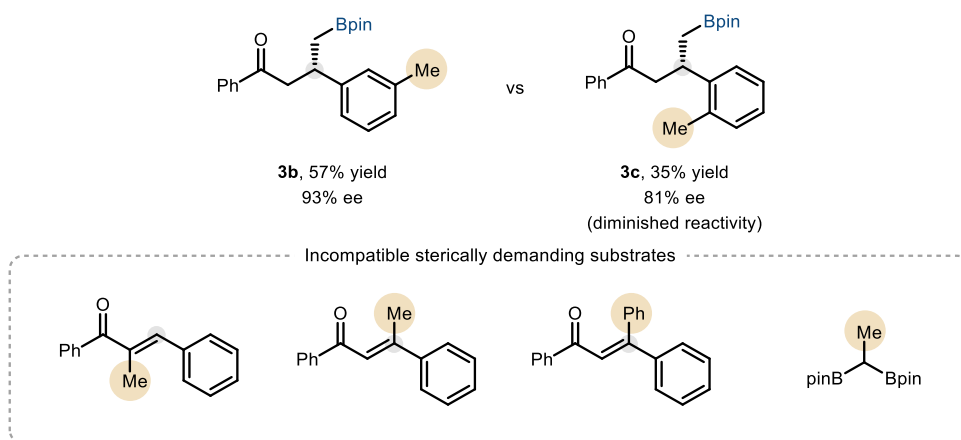
Table 3.2. Evaluation of the additives

entry ^a	ligand	additive	conversion	yield (%) ^b	ee (%) ^c
1	L1	Li(acac)	>99	70	92
2 ^d	L1	Li(acac)	>99	62	86
3 ^e	L1	Li(acac)	>99	53	83
4	L1	LiF	81	76	77
5	L1	LiCl	30	29	<5
6	L1	LiBr	28	28	<5
7	L1	LiClO ₄	<5	<5	-
8	L1	Li(TMHD)	44	35	<5
9	L1	Na(hfacH)	32	13	70
10	L1	TMSCl	36	24	7
11	L1	BF ₃ OEt ₂	<5	<5	-
12	L1	ZnBr	<5	<5	-

^aReaction conditions: CuBr (10 mol%), ligand (12 mol%), LiOt-Bu (1.2 equiv), additive (1.0 equiv), **2a** (1.5 equiv), and **1a** (0.3 mmol, 0.33 M) in THF (0.9 mL). ^bDetermined by GC analysis with *n*-dodecane as an internal standard. ^cDetermined by HPLC analysis. ^d5 mol% of CuBr and 6 mol% of L1 were used. ^e2.5 mol% of CuBr and 3 mol% of L1 were used. acac = acetylacetonate, TMHD = 2,2,6,6-tetramethyl-3,5-heptanedione, hfacH = hexafluoroacetylacetonate.

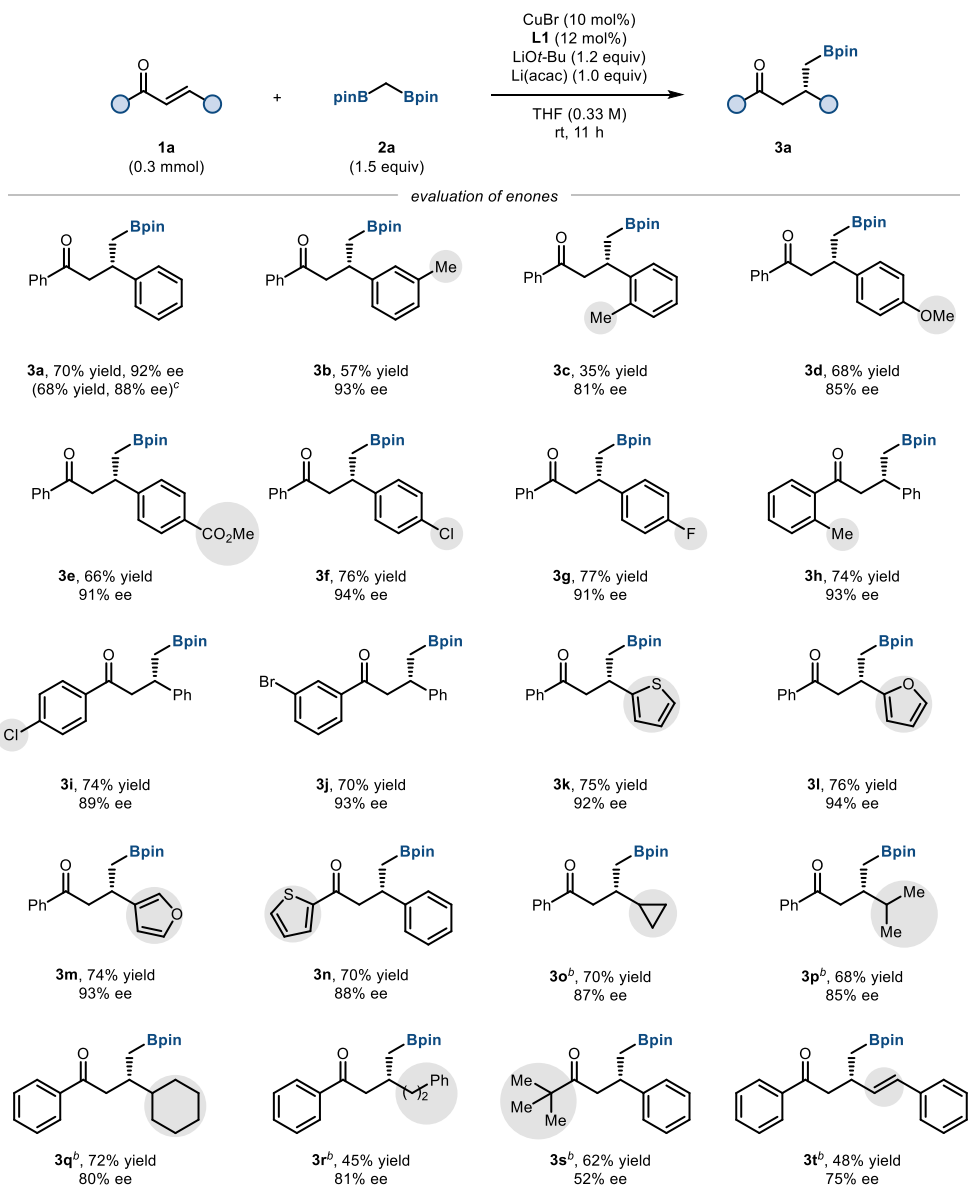
3.2.2. Applicability of the Protocol

With the optimized conditions, various α,β -unsaturated enone substrates were subjected to the reaction conditions for exploring the range of the developed reaction (Table 3.3). Reactions with chalcone derivatives with electron-donating or electron-withdrawing substituents on the arene ring at the β position of the enones resulted in the desired chiral boronic esters with great yield and enantioselectivity (**3a–3g**). However, when an ortho substituent was present on the arene, the yield substantially decreased (**3c**). In fact, the reaction utilizing other sterically demanding electrophiles and nucleophiles was also not compatible under the reaction conditions (Scheme 3.3). This implies that the steric hindrance of the substrates critically affected the efficiency of the protocol.



Scheme 3.3. Evaluations of sterically encumbered substrates

Table 3.3. Enantioselective conjugate addition 1,1-diborylmethane to α,β -unsaturated enones

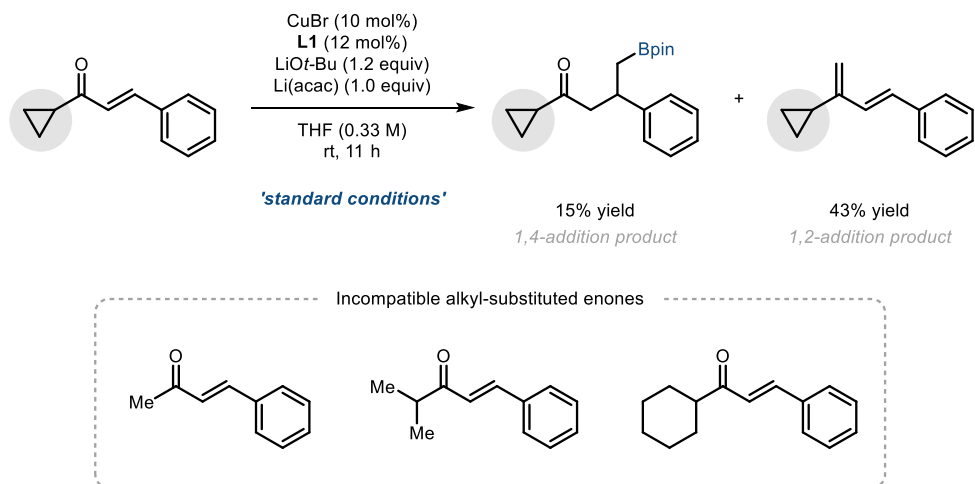


^aReaction conditions: **1a** (0.3 mmol), **2a** (1.5 equiv), CuBr (10 mol%), **L1** (12 mol%), LiOt-Bu (1.2 equiv), and Li(acac) (1.0 equiv) in THF (0.9 mL), rt, 11 h, under nitrogen. ^bThe reaction was conducted for 36 h. ^cThe reaction was carried out on a 3 mmol scale.

Notably, the efficiency of the reaction remained consistent even when conducted on a larger scale, demonstrating its robustness (**3a**). Variations on the phenyl ring directly attached to the carbonyl group were also well-tolerated (**3h–3j**). Importantly, the presence of halogen substituents, which can be utilized for further functionalization such as cross-coupling reactions, did not impact the outcome of the conjugate addition reaction (**3f, 3g, 3i, 3j**). Furthermore, biologically significant heterocycles like furan or thiofuran could be successfully incorporated into the substrate structure (**3k–3n**). In addition, the reactivity extended to alkyl-substituted α,β -unsaturated enones. The optimized conditions smoothly operated with a diverse array of alkyl groups introduced at the β -position of the enone substrate (**3o–3r**). However, the presence of an alkyl group at the carbonyl carbon significantly reduced the efficiency of product formation due to competitive 1,2-addition reactions. Only the substrate containing a bulky *tert*-butyl group proved viable for the conjugate addition (**3s**). Finally, an enone with an extended π -system produced the desired 1,4-addition products (**3t**). Of note, no side product resulting from competing 1,6-addition was observed.

As mentioned earlier, the reaction with enones bearing an alkyl group adjacent to the carbonyl exhibited lower reactivity and stereoselectivity. Therefore, at this point, we proceeded to vary the reaction parameters further to enhance the reactivity utilizing enones bearing cyclopropyl group as model substrates. However, we did not observe a significant improvement in

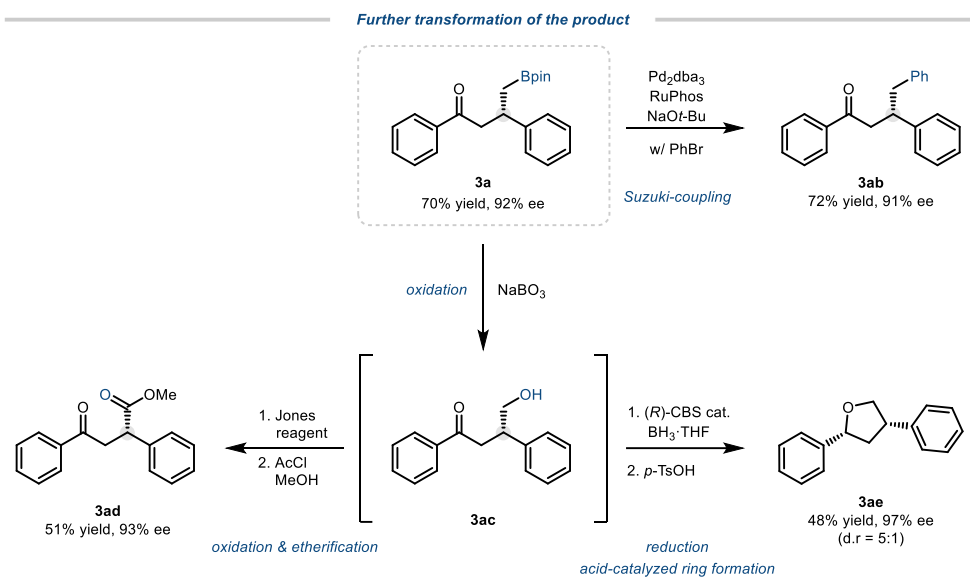
reactivity despite these efforts. Under the standard reaction conditions, unproductive 1,3-diene generated through sequence of 1,2-addition and boron-Wittig reaction was formed as major product (Scheme 3.4).



Scheme 3.4. Competitive 1,2-addition pathway with alkyl-substituted enones

Next, the synthetic versatility of the developed reaction was demonstrated using the stereochemically enriched γ -ketoboronic ester product **3a** as crucial intermediate. (Scheme 3.4). Employing the Suzuki-Miyaura cross-coupling reaction of (*S*)-**3a** and bromobenzene, the corresponding γ -phenyl ketone product was obtained with a 72% yield (**3ab**).⁹ During this C–C bond-forming process, the stereogenic center remained unaffected, maintaining its stereochemical integrity. Additionally, the C–B bond of (*S*)-**3a** could be easily oxidized in the presence of $\text{NaBO}_3 \cdot 4\text{H}_2\text{O}$, affording a γ -hydroxy ketone (**3ac**), which could be further functionalized to produce more complex products. A two-step sequence involving Jones oxidation and Fisher esterification

resulted in the corresponding methyl ester with an overall yield of 51% (**3ad**). Alternatively, by subjecting the carbonyl group to enantioselective reduction using the (*R*)-oxazaborolidine catalyst,¹⁰ followed by stereospecific benzylic displacement,¹¹ the enantiomeric form of the marine natural product calyxolane B was synthesized (**3ae**).¹²



Scheme 3.5. Transformation of the chiral products **3a**

3.2.3. NMR Investigations

To better understand the factors that contribute to the successful catalytic system containing Li(acac), catalytically relevant species were prepared and examined using ^{31}P and ^{11}B NMR experiments. First of all, when all the reaction components, including Li(acac), were introduced in the absence of the enone substrate, the potentially active nucleophilic species and ligand were observed at 113.4 ppm (Scheme 3.1F). Based on the observed reactivity towards the enone substrates and ^{31}P NMR analysis, the structure of the reactive species was assigned to be the ligand-bound alkyl copper complex.^{13,14} In addition to catalytically active species, the uncoordinated ligand L1 was the only significant species that was detected at 149.5 ppm (Scheme 3.1A and F). On the other hand, in the case of an identical mixture that did not contain Li(acac), no free ligand was observed (Scheme 3.1E). More importantly, the relative mass balance of active species diminished significantly. Instead, unidentified chemical species were found (137–147 ppm), indicating decomposition of catalytically responsible species based on L1 (*vide infra*).¹⁵

Subsequently, we conducted in-situ monitoring of the reaction mixture both with and without Li(acac) over 70 minutes for evaluation of the role of Li(acac) in the reaction mixture (Figure 3.1 and 3.2). Under the reaction conditions in the presence of Li(acac), only two resonance peak indicating ligands and catalytically active species respectively were detected over times.

However, interestingly, when monitoring the reaction without Li (acac), the region of new resonance, as shown in Figure 3.1E, gradually increased. The observed new resonance peak (137–147 ppm) were consistent with the chemical species derived from the reaction between ligand and alkoxide base (Figure 3.1B and Figure 3.2B). These results implied that Li(acac) could suppress the decomposition of the ligand under the reaction conditions.

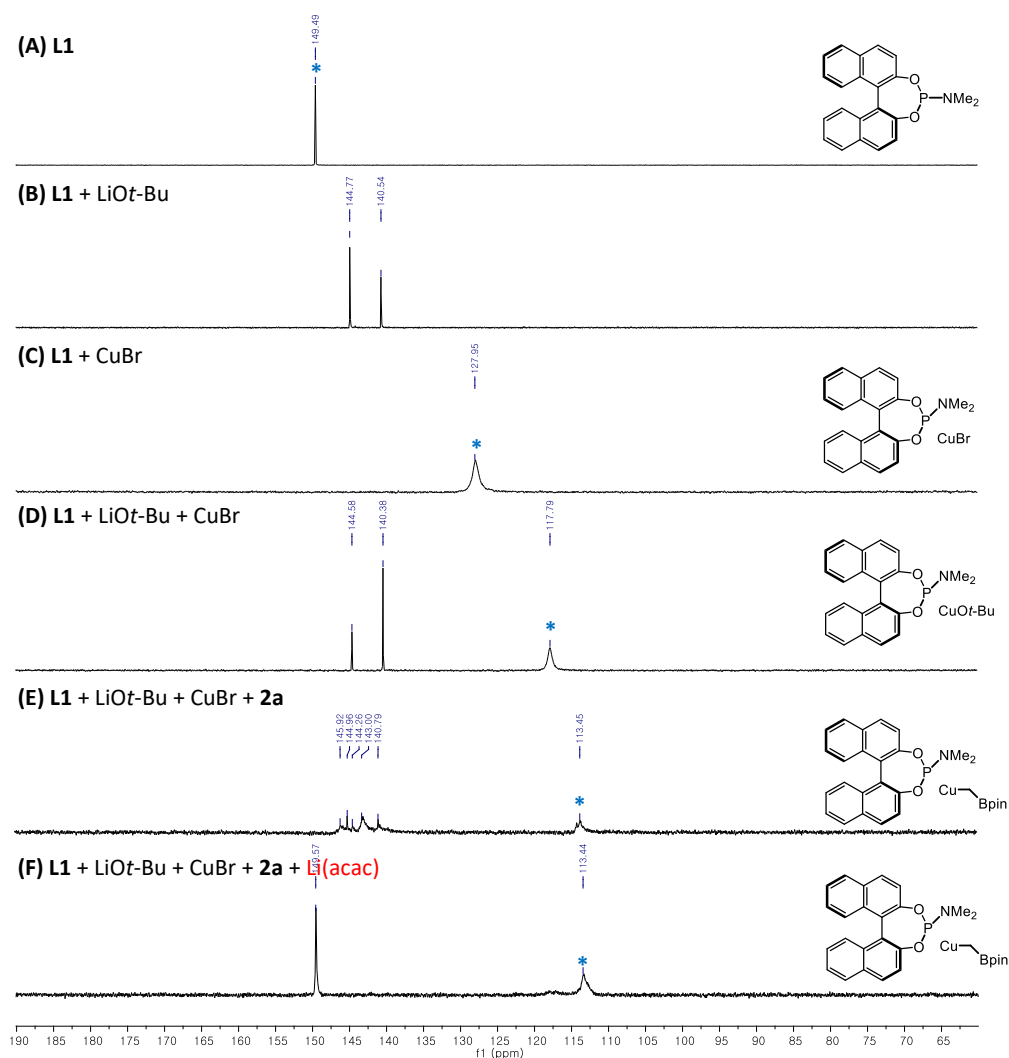


Figure 3.1. ^{31}P NMR spectra (162 MHz, THF- d_8 , rt) of the reaction mixture

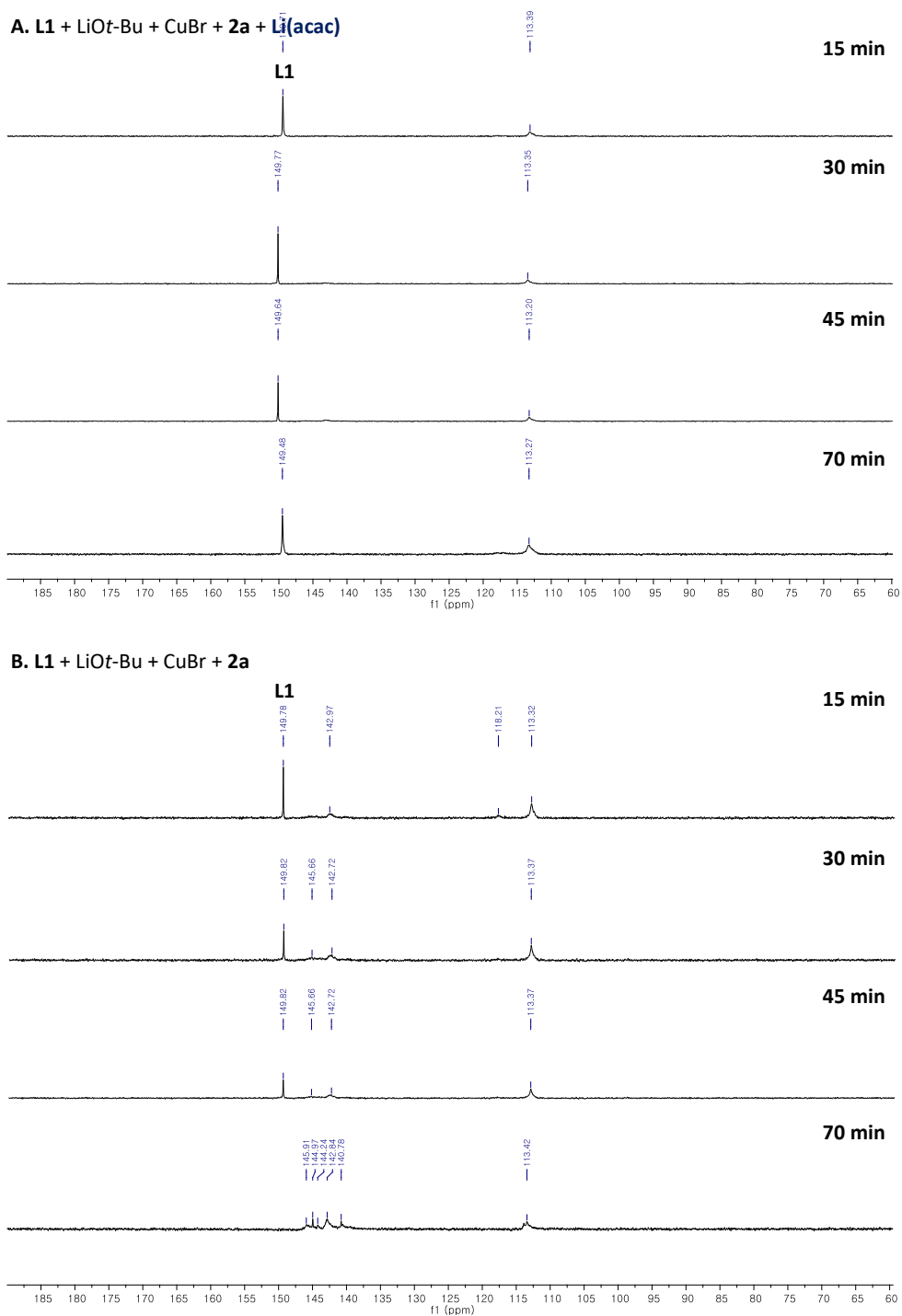
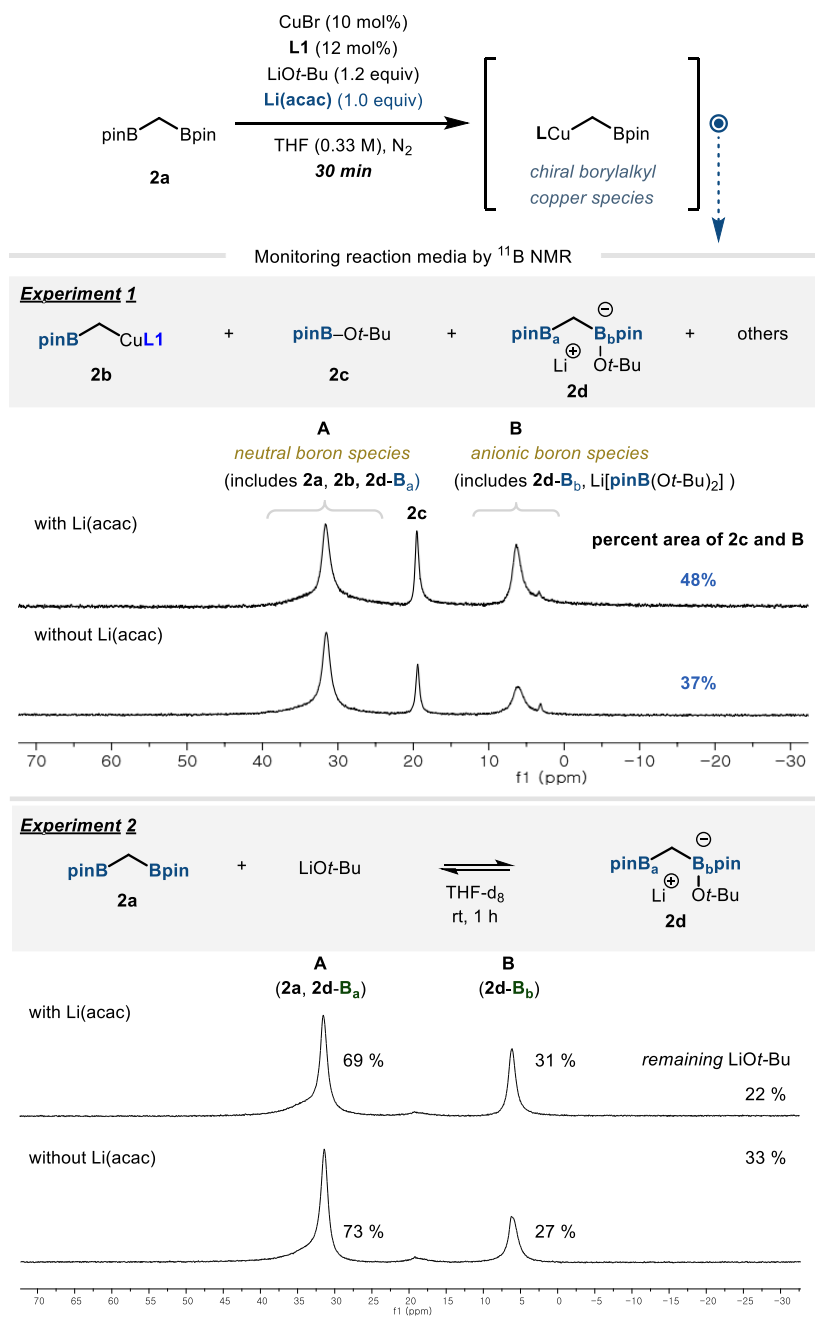


Figure 3.2. Monitoring of ligand decomposition over time by ^{31}P NMR spectroscopies

Next, the origin of the observed catalyst decomposition could be deduced using ^{11}B NMR studies (Figure 3.3, Experiment 1). The ^{11}B NMR spectra of the reaction mixture consists of three major signals originating from C-ligated neutral Bpin species, including **2a**, **2b**, and **2d-B_a** (A), heteroatom-bound neutral Bpin species (**2c**), and anionic complexes, such as **2d-B_b** or $\text{Li}[\text{pinB}(\text{O}t\text{-Bu})_2]$ (B).¹⁶ Complete quantitative analysis of all relevant species was difficult to perform because of the complexity of the system. It is evident, however, that the application of $\text{Li}(\text{acac})$ drove the equilibrium in the direction of increasing the amount of **2c** and **B**. Since the formation of **2c** and **B** stems from the coordination of the alkoxide at the boron centre, the result indicates an escalated level of the entrapped alkoxide nucleophile in the reaction mixture. Eventually, a reduced amount of alkoxide is available for ligand degradation to enhance the catalytic activity of the system.

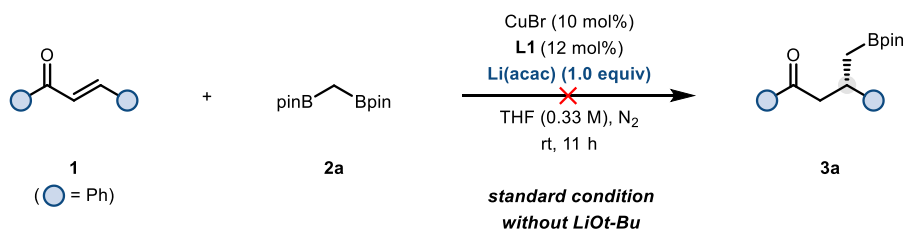
The impact of added $\text{Li}(\text{acac})$ was further investigated in a more controlled experiment in which **2a** was independently exposed to the $\text{LiO}t\text{-Bu}$ nucleophile (Figure 3.3, Experiment 2). The addition of $\text{Li}(\text{acac})$ shifted the equilibrium to the direction of the ate-complex formation (**2d**). During the reaction, a significant portion of the initially administered $\text{LiO}t\text{-Bu}$ nucleophiles was consumed: in the case of the $\text{Li}(\text{acac})$ -free conditions the effective concentration of $\text{LiO}t\text{-Bu}$ is 50% higher than that of the conditions with $\text{Li}(\text{acac})$.¹⁷

Figure 3.3. Monitoring the reaction mixture by ^{11}B NMR

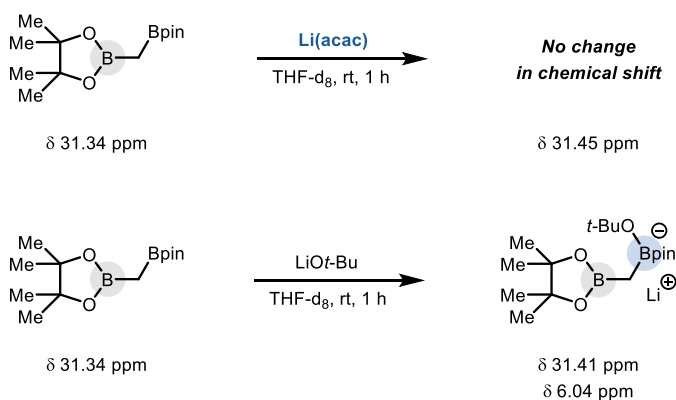


Reaction conditions: (Exp1) (a) L1 (1.0 equiv, 0.012 mmol), CuBr (0.83 equiv), **2a** (12.5 equiv), LiOt-Bu (10 equiv), and Li(acac) (8.3 equiv) in THF- d_8 (0.5 mL). **(Exp 2)** (a) **2a** (1.25 equiv, 0.15 mmol), LiOt-Bu (1.0 equiv), and Li(acac) (0.83 equiv) in THF- d_8 (0.5 mL).

A. Control experiments without LiOt-Bu



B. Li(acac) as activator for 2a



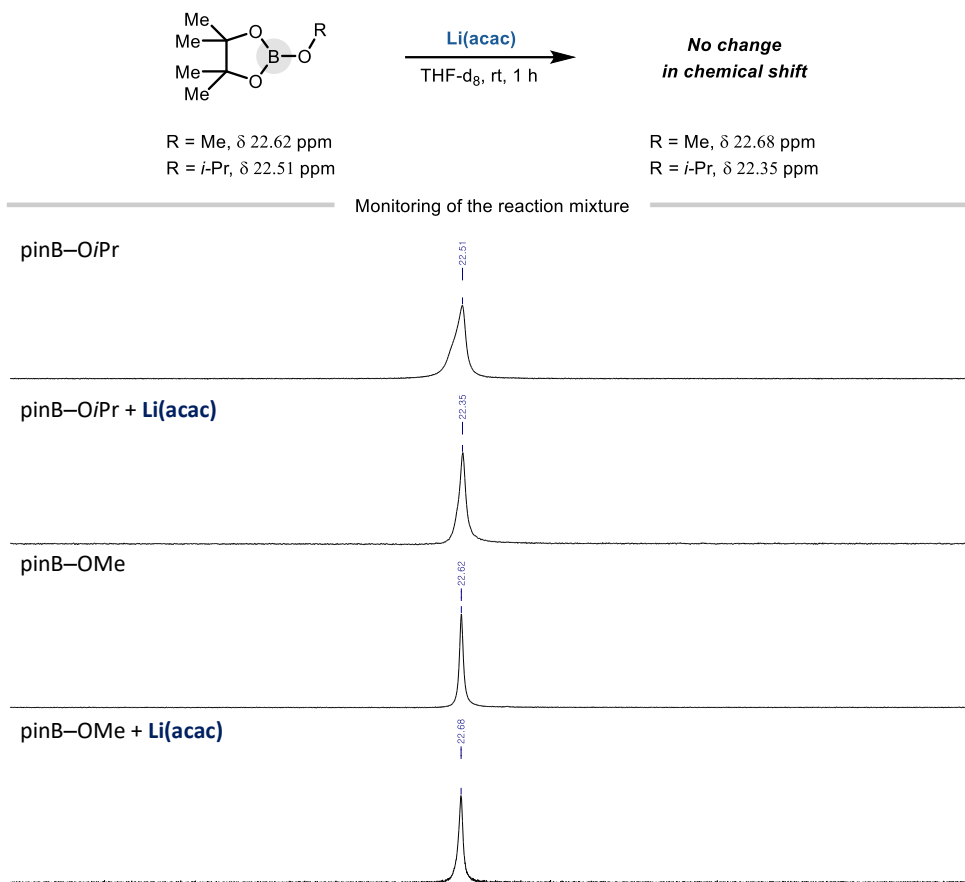
Scheme 3.6. Viability of Li(acac) as a better activator than LiOt-Bu

A series of NMR investigations demonstrated that Li(acac) acts as a promoter, facilitating the equilibrium conversion of 1,1-diborylalkanes into ate-complexes by consuming a larger amount of alkoxide base under the reaction conditions. However, it was unable to to exclude the possibility that Li(acac) might serve as a better activator of the boronic ester or that the acetylacetonate ligand could sequester the borate by-product. To test the viability of Li(acac) being a better activator for 1,1-diborylmethane (**2a**) than LiOt-Bu, a catalytic reaction was set up in the absence of Li(acac) (Scheme 3.6A). As expected, the desired reactivity was not observed at all: **1a** remained unconsumed and no addition product was observed. In addition, **2a**

was separately exposed to a stoichiometric amount of Li(acac) and monitored with ^{11}B NMR spectroscopy to better understand the interaction of Li(acac) with **2a** (Scheme 3.6B). Again, no change in chemical shift was observed suggesting a direct interaction is not taking place (δ 31.45 ppm). Overall, the possibility of Li(acac) to better activate **2a** than LiO*t*-Bu was set aside.

The other possibility of Li(acac) sequestering borate by-products, such as pinBO*t*-Bu (**2c**) or species “B”, to facilitate the overall process was also examined by ^{11}B -NMR experiments (Scheme 3.7). Since **2c** was not an easily accessible reagent, relevant experiments were carried out with commercially available pinBOMe and pinBO*i*-Pr, which should be even more reactive than **2c**. Both pinBOMe and pinBO*i*-Pr exhibited virtually no change in chemical shifts when treated with Li(acac) (δ 22.35 ppm and δ 22.68 ppm, respectively). Therefore, it was concluded that Li(acac), despite being a bidentate ligand, is not capable of scavenging a borate by-product. Combined, it is concluded that a more active form of participation is not operating for Li(acac).

Possibility of Li(acac) sequestering borate by-product

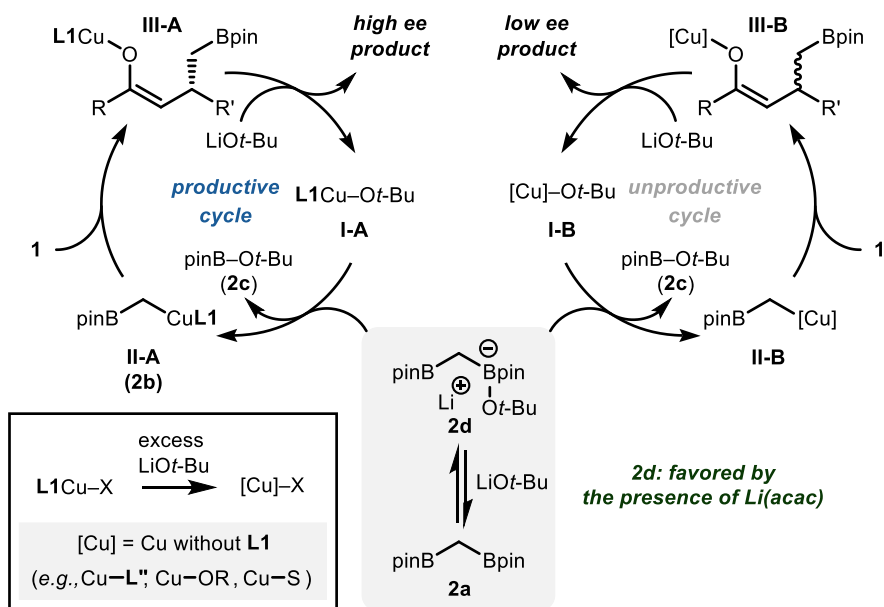


Scheme 3.7. Possibility of Li(acac) sequestering borate by-products

3.2.4. Proposed Mechanism

Based on these observations, a mechanistic scenario that consists of two independent catalytic cycles is presented (Figure 3.4). In the productive cycle, the active catalyst **I-A**, which is generated by the combination of **L1**, CuBr, and LiOt-Bu, undergoes transmetalation with **2a** to generate a copper alkyl species **II-A** (Figure 3.3, **2b**). The reactive carbon-based nucleophile should undergo an enantioselective conjugate addition reaction with enone substrate **1** to provide a copper enolate intermediate **III-A**, an immediate precursor of the desired product with high stereochemical integrity. During the operation of the major catalytic cycle, **2a** should be in equilibrium with its ate-complex form **2d**, a species responsible for the rate-determining transmetalation, by the involvement of LiOt-Bu.¹⁸ Ultimately, the equilibrium controls the amount of the alkoxide base in the reaction mixture that is available to destroy active catalytic species. The process includes the irreversible modification of the phosphoramidite ligand **L1**, which contributes to furnishing catalytically incompetent species ([Cu]). These species include Cu-complexes ligated with the decomposed ligand (**L''**), solvent (**S**), and/or other heteroatom-containing species present in the reaction mixture. Consequently, an alternative catalytic cycle with lower stereoselectivity operates with the intermediates **II-B** and **III-B**. As determined from the NMR experiments, the added Li(acac) controls the extent of the unproductive catalytic cycle by controlling the equilibrium of **2a**, LiOt-Bu, and **2d**.¹⁹

Figure 3.4. Plausible mechanistic scenario.



3.3. Conclusion

In conclusion, a novel reaction engineering strategy has been developed to allow for full utilisation of the catalytic activity of a transition-metal-catalysed reaction. By identifying the ligand decomposition pathway and using an additive-based restoration method, the efficiency of an underdeveloped reaction could be brought to synthetically useful levels. The method has been successfully applied to an enantioselective conjugate addition reaction with 1,1-bis[(pinacolato)boryl]methane catalysed by a Cu-phosphoramidite catalyst system. We believe that the strategy should have a broader impact on reactions catalysed by related metal-ligand complexes. It is anticipated that analogous reaction engineering systems will ultimately be implemented for transition metal catalysis in general.

3.4. References

- (1) Jang, W. J.; Yun, J. *Angew. Chem., Int. Ed.* **2019**, *58*, 18131.
- (2) Sun, C.; Potter, B.; Morken, J. P. *J. Am. Chem. Soc.* **2014**, *136*, 6534.
- (3) Shi, Y.; Hoveyda, A. H. *Angew. Chem., Int. Ed.* **2016**, *55*, 3455.
- (4) (a) Joannou, M. V.; Moyer, B. S.; Meek, S. J. *J. Am. Chem. Soc.* **2015**, *137*, 6176. (b) Murray, S. A.; Green, J. C.; Tailor, S. B.; Meek, S. J. *Angew. Chem., Int. Ed.* **2016**, *55*, 9065. (c) Zhan, M.; Li, R.-Z.; Mou, Z.-D.; Cao, C.-G.; Liu, J.; Chen, Y.-W.; Niu, D. *ACS Catal.* **2016**, *6*, 3381. (d) Kim, J. Ko, K. Cho, S. H. *Angew. Chem., Int. Ed.* **2017**, *56*, 11584. (e) Kim, J.; Shin, M.; Cho, S. H. *ACS Catal.* **2019**, *9*, 8503.
- (5) (a) Bannwarth, W.; Trzeciak, A. *Helv. Chim. Acta* **1987**, *70*, 175. (b) De Vries, K.; Feringa, B. L. *Tetrahedron Asymmetry* **1994**, *5*, 699. (c) McMurray, J. S.; Coleman IV, D. R.; Wang, W.; Campbell, M. L. *Biopolymer* **2001**, *60*, 3.
- (6) (a) Matteson, D. S.; Moody, R. J.; Jesthi, P. K. *J. Am. Chem. Soc.* **1977**, *99*, 3196. (c) Matteson, D. S.; Moody, R. J. *Organometallics* **1982**, *1*, 20. (d) Pelter, A.; Singaram, B.; Wilson, J. W. *Tetrahedron Lett.* **1983**, *24*, 635. (e) Pelter, A.; Williams, L.; Wilson, J. W. *Tetrahedron Lett.* **1983**, *24*, 627. (f) Matteson, D. S. *Tetrahedron* **1989**, *45*, 1859. (g) Pelter, A.; Drake, R.; *Tetrahedron* **1994**, *50*, 13801.
- (7) For review of additive effects in asymmetric catalysis, see: Hong, L.; Sun, W.; Yang, D.; Li, G.; Wang, R. *Chem. Rev.* **2016**, *116*, 4006.

- (8) For additive-promoted advancement of reactivity in conjugate addition, see: (a) Morikawa, S.; Yamazaki, S.; Tsukada, M.; Izuhara, S.; Morimoto, T.; Kakiuchi, K. *J. Org. Chem.* **2007**, *72*, 6459. (b) Yazaki, R.; Kumagai, N.; Shibasaki, M. *J. Am. Chem. Soc.* **2010**, *132*, 10275. (c) Jumde, R. P.; Lanza, F.; Veenstra, M. J.; Harutyunyan, S. R. *Science* **2016**, *352*, 433. (d) Rodríguez-Fernández, M.; Yan, X.; Collados, J. F.; White, P. B.; Harutyunyan, S. R. *J. Am. Chem. Soc.* **2017**, *139*, 14224.
- (9) Yang, C.-T.; Zhang, Z.-Q.; Tajuddin, H.; Wu, C.-C.; Liang, J.; Liu, J.-H.; Fu, Y.; Czyzewska, M.; Steel, P. G.; Marder, T. B.; Liu, L. *Angew. Chem., Int. Ed.* **2012**, *51*, 528.
- (10) Corey, E. J.; Helal, C. J. *Angew. Chem., Int. Ed.* **1998**, *37*, 1986.
- (11) Bunrit, A.; Srifa, P.; Rukkijakan, T.; Dahlstrand, C.; Huang, G.; Biswas, S.; Watile, R. A.; Samec, J. S. M. *ACS Catal.* **2020**, *10*, 1344.
- (12) (a) Hilt, G.; Bolze, P.; Harms, K. *Chem. Eur. J.* **2007**, *13*, 4312. (b) Liang, X.; Wei, K.; Yang, Y.-R. *Chem. Commun.* **2015**, *51*, 17471. (c) Gharpure, S. J.; Vishwakarma, D. S.; Nanda, S. K. *Org. Lett.* **2017**, *19*, 6534. (d) Zhao, F.; Li, N.; Zhang, T.; Han, Z.-Y.; Luo, S.-W.; Gong, L.-Z. *Angew. Chem., Int. Ed.* **2017**, *56*, 3247.
- (13) The assignment is based on the observed reactivity of the mixture to promote the asymmetric conjugate addition upon exposure to the enone substrate. In addition, the independent preparation of related Cu

complexes such as **L1CuBr** (^{31}P : δ 128 ppm) and **L1CuOt-Bu** (^{31}P : δ 118 ppm) supports this conclusion. See ESI for details.

- (14) At this time, we cannot rigorously rule out the possibility of **2b** existing in its multinuclear form. A related phosphoramidite-based Cu-alkyl species exhibiting such behavior has been prepared and characterized (^{31}P : δ 124 ppm). See: von Rekowski, F.; Koch, C.; Gschwind, R. M. *J. Am. Chem. Soc.* **2014**, *136*, 11389.
- (15) Some of the new species observed in this case could be generated by independently treating **L1** with LiOt-Bu. Therefore, it is believed that these species are the decomposition products of **L1** and their corresponding Cu complexes. In addition, the new species are being generated over time with concomitant consumption of **L1**. See ESI for details.
- (16) For studies associated with the identification of the borate derivatives by ^{11}B NMR, see: (a) Endo, K.; Ohkubo, T.; Shibata, T. *Org. Lett.* **2011**, *13*, 3368. (b) Joannou, M. V.; Moyer, B. S.; Goldfogel, M. J.; Meek, S. J. *Angew. Chem., Int. Ed.* **2015**, *54*, 14141. (c) Lee, B.; Chirik, P. J. *J. Am. Chem. Soc.* **2020**, *142*, 2429.
- (17) These values were quantitatively determined based on the assumption that all boron species exist as either **2a** or **2d**. For quantitative analysis based on ^{11}B NMR, see: Aguilera-Sáez, L. M.; Belmonte-Sánchez, J. R.;

Romero-González, R.; Martínez Vidal, J. L.; Arrebola, F. J.; Garrido Frenich, A.; Fernández, I. *Analyst* **2018**, *143*, 4707.

(18) Kim, M.; Park, B.; Shin, M.; Kim, S.; Kim, J.; Baik, M. H.; Cho, S. H. *J. Am. Chem. Soc.* **2021**, *143*, 1069.

(19) A more active participation of Li(acac) in the catalytic cycle, such as being an activator for **2a** or a scavenger for **2c**, was disregarded based on control experiments. See ESI for details.

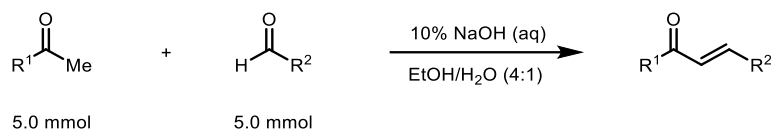
3.5. Experimental Section

3.5.1. General Information

Commercially available reagents were purchased from Sigma Aldrich, TCI, Alfa Aesar, Acros, Fluka and Strem, and used without further purification, unless otherwise noted. 1,1-bis[(pinacolato)boryl]methane and (*S*)-MonoPhos were purchased from Angene and Chemscene, respectively. Dry tetrahydrofuran (THF) was obtained by passing through an activated alumina column of solvent purification system, and further degassed by repeated sonication under house vacuum and vigorous purging with nitrogen gas. Yields represent chromatographically homogeneous product. All reactions were monitored by thin-layers chromatography (TLC) with 0.25 mm E. Merck silica gel plates (60F-254) using UV light or staining solution (potassium permanganate and *p*-anisaldehyde) for visualization. NMR spectra were recorded on an Agilent 400-MR DD2 Magnetic Resonance System, JNM-ECX 400 Spectrometer (JEOL) or/and Varian/Oxford As-500 instrument and calibrated using residual undeuterated solvent (CHCl₃ at δ 7.26 ppm for ¹H NMR and δ 77.16 ppm for ¹³C NMR) as internal reference. BF₃·OEt₂ (15% w/w in CDCl₃) and H₃PO₄ (85% w/w in H₂O) solution were used as external standards for obtaining ¹¹B and ³¹P NMR, respectively. For ¹⁹F NMR spectra, fluorobenzene was used as an external standard (−113.15 ppm). Chemical shifts (δ) are reported in parts per million (ppm). Coupling constants (*J*) are reported in hertz (Hz). For NMR spectra, multiplicities are

given as: s = singlet, d = doublet, t = triplet, q = quartet, m = multiplet, br = broad. Enantiomeric excess (ee) were determined by employing High-Performance Liquid Chromatography (HPLC) with columns containing chiral stationary phase and HPLC-grade solvent (*n*-hexane and isopropanol) as eluents. HPLC equipment was C196-E061W (Shimadzu, degassing unit: DGU-20A5R, pump : LC-20AD, auto sampler : SIL-20A, communication bus module : CBM-20A, UV/Vis detector : SPD-20A, and column oven : CTO-20A), unless otherwise noted. Optical rotations were record on JASCO P1030 polarimeter (D line of sodium vapor lamp) with a cylindrical glass cell from the same company. High resolution mass spectra (HRMS) were recorded on HRMS-ESI Q-TOF 5600 spectrometer at National Instrumentation Center for Environmental Management (NICEM) of Seoul National University.

3.5.2. General Procedure for Preparation of Enones



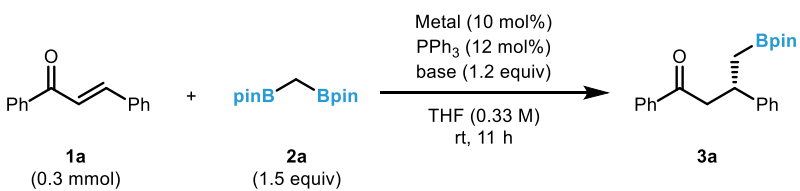
For preparation of enone substrates **2a**, **2b**, **2c**, **2d**, **2f**, **2g**, **2h**, **2i**, **2j**, **2k**, **2l**, **2m**, **2n**, **2o**, **2q**, **2s**, **2t** the following procedure was utilised.

To a 50 mL round bottom flask containing a magnetic stir bar were added the ketone (5.0 mmol), aldehyde (5.0 mmol) and 10 ml of ethanol/H₂O mixture (v/v = 4:1). The reaction mixture was vigorously stirred for 10 min. After further stirring for 5 min at 0 °C, aqueous sodium hydroxide solution (10% w/w, 5 mL) was added dropwise. The reaction system was warmed to room temperature and the progress was monitored by TLC. Upon completion of the reaction, ethanol was evaporated under reduced pressure and the remaining aqueous phase was diluted with ethyl acetate (30 mL) and saturated aqueous solution of ammonium chloride (30 mL). The aqueous phase was separated and extracted with ethyl acetate (3 × 30 mL). The combined organic phase was dried over anhydrous sodium sulfate (Na₂SO₄), filtered, and concentrated under reduced pressure. The crude product was purified by flash column chromatography on silica gel (EtOAc/hexanes).

2e¹, **2p**² and **2r**³ were prepared according to the literature procedures.

3.4.3. Evaluation on Reaction Conditions

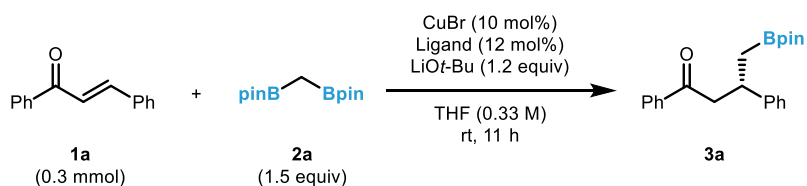
Table S3.1. Screening of metal and base


Reaction scheme showing the conversion of chalcone **1a** (0.3 mmol) to **3a** using pinacol borane **2a** (1.5 equiv). Reagents: Metal (10 mol%), PPh₃ (12 mol%), base (1.2 equiv) in THF (0.33 M) at room temperature for 11 hours.

Entry ^a	Metal	Base	Conv. (%)	Yield ^b (%)	ee (%)
1	CuBr	LiOt-Bu	>99	45	-
2	CuI	LiOt-Bu	>99	27	-
3	CuTC	LiOt-Bu	70	32	-
4	CuOAc	LiOt-Bu	65	13	-
5	CuCN	LiOt-Bu	57	25	-
6	Cu(CF ₃ -acac) ₂	LiOt-Bu	77	31	-
7	Cu(OAc) ₂	LiOt-Bu	>99	38	-
8	CuBr ₂	LiOt-Bu	>99	40	-
9	CuO	LiOt-Bu	87	<5	-
10	AgOTf	<i>n</i> -BuLi	56	15	-
11	AgOTf	NaOt-Bu	95	37	-

^aReaction conditions: Metal (10 mol%), PPh₃ (12 mol%), base (1.2 equiv), **2a** (1.5 equiv), and **1a** (0.3 mmol, 0.33 M) in THF (0.9 mL). ^bDetermined by GC analysis with n-dodecane as an internal standard. CF₃-acac = trifluoroacetylacetone.

Table S3.2. Screening of ligands



Entry ^a	Ligand	Conv. (%)	Yield ^b (%)	ee (%)
1	-	>99	20	-
2	<i>Pn</i> -Bu ₃	81	5	-
3	PPh ₃	>99	45	-
4	XPhos	>99	25	-
5	dppb	>99	22	-
6	dppe	23	<5	-
7	dppf	61	<5	-
8	<i>rac</i> -BINAP	>99	56	-
9	BBBPY	>99	21	-
10	1,10-Phenanthroline	>99	18	-
11	(1 <i>R</i> ,2 <i>R</i>)-DPEDA	61	20	-
12	(<i>S</i>)-MonoPhos	>99	63	-

^aReaction conditions: CuBr (10 mol%), ligand (12 mol%), LiOt-Bu (1.2 equiv), **2a** (1.5 equiv), and **1a** (0.3 mmol, 0.33 M) in THF (0.9 mL). ^bDetermined by GC analysis with n-dodecane as an internal standard.

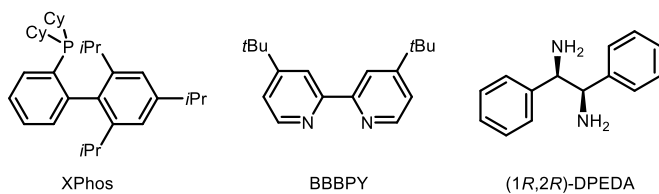
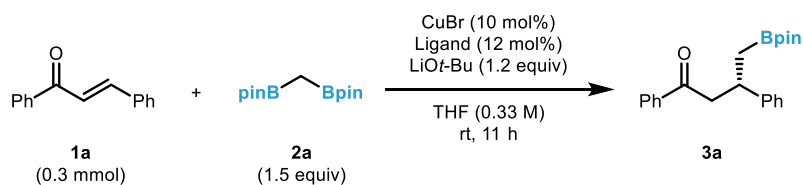
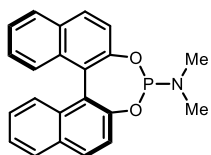


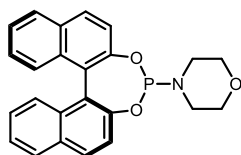
Table S3.3. Screening of chiral ligands

Entry ^a	Ligand	Conv. (%)	Yield ^b (%)	ee ^c (%)
1	L1	>99	63	76
2 ^d	L1	>99	68	79
3	L2	>99	40	55
4	L3	74	19	6
5	L4	98	40	4
6	L5	<5	trace	-
7	L6	28	trace	-
8	L7	29	trace	-
9	L8	<5	trace	-
10	L9	<5	trace	-
11	L10	<5	trace	-
12	L11	98	34	17
13	L12	>99	28	-1
14	L13	79	41	63

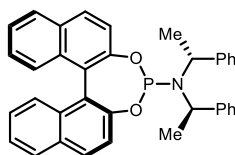
^aReaction conditions: CuBr (10 mol%), ligand (12 mol%), LiOt-Bu (1.2 equiv), **2a** (1.5 equiv), and **1a** (0.3 mmol, 0.33 M) in THF (0.9 mL). ^bDetermined by GC analysis with n-dodecane as an internal standard. ^cDetermined by HPLC analysis. ^dL1 of 24 mol% was used.



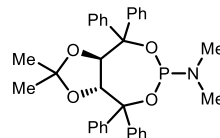
L1



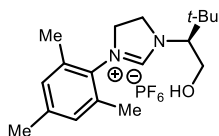
L2



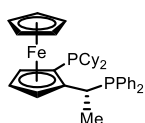
L3



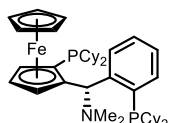
L4



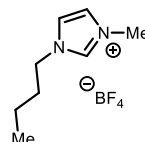
L5



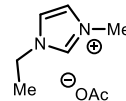
L6



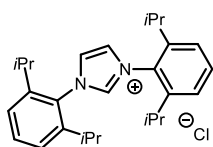
L7



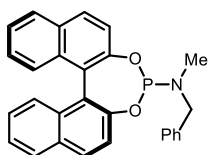
L8



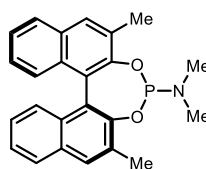
L9



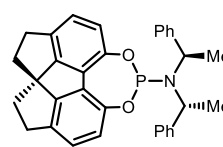
L10



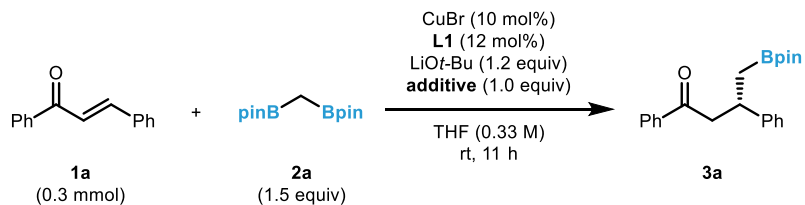
L11



L12



L13

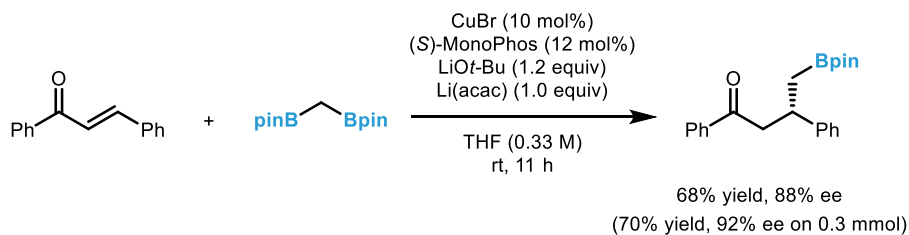
Table S3.4. Screening of additives

Entry ^a	Ligand	Additive	Conv. (%)	Yield ^b (%)	ee ^c (%)
1	-	-	>99	20	-
2	L1	-	>99	63	76
3	L1 ^d	-	>99	68	79
4	L1	Li(acac)	>99	70	92
5	L1	LiF	81	76	77
6	L1	LiCl	30	29	<5
7	L1	LiBr	28	28	<5
8	L1	LiClO ₄	<5	trace	-
9	L1	Li(TMHD)	44	35	<5
10	L1	Na(hfacH)	32	13	70
11	L1	TMSCl	36	24	7
12	L1	BF ₃ ·OEt ₂	<5	trace	-
13	L1	ZnBr ₂	<5	trace	-

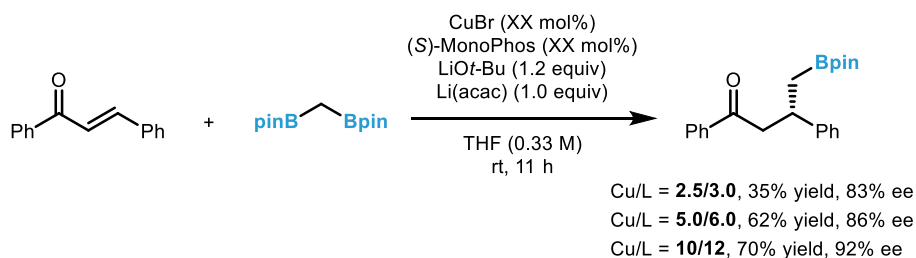
^aReaction conditions: CuBr (10 mol%), **L1** (12 mol%), LiOt-Bu (1.2 equiv), additive (1.0 equiv), **2a** (1.5 equiv), and **1a** (0.3 mmol, 0.33 M) in THF (0.9 mL). ^bDetermined by GC analysis with n-dodecane as an internal standard. ^cDetermined by HPLC analysis. ^d**L1** of 24 mol% was used. acac = acetylacetonate, TMHD = 2,2,6,6-tetramethyl-3,5-heptanedione, hfacH = hexafluoroacetylacetonate.

Scheme S3.1. Versatility of the reaction

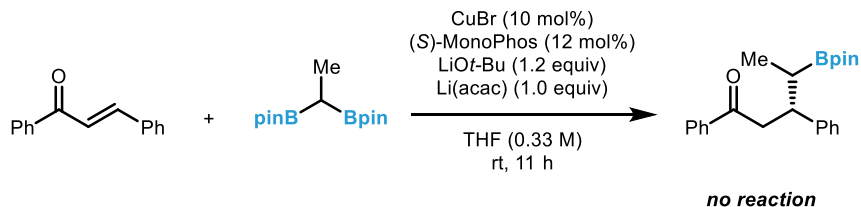
- Large scale (3.0 mmol scale)



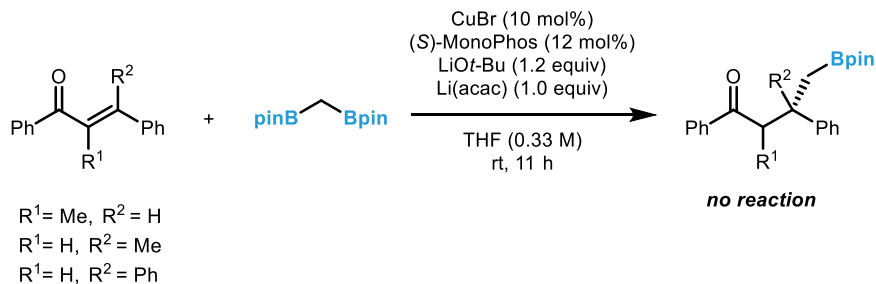
- Lower catalyst loading (0.3 mmol scale); *limited*



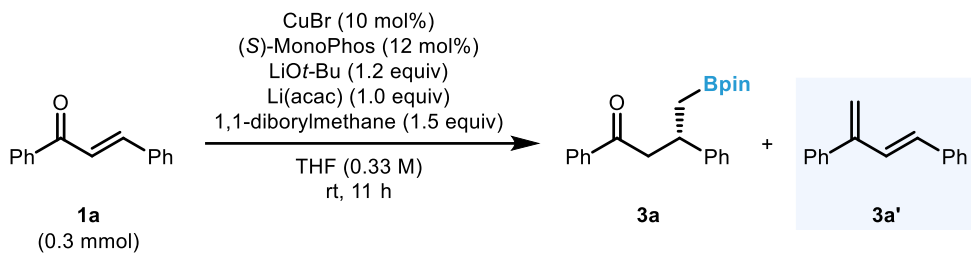
- Formation of two adjacent stereocenters (0.3 mmol scale); *limited*



- Sterically encumbered electrophile (0.3 mmol scale); *limited*



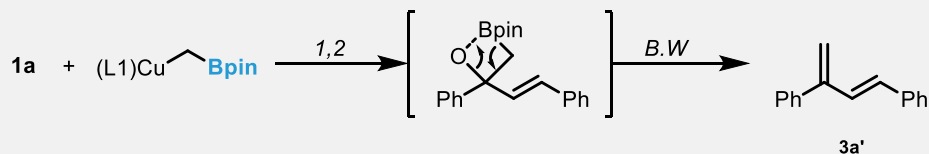
Scheme S3.2. Quantitative analysis of the side product.



Entry ^a	Ligand	Additive	Conv. (%)	3a ^b (%)	3a' ^c (%)	ee ^d (%)
1	-	-	>99	20	60	-
2	(S)-MonoPhos	-	>99	63	15	76
10	(S)-MonoPhos	Li(acac)	>99	70	18	92

^aReaction conditions: CuBr (10 mol%), ligand (12 mol%), LiOt-Bu (1.2 equiv), Li(acac) (1.0 equiv), 1,1-diborylmethane (1.5 equiv), and **1a** (0.3 mmol, 0.33 M) in THF (0.9 mL). ^{b,c}Determined by NMR with 1,1,2,2-tetrachloroethane as an internal standard. ^dDetermined by HPLC analysis. acac = acetylacetonate.

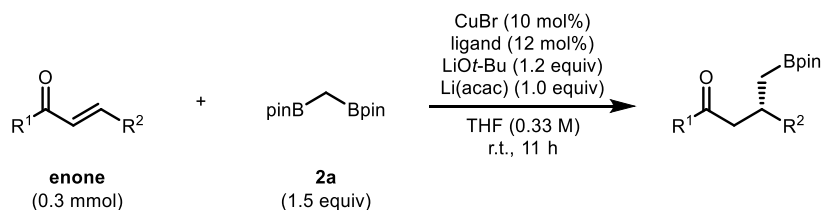
[Plausible mechanism]



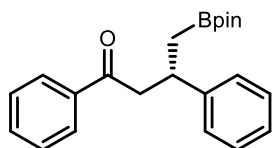
1,2 : 1,2-addition

B.W : Boron-Wittig reaction

3.5.4. General Procedure for Enantioselective Conjugate Addition



In a nitrogen-filled glove box, an oven-dried 4 mL dram-vial was charged with a magnetic stir bar, CuBr (0.030 mmol, 10 mol%, 4.2 mg), (*S*)-MonoPhos (0.036 mmol, 12 mol%, 9.6 mg), LiO*t*-Bu (0.36 mmol, 1.2 equiv, 28.8 mg), 1,1-bis[(pinacolato)boryl]methane (**2**, 0.45 mmol, 1.5 equiv, 120.6 mg), and Li(acac) (0.30 mmol, 1.0 equiv, 31.8 mg). Subsequently, THF (0.6 mL) was added to the mixture via a syringe and the system was sealed with an open-top teflon faced screw cap. The vial was removed from the glovebox and the reaction mixture was vigorously stirred for one hour. To the system was added a solution of enone (0.3 mmol) in 0.3 mL of THF via a syringe. Then, the reaction mixture was vigorously stirred at room temperature for 11 hours. Upon completion of the reaction, brine (20 mL) was added in one portion to quench the reaction. The aqueous phase was separated and extracted with ethyl acetate (3 × 20 mL). The combined organic phase was dried over anhydrous sodium sulfate (Na₂SO₄), filtered, and concentrated under reduced pressure. The crude product was purified by flash column chromatography on silica gel (EtOAc/hexanes). For the preparation of racemic samples, triphenylphosphine (12 mol%) or a mixture of (*R*)-MonoPhos (6 mol%) and (*S*)-MonoPhos (6 mol%) was used.



(S)-1,3-diphenyl-4-(4,4,5,5-tetramethyl-1,3,2-dioxaborolan-2-yl)butan-1-one (3a) Following general procedure, the crude product was purified by silica gel chromatography (hexanes : DCM = 100 : 0 → 5 : 95) to provide **3a** as a yellowish liquid (74 mg, 70%, 92% ee). An identical reaction was performed on a 3 mmol scale to provide similar results (714 mg, 68% yield, 88% ee).

¹H NMR (400 MHz, CDCl₃) δ 7.92 (m, 2H), 7.55–7.48 (m, 1H), 7.46–7.37 (m, 2H), 7.31–7.20 (m, 4H), 7.18–7.10 (m, 1H), 3.62 (m, *J* = 1H), 3.32 (dd, *J* = 16.1, 7.0 Hz, 1H), 3.26 (dd, *J* = 16.1, 7.2 Hz, 1H), 1.33 (dd, *J* = 15.5, 6.8 Hz, 1H), 1.24 (dd, *J* = 15.5, 8.8 Hz, 1H), 1.10 (s, 6H), 1.08 (s, 6H) ppm.

¹³C NMR (101 MHz, CDCl₃) δ 199.03, 146.31, 137.20, 132.70, 128.37, 128.16, 128.08, 127.22, 126.06, 82.96, 47.69, 37.29, 24.65, 24.56 ppm. The carbon bound to the boron was not detected due to quadrupolar relaxation.

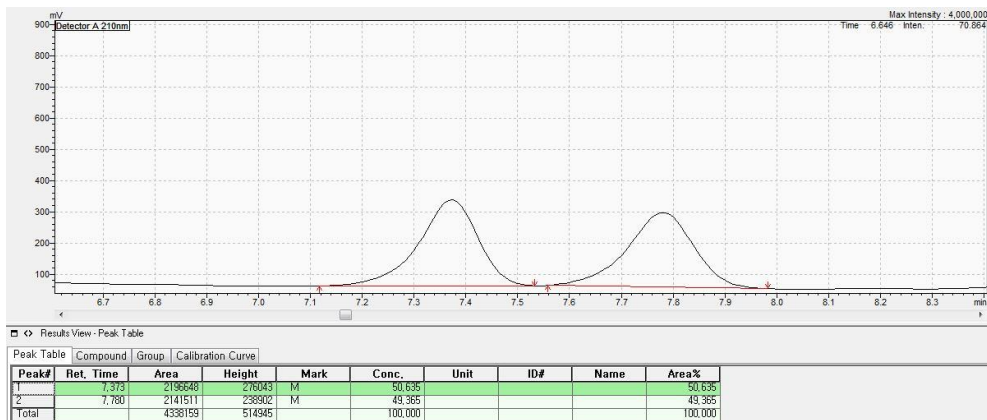
¹¹B NMR (128 MHz, CDCl₃) δ 33.5 ppm.

HRMS (ESI) calculated for [C₂₂H₂₇BO₃+H]⁺: 351.2126, found: 351.2138.

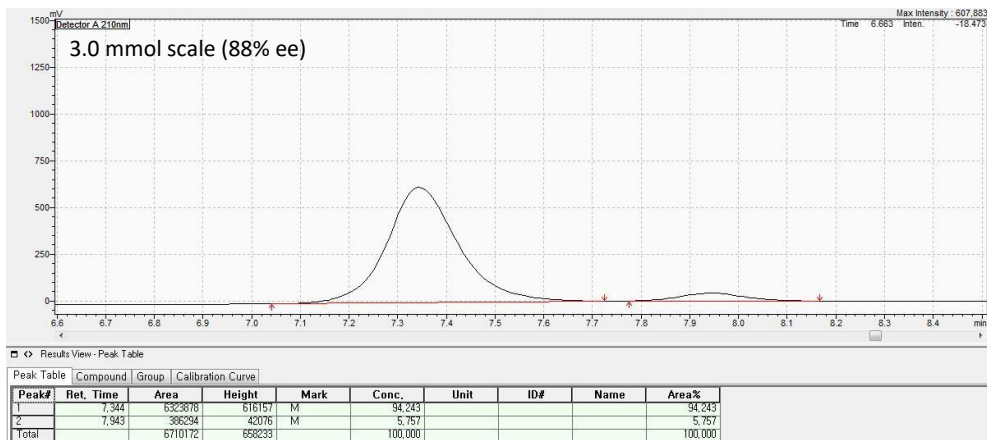
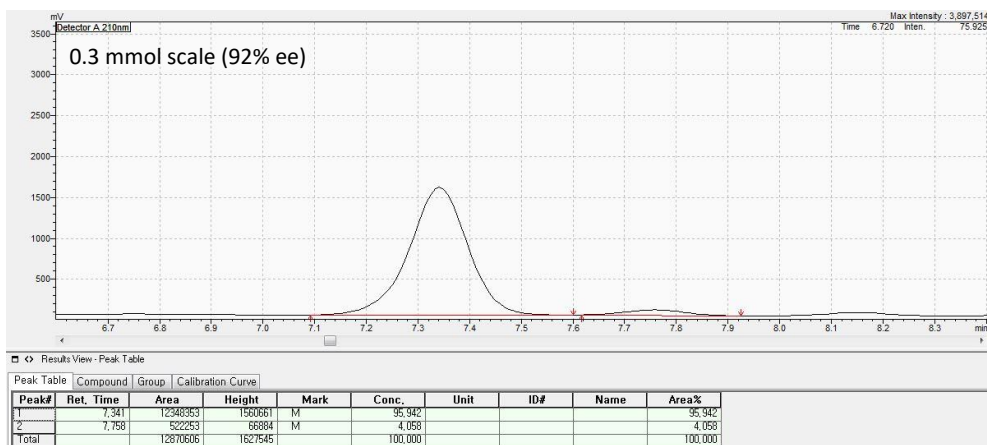
Optical rotation, [α]_D²² = -7.9 (c = 1.04, DCM).

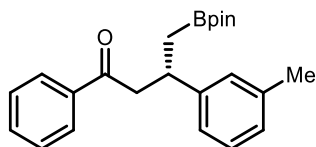
Enantiomeric excess, 92% ee was measured by HPLC (CHIRALPAK IA, *n*-hexane : *i*-PrOH = 98.5 : 1.5 → 98 : 2, 1.0 mL/min, wavelength = 210 nm, 30 °C); t_R = 7.34 min (major), t_R = 7.75 min (minor).

[Racemic 3a]



[Enantioenriched 3a]





(S)-1-phenyl-4-(4,4,5,5-tetramethyl-1,3,2-dioxaborolan-2-yl)-3-(*m*-tolyl)butan-1-one (3b) Following general procedure, the crude product was purified by silica gel chromatography (hexanes : DCM = 100 : 0 → 0 : 100, then DCM : MeOH = 100 : 0 → 99 : 1) to provide **3b** as a yellowish liquid (62 mg, 57%, 93% ee).

¹H NMR (400 MHz, CDCl₃) δ 7.97–7.89 (m, 2H), 7.56–7.49 (m, 1H), 7.47–7.37 (m, 2H), 7.11 (m, 3H), 6.96 (d, *J* = 7.2 Hz, 1H), 3.58 (m, 1H), 3.32 (dd, *J* = 16.1, 7.1 Hz, 1H), 3.26 (dd, *J* = 16.0, 7.1 Hz, 1H), 2.30 (s, 3H), 1.31 (dd, *J* = 15.5, 6.8 Hz, 1H), 1.21 (dd, *J* = 15.5, 8.8 Hz, 1H), 1.11 (s, 6H), 1.09 (s, 6H) ppm.

¹³C NMR (101 MHz, CDCl₃) δ 199.17, 146.32, 137.56, 137.29, 132.70, 128.39, 128.14, 128.11, 128.10, 126.80, 124.16, 82.97, 47.63, 37.22, 24.69, 24.60, 21.41 ppm.

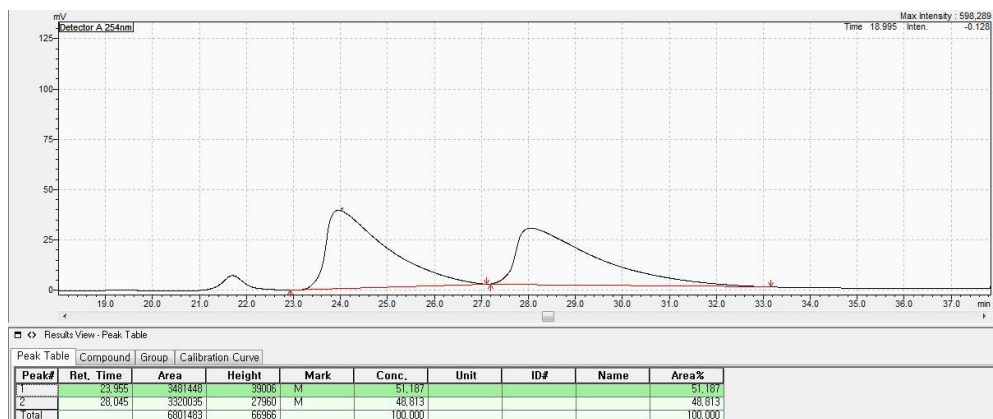
¹¹B NMR (128 MHz, CDCl₃) δ 33.0 ppm.

HRMS (ESI) calculated for [C₂₃H₂₉BO₃+H]⁺: 365.2282, found: 365.2296.

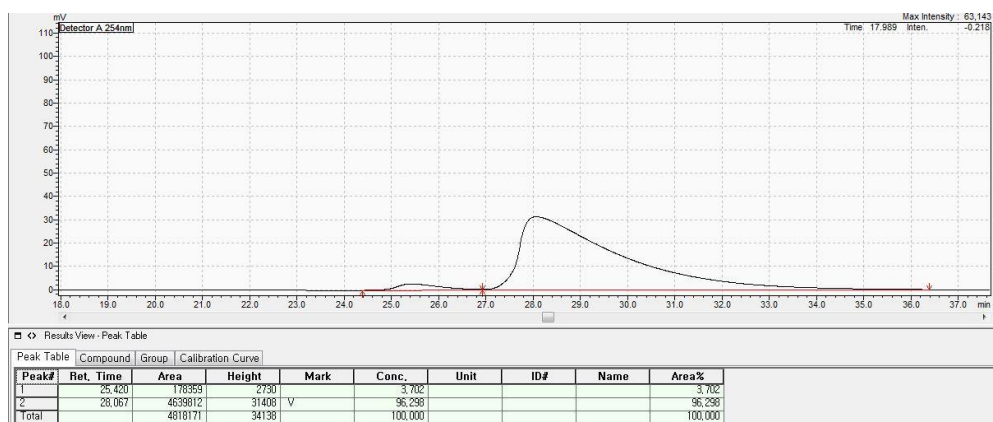
Optical rotation, [α]_D²² = +4.7 (c = 1.23, DCM).

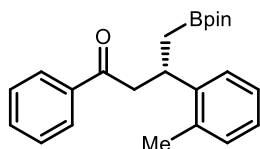
Enantiomeric excess, 93% ee was measured by HPLC (CHIRALPAK IA, *n*-hexane : *i*-PrOH = 99.8 : 0.2, 1.0 mL/min, wavelength = 254 nm, 28 °C); t_R = 28.06 min (major), t_R = 25.42 min (minor).

[Racemic 3b]



[Enantioenriched 3b]





(S)-1-phenyl-4-(4,4,5,5-tetramethyl-1,3,2-dioxaborolan-2-yl)-3-(o-tolyl)butan-1-one (3c) Following general procedure, the crude product was purified by silica gel chromatography (hexanes : DCM = 100 : 0 → 0 : 100, then DCM : MeOH = 100 : 0 → 99 : 1) to provide **3c** as a yellowish liquid (38 mg, 35%, 81% ee).

¹H NMR (400 MHz, CDCl₃) δ 7.92 (m, 2H), 7.52 (m, 1H), 7.41 (m, 2H), 7.27–7.23 (m, 1H), 7.13 (m, 1H), 7.09–6.99 (m, 2H), 3.87 (m, 1H), 3.32–3.19 (m, 2H), 2.39 (s, 3H), 1.29 (dd, *J* = 15.4, 6.6 Hz, 1H), 1.21 (dd, *J* = 15.4, 9.4 Hz, 1H), 1.05 (s, 6H), 1.02 (s, 6H) ppm.

¹³C NMR (101 MHz, CDCl₃) δ 199.29, 144.66, 137.30, 135.70, 132.76, 130.15, 128.44, 128.12, 126.05, 125.77, 125.76, 82.96, 47.45, 32.01, 24.57, 19.76 ppm.

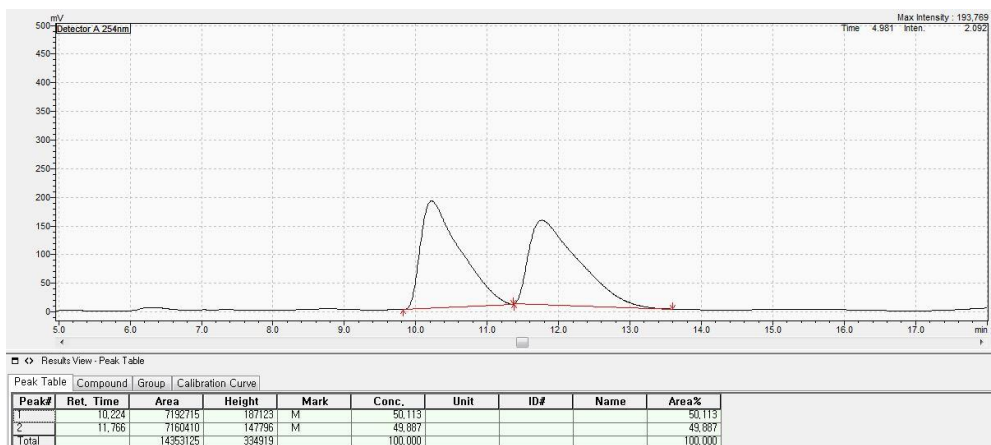
¹¹B NMR (128 MHz, CDCl₃) δ 33.0 ppm.

HRMS (ESI) calculated for [C₂₃H₂₉BO₃+H]⁺: 365.2282, found: 365.2296.

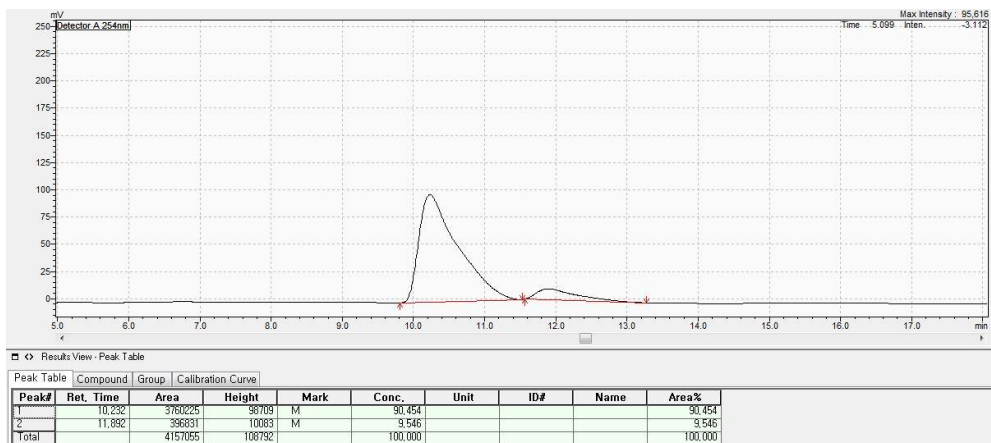
Optical rotation, [α]_D²² = -2.0 (c = 0.76, DCM).

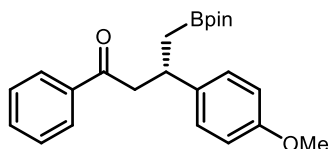
Enantiomeric excess, 81% ee was measured by HPLC (CHIRALCEL OD-H, *n*-hexane : *i*-PrOH = 99.3 : 0.7, 1.2 mL/min, wavelength = 254 nm, 28 °C); t_R = 10.23 min (major), t_R = 11.89 min (minor).

[Racemic 3c]



[Enantioenriched 3c]





(S)-3-(4-methoxyphenyl)-1-phenyl-4-(4,4,5,5-tetramethyl-1,3,2-dioxaborolan-2-yl)butan-1-one (3d) Following general procedure, the crude product was purified by silica gel chromatography (hexanes : DCM = 100 : 0 → 0 : 100, then DCM : MeOH = 100 : 0 → 98 : 2) to provide **3d** as a yellowish liquid (75 mg, 68%, 85% ee).

¹H NMR (400 MHz, CDCl₃) δ 7.95–7.88 (m, 2H), 7.55–7.49 (m, 1H), 7.46–7.37 (m, 2H), 7.21–7.14 (m, 2H), 6.82–6.75 (m, 2H), 3.75 (s, 3H), 3.55 (m, 1H), 3.29 (dd, *J* = 15.9, 6.8 Hz, 1H), 3.21 (dd, *J* = 15.9, 7.4 Hz, 1H), 1.29 (dd, *J* = 15.5, 6.9 Hz, 1H), 1.20 (dd, *J* = 15.5, 8.8 Hz, 1H), 1.11 (s, 6H), 1.09 (s, 6H) ppm.

¹³C NMR (101 MHz, CDCl₃) δ 199.29, 157.88, 138.52, 137.29, 132.72, 128.43, 128.16, 128.17, 113.60, 83.03, 55.21, 48.01, 36.65, 24.75, 24.63 ppm. The carbon bound to the boron was not detected due to quadrupolar relaxation.

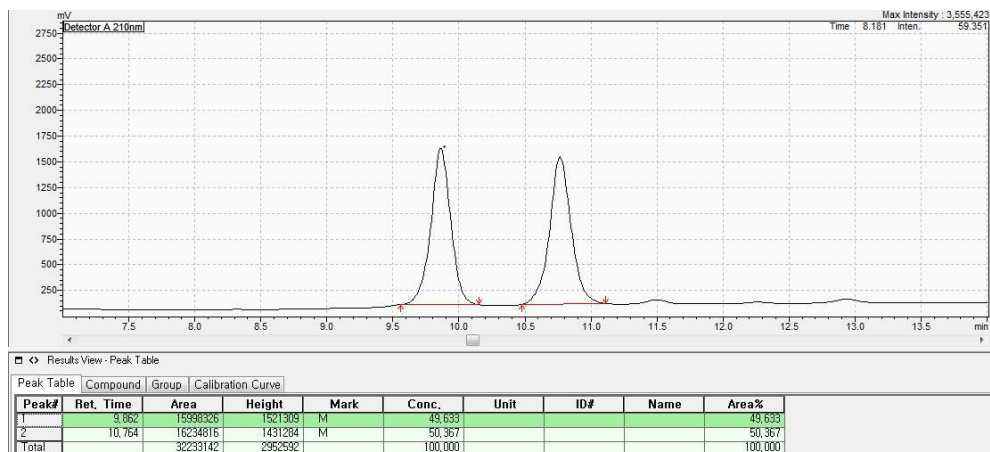
¹¹B NMR (128 MHz, CDCl₃) δ 33.3 ppm.

HRMS (ESI) calculated for [C₂₃H₂₉BO₄+H]⁺: 381.2231, found: 381.2240.

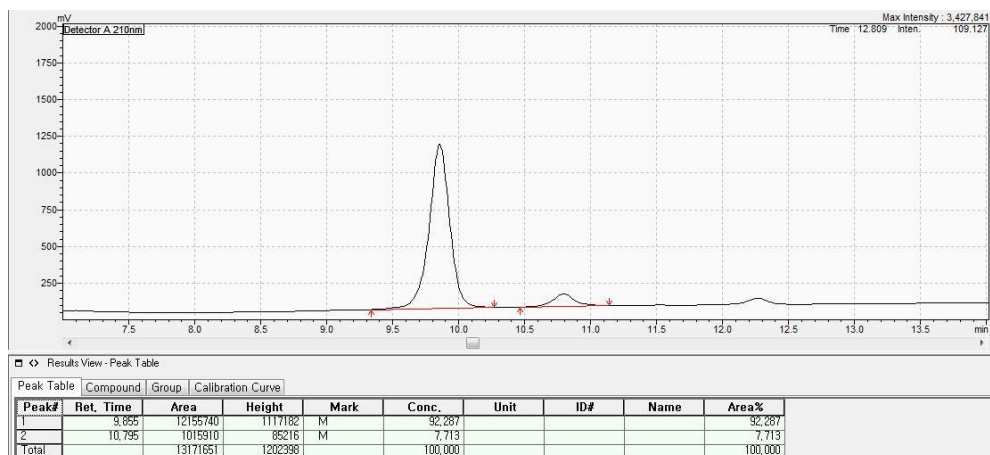
Optical rotation, [α]_D²² = +3.98 (c = 0.58, DCM).

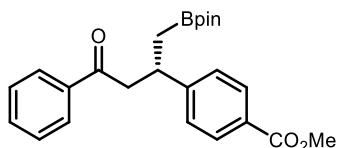
Enantiomeric excess, 85% ee was measured by HPLC (CHIRALPAK IA, *n*-hexane : *i*-PrOH = 98.5 : 1.5 → 98 : 2, 1.0 mL/min, wavelength = 210 nm, 30 °C); t_R = 9.85 min (major), t_R = 10.79 min (minor).

[Racemic 3d]



[Enantioenriched 3d]





Methyl-(*S*)-4-(4-oxo-4-phenyl-1-(4,4,5,5-tetramethyl-1,3,2-dioxaborolan-2-yl)butan-2-yl)benzoate (3e) Following general procedure, the crude product was purified by silica gel chromatography (hexanes : DCM = 50 : 50 → 0 : 100, DCM : MeOH = 100 : 0 → 98 : 2) to provide **3c** as a colorless liquid (81 mg, 66%, 91% ee).

¹H NMR (400 MHz, CDCl₃) δ 7.91–7.86 (m, 4H), 7.57–7.49 (m, 1H), 7.46–7.38 (m, 2H), 7.37–7.31 (m, 2H), 3.88 (s, 3H), 3.68 (m, 1H), 3.34 (dd, *J* = 16.4, 6.6 Hz, 1H), 3.27 (dd, *J* = 16.4, 7.5 Hz, 1H), 1.32 (dd, *J* = 15.6, 6.7 Hz, 1H), 1.22 (dd, *J* = 14.5, 9.4 Hz, 1H), 1.10 (s, 6H), 1.07 (s, 6H) ppm.

¹³C NMR (101 MHz, CDCl₃) δ 198.81, 167.26, 152.06, 137.21, 133.10, 129.81, 128.67, 128.25, 128.18, 127.55, 83.35, 52.08, 47.38, 37.39, 24.89, 24.76 ppm. The carbon bound to the boron was not detected due to quadrupolar relaxation.

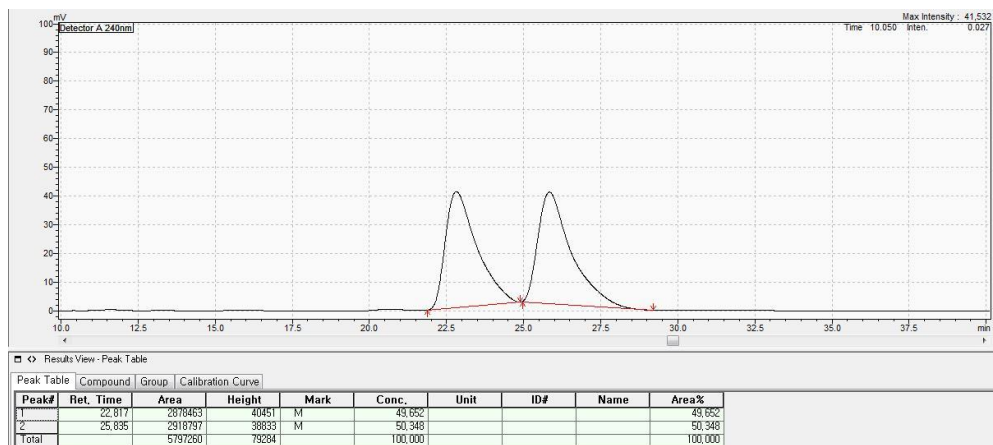
¹¹B NMR (128 MHz, CDCl₃) δ 33.39 ppm.

HRMS (ESI) calculated for [C₂₄H₂₉BO₅+H]⁺: 409.2180, found: 409.2194.

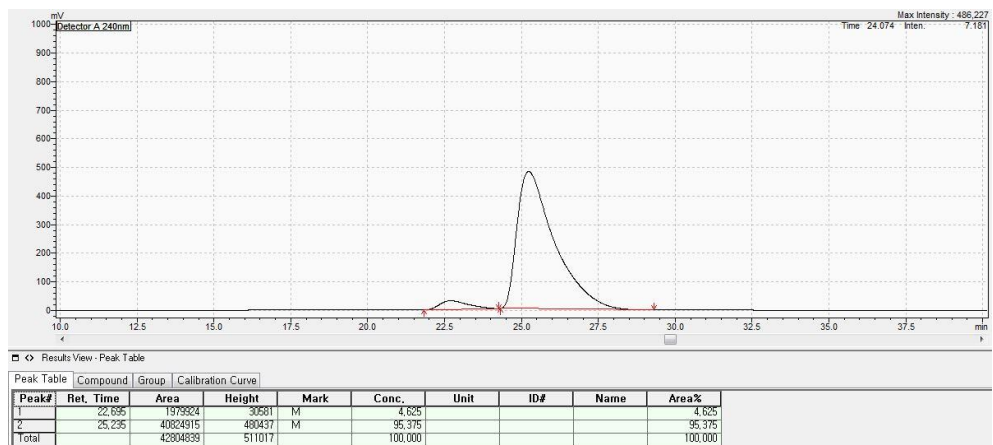
Optical rotation, [α]_D²² = -2.49 (c = 0.88, DCM).

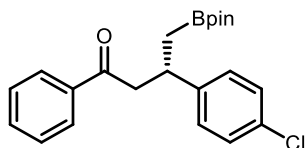
Enantiomeric excess, 91% ee was measured by HPLC (CHIRALCEL OD, *n*-hexane : *i*-PrOH = 99 : 1, 1.0 mL/min, wavelength = 240 nm, 28 °C); t_R = 22.69 min (major), t_R = 25.23 min (minor).

[Racemic 3e]



[Enantioenriched 3e]





(S)-3-(4-chlorophenyl)-1-phenyl-4-(4,4,5,5-tetramethyl-1,3,2-dioxaborolan-2-yl)butan-1-one (3f) Following general procedure, the crude product was purified by silica gel chromatography (hexanes : DCM = 100 : 0 → 0 : 100, then DCM : MeOH = 100 : 0 → 99 : 1) to provide **3f** as a yellowish liquid (86 mg, 76%, 94% ee).

¹H NMR (400 MHz, CDCl₃) δ 7.96–7.85 (m, 2H), 7.55–7.50 (m, 1H), 7.42 (m, 2H), 7.22–7.19 (m, 4H), 3.65–3.55 (m, 1H), 3.31 (dd, *J* = 16.3, 6.5 Hz, 1H), 3.23 (dd, *J* = 16.3, 7.7 Hz, 1H), 1.30 (dd, *J* = 15.6, 6.8 Hz, 1H), 1.19 (dd, *J* = 15.6, 8.7 Hz, 1H), 1.12 (s, 6H), 1.10 (s, 6H) ppm.

¹³C NMR (101 MHz, CDCl₃) δ 198.73, 144.86, 137.08, 132.87, 131.65, 128.69, 128.47, 128.27, 128.07, 83.14, 47.46, 36.67, 24.72, 24.60 ppm. The carbon bound to the boron was not detected due to quadrupolar relaxation.

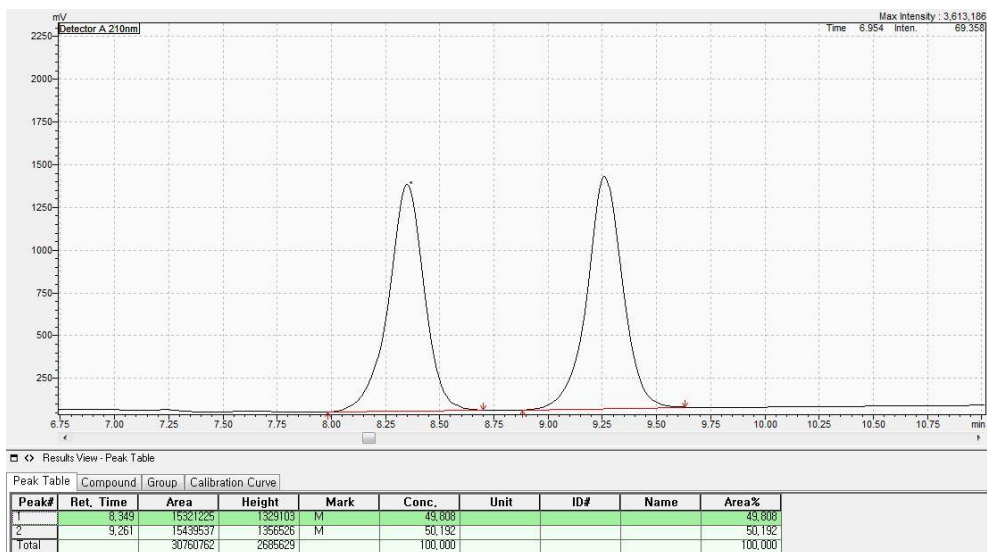
¹¹B NMR (128 MHz, CDCl₃) δ 33.2 ppm.

HRMS (ESI) calculated for [C₂₂H₂₆BClO₃+H]⁺: 385.1736, found: 385.1737.

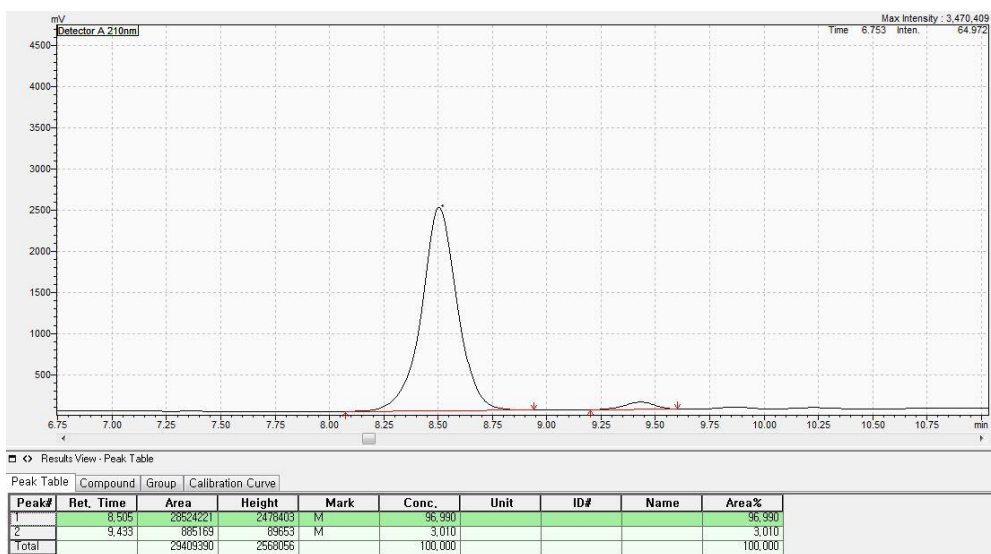
Optical rotation, [α]_D²² = -3.42 (c = 0.99, DCM).

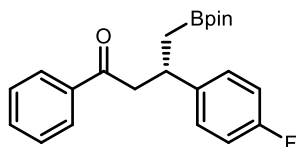
Enantiomeric excess, 94% ee was measured by HPLC (CHIRALPAK IA, *n*-hexane : *i*-PrOH = 98.5 : 1.5 → 98 : 2, 1.0 mL/min, wavelength = 210 nm, 30 °C); t_R = 8.50 min (major), t_R = 9.43 min (minor).

[Racemic 3f]



[Enantioenriched 3f]





(S)-3-(4-fluorophenyl)-1-phenyl-4-(4,4,5,5-tetramethyl-1,3,2-dioxaborolan-2-yl)butan-1-one (3g) Following general procedure, the crude product was purified by silica gel chromatography (hexanes : DCM = 100 : 0 → 0 : 100, then DCM : MeOH = 100 : 0 → 99 : 1) to provide **3g** as an orange liquid (89 mg, 77%, 91% ee).

¹H NMR (400 MHz, CDCl₃) δ 7.94–7.88 (m, 2H), 7.55–7.49 (m, 1H), 7.45–7.38 (m, 2H), 7.25–7.19 (m, 2H), 6.97–6.87 (m, 2H), 3.65–3.56 (m, 1H), 3.30 (dd, *J* = 16.1, 6.6 Hz, 1H), 3.22 (dd, *J* = 16.1, 7.6 Hz, 1H), 1.30 (dd, *J* = 15.5, 6.7 Hz, 1H), 1.20 (dd, *J* = 15.5, 9.0 Hz, 1H), 1.11 (s, 6H), 1.09 (s, 6H) ppm.

¹³C NMR (101 MHz, CDCl₃) δ 198.91, δ 161.27 (d, *J* = 243.6 Hz), 141.96 (d, *J* = 3.2 Hz), 137.15, 132.83, 128.70 (d, *J* = 7.8 Hz), 128.46, 128.08, 114.87 (d, *J* = 21.1 Hz), 83.09, 47.79, 36.64, 24.71, 24.59 ppm. The carbon bound to the boron was not detected due to quadrupolar relaxation.

¹¹B NMR (128 MHz, CDCl₃) δ 33.1 ppm.

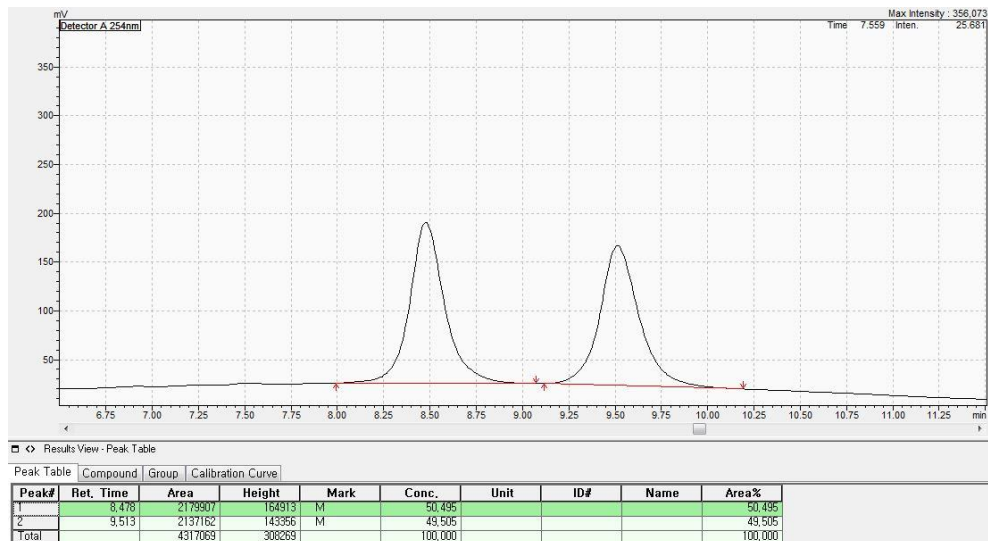
¹⁹F NMR (376 MHz, CDCl₃) δ –117.38 ppm.

HRMS (ESI) calculated for [C₂₂H₂₆BF₃O₃+H]⁺: 369.2032, found: 369.2044.

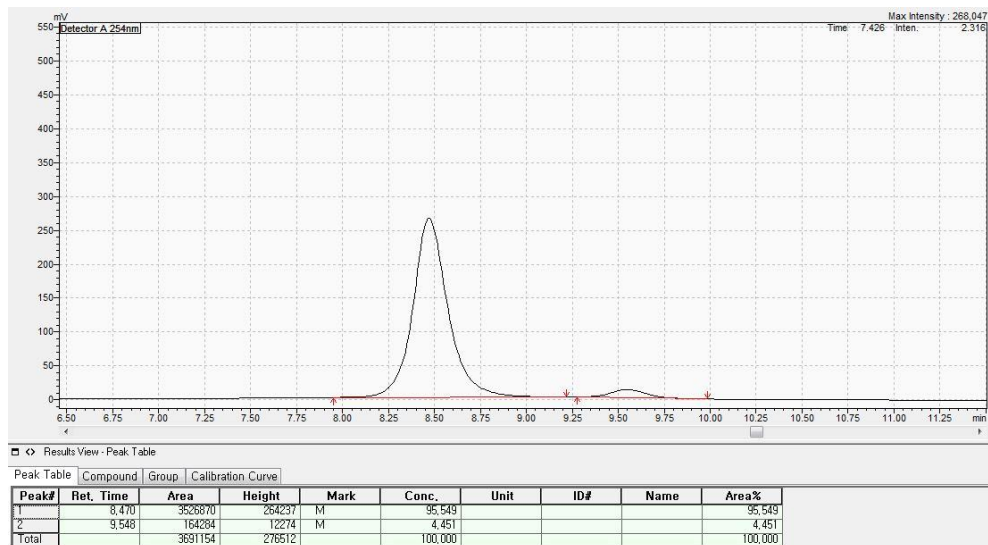
Optical rotation, [α]_D²² = –0.85 (c = 1.50, DCM).

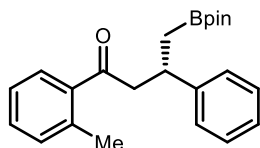
Enantiomeric excess, 91% ee was measured by HPLC (CHIRALPAK IA, *n*-hexane : *i*-PrOH = 99 : 1, 1.0 mL/min, wavelength = 254 nm, 28 °C); $t_R = 8.47$ min (major), $t_R = 9.54$ min (minor).

[Racemic 3g]



[Enantioenriched 3g]





(S)-3-phenyl-4-(4,4,5,5-tetramethyl-1,3,2-dioxaborolan-2-yl)-1-(o-tolyl)butan-1-one (3h) Following general procedure, the crude product was purified by silica gel chromatography (hexanes : DCM = 100 : 0 → 0 : 100) to provide **3h** as a yellowish liquid (81 mg, 74%, 93% ee).

¹H NMR (400 MHz, CDCl₃) δ 7.51–7.55 (m, 1H), 7.28–7.34 (m, 1H), 7.27–7.09 (m, 6H), 3.60–3.48 (m, 1H), 3.29 (dd, *J* = 16.0, 6.7 Hz, 1H), 3.16 (dd, *J* = 16.0, 8.0 Hz, 1H), 2.26 (s, 3H), 1.29 (dd, *J* = 15.5, 7.0 Hz, 1H), 1.21 (dd, *J* = 15.5, 8.7 Hz, 1H), 1.11 (s, 6H), 1.09 (s, 6H) ppm.

¹³C NMR (101 MHz, CDCl₃) δ 203.72, 146.01, 138.59, 137.78, 131.66, 130.79, 128.19, 128.15, 127.34, 126.12, 125.41, 83.04, 50.79, 37.58, 24.71, 24.64, 20.71 ppm. The carbon bound to the boron was not detected due to quadrupolar relaxation.

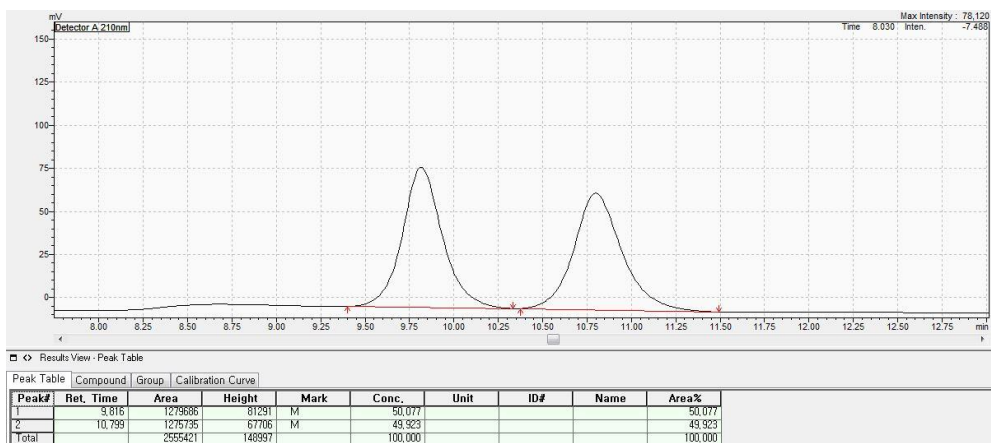
¹¹B NMR (128 MHz, CDCl₃) δ 33.0 ppm.

HRMS (ESI) calculated for [C₂₃H₂₉BO₃+H]⁺: 365.2282, found: 365.2296.

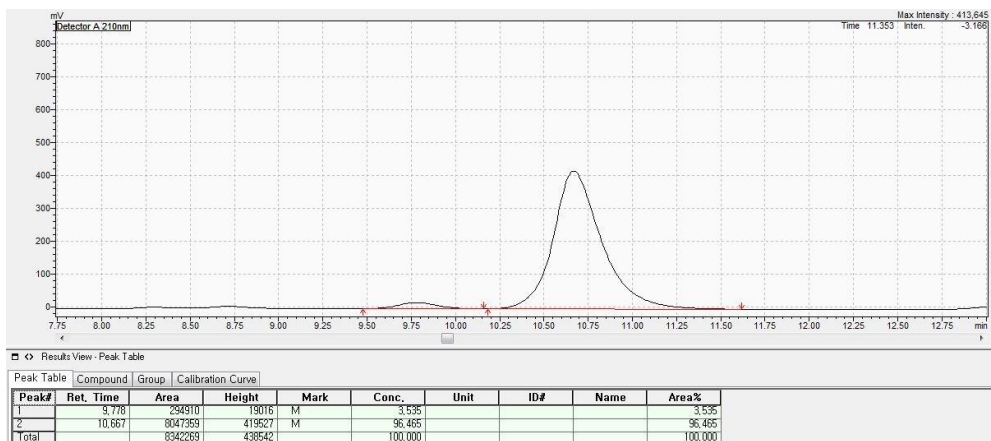
Optical rotation, [α]_D²² = -2.6 (c = 1.05, DCM).

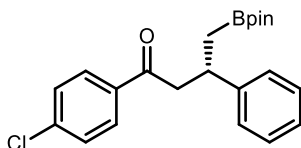
Enantiomeric excess, 93% ee was measured by HPLC (CHIRALPAK IA, *n*-hexane : *i*-PrOH = 99 : 1, 0.6 mL/min, wavelength = 210 nm, 28 °C); t_R = 10.66 min (major), t_R = 9.77 min (minor).

[Racemic 3h]



[Enantioenriched 3h]





(S)-1-(4-chlorophenyl)-3-phenyl-4-(4,4,5,5-tetramethyl-1,3,2-dioxaborolan-2-yl)butan-1-one (3i) Following general procedure, the crude product was purified by silica gel chromatography (hexanes : EtOAc = 10 : 1) to provide **3i** as a colorless oil (85 mg, 74%, 89% ee).

¹H NMR (400 MHz, CDCl₃) δ 7.81–7.75 (m, 2H), 7.35–7.29 (m, 2H), 7.21–7.15 (m, 4H), 7.11–7.04 (m, 1H), 3.50 (m, 1H), 3.22 (dd, *J* = 16.0, 6.8 Hz, 1H), 3.14 (dd, *J* = 15.9, 7.4 Hz, 1H), 1.24 (dd, *J* = 15.5, 7.0 Hz, 1H), 1.15 (dd, *J* = 15.9, 8.6 Hz, 1H), 1.03 (s, 6H), 1.01 (s, 6H) ppm.

¹³C NMR (101 MHz, CDCl₃) δ 197.95, 146.11, 139.16, 135.60, 129.57, 128.72, 128.25, 127.21, 126.20, 83.08, 47.68, 37.46, 24.70, 24.61 ppm. The carbon bound to the boron was not detected due to quadrupolar relaxation.

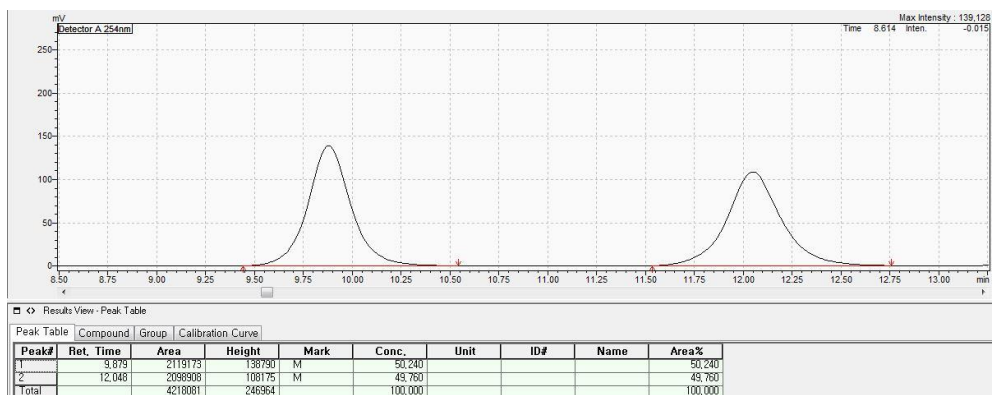
¹¹B NMR (128 MHz, CDCl₃) δ 32.8 ppm.

HRMS (ESI) calculated for [C₂₂H₂₆BClO₃+H]⁺: 385.1736, found: 385.1734.

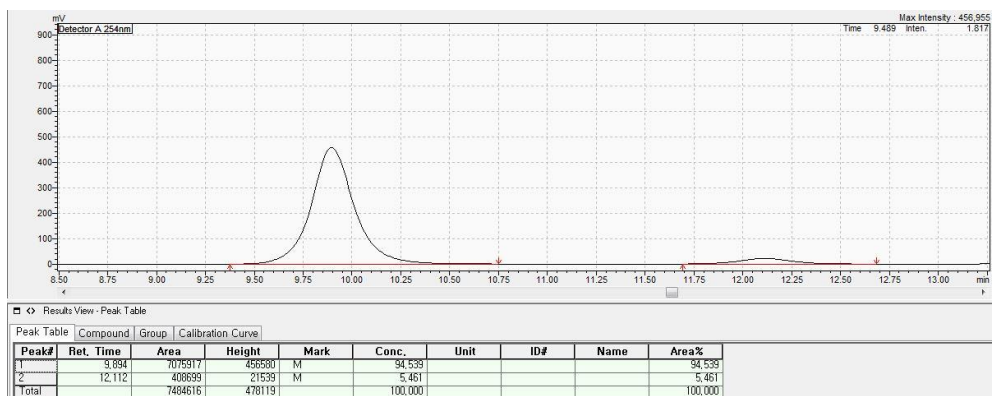
Optical rotation, [α]_D²² = +0.31 (c = 1.5, DCM).

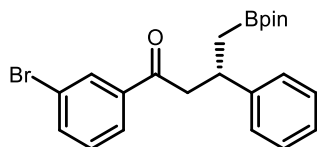
Enantiomeric excess, 89% ee was measured by HPLC (CHIRALPAK IA, *n*-hexane : *i*-PrOH = 99 : 1, 1.0 mL/min, wavelength = 254 nm, 28 °C); t_R = 9.89 min (major), t_R = 12.11 min (minor).

[Racemic 3i]



[Enantioenriched 3i]





(S)-1-(3-bromophenyl)-3-phenyl-4-(4,4,5,5-tetramethyl-1,3,2-dioxaborolan-2-yl)butan-1-one (3j) Following general procedure, the crude product was purified by silica gel chromatography (hexanes : DCM = 50 : 50 → 0 : 100, DCM : MeOH = 100 : 0 → 98 : 2) to provide **3j** as a pale yellow oil (90 mg, 70%, 93% ee).

¹H NMR (500 MHz, CDCl₃) δ 8.06–8.02 (m, 1H), 7.85–7.80 (m, 1H), 7.67–7.61 (m, 1H), 7.32–7.27 (m, 1H), 7.26–7.21 (m, 4H), 7.18–7.11 (m, 1H), 3.63–3.52 (m, 1H), 3.30 (dd, *J* = 16.0, 6.8 Hz, 1H), 3.20 (dd, *J* = 16.0, 7.4 Hz, 1H), 1.31 (dd, *J* = 15.6, 7.0 Hz, 1H), 1.23 (dd, *J* = 15.8, 8.6 Hz, 1H), 1.11 (s, 6H), 1.09 (s, 6H) ppm.

¹³C NMR (126 MHz, CDCl₃) δ 197.79, 135.58, 131.24, 130.02, 128.48, 128.27, 127.21, 126.65, 126.55, 126.24, 122.82, 83.12, 47.75, 37.39, 24.70, 24.63 ppm. The carbon bound to the boron was not detected due to quadrupolar relaxation.

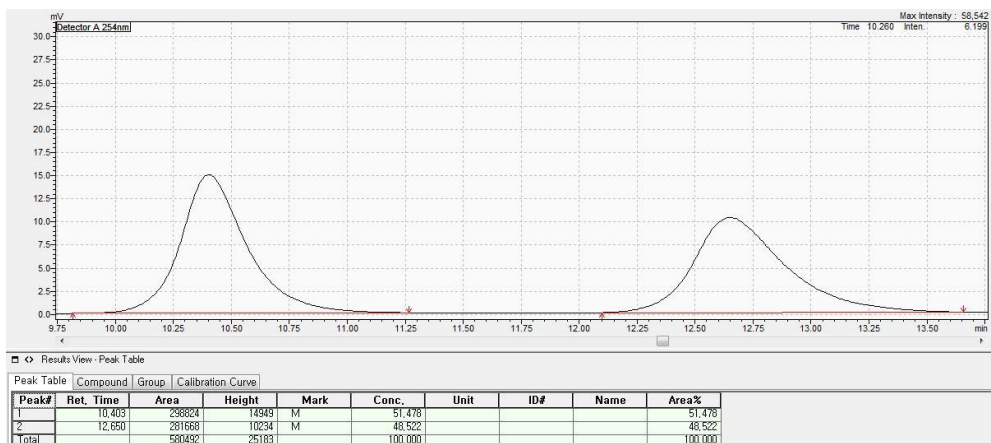
¹¹B NMR (128 MHz, CDCl₃) δ 33.5 ppm.

HRMS (ESI) calculated for [C₂₂H₂₆BBro₃+H]⁺: 429.1231, found: 429.1234.

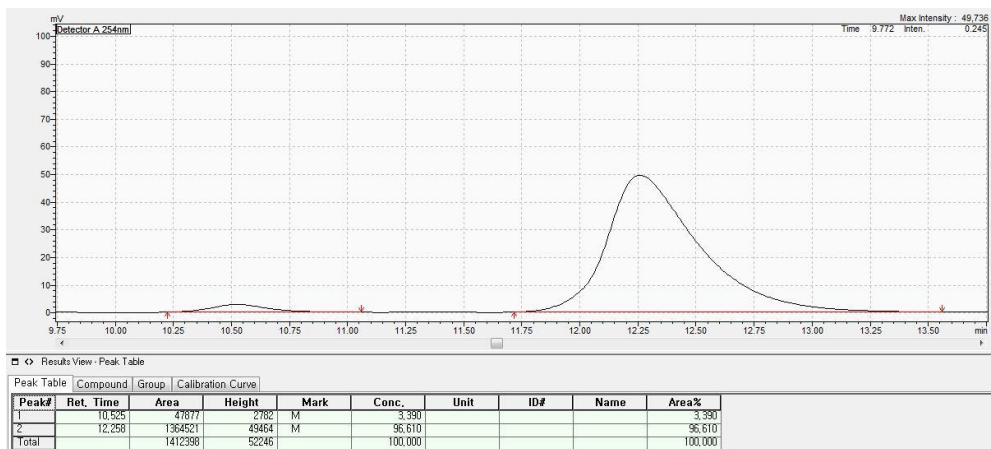
Optical rotation, [α]_D²² = -4.14 (c = 1.2, DCM).

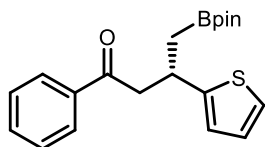
Enantiomeric excess, 93% ee was measured by HPLC (CHIRALPAK IA, *n*-hexane : *i*-PrOH = 99.5 : 0.5, 1.0 mL/min, wavelength = 254 nm, 28 °C); t_R = 12.25min (major), t_R = 10.52min (minor).

[Racemic 3j]



[Enantioenriched 3j]





(S)-1-phenyl-4-(4,4,5,5-tetramethyl-1,3,2-dioxaborolan-2-yl)-3-(thiophen-2-yl)butan-1-one (3k) Following general procedure, the crude product was purified by silica gel chromatography (hexanes : DCM = 50 : 50 → 0 : 100, DCM : MeOH = 100 : 0 → 97 : 3) to provide **3k** as a colorless liquid (80 mg, 75%, 92% ee).

¹H NMR (500 MHz, CDCl₃) δ 7.98–7.90 (m, 2H), 7.56–7.51 (m, 1H), 7.47–7.40 (m, 2H), 7.10–7.03 (m, 1H), 6.89–6.82 (m, 2H), 4.01–3.91 (m, 1H), 3.36 (dd, *J* = 14.9, 5.4 Hz, 1H), 3.32 (dd, *J* = 14.9, 5.6 Hz, 1H), 1.37 (dd, *J* = 15.7, 6.7 Hz, 1H), 1.31 (dd, *J* = 15.6, 8.3 Hz, 1H), 1.15 (s, 6H), 1.13 (s, 6H) ppm.

¹³C NMR (126 MHz, CDCl₃) δ 198.69, 150.56, 137.15, 132.87, 128.46, 128.13, 126.30, 123.33, 122.64, 83.17, 48.35, 32.62, 24.71, 24.65 ppm. The carbon bound to the boron was not detected due to quadrupolar relaxation.

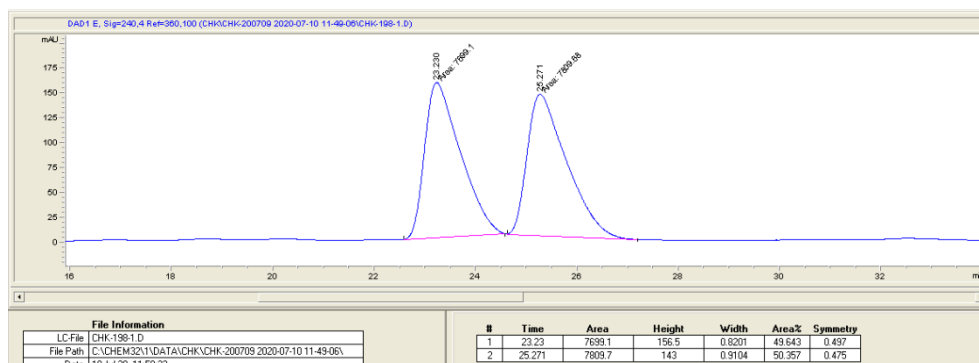
¹¹B NMR (128 MHz, CDCl₃) δ 31.87 ppm.

HRMS (ESI) calculated for [C₂₀H₂₅BO₃S+H]⁺: 357.1690, found: 357.1698.

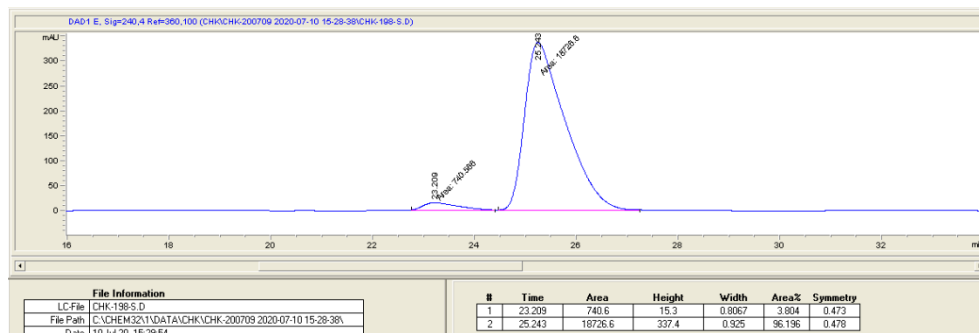
Optical rotation, [α]_D²² = +4.31 (c = 1.01, DCM).

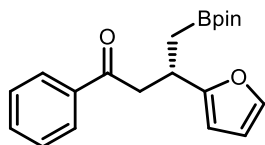
Enantiomeric excess, 92% ee was measured by HPLC (CHIRALCEL OD, *n*-hexane : *i*-PrOH = 99.9 : 0.1, 0.2 mL/min, wavelength = 240 nm, 25 °C); t_R = 25.24 min (major), t_R = 23.20 min (minor). Determined on equipment combined an Agilent Technologies 1200 series Infinity LC and Hewlett Packard 1100 series LC.

[Racemic 3k]



[Enantioenriched 3k]





(S)-3-(furan-2-yl)-1-phenyl-4-(4,4,5,5-tetramethyl-1,3,2-dioxaborolan-2-yl)butan-1-one (3I) Following general procedure, the crude product was purified by silica gel chromatography (hexanes : DCM = 100 : 0 → 0 : 100, then DCM : MeOH = 100 : 0 → 99 : 1) to provide **3I** as a yellowish liquid (77 mg, 76%, 94% ee).

¹H NMR (400 MHz, CDCl₃) δ 7.99–7.92 (m, 2H), 7.57–7.50 (m, 1H), 7.47–7.40 (m, 2H), 7.29–7.21 (m, 1H), 6.25–6.18 (m, 1H), 6.01 (d, *J* = 3.2 Hz, 1H), 3.79–3.68 (m, 1H), 3.37 (dd, *J* = 16.3, 6.7 Hz, 1H), 3.25 (dd, *J* = 16.3, 7.1 Hz, 1H), 1.25 (d, *J* = 7.3 Hz, 2H), 1.19 (s, 6H), 1.17 (s, 6H) ppm.

¹³C NMR (101 MHz, CDCl₃) δ 198.86, 159.11, 140.68, 137.19, 132.82, 128.44, 128.15, 109.87, 104.26, 83.13, 44.68, 30.79, 24.78, 24.70 ppm. The carbon bound to the boron was not detected due to quadrupolar relaxation.

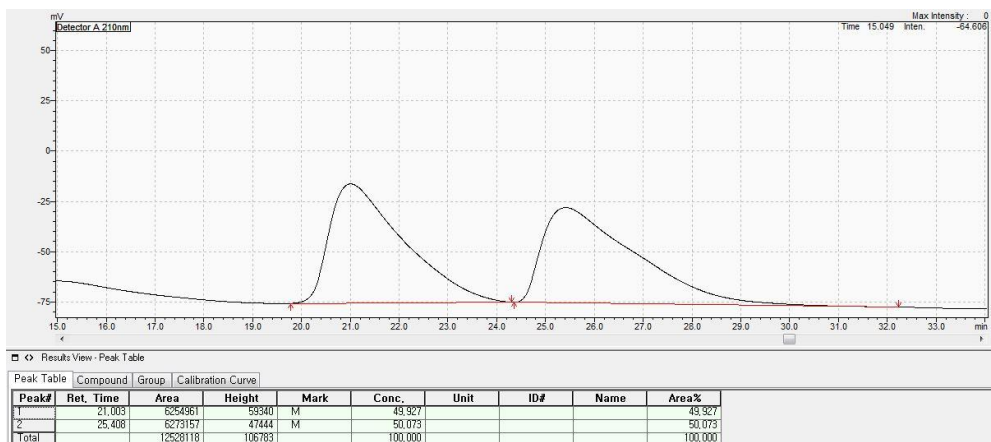
¹¹B NMR (128 MHz, CDCl₃) δ 33.1 ppm.

HRMS (ESI) calculated for [C₂₀H₂₅BO₄+H]⁺: 341.1918, found: 341.1930.

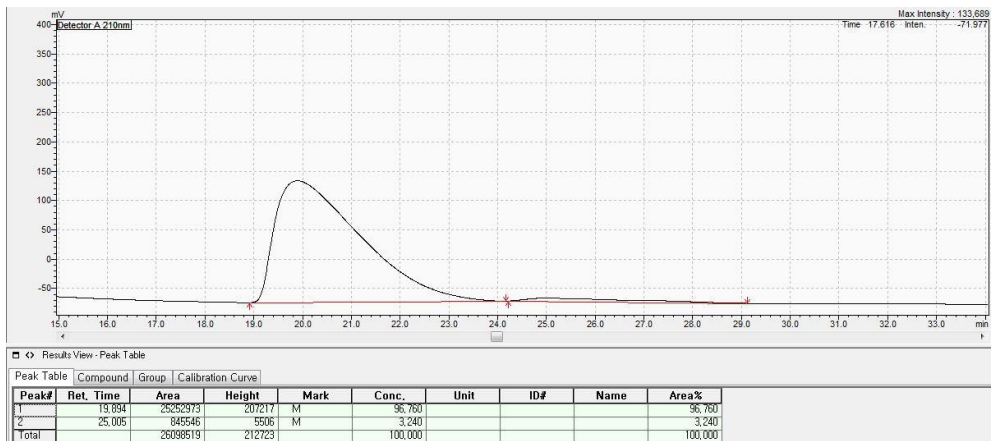
Optical rotation, [α]_D²² = -9.5 (c = 0.79, DCM).

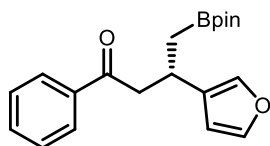
Enantiomeric excess, 94% ee was measured by HPLC (CHIRALCEL OD-H, *n*-hexane : *i*-PrOH = 99.8 : 0.2, 1.0 mL/min, wavelength = 210 nm, 28 °C); t_R = 19.89 min (major), t_R = 25.00 min (minor).

[Racemic 3I]



[Enantioenriched 3I]





(S)-3-(furan-3-yl)-1-phenyl-4-(4,4,5,5-tetramethyl-1,3,2-dioxaborolan-2-yl)butan-1-one (3m) Following general procedure, the crude product was purified by silica gel chromatography (hexanes : DCM = 100 : 0 → 0 : 100, then DCM : MeOH = 100 : 0 → 99 : 1) to provide **3m** as a yellowish liquid (76 mg, 74%, 93% ee).

¹H NMR (400 MHz, CDCl₃) δ 7.98–7.90 (m, 2H), 7.56–7.50 (m, 1H), 7.47–7.40 (m, 2H), 7.30–7.27 (m, 1H), 7.25–7.21 (m, 1H), 6.33 (m, 1H), 3.62–3.51 (m, 1H), 3.26 (dd, *J* = 16.1, 6.5 Hz, 1H), 3.16 (dd, *J* = 16.1, 7.5 Hz, 1H), 1.22 (m, 2H), 1.17 (s, 6H), 1.16 (s, 6H).

¹³C NMR (101 MHz, CDCl₃) δ 199.21, 142.56, 138.50, 137.28, 132.82, 129.90, 128.47, 128.15, 109.67, 83.13, 46.95, 27.86, 24.76, 24.68 ppm. The carbon bound to the boron was not detected due to quadrupolar relaxation.

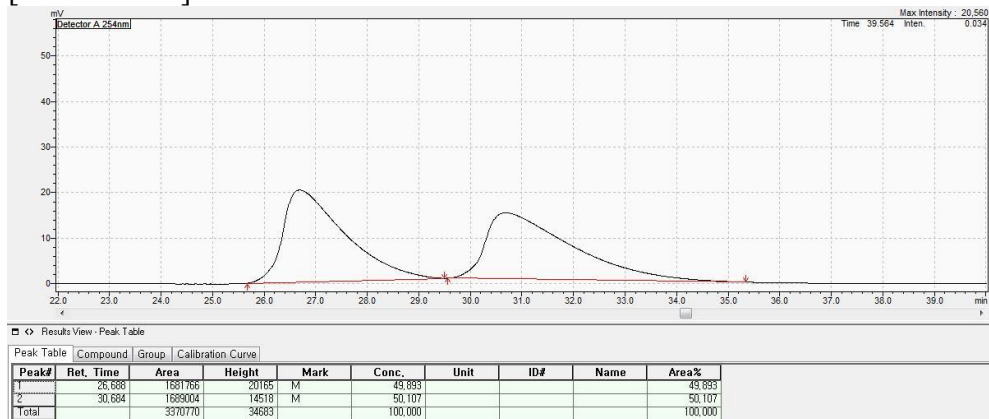
¹¹B NMR (128 MHz, CDCl₃) δ 33.10 ppm.

HRMS (ESI) calculated for [C₂₀H₂₅BO₄+H]⁺: 341.1918, found: 341.1921.

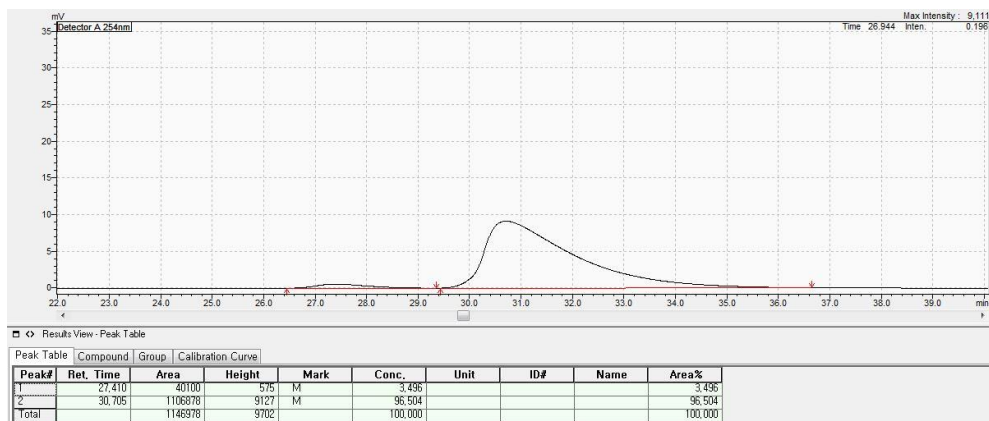
Optical rotation, [α]_D²² = +0.59 (c = 0.71, DCM).

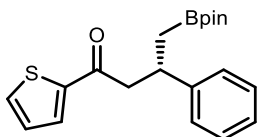
Enantiomeric excess, 93% ee was measured by HPLC (CHIRALPAK IA, *n*-hexane : *i*-PrOH = 99.8 : 0.2, 1.0 mL/min, wavelength = 254 nm, 30 °C); t_R = 30.71 min (major), t_R = 27.41 min (minor).

[Racemic 3m]



[Enantioenriched 3m]





(S)-3-phenyl-4-(4,4,5,5-tetramethyl-1,3,2-dioxaborolan-2-yl)-1-(thiophen-2-yl)butan-1-one (3n). Following general procedure, the crude product was purified by silica gel chromatography (hexanes : EtOAc = 100 : 0 → 85 : 15) to provide **3n** as a colorless liquid (75 mg, 70%, 88% ee).

¹H NMR (500 MHz, CDCl₃) δ 7.67 (d, *J* = 3.5 Hz, 1H), 7.57 (d, *J* = 4.8 Hz, 1H), 7.29–7.20 (m, 4H), 7.17–7.10 (m, 1H), 7.09–7.04 (m, 1H), 3.65–3.55 (m, 1H), 3.26–3.14 (m, 2H), 1.32 (dd, *J* = 15.0, 8.8 Hz, 1H), 1.23 (dd, 1H), 1.09 (s, 6H), 1.07 (s, 6H) ppm.

¹³C NMR (126 MHz, CDCl₃) δ 191.98, 146.08, 144.87, 133.30, 131.80, 128.22, 127.88, 127.24, 126.17, 83.03, 48.57, 37.80, 24.69, 24.58 ppm. The carbon bound to the boron was not detected due to quadrupolar relaxation.

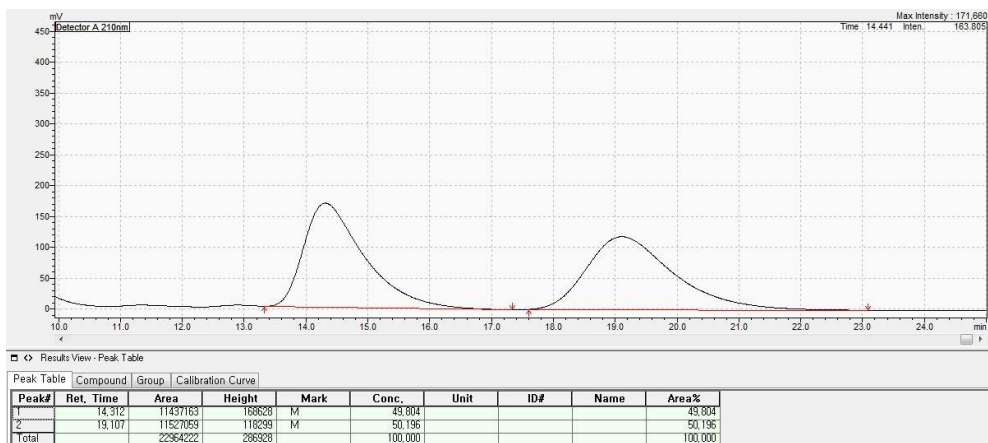
¹¹B NMR (128 MHz, CDCl₃) δ 33.27 ppm.

HRMS (ESI) calculated for [C₂₀H₂₅BO₃S+H]⁺: 357.1690, found: 357.1692.

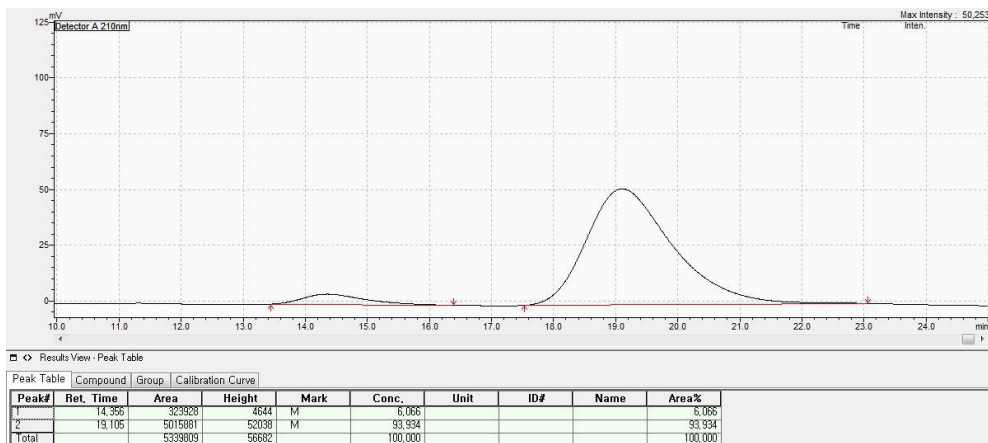
Optical rotation, [α]_D²² = +13.7 (c = 1.42, DCM).

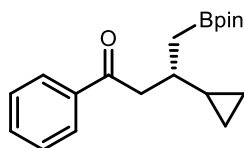
Enantiomeric excess, 88% ee was measured by HPLC (CHIRALCEL OJ-H, *n*-hexane : *i*-PrOH = 95 : 5, 1.0 mL/min, wavelength = 210 nm, 28 °C); t_R = 19.10 min (major), t_R = 14.35 min (minor).

[Racemic 3n]



[Enantioenriched 3n]





(S)-3-cyclopropyl-1-phenyl-4-(4,4,5,5-tetramethyl-1,3,2-dioxaborolan-2-yl)butan-1-one (30) Following general procedure stirring for 36 hours instead of 11 hours, the crude product was purified by silica gel chromatography (hexanes : DCM = 50 : 50 → 0 : 100, DCM : MeOH = 100 : 0 → 99.5 : 0.5) to provide **30** as a colorless liquid (66 mg, 70%, 87% ee).

¹H NMR (400 MHz, CDCl₃) δ 8.03–7.95 (m, 2H), 7.56–7.49 (m, 1H), 7.47–7.40 (m, 2H), 3.16 (dd, *J* = 14.9, 6.9 Hz, 1H), 2.98 (dd, *J* = 14.9, 6.8 Hz, 1H), 1.61–1.48 (m, 1H), 1.24 (s, 12H), 1.06–0.93 (m, 2H), 0.78–0.66 (m, 1H), 0.43–0.28 (m, 2H), 0.20–0.11 (m, 1H), 0.05–0.01 (m, 1H) ppm.

¹³C NMR (101 MHz, CDCl₃) δ 200.62, 137.61, 132.61, 128.39, 128.29, 82.99, 46.29, 37.60, 24.94, 24.85, 18.60, 4.86, 4.27 ppm.

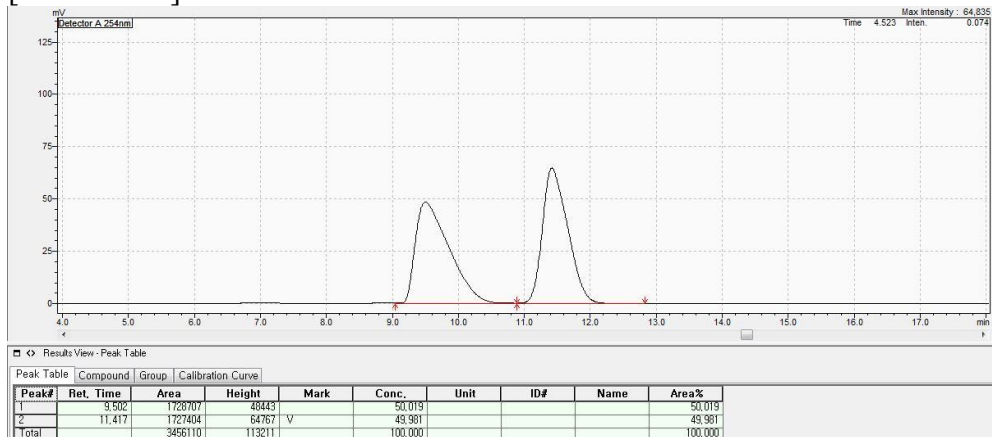
¹¹B NMR (128 MHz, CDCl₃) δ 33.25 ppm.

HRMS (ESI) calculated for [C₁₉H₂₇BO₃+H]⁺: 315.2126, found: 315.2135.

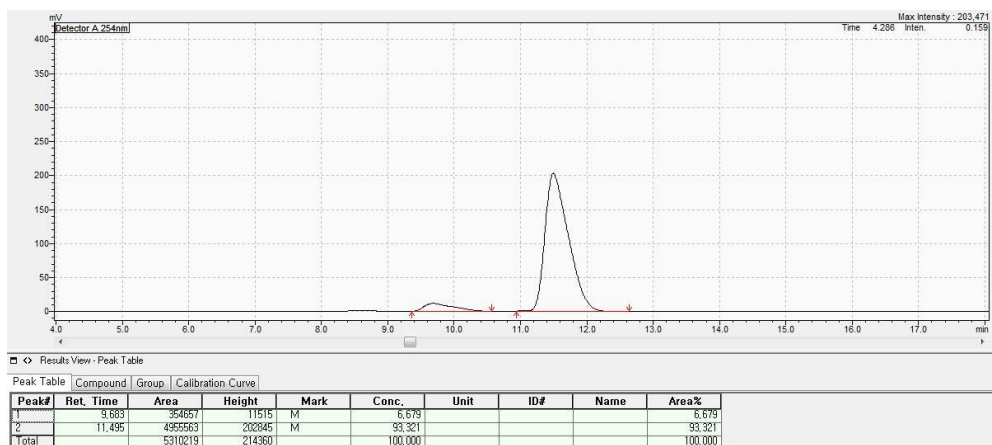
Optical rotation, [α]_D²² = -11.6 (c = 1.11, DCM).

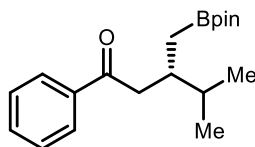
Enantiomeric excess, 87% ee was measured by HPLC (CHIRALCEL OD-H, *n*-hexane : *i*-PrOH = 99.7 : 0.3, 1.0 mL/min, wavelength = 254 nm, 28 °C); t_R = 11.49 min (major), t_R = 9.68 min (minor).

[Racemic 3o]



[Enantioenriched 3o]





(S)-4-methyl-1-phenyl-3-((4,4,5,5-tetramethyl-1,3,2-dioxaborolan-2-yl)methyl) pentan-1-one (3p) Following general procedure stirring for 36 hours instead of 11 hours, the crude product was purified by silica gel chromatography (hexanes : DCM = 50 : 50 \rightarrow 0 : 100, DCM : MeOH = 100 : 0 \rightarrow 99.5 : 0.5) to provide **3p** as a yellowish liquid (64 mg, 68%, 85% ee).

¹H NMR (400 MHz, CDCl₃) δ 8.02–7.98 (m, 2H), 7.56–7.50 (m, 1H), 7.48–7.40 (m, 2H), 2.97 (dd, J = 15.6, 7.1 Hz, 1H), 2.86 (dd, J = 15.6, 6.5 Hz, 1H), 2.33–2.23 (m, 1H), 1.78–1.64 (m, 1H), 1.22 (s, 6H), 1.21 (s, 6H), 0.88 (m, 1H), 0.87 (dd, J = 6.8, 1.7 Hz, 6H), 0.75 (dd, J = 15.7, 8.5 Hz, 1H) ppm.

¹³C NMR (101 MHz, CDCl₃) δ 200.82, 137.50, 132.60, 128.37, 128.26, 82.94, 42.67, 36.60, 31.84, 24.85, 24.81, 19.69, 18.36 ppm.

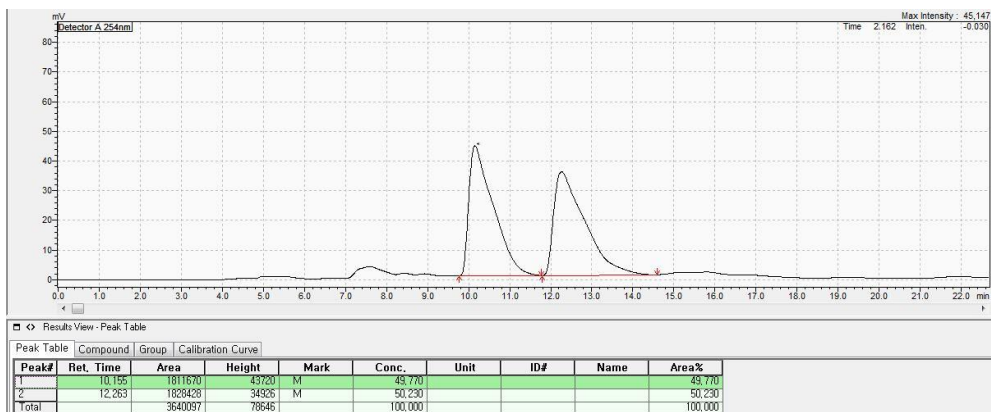
¹¹B NMR (128 MHz, CDCl₃) δ 34.20 ppm.

HRMS (ESI) calculated for [C₁₉H₂₉BO₃+H]⁺: 317.2282, found: 317.2292.

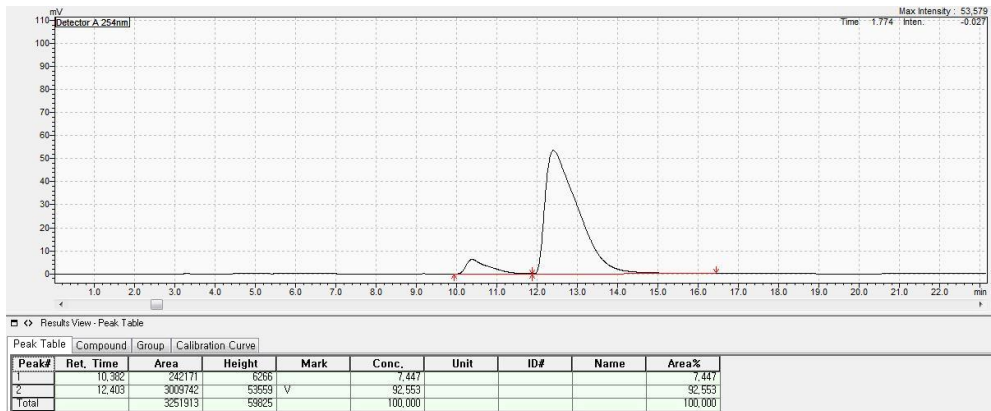
Optical rotation, $[\alpha]_D^{22} = -10.6$ ($c = 1.06$, DCM).

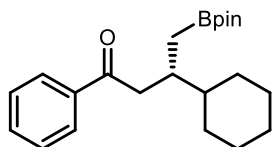
Enantiomeric excess, 85% ee was measured by HPLC (CHIRALCEL OD-H, *n*-hexane : *i*-PrOH = 99.3 : 0.7, 1.0 mL/min, wavelength = 254 nm, 28 °C); $t_R = 12.40$ min (major), $t_R = 10.38$ min (minor).

[Racemic 3p]



[Enantioenriched 3p]





(S)-3-cyclohexyl-1-phenyl-4-(4,4,5,5-tetramethyl-1,3,2-dioxaborolan-2-yl)butan-1-one (3q) Following general procedure stirring for 36 hours instead of 11 hours, the crude product was purified by silica gel chromatography (hexanes : DCM = 50 : 50 → 0 : 100, DCM : MeOH = 100 : 0 → 99.5 : 0.5) to provide **3q** as a colorless liquid (77 mg, 72%, 80% ee).

¹H NMR (400 MHz, CDCl₃) δ 8.03–7.96 (m, 2H), 7.56–7.49 (m, 1H), 7.47–7.40 (m, 2H), 2.94 (d, *J* = 6.8 Hz, 2H), 2.31–2.21 (m, 1H), 1.78–1.57 (m, 5H), 1.36–1.27 (m, 1H), 1.21 (s, 6H), 1.21 (s, 6H), 1.18 – 0.95 (m, 5H), 0.89 (dd, *J* = 15.7, 5.9 Hz, 1H), 0.79 (dd, *J* = 15.7, 8.1 Hz, 1H) ppm.

¹³C NMR (101 MHz, CDCl₃) δ 200.85, 137.52, 132.58, 128.36, 128.24, 82.90, 42.77, 42.69, 36.10, 30.11, 29.31, 26.75, 26.69, 26.68, 24.82, 24.79 ppm. The carbon bound to the boron was not detected due to quadrupolar relaxation.

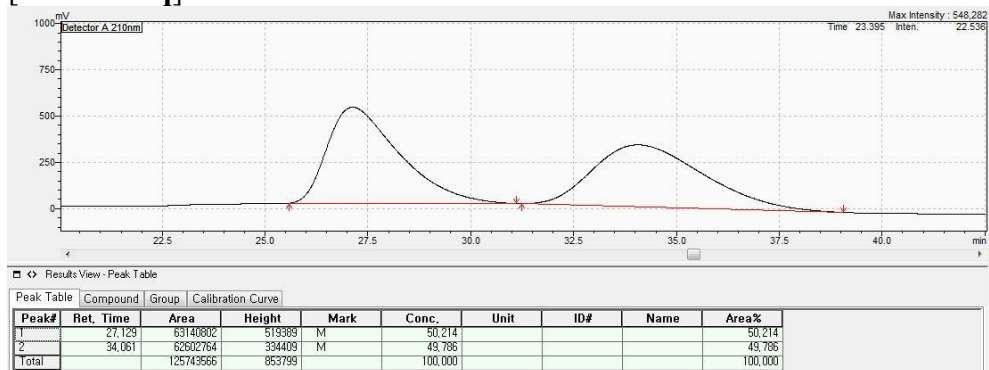
¹¹B NMR (128 MHz, CDCl₃) δ 33.29 ppm.

HRMS (ESI) calculated for [C₂₂H₃₃BO₃+H]⁺: 357.2595, found: 357.2610.

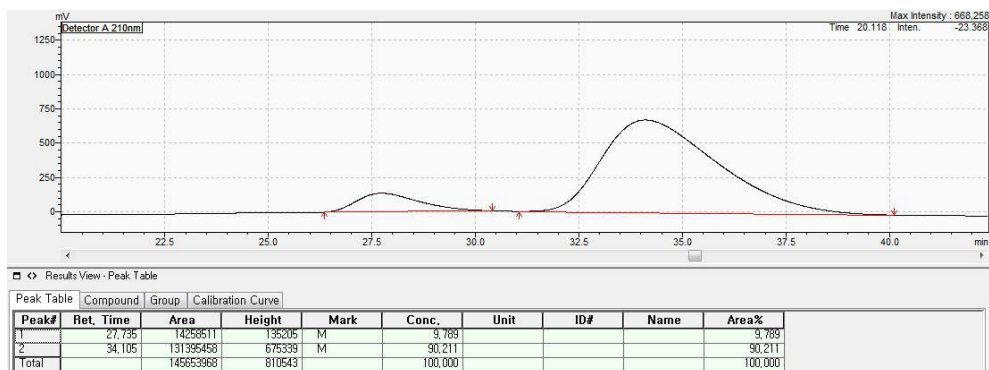
Optical rotation, [α]_D²² = –9.4 (c = 0.8, DCM).

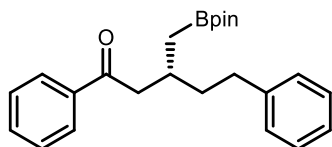
Enantiomeric excess, 80% ee was measured by HPLC (CHIRALCEL OJ-H, *n*-hexane : *i*-PrOH = 99.8 : 0.2), 0.2 mL/min, wavelength = 210 nm, 30 °C); t_R = 34.10 min (major), t_R = 27.73 min (minor).

[Racemic 3q]



[Enantioenriched 3q]





(R)-1,5-diphenyl-3-((4,4,5,5-tetramethyl-1,3,2-dioxaborolan-2-yl)methyl)pentan-1-one (3r) Following general procedure stirring for 36 hours instead of 11 hours, the crude product was purified by silica gel chromatography (hexanes : DCM = 50 : 50 \rightarrow 0 : 100, DCM : MeOH = 100 : 0 \rightarrow 99.5 : 0.5) to provide **3r** as a yellowish liquid (51 mg, 45%, 81% ee).

$^1\text{H NMR}$ (400 MHz, CDCl_3) δ 8.05–7.93 (m, 2H), 7.58–7.50 (m, 1H), 7.49–7.41 (m, 2H), 7.29–7.21 (m, 2H), 7.20–7.12 (m, 3H), 3.09 (dd, J = 15.6, 6.6 Hz, 1H), 2.93 (dd, J = 15.6, 7.0 Hz, 1H), 2.75–2.55 (m, 2H), 2.48–2.37 (m, 1H), 1.81–1.59 (m, 2H), 1.26 (s, 12H), 1.02 (dd, J = 15.8, 6.1 Hz, 1H), 0.95 (dd, J = 15.9, 7.2 Hz, 1H) ppm.

$^{13}\text{C NMR}$ (101 MHz, CDCl_3) δ 200.40, 142.61, 137.43, 132.72, 128.43, 128.30, 128.23 (2C), 125.56, 83.04, 45.42, 38.60, 33.28, 31.16, 24.88, 24.87 ppm. The carbon bound to the boron was not detected due to quadrupolar relaxation.

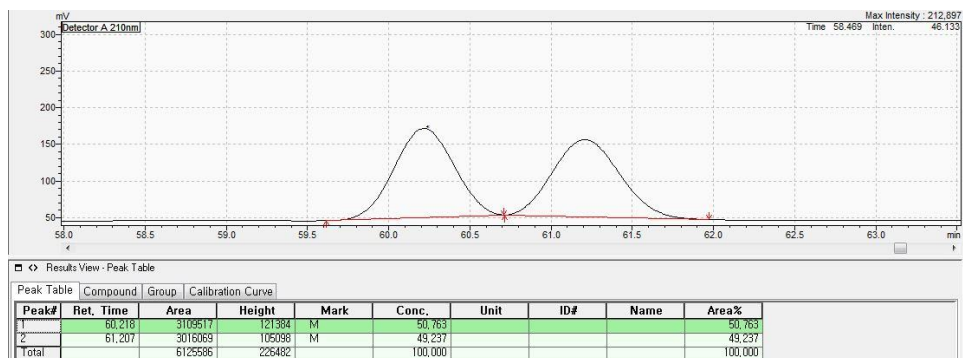
$^{11}\text{B NMR}$ (128 MHz, CDCl_3) δ 33.49 ppm.

HRMS (ESI) calculated for $[\text{C}_{24}\text{H}_{31}\text{BO}_3+\text{H}]^+$: 379.2439, found: 379.2448.

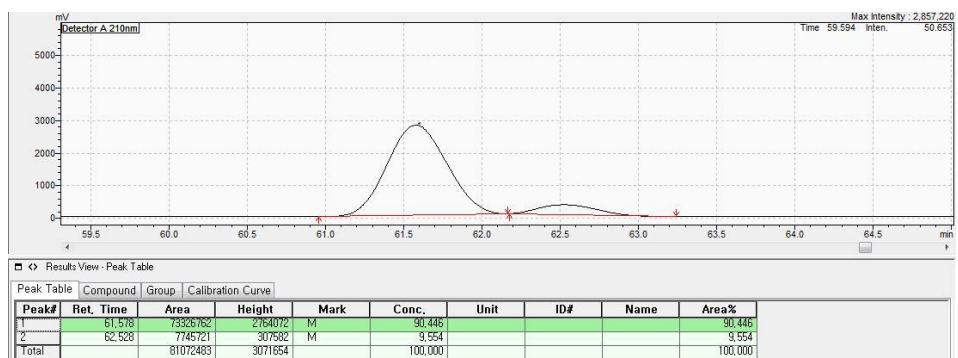
Optical rotation, $[\alpha]_{\text{D}}^{22} = +5.3$ (c = 0.28, DCM).

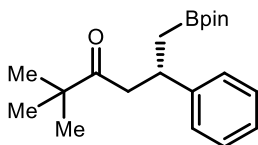
Enantiomeric excess, 81% ee was measured by HPLC (CHIRALPAK AD-H, *n*-hexane : *i*-PrOH = 98 : 2, 0.2 mL/min, wavelength = 210 nm, 30 °C); t_{R} = 61.57 min (major), t_{R} = 62.52 min (minor).

[Racemic 3r]



[Enantioenriched 3r]





(S)-2,2-dimethyl-5-phenyl-6-(4,4,5,5-tetramethyl-1,3,2-dioxaborolan-2-yl)hexan-3-one (3s) Following general procedure stirring for 36 hours instead of 11 hours, the crude product was purified by silica gel chromatography (hexanes : DCM = 100 : 0 → 0 : 100) to provide **3s** as a yellowish liquid (61 mg, 62%, 52% ee).

¹H NMR (500 MHz, CDCl₃) δ 7.24–7.18 (m, 4H), 7.16–7.10 (m, 1H), 3.52–3.43 (m, 1H), 2.81 (dd, *J* = 15.6, 5.6 Hz, 1H), 2.77 (dd, *J* = 15.7, 5.7 Hz, 1H), 1.19 (dd, *J* = 15.3, 6.5 Hz, 1H), 1.14–1.10 (m, 1H), 1.08 (s, 6H), 1.06 (s, 6H), 1.01 (s, 9H) ppm.

¹³C NMR (126 MHz, CDCl₃) δ 214.07, 146.69, 128.04, 127.33, 125.89, 82.91, 45.82, 43.96, 36.43, 26.03, 24.66, 24.57 ppm. The carbon bound to the boron was not detected due to quadrupolar relaxation.

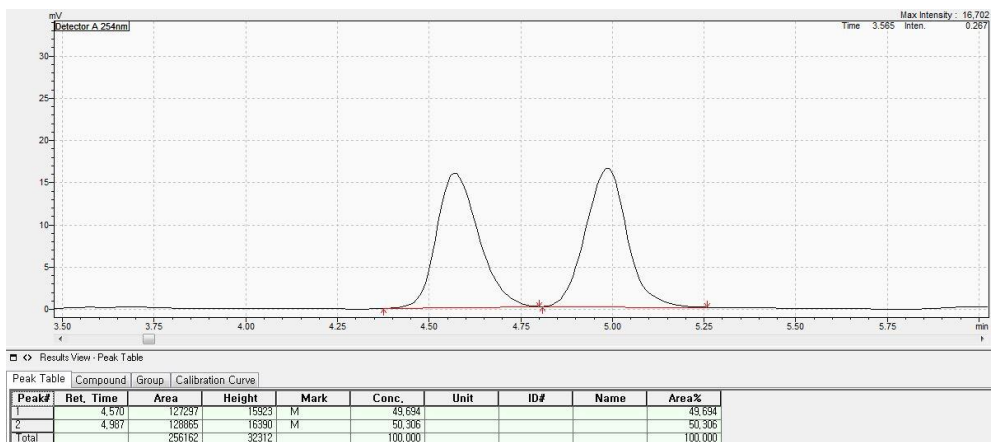
¹¹B NMR (128 MHz, CDCl₃) δ 32.40 ppm.

HRMS (ESI) calculated for [C₂₀H₃₁BO₃+H]⁺: 331.2439, found: 331.2441.

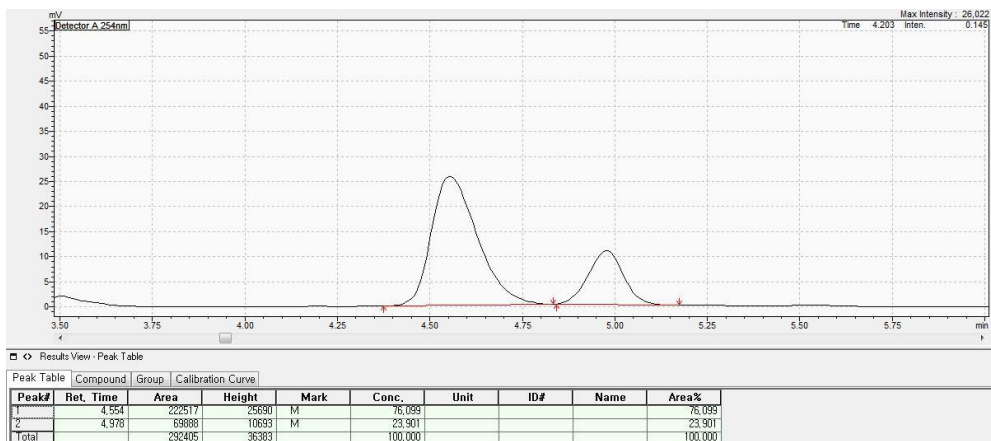
Optical rotation, [α]_D²² = +6.61 (c = 1.50, DCM).

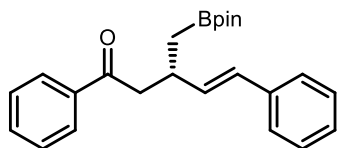
Enantiomeric excess, 52% ee was measured by HPLC (CHIRALPAK IA, *n*-hexane : *i*-PrOH = 99 : 1, 1.0 mL/min, wavelength = 254 nm, 28 °C); t_R = 4.97 min (major), t_R = 4.55 min (minor).

[Racemic product 3s]



[Enantioenriched 3s]





(R)-1,5-diphenyl-3-((4,4,5,5-tetramethyl-1,3,2-dioxaborolan-2-yl)methyl)pentan-1-one (3t) Following general procedure stirring for 36 hours instead of 11 hours, the crude product was purified by silica gel chromatography (hexanes : DCM = 50 : 50 \rightarrow 0 : 100, DCM : MeOH = 100 : 0 \rightarrow 99.5 : 0.5) to provide **3t** as a yellowish solid (54 mg, 48%, 75% ee).

$^1\text{H NMR}$ (400 MHz, CDCl_3) δ 8.01–7.92 (m, 2H), 7.57–7.49 (m, 1H), 7.47–7.39 (t, $J = 7.6$ Hz, 2H), 7.30–7.20 (m, 4H), 7.18–7.11 (m, 1H), 6.37 (d, $J = 15.9$ Hz, 1H), 6.20 (dd, $J = 15.9, 7.5$ Hz, 1H), 3.23–3.12 (m, 2H), 3.10–3.00 (m, 1H), 1.20 (s, 12H), 1.12 (dd, $J = 15.6, 6.0$ Hz, 1H), 1.05 (dd, $J = 15.7, 7.5$ Hz, 1H) ppm.

$^{13}\text{C NMR}$ (101 MHz, CDCl_3) δ 199.35, 137.55, 137.36, 134.81, 132.80, 128.85, 128.48, 128.35, 128.22, 126.87, 126.10, 83.15, 46.00, 35.11, 24.94, 24.79 ppm. The carbon bound to the boron was not detected due to quadrupolar relaxation.

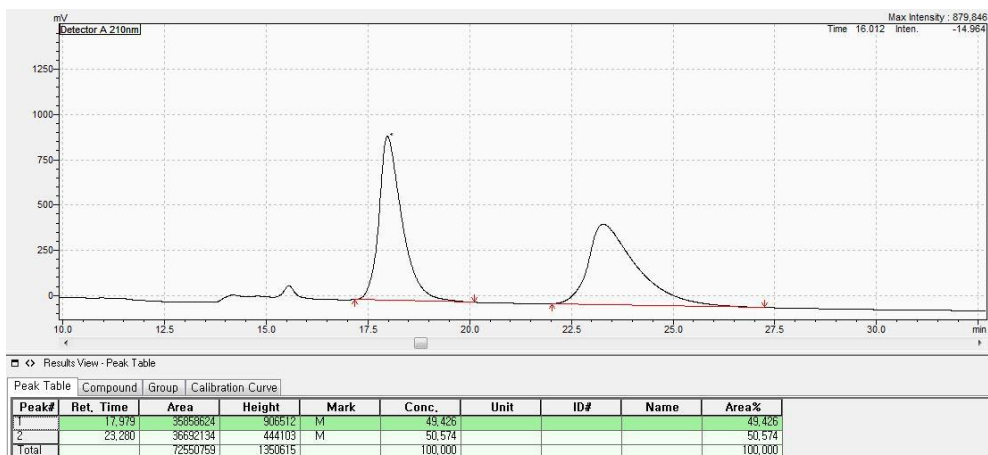
$^{11}\text{B NMR}$ (128 MHz, CDCl_3) δ 33.07 ppm.

HRMS (ESI) calculated for $[\text{C}_{24}\text{H}_{29}\text{BO}_3+\text{H}]^+$: 377.2282, found: 377.2279.

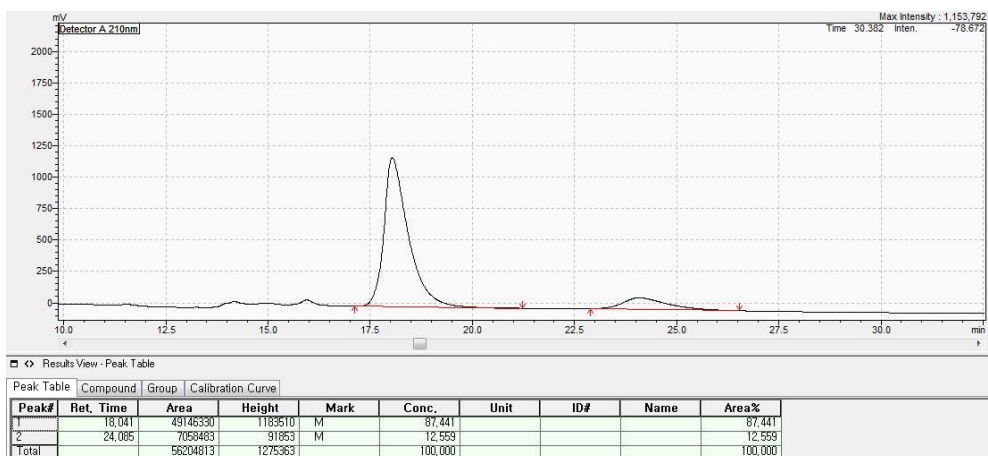
Optical rotation, $[\alpha]_{\text{D}}^{22} = +12.9$ ($c = 0.88$, DCM).

Enantiomeric excess, 75% ee was measured by HPLC (CHIRALPAK IA, *n*-hexane : *i*-PrOH = 99.8 : 0.2, 0.6 mL/min, wavelength = 210 nm, 30 °C); $t_{\text{R}} = 18.04$ min (major), $t_{\text{R}} = 24.08$ min (minor).

[Racemic product 3t]

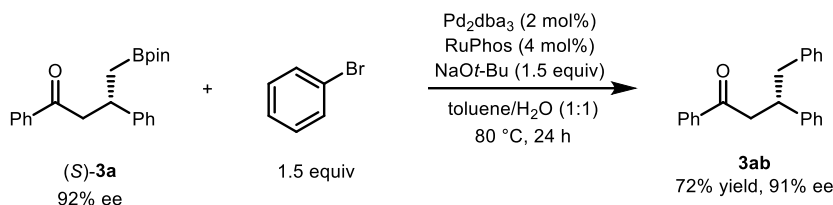


[Enantioenriched 3t]



3.5.5. General Procedure for Further Derivatizations

3.5.5.1. Palladium-catalysed cross coupling



(S)-(-)-1,3,4-triphenylbutan-1-one (3ab).⁴

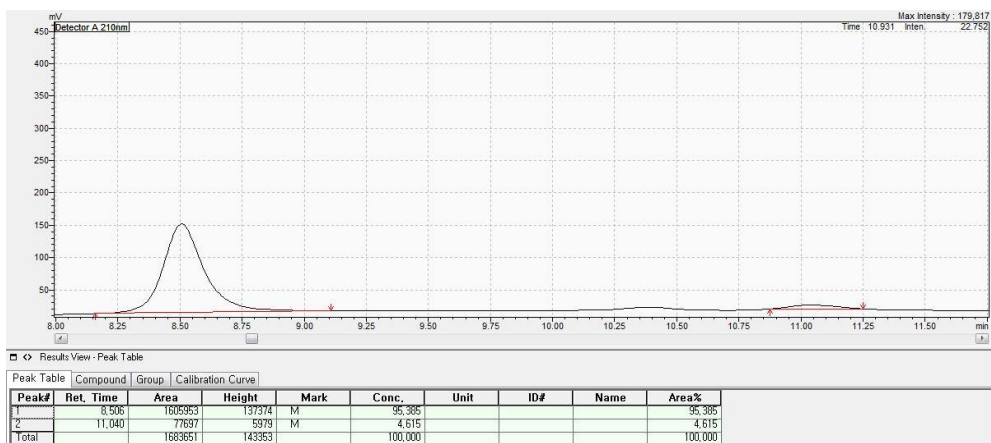
In a nitrogen-filled glove box, an oven-dried 4 mL dram-vial was charged with a magnetic stir bar, (S)-3a (92% ee, 0.47 mmol, 1.0 equiv, 164 mg), Pd₂dba₃ (0.009 mmol, 2 mol%, 8.7 mg), RuPhos (0.019 mmol, 4 mol%, 8.8 mg), NaOt-Bu (1.9 mmol, 4.0 equiv, 179 mg), and bromobenzene (0.71 mmol, 1.5 equiv, 73 μ L). Subsequently, anhydrous toluene (1.6 mL) was added to the mixture via a syringe and the system was sealed with an open-top teflon faced screw cap. The vial was removed from the glovebox and then, H₂O (0.16 mL) was added. The reaction mixture was vigorously stirred for 24 hours at 80 °C. Upon completion of the reaction, the reaction mixture was cooled to room temperature and brine (20 mL) was added in one portion to quench the reaction. The aqueous phase was separated and extracted with ethyl acetate (3 \times 20 mL). The combined organic phase was dried over anhydrous sodium sulfate (Na₂SO₄), filtered, and concentrated under reduced pressure. The crude product was purified by flash column chromatography on

silica gel (hexanes : EtOAc = 100 : 0 → hexanes : EtOAc = 97 : 3) to provide **3ab** (95 mg, 72%, 91% ee). **¹H NMR** (400 MHz, CDCl₃) δ 7.90–7.82 (m, 2H), 7.56–7.49 (m, 1H), 7.46–7.37 (m, 2H), 7.31–7.13 (m, 8H), 7.12–7.05 (m, 2H), 3.74–3.63 (m, 1H), 3.36 (dd, *J* = 16.8, 7.3 Hz, 1H), 3.29 (dd, *J* = 16.8, 6.6 Hz, 1H), δ 3.02 (dd, *J* = 13.9, 7.6 Hz, 1H), 2.97 (dd, *J* = 13.7, 8.0 Hz, 1H). **¹³C NMR** (101 MHz, CDCl₃) δ 197.53, 173.79, 138.36, 136.35, 133.29, 128.90, 128.58, 128.05, 127.81, 127.55, 52.26, 46.34, 42.78 ppm. **Enantiomeric excess**, 91% ee was measured by HPLC (CHIRALPAK IA, *n*-hexane : *i*-PrOH = 98.5 : 1.5 → 98:2, 1.0 mL/min, wavelength = 210 nm, 30 °C); *t*_R = 8.51 min (major), *t*_R = 11.04 min (minor); [α]_D²² = -5.5 (c = 0.72, DCM).

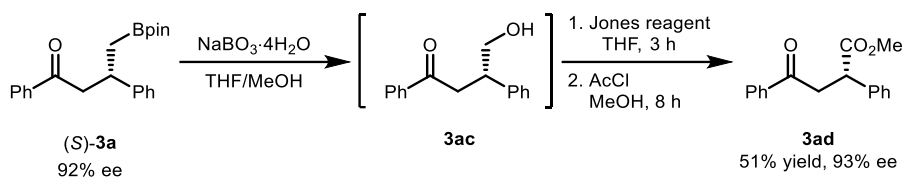
[Racemic 3ab]



[Enantioenriched 3ab]



3.5.5.2. Oxidation and esterification.

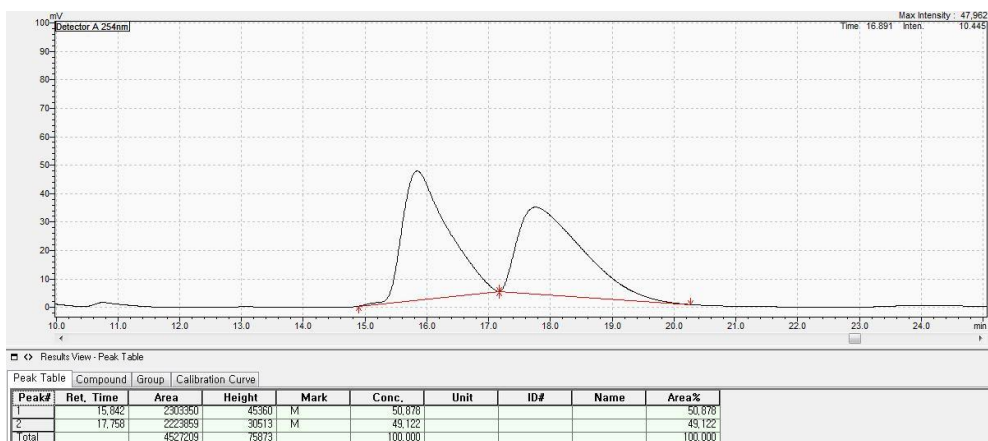


Methyl (*S*)-4-oxo-2,4-diphenylbutanoate (3ad).⁵

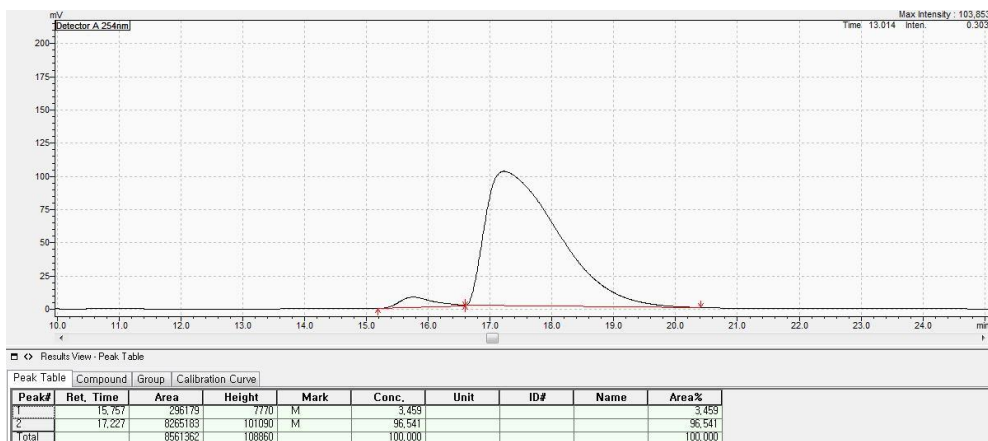
A 4 mL dram-vial containing a magnetic stir bar was charged with (*S*)-**3a** (92% ee, 0.37 mmol, 1.0 equiv, 128 mg) and NaBO₃·4H₂O (0.74 mmol, 2.0 equiv, 114 mg). Subsequently, 1.6 mL of THF/MeOH mixture (v/v = 1:1) were added to the mixture via a syringe. The reaction mixture was vigorously stirred for 4 hours. Upon completion of the reaction, brine (10 mL) was added in one portion to quench the reaction. The aqueous phase was separated and extracted with ethyl acetate (3 × 10 mL). The combined organic phase was dried over anhydrous sodium sulfate (Na₂SO₄), filtered, and concentrated under reduced pressure. Subsequently, the crude product was dissolved in THF (0.8 mL) and then, 2.5 M Jones reagent (CrO₃/H₂SO₄, 0.56 mmol, 1.5 equiv, 0.23 mL) was added. After stirring 3 hours, brine (10 mL) was added in one portion to quench the reaction. The aqueous phase was separated and extracted with ethyl acetate (3 × 10 mL). The combined organic phase was dried over anhydrous sodium sulfate (Na₂SO₄), filtered, and concentrated *in vacuo*. The crude product was dissolved in MeOH (1 mL) and acetyl chloride

(AcCl) (0.74 mmol, 2.0 equiv, 52 μ L) was added to the reaction mixture. After stirring for 8 hours, the reaction mixture was diluted with brine (10 mL), extracted with ethyl acetate (3×20 mL). The organic layer was dried over anhydrous sodium sulfate (Na_2SO_4), and concentrated under reduced pressure. The resulting residue was purified by flash column chromatography (hexanes : EtOAc = 100 : 0 \rightarrow hexanes : EtOAc = 75 : 25) to provide **3ad** (51 mg, 51%, 93% ee). **^1H NMR** (400 MHz, CDCl_3) δ 8.02–7.93 (m, 2H), 7.60–7.53 (m, 1H), 7.50–7.42 (m, 2H), 7.41–7.26 (m, 5H), 4.31 (dd, $J = 10.3, 4.1$ Hz, 1H), 3.96 (dd, $J = 18.0, 10.3$ Hz, 1H), 3.70 (s, 3H), 3.28 (dd, $J = 18.0, 4.1$ Hz, 1H) ppm. **^{13}C NMR** (101 MHz, CDCl_3) δ 197.58, 173.81, 138.31, 136.35, 133.28, 128.88, 128.56, 128.05, 127.79, 127.52, 52.31, 46.32, 42.77 ppm. **Enantiomeric excess**, 93% ee was measured by HPLC (CHIRALCEL OD-H, *n*-hexane : *i*-PrOH = 98.3 : 1.7, 1.0 mL/min, wavelength = 254 nm, 28 $^\circ\text{C}$); $t_{\text{R}} = 17.22$ min (major), $t_{\text{R}} = 15.75$ min (minor); $[\alpha]_{\text{D}}^{22} = +84.4$ ($c = 0.73$, DCM).

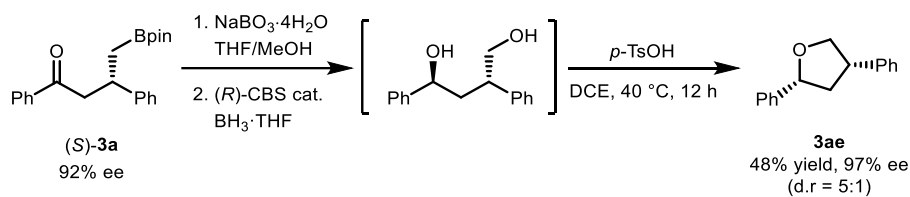
[Racemic 3ad]



[Enantioenriched 3ad]



3.5.5.3. Oxidation, reduction and acid-catalysed ring formation.

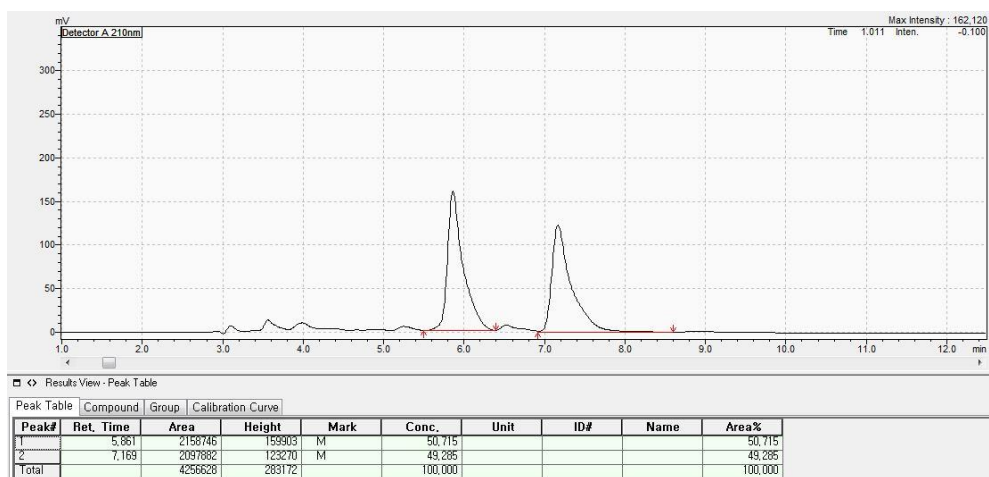


(2*R*,4*S*)-2,4-diphenyltetrahydrofuran (*ent*-Calyxolane B, **3ae**).⁶

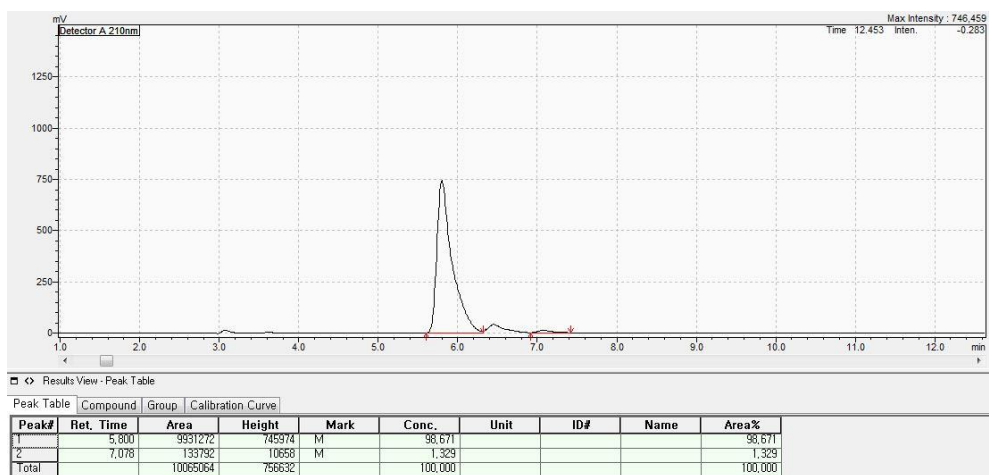
A 4 mL dram-vial containing a magnetic stir bar was charged with (*S*)-**3a** (92% ee, 0.37 mmol, 1.0 equiv, 128 mg), NaBO₃·4H₂O (0.74 mmol, 2.0 equiv, 114 mg). Subsequently, 1.6 mL of THF/MeOH mixture (v/v = 1:1) were added to the mixture via a syringe. The reaction mixture was vigorously stirred for 4 hours. Upon completion of the reaction, brine (10 mL) was added in one portion to quench the reaction. The aqueous phase was separated and extracted with ethyl acetate (3 × 10 mL). The combined organic phase was dried over anhydrous sodium sulfate (Na₂SO₄), filtered, and concentrated under reduced pressure. The resulting mixture was dissolved in THF (0.3 mL). To an another 4 ml vial containing a magnetic stir bar were added (*R*)-CBS catalyst (0.08 mmol, 20 mol%, 22 mg) and anhydrous THF (0.5 mL). Subsequently, BH₃·THF solution (1.0 M in THF, 0.74 mmol, 2.0 equiv, 0.74 mL) solution was added to the reaction mixture at 0 °C. After stirring for 30 mins, the crude mixture was added to the vial containing pre-activated (*R*)-CBS catalyst solution. The system was vigorously stirred for 8 hours at room temperature. Upon completion of the reaction, brine (10 mL) was added in

one portion to quench the reaction. The aqueous phase was separated and extracted with ethyl acetate (3×10 mL). The combined organic phase was dried over anhydrous sodium sulfate (Na_2SO_4), filtered, and concentrated under reduced pressure. The crude product (diol) and PTSA (0.04 mmol, 10 mol%, 6.9 mg) was dissolved in 1,2-DCE (1 mL) and stirred for 12 hours at 40 °C. Upon completion of the reaction, brine (10 mL) was added to quench the reaction. The aqueous phase was separated and extracted with ethyl acetate (3×10 mL). The organic layer, which was dried by sodium sulfate Na_2SO_4 , was concentrated *in vacuo*. The concentrated crude product was purified by flash column chromatography (Petroleum ether : EtOAc = 100 : 0 \rightarrow Petroleum ether : EtOAc = 98 : 2) to provide **3ae** (40 mg, 48%, 97% ee). The *rac*-**3ae** was synthesized using *rac*-**3a**; ketone reduction was performed using NaBH_4 (0.6 mmol, 200 mol%, 23mg) instead of (*R*)-CBS catalyst. **¹H NMR** (400 MHz, CDCl_3) δ 7.46–7.17 (m, 10H), 5.08 (dd, $J = 10.2, 5.7$ Hz, 1H), 4.37 (t, $J = 8.3$ Hz, 1H), 4.03 (t, $J = 8.5$ Hz, 1H), 3.75–3.58 (m, 1H), 2.84–2.74 (m, 1H), 2.11–1.98 (m, 1H) ppm. **¹³C NMR** (101 MHz, CDCl_3) δ 142.65, 141.70, 128.61, 128.43, 127.40, 127.25, 126.65, 125.71, 81.84, 75.11, 46.03, 43.73 ppm. **Enantiomeric excess**, 97% ee was measured by HPLC (CHIRALCEL OD, *n*-hexane : *i*-PrOH = 90 : 10, 1.0 mL/min, wavelength = 210 nm, 30 °C); $t_R = 5.80$ min (major), $t_R = 7.08$ min (minor); $[\alpha]_D^{22} = +46.4$ ($c = 0.61$, DCM).

[Racemic product of 3ae]



[Enantioenriched product of 3ae]



3.5.6. ^{31}P and ^{11}B NMR studies

3.5.6.1. In situ monitoring of reaction system by ^{31}P NMR spectroscopies

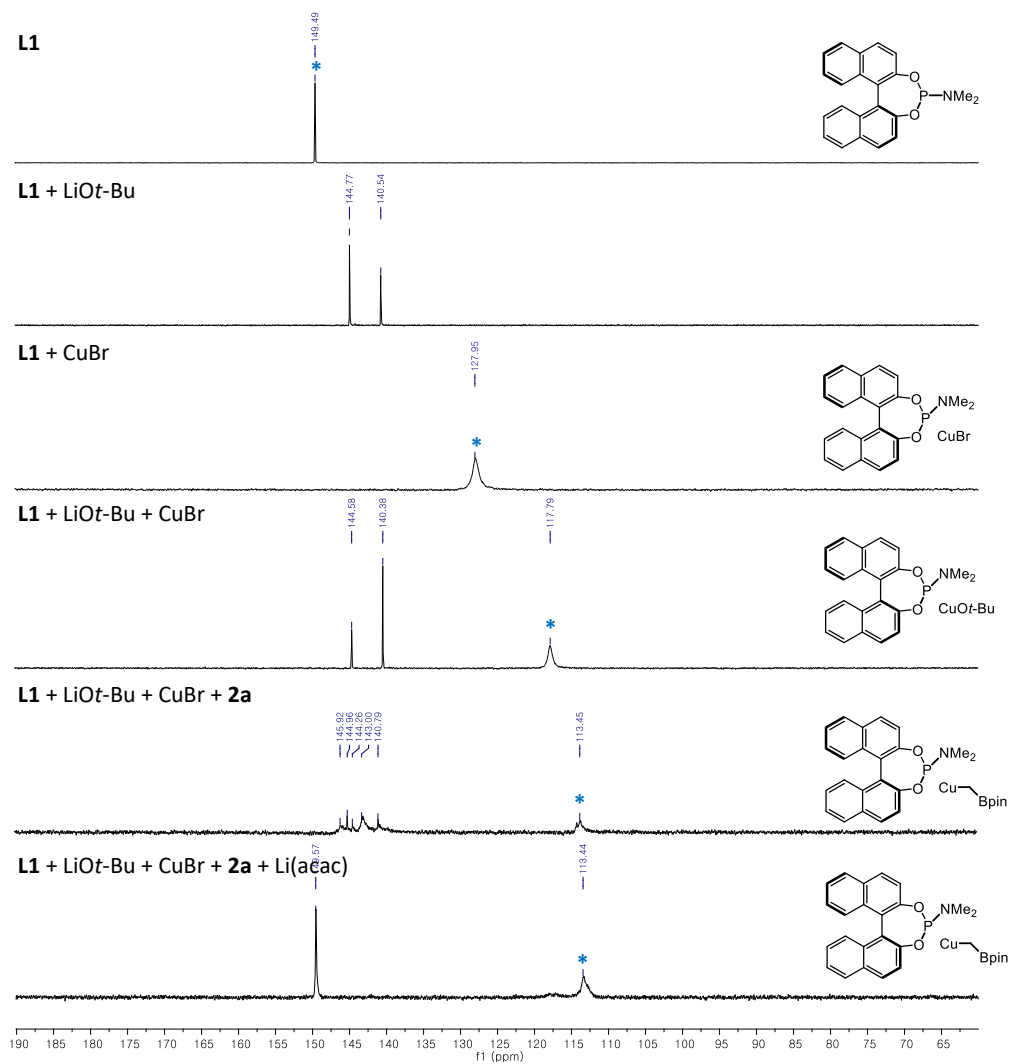


Figure S3.1. ^{31}P NMR spectra (162 MHz, THF- d_8 , rt) of the reaction mixture

3.5.6.2. Monitoring of ligand decomposition over time by ^{31}P NMR spectroscopies

L1 + LiOt-Bu + CuBr + **2a** + Li(acac)

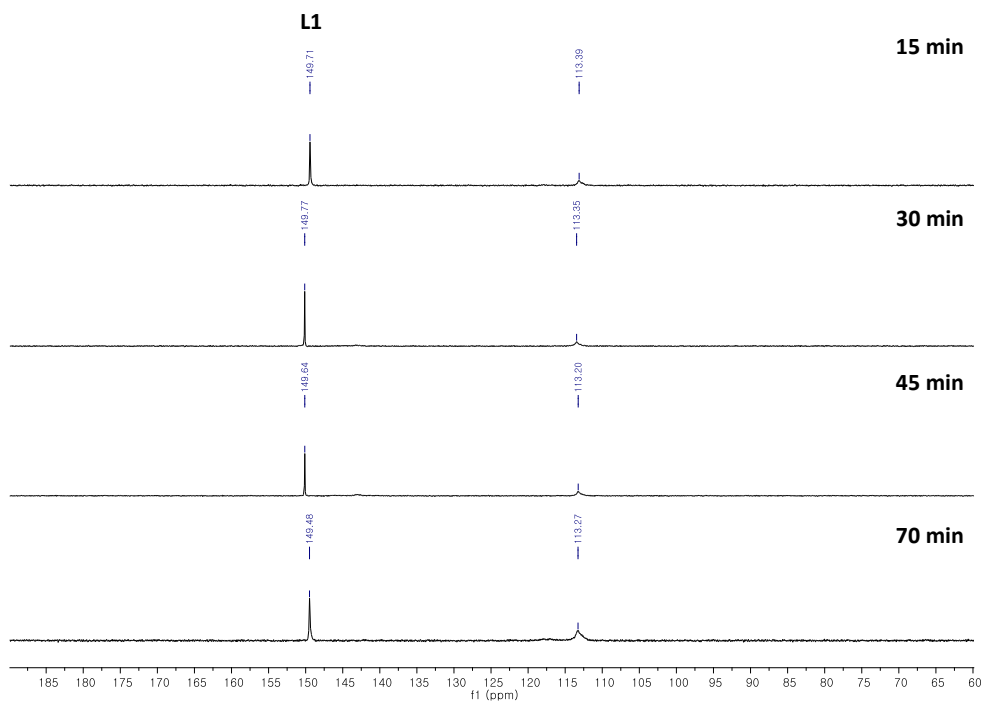


Figure S3.2. ^{31}P NMR spectra (162 MHz, THF- d_8 , rt) of the reaction mixture in the presence of Li(acac).

L1 + LiOt-Bu + CuBr + 2a

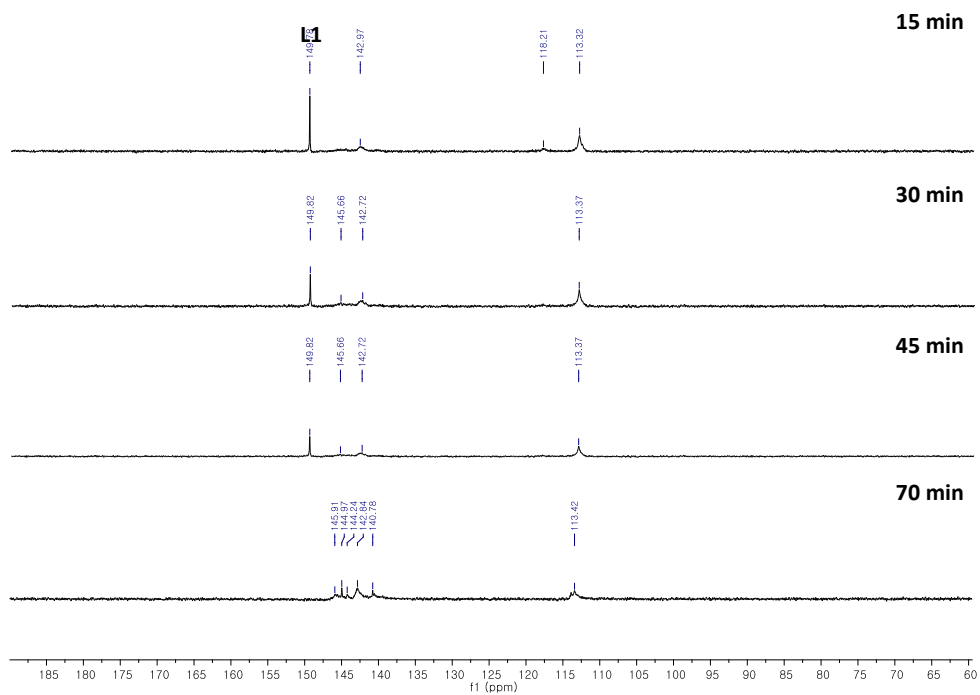
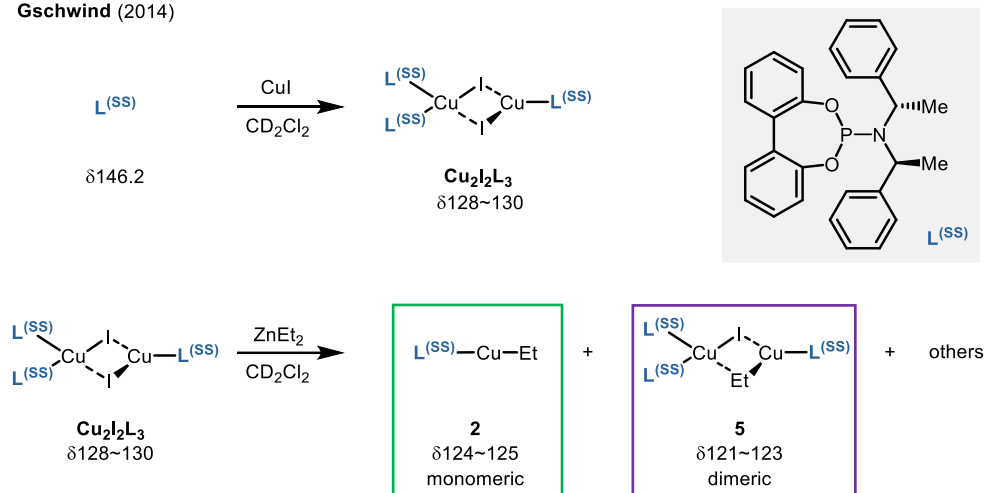


Figure S3.3. ^{31}P NMR spectra (162 MHz, THF- d_8 , rt) of the reaction mixture in the absence of Li(acac)

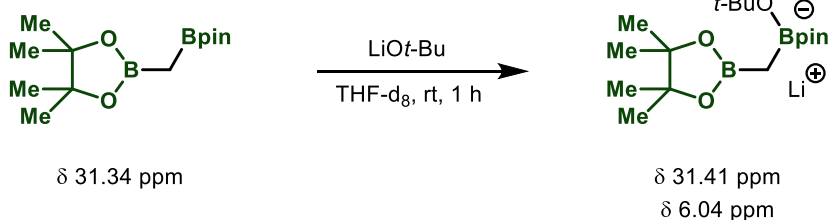
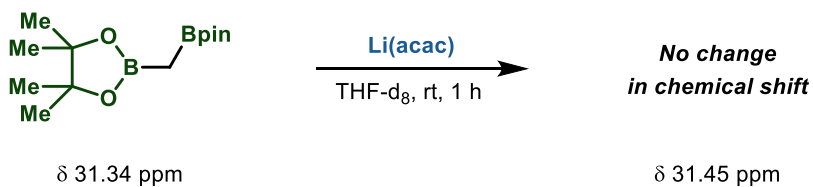
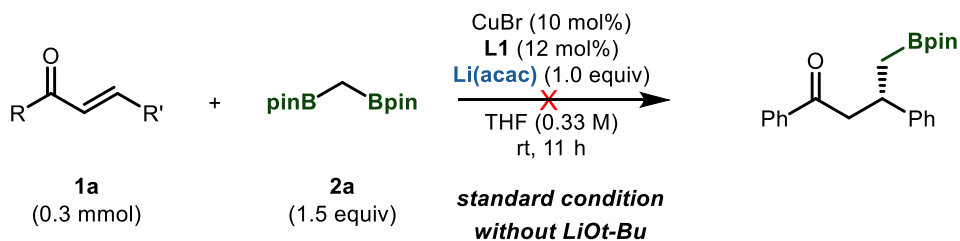
3.5.6.3. A related phosphoramidite-based copper-alkyl species.⁷

Gschwind (2014)

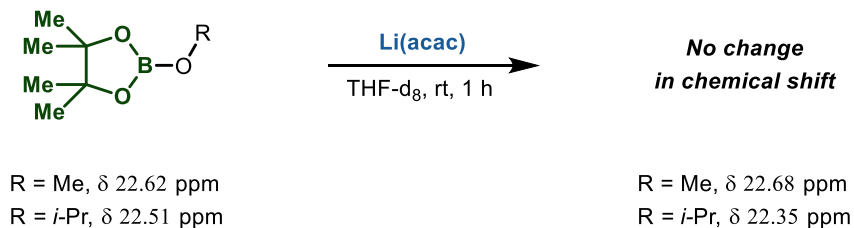


3.5.6.4. Studies to elucidate the role of Li(acac).

- Viability of Li(acac) as a better activator than LiOt-Bu



- Possibility of Li(acac) sequestering borate by-product



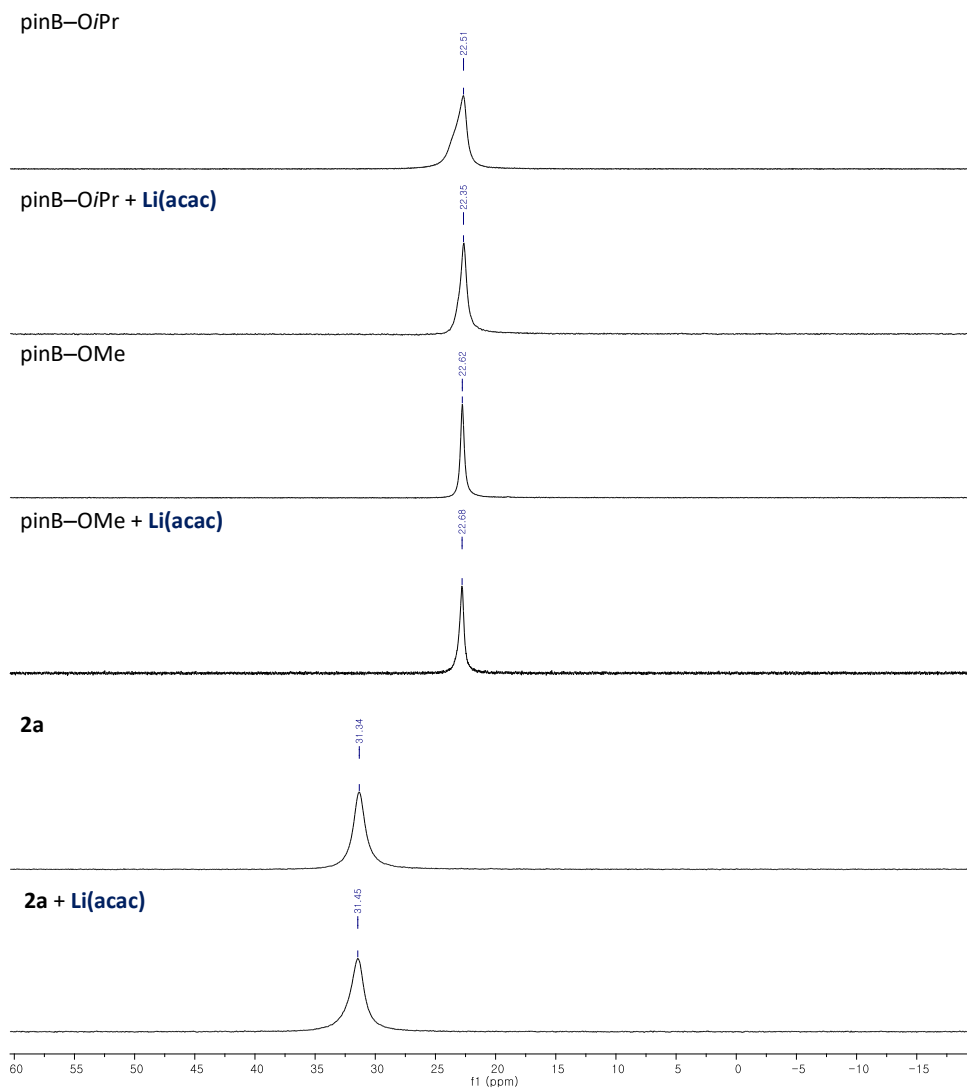
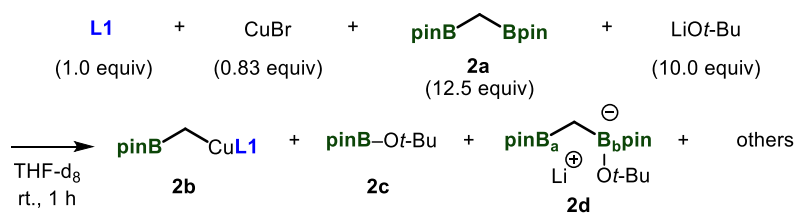


Figure S3.4. ^{11}B NMR spectra (128 MHz, THF- d_8 , rt) of the reaction mixture

3.5.6.5. In situ monitoring of reaction system by ^{11}B NMR spectroscopies



In a nitrogen-filled glove box, an oven-dried 4 mL dram-vial was charged with a magnetic stir bar, **L1** (0.012 mmol, 1.0 equiv), CuBr (0.83 equiv), 1,1-bis[(pinacolato)boryl]methane (**2a**, 12.5 equiv), LiOt-Bu (10 equiv) and Li(acac) (8.3 equiv). Subsequently, THF- d_8 (0.5 mL) was added to the mixture via a syringe and the system was sealed with a screw cap. After stirring for 1 hour, the reaction mixture was transferred to an NMR tube equipped with a J-Young valve. The valve was closed and then, the NMR tube was removed from the glovebox. ^{11}B NMR spectra were obtained immediately. For the control experiment, the same procedure was conducted in the absence of Li(acac). **A** = neutral Bpin species, including **2a**, **2b**, and **2d-B_a**, **B** = anionic complexes, including **2d-B_b**.

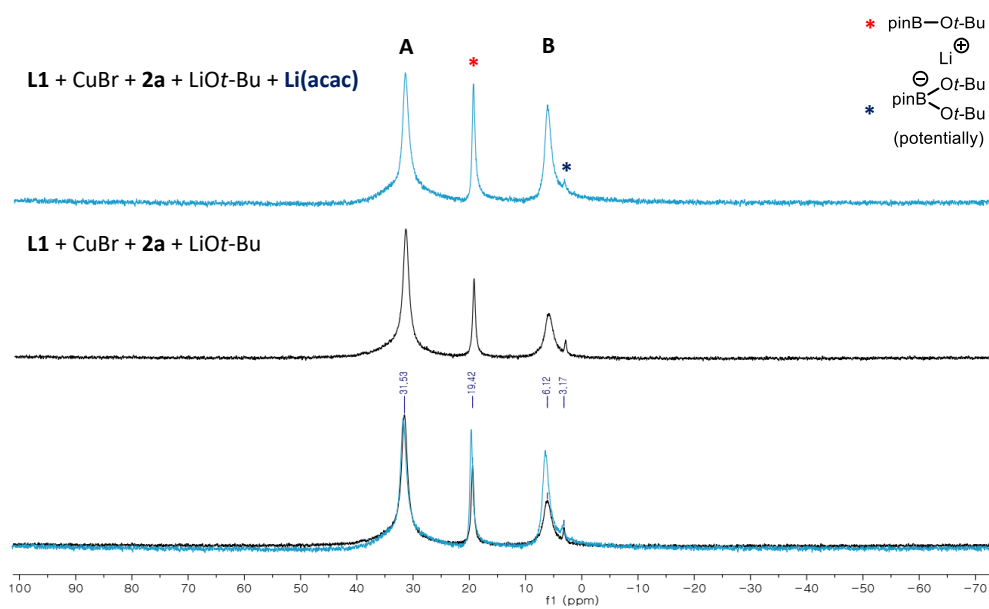
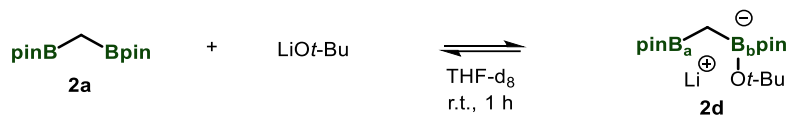


Figure S3.5. ^{11}B NMR spectra (128 MHz, THF- d_8 , rt) of the reaction mixture

3.5.6.6. In situ monitoring of equilibrium of **2a** with Li*O**t*-Bu by ¹¹B NMR spectroscopies



In a nitrogen-filled glove box, an oven-dried 4 mL dram-vial was charged with a magnetic stir bar, 1,1-bis[(pinacolato)boryl]methane (**2a**, 1.25 equiv, 0.15 mmol), Li*O**t*-Bu (1.0 equiv), Li(acac) (0.83 equiv). Subsequently, THF-*d*₈ (0.5 mL) was added to the mixture via a syringe and the system was sealed with a screw cap. After stirring for 1 hour, the reaction mixture was transferred to an NMR tube equipped with a J-Young valve. The valve was closed and then, the NMR tube was removed from the glovebox. ¹¹B NMR spectra were obtained immediately. For the control experiment, the same procedure was conducted in the absence of Li(acac). **A** = neutral Bpin species, including **2a**, **2b**, and **2d-B_a**, **B** = anionic complexes, including **2d-B_b**.

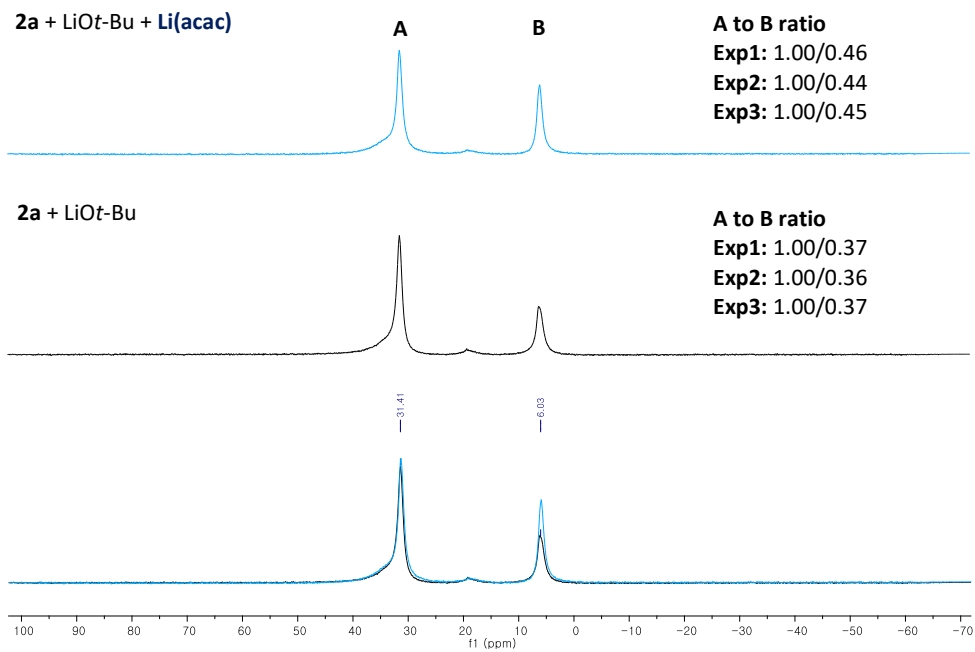
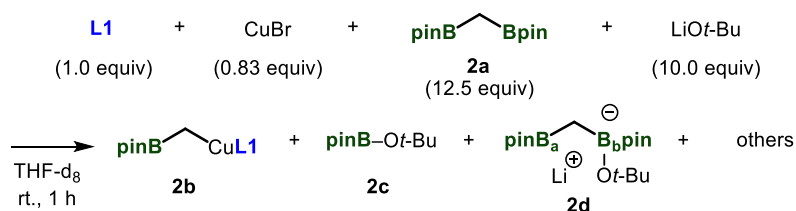
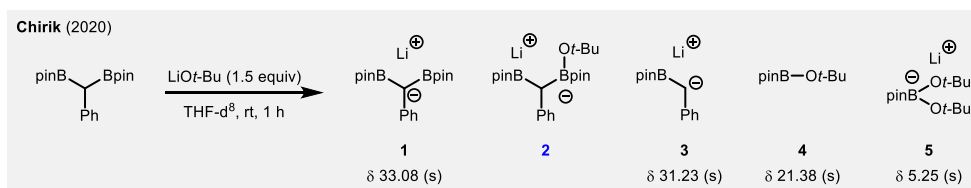
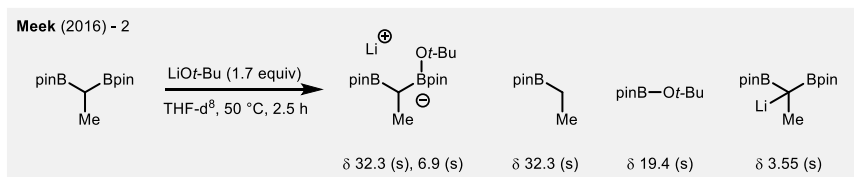
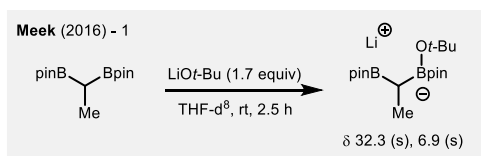


Figure S3.6. ^{11}B NMR spectra (128 MHz, THF- d_8 , rt) of the reaction mixture

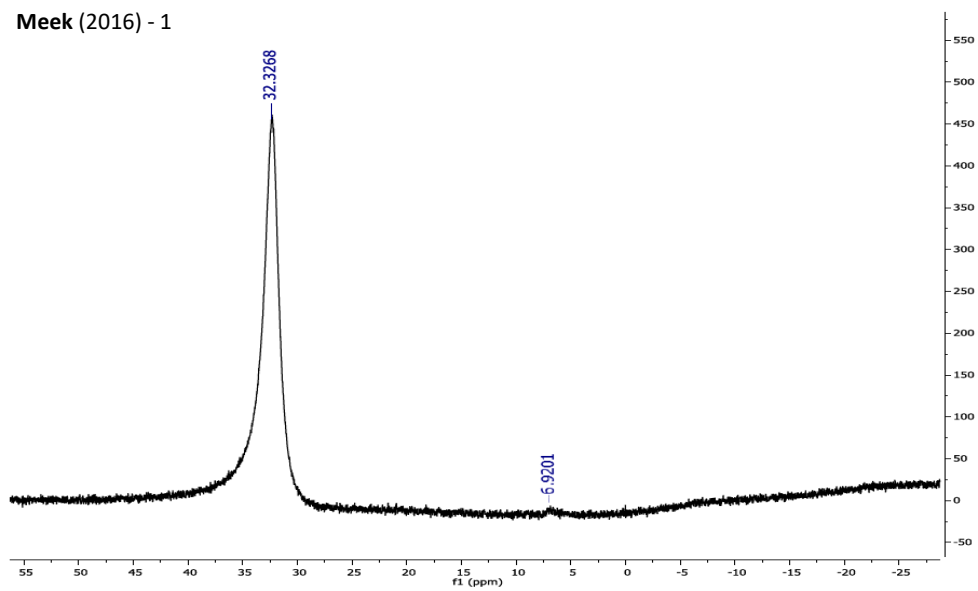
3.5.6.7. Identification of borate derivatives



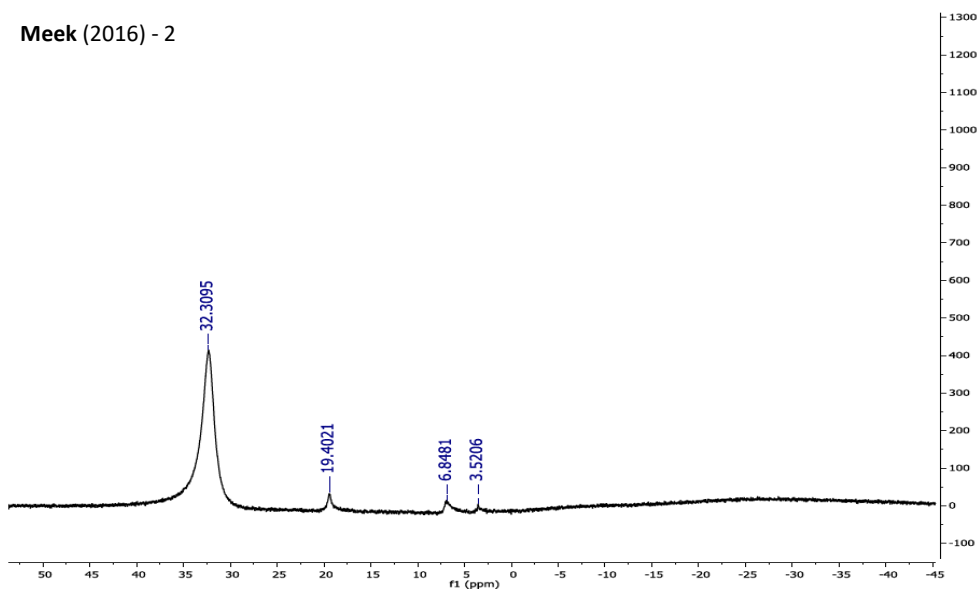
The following ^{11}B NMR data are reported (Meek 2016 and Chirik 2020).^{8,9} The ^{11}B NMR spectrum of the reaction mixture consists of three major signals originating from C-ligated neutral Bpin species (δ 31.5 ppm), including **2a**, **2b**, and **2d-B_a**, heteroatom-bound neutral Bpin species (**2c**, δ 19.4 ppm), and anionic complexes, such as **2d-B_b** (δ 6.12 ppm) or $\text{Li}[\text{pinB}(\text{Ot-Bu})_2]$ (δ 3.17 ppm).



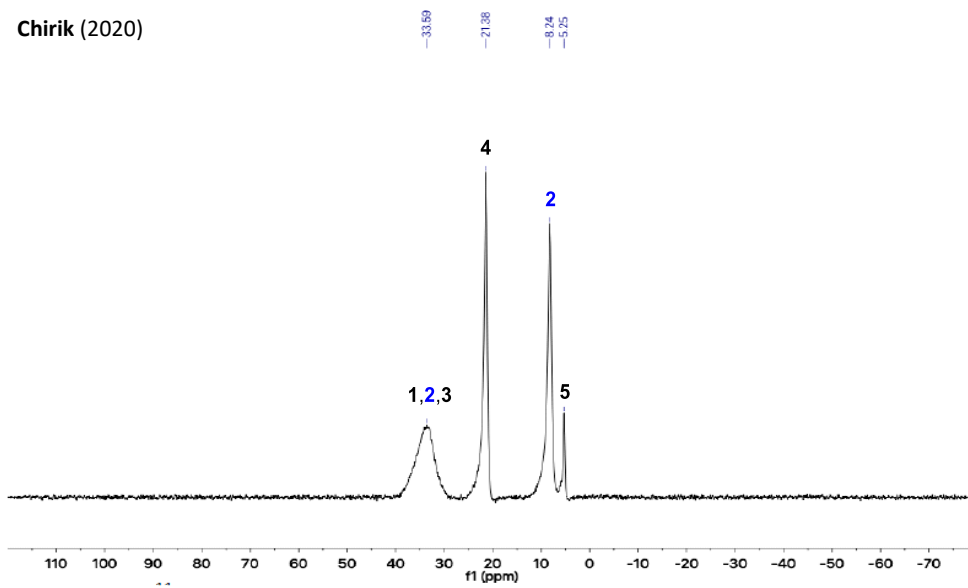
Meek (2016) - 1



Meek (2016) - 2

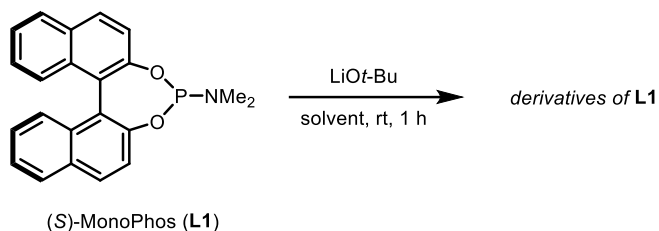


Chirik (2020)



3.5.7. Preliminary Mass Spectroscopic Data (HRMS)

3.5.7.1. General procedure for monitoring of decomposition pathway of (S)-MonoPhos



Condition A. In a nitrogen-filled glove box, an oven-dried 4 mL dram-vial was charged with a magnetic stir bar, (S)-MonoPhos (0.012 mmol, 1.0 equiv). Subsequently, acetonitrile (0.5 mL) was added to the mixture via a syringe and the system was sealed with a screw cap. After stirring for 1 hour, the mixture was diluted in acetonitrile for HRMS analysis. HRMS were recorded within 1 hour.

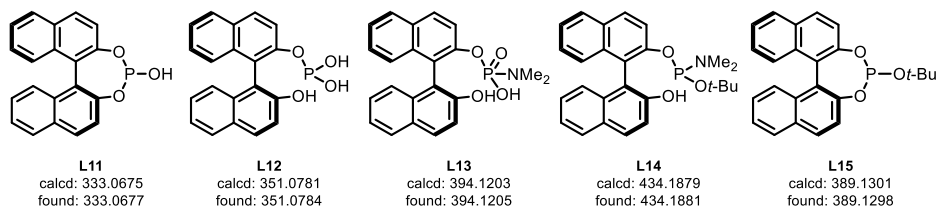
Condition B. In a nitrogen-filled glove box, an oven-dried 4 mL dram-vial was charged with a magnetic stir bar, (S)-MonoPhos (0.012 mmol, 1.0 equiv), and LiOt-Bu (10 equiv). Subsequently, anhydrous THF (0.5 mL) was added to the mixture via a syringe and the system was sealed with a screw cap. After stirring for 1 hour, the reaction mixture was filtered and concentrated under reduced pressure. The filtrate was diluted in acetonitrile for HRMS analysis. HRMS were recorded within 1 hour.

Condition C. In a nitrogen-filled glove box, an oven-dried 4 mL dram-vial was charged with a magnetic stir bar, (*S*)-MonoPhos (0.012 mmol, 1.0 equiv), and LiO*t*-Bu (10 equiv). Subsequently, acetonitrile (0.5 mL) was added to the mixture via a syringe and the system was sealed with a screw cap. After stirring for 1 hour, the vial was removed from the glovebox.

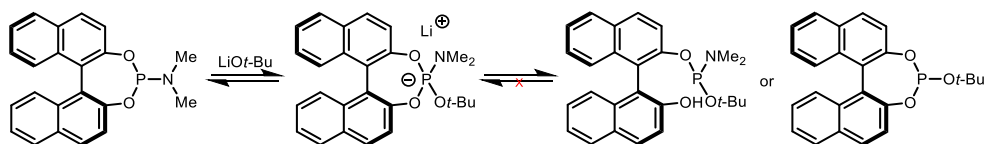
The reaction mixture was filtered quickly and HRMS were recorded within 1 hour.

Condition D. A 4 mL dram-vial was charged with a magnetic stir bar, (*S*)-MonoPhos (0.012 mmol, 1.0 equiv), and LiO*t*-Bu (10 equiv). Subsequently, acetonitrile (0.5 mL) was added to the mixture via a syringe. After stirring 1 hour under air, brine (5 mL) was added in one portion to quench the reaction. The aqueous phase was separated and extracted with ethyl acetate (3 × 10 mL). The combined organic phase was dried over anhydrous sodium sulfate (Na₂SO₄), filtered, and concentrated under reduced pressure. Subsequently, the crude product was diluted with acetonitrile for HMRS analysis. HRMS were recorded within 1 hour.

3.5.7.2. The observation of the related phosphoramidite-based species

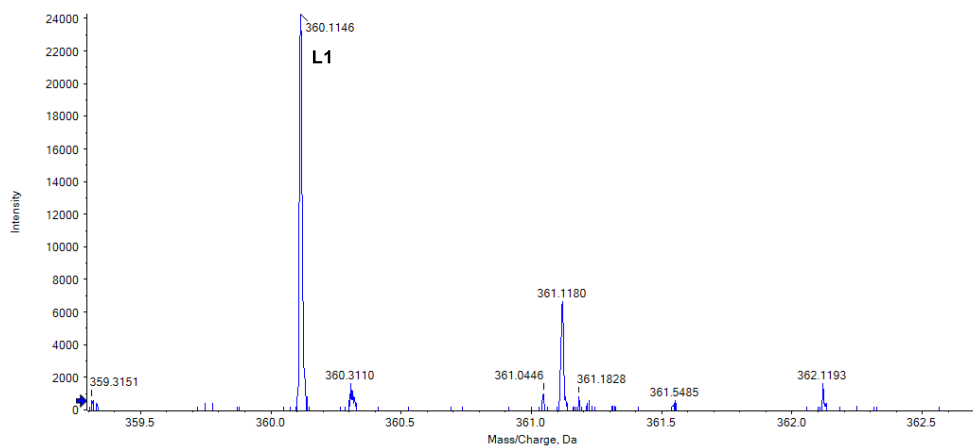


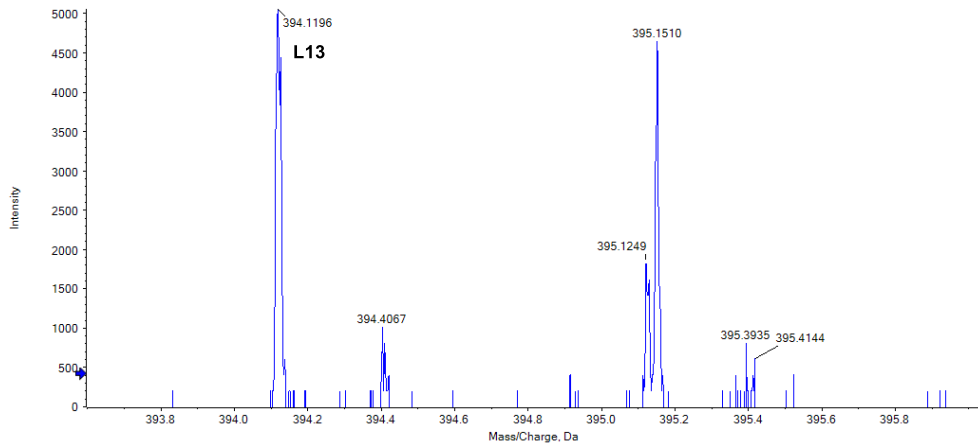
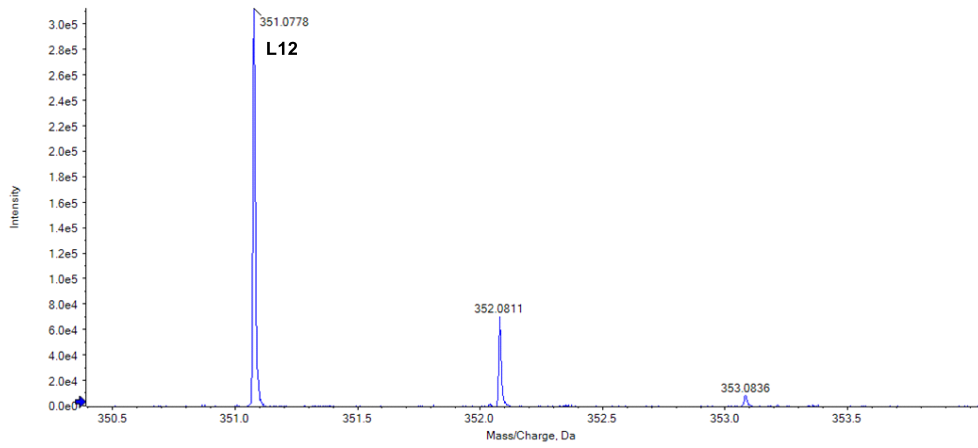
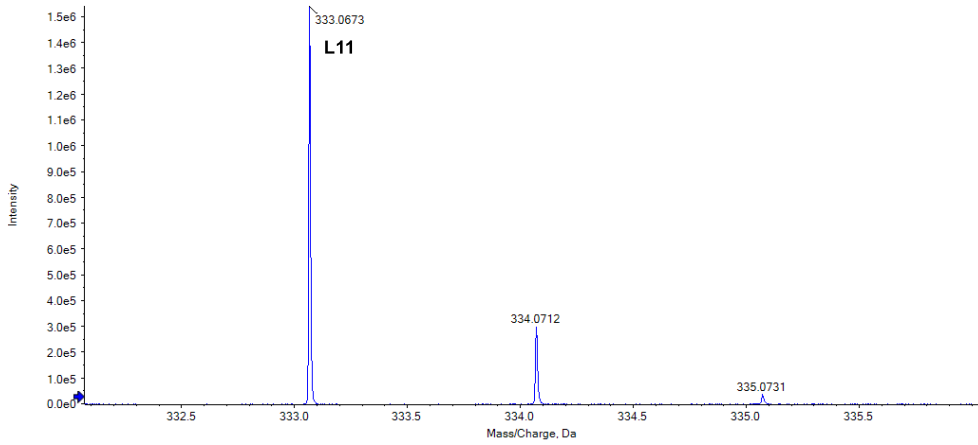
3.5.7.3. Plausible mechanistic scenario



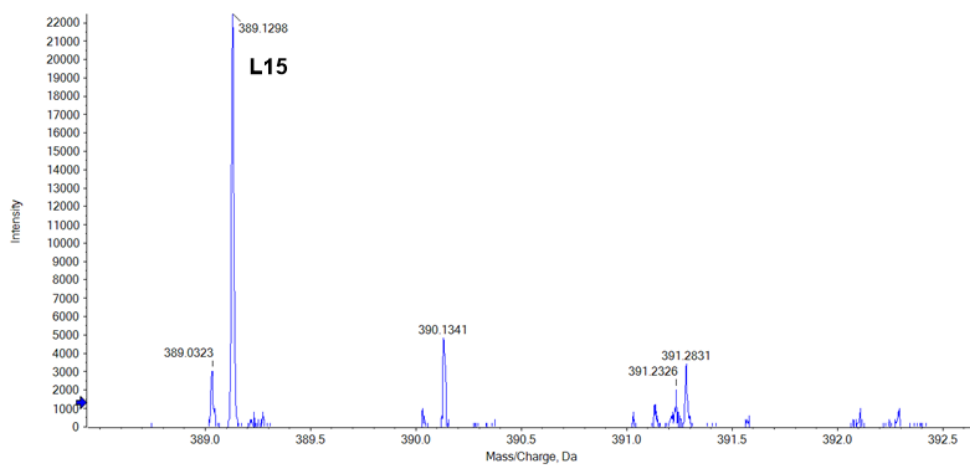
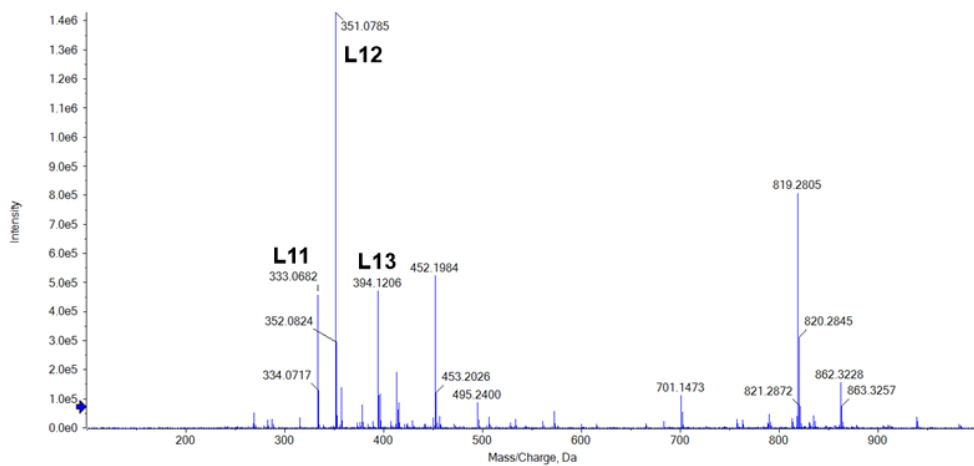
3.5.7.4. HRMS analysis (ESI-MS, $[M+H]^+$)

(a) Under condition A (**L1** in MeCN)

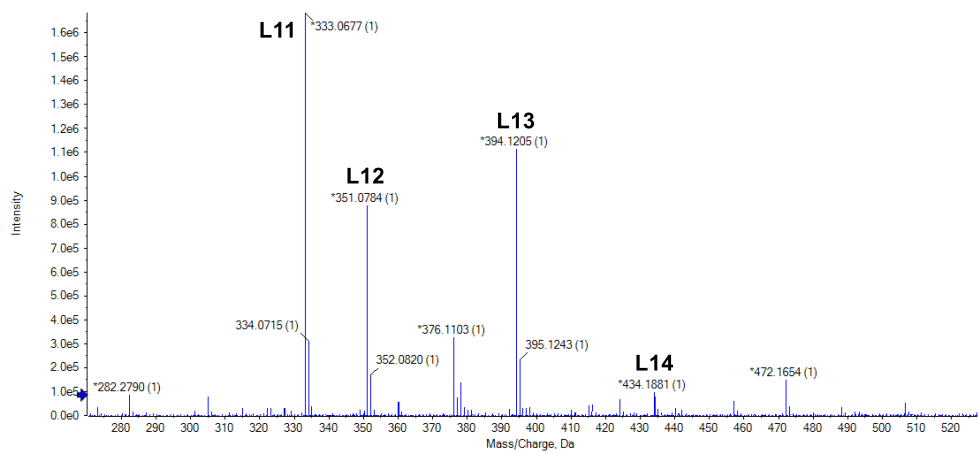




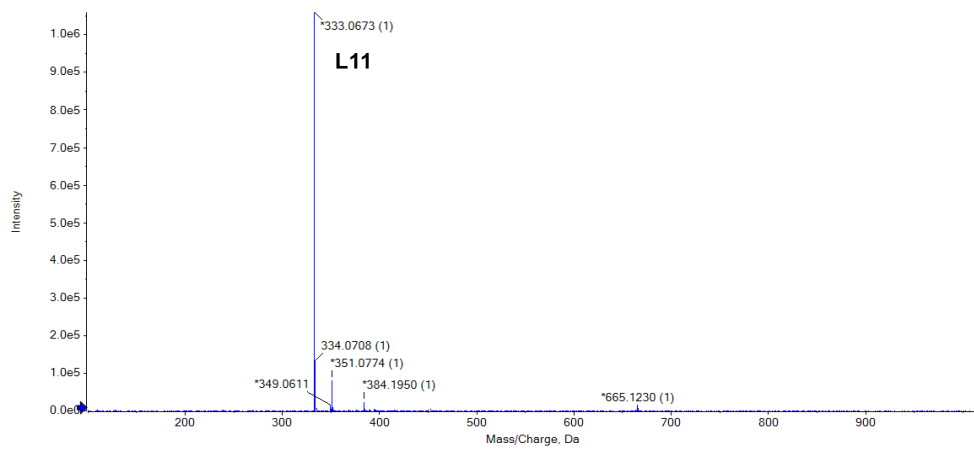
(b) Under condition B (L1 + LiO*t*-Bu in THF)



(c) Under condition C (L1 + LiOt-Bu in MeCN)



(d) Under condition D (L1 + LiOt-Bu in MeCN and work-up)



3.5.8 References in Experimental Section

- (1) For preparation of enone **2e**, see: Kazi, I.; Guha, S.; Sekar, G. *Org. Lett.* **2017**, *19*, 1244.
- (2) For preparation of enone **3p**, see: Kan, J.; Zhang, M.; Zhang, X.; Lou, X.; Shang, Y.; Xu, B.; Yang, F.; Su, W. *Chem. Eur. J.* **2019**, *25*, 15233.
- (3) For preparation of enone **3r**, see: Cao, J.-J.; Zhou, F.; Zhou, J. *Angew. Chem., Int. Ed.* **2010**, *49*, 4976.
- (4) Matsumura, S.; Maeda, Y.; Nishimura, T.; Umeura, S. *J. Am. Chem. Soc.* **2003**, *125*, 8862.
- (5) Kin, S.; Nibbs, A. E.; Türkmen, Y. E.; Rawal, V. H. *J. Am. Chem. Soc.* **2013**, *135*, 16050.
- (6) (a) Liang, X.; Wei, K.; Yang, Y.-R. *Chem. Commun.* **2015**, *51*, 17471. (b) Gharpure, S. J.; Vishwakarma, D. S.; Nanda, S. K. *Org. Lett.* **2017**, *19*, 6534. (c) Zhao, F.; Li, N.; Zhang, T.; Han, Z.-Y.; Luo, S.-W.; Gong, L.-Z. *Angew. Chem., Int. Ed.* **2017**, *56*, 3247.
- (7) Rekowski, F. von.; Koch, C.; Gschwind, R. M. *J. Am. Chem. Soc.* **2014**, *136*, 11389.
- (8) Joannou, M. V.; Moyer, B. S.; Meek, S. J. *J. Am. Chem. Soc.* **2015**, *137*, 6176.
- (9) Lee, B.; Chirik, P. J. *J. Am. Chem. Soc.* **2020**, *142*, 2429.

CHAPTER 4

Stereospecific Transformation of Enantioenriched Alkylboron

The majority of this chapter will be published:

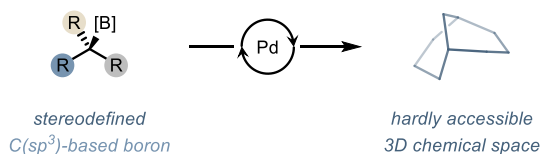
Roh, B.; Lee, H. G.* *Synthesis*. **2023** (invited review article)

© 2023. Thieme.

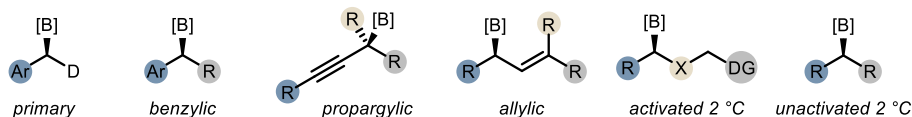
4.1. Introduction

The efficient formation of key carbon-carbon bonds is of the most important process to access complex molecules. Among the various methods, transition-metal catalyzed cross-coupling reaction has revolutionized modern synthesis. Currently, Suzuki-Miyaura cross-couplings (SMC) reaction has been recognized as the most powerful and indispensable toolkit due to the applicability and utility of the organoboron compounds. Despite their advantages, the most examples of Suzuki-Miyaura cross-coupling are limited to the use of $C(sp^2)$ -hybridized carbon based organoboron species, enabling access to only flat chemical structures via the formation of $C(sp^2)-C(sp^2)$ bonds. To expand the applicability of this protocol to synthesize three dimensional chemical structures, understanding the mechanism and development of the protocols utilizing $C(sp^3)$ -based alkylboron is essential.

A. Stereospecific Suzuki-Miyaura cross-coupling



B. Classification



Scheme 4.1. Stereospecific Suzuki-Miyaura coupling

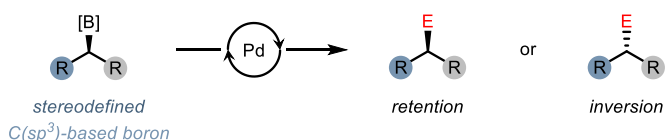
In this context, Chapter 4 describes the pioneering work and recent progress of stereospecific Suzuki-Miyaura cross-coupling, that is one of the powerful strategies allowing facile access to enantioenriched three-dimensional chemical structures (Scheme 4.1A). The related contents are classified and explained according to the types of nucleophiles, that is, primary-, benzylic-, allylic-, propargylic-, activated secondary-, and unactivated secondary enantioenriched alkylboron (Scheme 4.1B).

4.2. Stereospecific Suzuki-Miyaura Cross-Coupling (SSMC) reactions

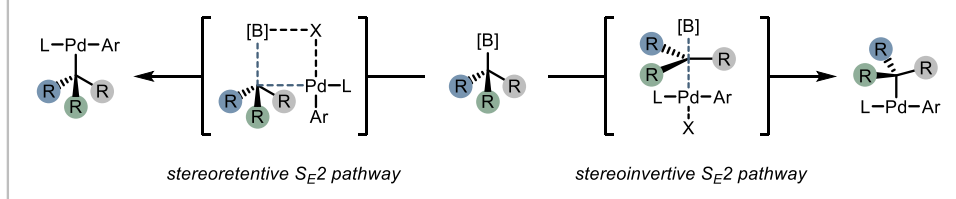
4.2.1. SSMC reactions with primary alkylboron

Stereospecific Suzuki-Miyaura cross-coupling reactions occurs with chiral boronates bearing stereochemical information as starting material (Scheme 4.2A).¹ The key feature of these protocols is the transmetalation process occurring with either retention or inversion of configuration (Scheme 4.2B). At this point, it might be expected that chiral secondary boronates must be utilized in the reactions to observe the stereochemical courses.

A. Stereospecific Suzuki-Miyaura cross-coupling



B. Putative mechanistic pathway in transmetalation

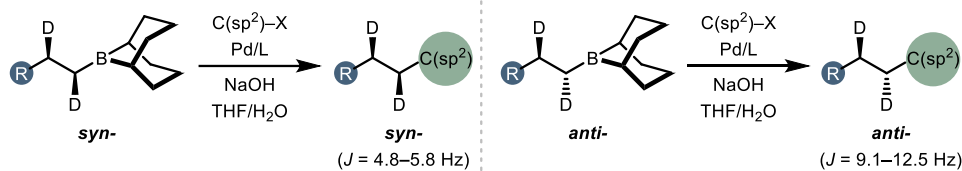


Scheme 4.2. Stereochemical courses of transmetalation in Stereospecific Suzuki-Miyaura coupling

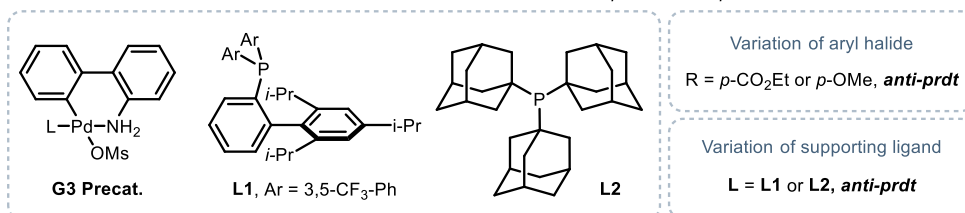
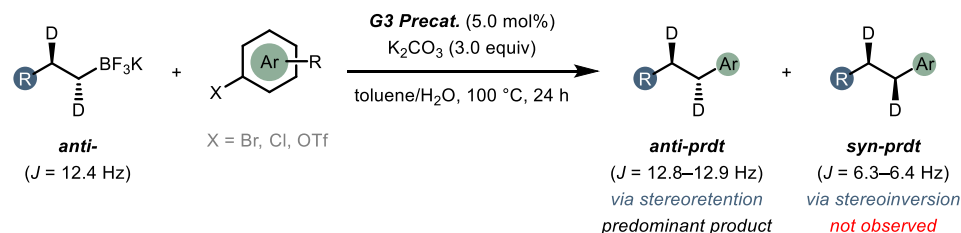
Interestingly, the initial investigations to understand the stereochemical course during the transmetalation process in stereospecific Suzuki-Miyaura cross-coupling reactions were first disclosed with primary alkylboranes. In the pioneering works performed independently by Woerpel² and Soderquis³ in 1998, detail mechanistic studies were conducted on the basis of Whitesides'

protocol⁴ using vicinal deuterated primary alkylborane (9-BBN) (Scheme 4.3A). By comparing the vicinal $J_{(H-H)}$ coupling constant in ¹H NMR investigations, the stereochemical information of the products were obtained indicating the retention of configuration.

A. Woerpel and Soderquist (1998): stereoretentive transmetalation



B. Biscoe (2021): stereoretentive transmetalation



Scheme 4.3. Stereochemical course of primary alkylboronates

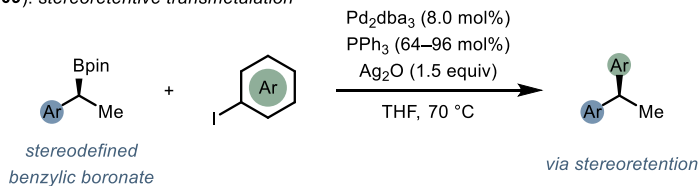
In recent 2021, after the seminal studies stated above, Biscoe and colleagues reported in-depth investigations of the stereochemical behavior of primary alkyl trifluoroborates in the stereospecific Suzuki-Miyaura cross-coupling reactions (Scheme 4.3B).⁵ The authors chose the less reactive primary alkyl trifluoroborates as nucleophiles because 9-BBN-based

alkylboranes are too nucleophilic to be suitable for investigating various parameters affecting the stereochemical course of transmetalation process. Notably, the stereochemical course of transmetalation under the reaction conditions affords the complete retention of configuration, not depending upon either the electronic- or steric properties of the supporting phosphine ligand and aryl electrophiles. These results indicated that it is hard to predict the stereochemical outcome in the stereospecific Suzuki-Miyaura cross coupling reactions.

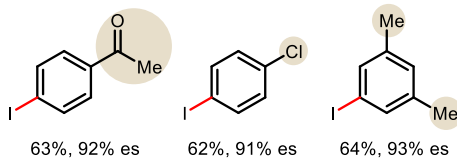
4.2.2. SSMC reactions with benzylic alkylboron

In 2009, Crudden and co-workers disclosed the first stereospecific Suzuki-Miyaura cross-coupling using enantioenriched secondary benzylic boronic ester and aryl iodides, affording the desired chiral 1,1-diarylethane products (Scheme 4.4A).⁶ The stereochemical information of the starting materials was efficiently transferred to the desired products in stereoretentive manner, showing high enantiospecificity. Of note, the use of silver-based additive was proved to be critical for the reactivity in this protocol. The reaction with either Ag₂O or Ag₂CO₃ only showed a certain level of reactivity and Ag₂O exhibited the best performance. The authors suggested that Ag₂O as base might play an important role, facilitating the slow transmetalation step through enabling the formation of oxo-palladium species.⁷ The applicability of the developed process was further evaluated, displaying that aryl iodides with different electronic properties were tolerated (Scheme 4.4B). But, the reaction with aryl bromide or substituted benzylic boronic ester gave the diminished reactivity. After their initial discovery, Crudden and co-workers further disclosed the unique chemoselectivity of this protocol using either chiral benzylic secondary boronic ester bearing vinyl group or external styrene (Scheme 4.4D).⁸ Highly chemoselective Suzuki-Miyaura reactions proceeded over potential Heck reactions. Based on this pioneering report, Burke and co-workers were explored the potential of this protocol for construction of complex compound (Scheme 4.4C).⁹

A. Crudden (2009): stereoretentive transmetalation

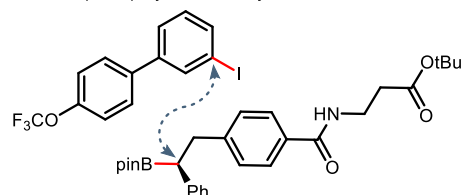


B. Selected examples



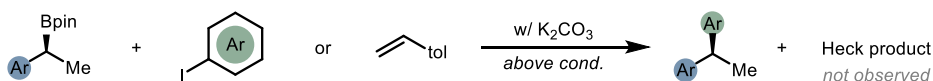
complete retention of configuration was observed

C. Burke (2011): synthetic utility



Condition: Pd₂dba₃, PPh₃, Ag₂O, K₂CO₃, DME, 60 °C "40% yield, 98% es"

D. Crudden (2013): chemoselectivity

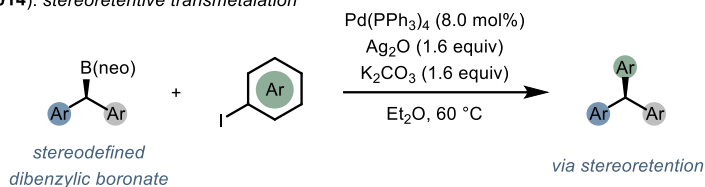


Scheme 4.4. Stereospecific Suzuki reaction with enantioenriched benzylic boronates

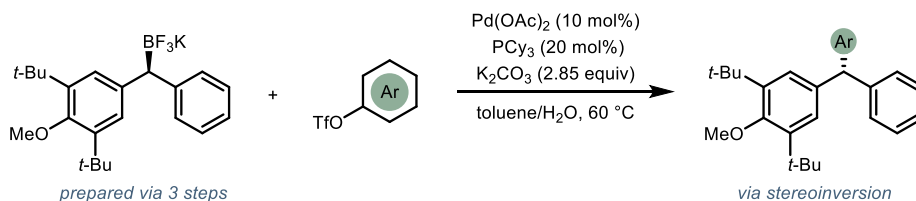
After that, Crudden and co-workers investigated the expandability of the protocol for access to chiral triarylmethane structures (Scheme 4.5A).¹⁰ Under slightly modified reaction conditions, a variety of chiral triarylmethane products were synthesized in high enantiospecificity with complete retention of configuration. Liao and co-workers developed new catalytic asymmetric method, providing structurally various chiral diarylmethine boronic ester (Scheme 4.5B).¹¹ To demonstrate the utility of their catalytic system, they further explored stereospecific transformation of their substrates. After transformation of chiral boronic esters to potassium trifluoroborate salts, the newly formed chiral trifluoroborates were further applied to Pd-catalyzed

stereospecific cross-coupling reactions with aryl triflates. In results, a series of enantioenriched triarylmethanes were smoothly constructed and stereochemical information of chiral boronic ester was successfully transferred to the products with high enantiospecificity. Notably, it was found that the reactions proceeded with inversion of configuration, which is the opposite of the protocol developed by Crudden and co-workers, although there were no rigorously mechanistic investigations in this system.

A. Crudden (2014): stereoretentive transmetalation



B. Liao (2015): stereoinvertive transmetalation

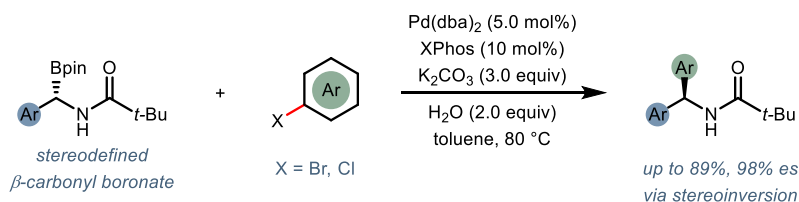


Scheme 4.5. Utilization of stereo-enriched diarylboronates.

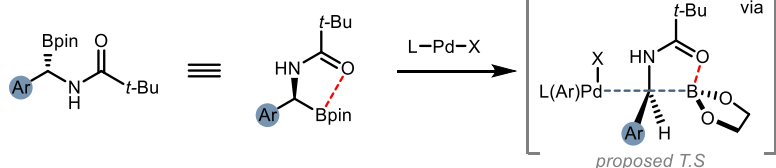
In 2010, Ohmura and Suginome group reported first stereoinvertive Suzuki-Miyaura reactions (Scheme 4.6A).¹² It was postulated that carbonyl oxygen of α -amide functional group on chiral benzylic boronic ester could involve in intramolecular coordination to the boron center during key transmetalation event. These interactions are believed to impede the potential

coordination of palladium to boron center (Scheme 4.6B). In turn, this causes the palladium to approach the boron center from the opposite side, facilitating the transmetalation pathway in a stereoinvertive manner. Of note, highly stereospecific transfer of stereochemical information was only achieved with a chiral boronic ester bearing a sterically encumbered pivaloyl group.

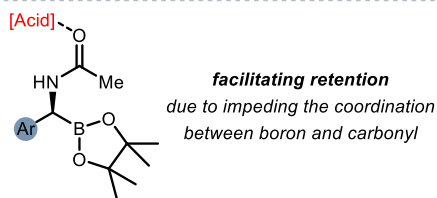
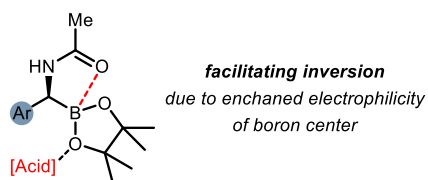
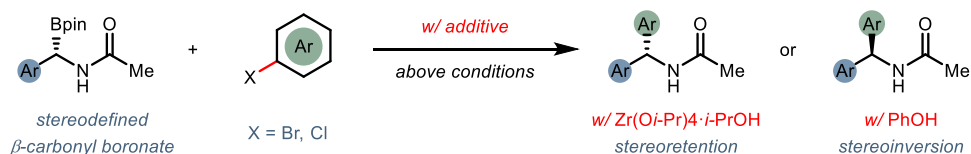
A. Ohmura & Suginome (2010): stereoinvertive transmetalation



B. Key feature



C. Ohmura & Suginome (2011): additive effect for stereochemical course

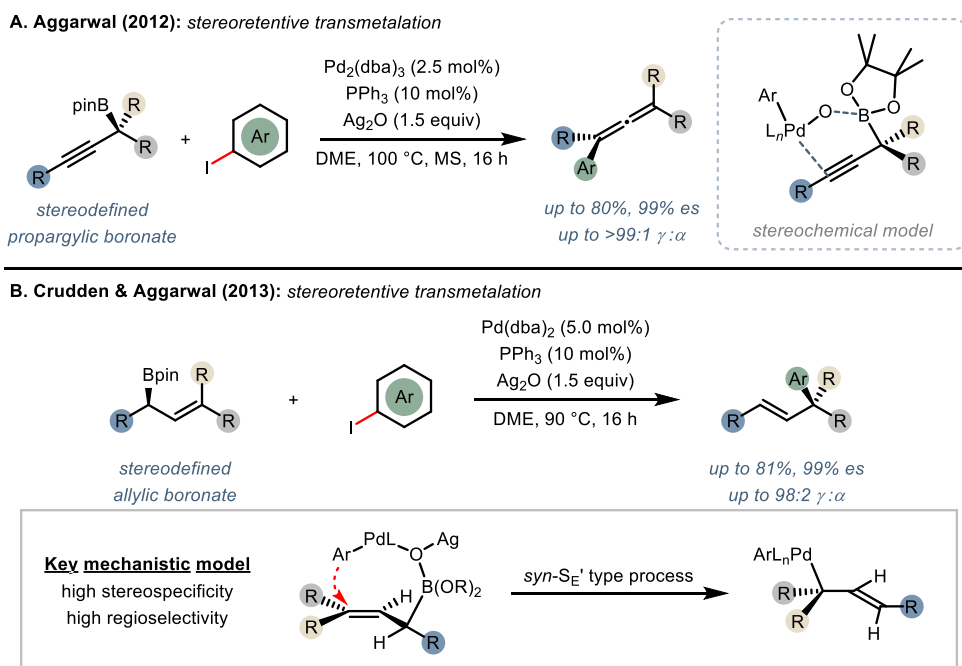


Scheme 4.6. Early discovery of stereoinvertive cross-coupling

Later, Ohmura and Suginome group further supported their postulation by conducting a series of experimental investigations in 2011 (Scheme 4.6C).¹³ Control experiments with various Brønsted or Lewis acid additives were carried out with chiral benzylic boronic ester bearing acetyl protected α -amide group. As expected, in the absence of additives, low enantiospecificity was observed. Notably, the stereospecificity was significantly enhanced by the addition of phenol in stereoinvertive manner. On the other hand, the retention of stereochemistry was primarily observed and the addition of $\text{Zr}(\text{O}i\text{-Pr})_4 \cdot i\text{PrOH}$ displayed the best performance. The roles of the additives were rationalized based on the original postulation (Scheme 4.6B).¹² Acid additive can interact with either oxygen atom on pinacol or oxygen atom of carbonyl on amide group. When additives are coordinated with oxygen atom on pinacol, the electrophilicity of boron center could be enhanced, facilitating the intramolecular coordination of carbonyl to boron center. As such, the invertive transmetalation pathway was made easier. The coordination of acid additive to amide hinder the direct formation of oxygen-boron bonds giving tricoordinated boron species and it undergoes retentive transmetalation process via four-membered-ring transition state.

4.2.3. SSMC reactions with allylic/propargylic alkyboron

Enantioenriched allylic and propargylic boronic esters have been also recognized as versatile building block in synthetic organic chemistry. Due to the presence of C(sp²)-hybridized carbon at α -position, these species have also better reactivity than unactivated alkyl boronates. Unlike the prototypical reactions such as nucleophilic addition to carbonyl groups, Suzuki-Miyaura cross-coupling of racemic secondary allylic boronic esters with aryl iodides was first reported by Crudden and co-workers in 2012.¹⁴



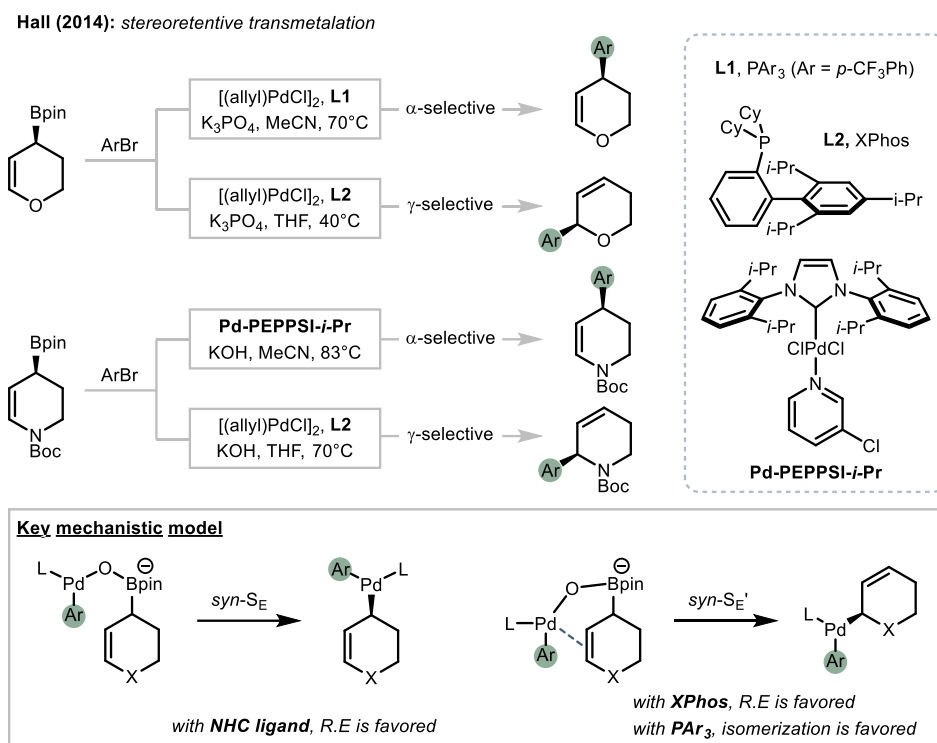
Scheme 4.7. Coupling with enantioenriched allylic- and propargylic boronate

Since this initial discovery, Aggarwal and co-workers developed the first stereospecific Suzuki reaction of enantioenriched propargylic boronic esters with aryl iodides.¹⁵ Using the slightly modified conditions of Crudden, chiral allene products were synthesized in high yield and excellent enantiospecificity (Scheme 4.7A).

After that, Aggarwal and Crudden reported cross-coupling reactions of enantioenriched allylic boronic esters with aryl iodides in 2013 (Scheme 4.7B).¹⁶ In both stereospecific cross-coupling reactions of enantioenriched allylic and propargylic boronic ester, γ -selectivity were primarily favored. Although the pioneering discoveries¹⁷ describing that regioselectivity can be controlled by choice of the supporting ligand, it was proposed that these reactions proceeded via *syn*-S_E' type mechanism. The Pd-O-B bonds is preferentially formed and the following intramolecular transmetalation process occurs via cyclic transition state, promoting the formation of chiral γ -selective products.

In 2014, Hall and co-workers demonstrated that both potential regioisomer products derived from one chiral allylic boronates could be obtained under the stereospecific Pd-catalyzed Suzuki-Miyaura cross-coupling reactions (Scheme 4.8A).¹⁸ First of all, enantioenriched pyranyl and piperidyl allylic boronates were prepared by their previous methods which are catalytic enantioselective borylation of alkenyl triflates. By designing the catalytic system using different ligands and palladium precatalyst, high level

of regiochemical control was accomplished, allowing the formation of both α and γ products with retention of configuration.

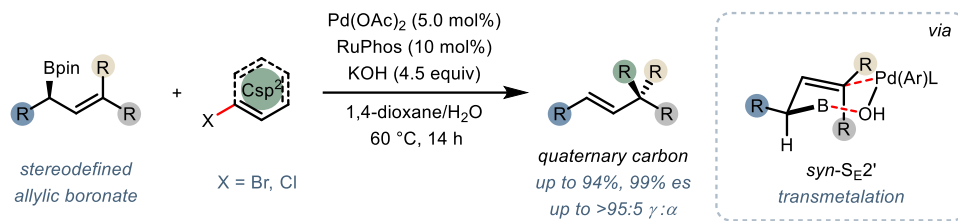


Scheme 4.8. Coupling with enantioenriched cyclic allylic boronate

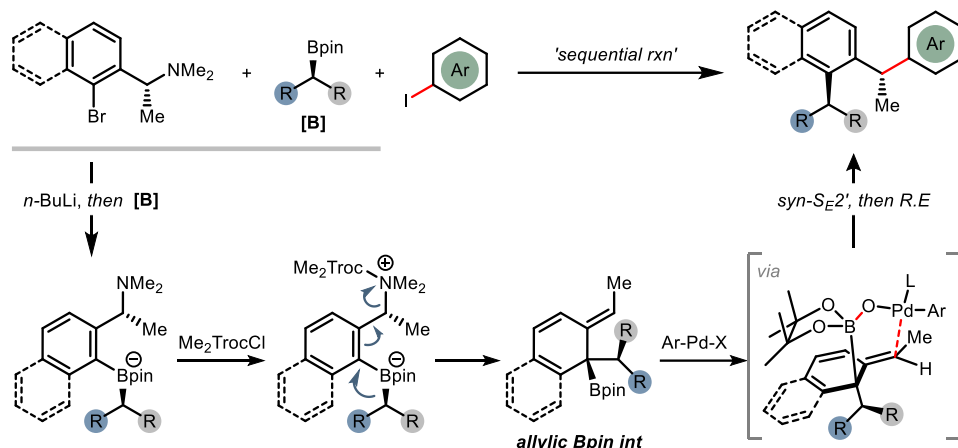
The reaction mechanism proposed for transmetalation follows the unified $\text{syn-SE}'$ type process. The oxo-Pd(II) species formed under basic conditions undergoes the following Pd transmetalation with chiral allylic boronates, affording the allylic Pd(II) complex. The Pd(II) intermediates bearing XPhos or PAR_3 ($\text{Ar} = 4\text{-CF}_3\text{-C}_6\text{H}_4$) as supporting ligands primarily coordinate with the electron-rich alkenes due to their electron deficient state, first giving α -bonded allylic Pd(II) complex. With XPhos ligand which is bulkier and

stronger α -donor phosphine, the following fast reductive elimination process leads to the formation of γ -selective products. The allylic Pd(II) complex bearing electron-deficient and the weaker α -donor phosphine PAr₃ (Ar = 4-CF₃-C₆H₄) leads to the formation of η^3 π -allylic intermediate, and provides the thermodynamically favored α -bonded allylic Pd(II) complex due to the absence of adjacent heteroatom. Lastly, reductive elimination of this complex affords the α -selective products. On the other hands, the catalytic system having NHC-type ligands is thought to undergoes fast reductive elimination, providing α -selective products. As such, it was proposed that the preference of NHC ligated Pd(II) complex into S_E transmetalation over alkene-directed S_E' type process is attributed the bulky and non-dissociative nature of the NHC ligand. A year later, Hall and co-workers expanded their designed protocol for utilization of 2-alkoxy pyran units as useful building block in 2015.¹⁹ Under the modified catalytic systems with chiral 2-ethoxy dihydropyranyl boronates, both 2- and 4-substituted chiral pyran product were obtained in high optical purity through ligand-controlled regiodivergent and stereospecific Suzuki-Miyaura cross-coupling reactions. This approach was further used for synthesis and confirmation of absolute stereochemistry of natural product diospongin B.

A. Morken (2014): stereoretentive transmetalation



B. Aggarwal (2018): stereoretentive transmetalation



Scheme 4.9. Synthesis quaternary carbon and sequential reactions utilizing enantioenriched allylic boronate

After that, Morken group reported the use of chiral γ,γ -disubstituted allylboronates as suitable substrates in stereospecific Suzuki reactions (Scheme 4.9A).²⁰ This strategy was achieved with high regioselectivity and enantiospecificity, enabling the construction of quaternary carbon stereocenters. Mechanistic studies suggested that the reaction process occurs stereospecific *syn* S_E' transmetalation with allyl migration, followed by fast reductive elimination. This postulation was rationalized by control experiments with two different secondary allylic boronic esters. In both cases, it was observed that the products expected to be formed through S_E'

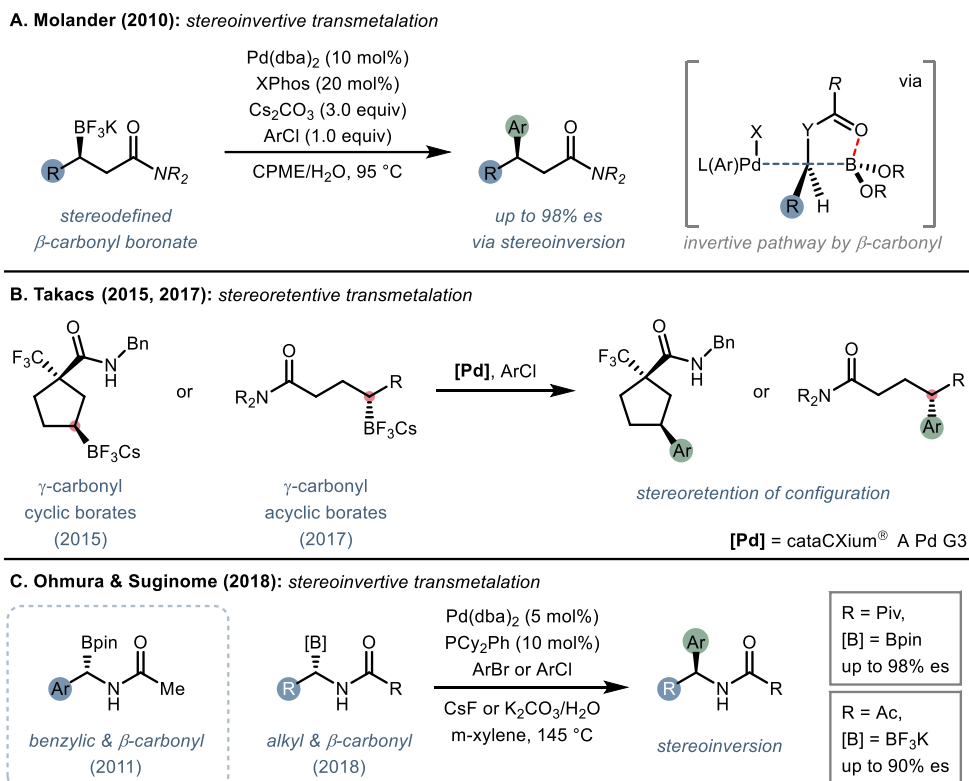
transmetalation were generated in high regioselectivity. These results are in line with the proposed reaction mechanism.

In addition, the unique sequential process of benzylamines, boronic acid and aryl iodides were demonstrated in 2019 by Aggarwal and co-workers (Scheme 4.9B).²¹ They found that chiral allylboronates intermediate, generated through sequential stereospecific 1,2-metalate rearrangement/*anti*-S_N2' elimination process of an *ortho*-lithiated benzylamine and alkyl boronates, undergoes the following stereospecific allylic Suzuki-Miyaura reactions. It was proposed that the transmetalation occurs through γ -selective S_E' type process and this process was facilitated by re-aromatization of dearomatized allylboronates intermediate, affording sterically encumbered chiral 1,1-diarylethane with high stereospecificity.

4.2.4. SSMC reactions with activated secondary alkylboron

Direct use of the unactivated chiral secondary boronate as nucleophile is highly challenging due to the slow transmetalation and competitive β -hydride elimination. To circumvent these challenges, there have been various activation modes. For examples, the introduction of either sp^2 -hybridized carbon (Section 4.2.2 and 4.2.3) or heteroatom at α -position or/and inclusion of coordinating group at β or γ position (Section 4.2.4) can facilitate the transmetalation of alkyl boronates.

Installation of carbonyl group on alkylboronates have been widely used for facilitation of transmetalation. In 2010, Molander and co-workers first reported that enantioenriched nonbenzylic secondary alkylboronates were found to participate easily in stereospecific cross-coupling reactions (Scheme 4.10A).²² Enantioenriched trifluoroborate salts bearing amide at β position with aryl chlorides could be employed in stereospecific coupling, revealing the complete inversion of configuration. Notably, it was found that neither the analogous ketone nor ester-containing chiral borates were not compatible with this protocol. Overall, proposed was that the auxiliary carbonyl oxygen serve as hemilabile ligand to enhance transmetalation and inhibit β -hydride elimination through coordinating with either boron or palladium during the process. The proposed S_E2 -type process affording inversion of configuration were consistent with previous work developed by Ohmura and Suginome.^{12,13}



Scheme 4.10. Suzuki coupling with carbonyl-substituted enantioenriched boronates

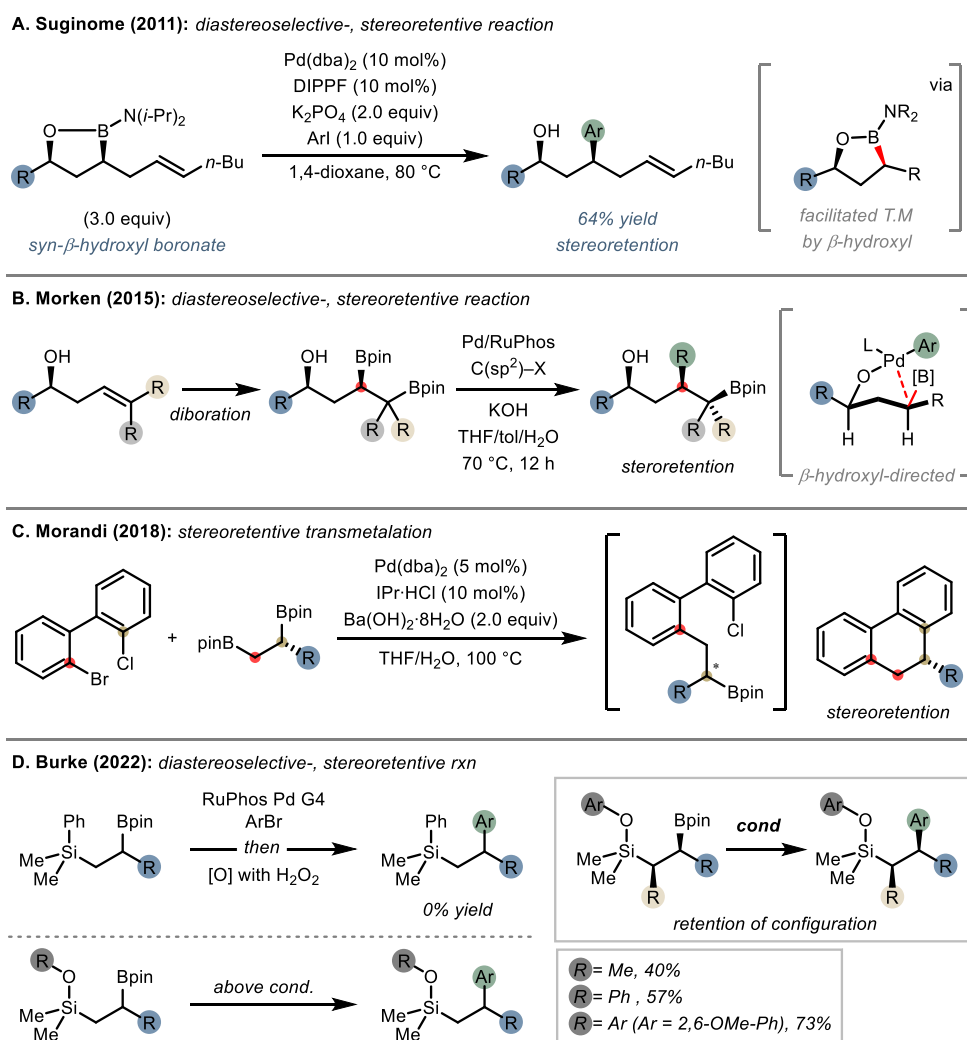
After that, Takacs and co-workers demonstrated that stereospecific cross-couplings of enantioenriched γ -borylated amide in highly stereoretentive manner in 2015 (Scheme 4.10B).²³ These results were the opposite of coupling with β -borylated amide developed by Suginome^{12,13} and Molander²², implying that carbonyl at β position is critical for inversion of configuration. In 2017, similar stereoretentive cross-coupling of chiral acyclic secondary γ -borylated amide was disclosed by Takacs group.²⁴ The protocol was extended to acyclic secondary γ -borylated amide prepared through their Rh-catalyzed

enantioselective borylation. These chiral amides underwent stereospecific Suzuki-coupling in stereoretentive manner with high enantiospecificity.

In 2018, Ohmura and Suginome extended their previous protocols^{12,13} for the use of chiral α -amide benzylic boronates to non-benzylic catalytic system. (Scheme 4.10C).²⁵ Notably, optically pure α -amide non-benzylic borates participated in the cross-coupling with various aryl bromides and aryl chlorides under modified catalytic system. In all cases, the inversion of configuration was favored, which is in accord with the results in their previous work.¹³ The most sterically encumbered group afford highest stereospecificity, indicating that stereoselectivity strongly depends on the structure of the acyl moiety. Overall, it was proposed that the observed inversion of configuration is derived from intramolecular coordination of the carbonyl group with the boron atom, blocking the approach of the palladium. As such, the enhanced stereospecificity with more sterically demanding groups is attributed to avoiding steric repulsion with alkyl groups.

Like the coordination effect of carbonyls, hydroxyl groups have also played a role in directing the stereospecific cross-coupling reactions. Suginome and co-workers demonstrated stereoselective cyclizative carboboration affording β -hydroxy secondary alkyl boronates in 2011 (Scheme 4.11A).²⁶ Then, the corresponding boronate were transformed to arylation products through Suzuki coupling with iodobenzene, showing that complete retention of configuration. It was proposed that the origin of the

enhanced reactivity of β -hydroxy secondary alkyl boronates is attributed to intramolecular coordination of the oxygen atom although the stereochemical course of the protocol was not clear.



Scheme 4.11. β -Hydroxyl-directed Suzuki reactions

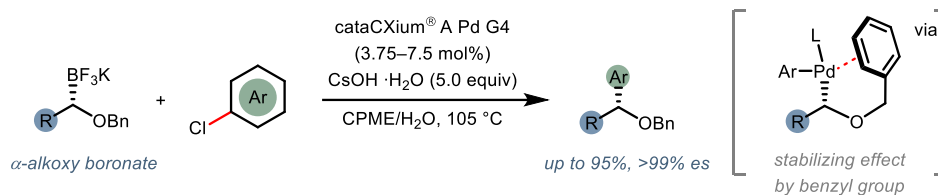
In 2015, Morken and colleagues demonstrated hydroxyl group-directed highly regioselective Suzuki-Miyaura cross-couplings (Scheme 4.11B).²⁷ They prepared 1,2-vicinal bis(boronates) by utilizing their previous diboration method and applied it to Pd-catalyzed Suzuki-coupling. Notably, β -hydroxy group provide the directing effect providing high regioselectivity. Only when hydroxyl group positioned at β -position, cross-coupling products were efficiently formed suggesting the ability of β -hydroxyl group to activate preferentially a secondary alkyl boronates over primary alkyl analogues. Importantly, this protocol occurs with complete retention of configuration. As such, they proposed the distinct reaction mechanism relative to the β -carbonyl group-promoted cross-coupling which proceeded with inversion of configuration. The binding of the β -hydroxyl group on boronates to the oxidative addition complex occurs with displacement of a halide. Subsequently, inner-sphere transmetalation in stereoretentive manner affords organopalladium complex, delivering the corresponding coupling products.

In 2021, Morandi group reported cascade annulation reactions utilizing alkyl 1,2-bisboronic pinacol ester as nucleophile. configuration (Scheme 4.11C).²⁸ The mechanistic studies showed that chlorinated intermediate could be isolated, then participating in the secondary cross-coupling reaction to afford the annulated product. Notably, the reactions proceeded efficiently with alkyl 1,2-bisboronic pinacol ester not containing β -hydroxyl group. This challenging cross-coupling of a secondary alkyl boronate was enabled by the

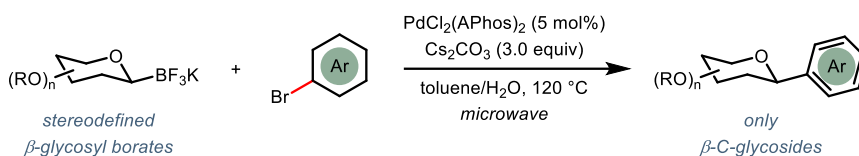
proximity of the reactive site during the intramolecular process. In addition, the protocol was also successfully applied to stereospecific versions of cross-couplings, showing the retention of configuration which is in accordance with Morcken's work.

Most recently, Burke and Hein designed β -silyl-substituted secondary alkyl boronic acid and successfully applying it to the stereospecific cross-coupling reactions (Scheme 4.11D).²⁹ The authors strategically utilized the silyl group as stable β -oxygen surrogates and transmetalation-promoting groups. Notably, when the alkoxide or phenoxide were installed on silyl center, the reactivity was dramatically increased, suggesting that the Lewis basic substituent might play a critical role in promoting the transmetalation, which are similar with carbonyl or hydroxyl group. Moreover, the enantioenriched secondary alkyl β -aryloxysilyl pinacol boronic esters were synthesized and submitted to the stereospecific cross-coupling/oxidation sequence, revealing the perfect stereoretention.

A. Molander (2012): stereoretentive reaction



B. Higashibayashi (2023): stereoretentive reaction



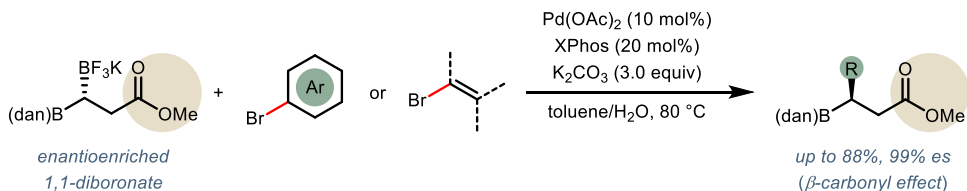
Scheme 4.12. Suzuki reactions of α -alkoxy-substituted enantioenriched boronate

Like directing group such as carbonyl and hydroxyl group, the presence of heteroatom at α -position also facilitates the transmetalation of alkyl boronates. The first report of stereospecific Suzuki-Miyaura cross-coupling with chiral α -alkoxy boronates was disclosed by Molander and co-workers in 2012. configuration (Scheme 4.12A).³⁰ They demonstrated a variety of α -hydroxyl alkyl trifluoroborates can be synthesized through one-pot procedure under the modified reaction conditions based on Sadighi diboration protocol.³¹ Next, the ability of protecting group on the alcohol were evaluated for the desired cross-coupling. Of note, benzyl protected α -alkoxy alkyl trifluoroborates were only compatible with Suzuki cross-coupling reaction, affording the desired coupling products. These results were in accord with their postulation that benzyl group can stabilize the palladium intermediate formed after transmetalation process by coordination to palladium center,

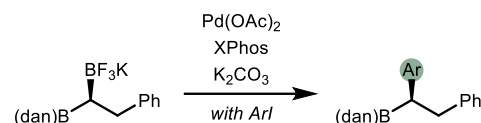
resulting in both impeding the competitive β -hydride elimination. For further investigations of stereospecificity of the reaction, enantiomerically enriched α -alkoxyl trifluoroborates were prepared and subjected to the cross-coupling reaction, revealing that the transformation proceeded with retention of configuration in complete stereospecificity. Unlike the coordination mode of carbonyl group to boron center enforcing palladium to approach on backside, benzyl group have less ability for coordination to boron center. As such, transmetalation in this protocol was believed to proceeds through a four-membered transition structure with retention.

In recent 2023, Higashibayashi and colleagues developed the copper-catalyzed stereoselective borylation enabling access to β -glycosyl boronates (Scheme 4.12B).³² They utilized a series of β -glycosyl boronates as versatile intermediate for subsequent palladium-catalyzed cross-coupling. In the process, the stereochemical information of the anomeric carbon on the β -glycosyl trifluoroborates were transferred to the desired coupling products in stereoretentive manner without formation of α -C-glycoside. The resulting stereochemistry were similar with that of Molander's protocol.³⁰

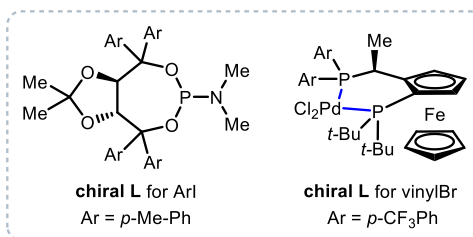
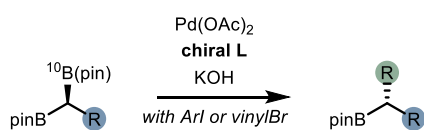
A. Hall (2011): stereoinvertive transmetalation



B. Yun (2013): stereoretentive transmetalation



C. Morken (2014): stereoinvertive transmetalation



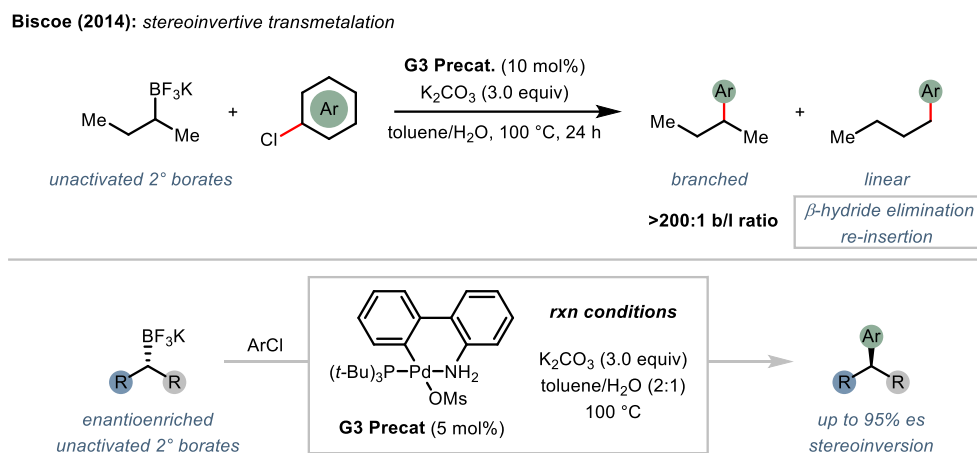
Scheme 4.13. Suzuki reactions of enantioenriched 1,1-diboronates

In 2011, Hall and co-workers developed a method for synthesis of enantioenriched 1,1-diboron species and further showed the applicability of the products to the stereospecific Suzuki-Miyaura cross-coupling (Scheme 4.13A).³³ The chemoselective cross-coupling was enabled by the proximity of pinacol ester and β -carbonyl group observed in their X-ray crystallographic structure. Also, it was proposed that the stabilization effect from the second boronyl unit facilitate the challenging transmetalation. The observed stereoinversion of configuration were similar with those observed in the stereospecific couplings of chiral boronates bearing β -carbonyl group developed by Suginome and Molander.^{12,13}

Later in 2013, Yun and colleague reported copper-catalyzed enantioselective hydroboration strategy, providing enantiomerically enriched 1,1-diborylalkanes.³² Further utility of the chiral diborylalkanes were evaluated by application to Suzuki-Miyaura cross-coupling reactions (Scheme 4.13B). Of interest is that stereochemical information was transferred to the coupling product in stereoretentive manner. These results exhibited that inclusion of carbonyl groups is critical for reactivity and stereoinversion of configuration. A year later, in 2014, Morken and co-workers published asymmetric cross-coupling of 1,1-bisboronates with either aryl halide³⁵ or vinyl halides³⁶ to furnish chiral benzylic or allylic boronates. To prove which step can be involved in the stereochemistry-determining step, ¹⁰B-labeled chiral secondary 1,1-diboronates were subjected to the Suzuki-Miyaura cross-coupling (Scheme 4.13C). In control experiments, it was found that the coupling proceeded with inversion of configuration despite the absence of coordinating group. These observations were not in accordance with Hall³³ and Yun's³⁴ observations. Overall, although the origin of the stereochemical course was not mentioned, it seems likely that different kinds of 1,1-diborylalkanes might follow the distinct transmetalation reaction mechanism.

4.2.5. SSMC reactions with unactivated secondary alkylboron

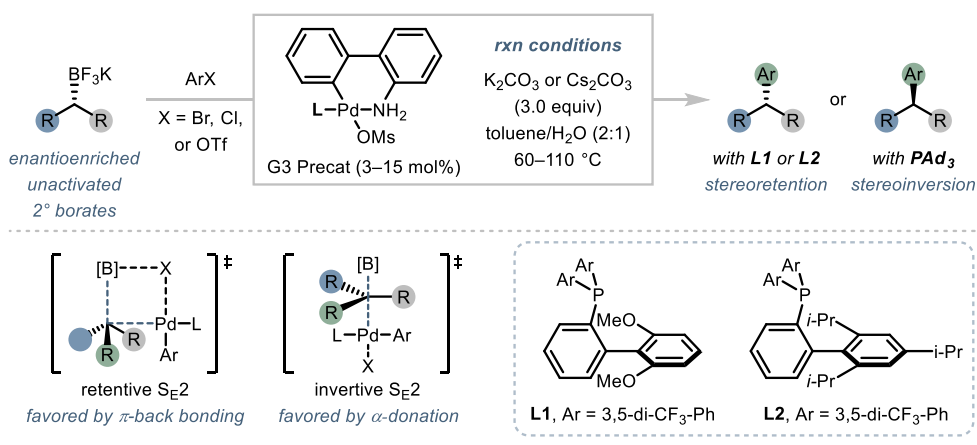
As discussed in the previous sections, for the successful applications of stereospecific Suzuki-Miyaura cross-coupling, it has been thought that various activation modes must be considered not only to improve reactivity but also to avoid the competitive side pathway. In 2014, however, Biscoe group first disclosed the Pd-catalyzed stereospecific Suzuki-Miyaura cross-coupling using unactivated secondary alkyl boronates, which has been regarded as the most challenging due to its propensity undergoing β -hydride elimination followed by isomerization and racemization (Scheme 4.14).³⁷ This method was achieved with P(*t*-Bu)₃-ligated G3-Pd precatalyst and K₂CO₃ in aqueous toluene system, showing unprecedented selectivity to afford the branched product (>200:1).



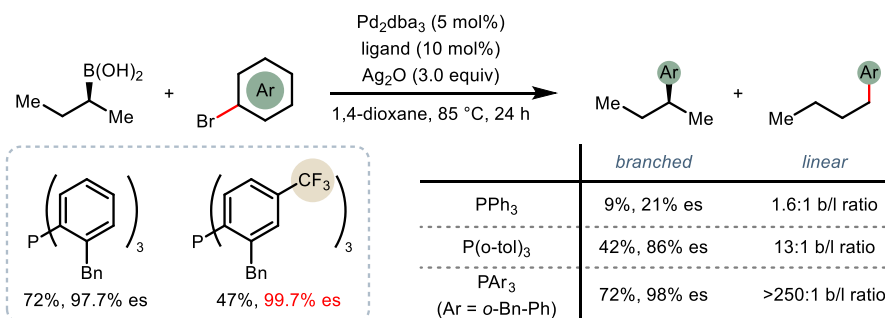
Scheme 4.14. Pioneering discovery for Suzuki-coupling of enantioenriched unactivated secondary

Next, to evaluate the stereochemical course of the protocol, chiral unactivated secondary alkyl trifluoroborates were also subjected to the standard reaction conditions. Interestingly, the reaction proceeded with inversion of configuration despite the absence of directing group. These observations suggested that the parameters influencing the stereochemical course in stereospecific Suzuki-Miyaura cross-coupling reactions are more complicated, making it difficult to correctively predict the stereochemical outcome.

Biscoe & Sigman (2018): stereodivergent transmetalation



Burke (2021): stereoretentive transmetalation



Scheme 4.15. Suzuki cross-coupling of enantioenriched unactivated secondary

Later in 2018, the Biscoe and Sigman groups reported more thorough mechanistic investigations in the Suzuki-Miyaura cross-coupling of chiral unactivated secondary alkyl boronates, and this method enabled control of the stereochemical outcome by the design and choice of the supporting ligand (Scheme 4.15A).³⁸ Interestingly, the electronic properties of aryl chlorides influenced the stereochemical outcome in the reactions. The steric and electronic properties also significantly affected the stereochemistry of the products. To gain mechanistic insight based on the observation describing that the stereospecificity depends on complex factors, predictive statistical model was established by developing a series of molecular descriptors of phosphine ligands. By applying this model, two different phosphine ligands were strategically designed and it enabled to facilitate stereoretentive-biased pathway. The key features of the designed ligands are sterically bulky and electron deficient, which are expected to impede β -hydride elimination pathway, facilitate the stereoretentive transmetalation and accelerate reductive elimination simultaneously. On the other hand, bulky and electron-rich ligand $P(t\text{-Bu})_3$ or PAd_3 promoted the stereoinvertive transmetalation pathway. Based on a series of experimental and computational observations, the origin of the stereochemistry was proposed. The sterically bulky property of the ligand is critical for the high enantioselectivity by suppressing the competitive β -hydride elimination pathway, followed by avoiding sequential process of reinsertion/racemization. At the same time, the electronic

properties of the ligand influence the transmetalation steps. The stereoinvertive pathway depends on strong α -donating property of the supporting ligand, stabilizing cationic palladium intermediate during the transmetalation process. On the contrary, the π -back bonding of the ligands can enhance the stereoretentive pathway by stabilizing the coordination of additional π -donor ligand to palladium center. Overall, the stereodivergent Pd-catalyzed Suzuki-Miyaura cross-coupling were achieved using one enantiomerically enriched unactivated boronates, enabling access to both chiral products with high stereospecificity.

A year later, Burke and colleagues utilized the unactivated secondary alkyl boronic acid and subjected to Suzuki-Miyaura cross-coupling reactions, revealing the complete stereoretention of configuration (Scheme 4.15B).³⁹ In the presence of bulky triarylphosphine as the supporting ligand, the reaction proceeded with perfect enantiospecificity and branch/linear ratio. Additional control experiments with electronically tuning bulky triarylphosphines resulted in the positive correlation between electron deficiency and stereospecificity. These experimental results were in accord with the protocol developed by Biscoe and Sigman. Overall, it was proposed that the bulky triarylphosphine preferentially facilitates the stereoretentive pathway by shielding the axial positions, resulting in blocking the stereoinvertive pathway.

4.3. References

- (1) (a) Wang, C.-Y.; Derosa, J.; Biscoe, M. R. *Chem. Sci.* **2015**, *6*, 5105. (b) Leonori, D.; Aggarwal, V. K. *Angew. Chem., Int. Ed.* **2015**, *54*, 1082. (c) Cherney, A. H.; Kadunce, N. T.; Reisman, S. E. *Chem. Rev.* **2015**, *115*, 9587. (d) Rygus, J. P. G.; Crudden, C. M. *J. Am. Chem. Soc.* **2017**, *139*, 18124. (e) Ma, X.; Murray, B.; Biscoe, M. R. *Nat. Rev. Chem.* **2020**, *4*, 584.
- (2) Ridgway, B. H.; Woerpel, K. A. *J. Org. Chem.* **1998**, *63*, 458.
- (3) Matos, K.; Soderquist, J. A. *J. Org. Chem.* **1998**, *63*, 461.
- (4) Bock, P. L.; Boschetto, D. M.; Rasmussen, J. R.; Demers, J. P.; Whitesides, G. M. *J. Am. Chem. Soc.* **1974**, *96*, 2814.
- (5) Murray, B.; Zhao, S.; Aramini, J. M.; Wang, H.; Biscoe, M. R. *ACS Catal.* **2021**, *11*, 2504.
- (6) Imao, D.; Glassponle, B. W.; Laberge, V. S.; Crudden, C. M. *J. Am. Chem. Soc.* **2009**, *131*, 5024.
- (7) (a) Uenishi, J.; Beau, J. M.; Armstrong, R. W.; Kishi, Y. *J. Am. Chem. Soc.* **1987**, *109*, 4756 (b) Hirabayashi, K.; Kawashima, J.; Nishihara, Y.; Mori, A.; Hiyama, T. *Org. Lett.* **1999**, *1*, 299.
- (8) Glasspoole, B. W.; Oderinde, M. S.; Moore, B. D.; Antoft-Finch, A.; Crudden, C. M. *Synthesis* **2013**, *45*, 1759.

- (9) Li, J.; Burke, M. *J. Am. Chem. Soc.* **2011**, *133*, 13774.
- (10) Matthew, S. C.; Glasspoole, B. W.; Eisenberger, P.; Crudden, C. M. *J. Am. Chem. Soc.* **2014**, *136*, 5828.
- (11) Lou, Y.; Cao, P.; Jia, T.; Zhang, Y.; Wang, M.; Liao, J. *Angew. Chem., Int. Ed.* **2015**, *54*, 12134
- (12) Ohmura, T.; Awano, T. Suginome, M. *J. Am. Chem. Soc.* **2010**, *132*, 13191.
- (13) Awano, T.; Ohmura, T.; Suginome, M. *J. Am. Chem. Soc.* **2011**, *133*, 20738.
- (14) Glasspoole, B. W.; Ghozati, K.; Moir, J. W.; Crudden, C. M. *Chem. Commun.* **2012**, *48*, 1230.
- (15) Partridge, B. M.; Chausset-Boissarie, L.; Burns, M.; Pulis, A. P.; Aggarwal, V. K. *Angew. Chem. Int. Ed.* **2012**, *51*, 11795.
- (16) Chausset-Boissarie, L.; Ghozati, K.; LaBine, E.; Chen, J. L. Y.; Aggarwal, V. K.; Crudden, C. M. *Chem. Eur. J.* **2013**, *19*, 17698
- (17) (a) Kálmán J. Szabó* *J. Am. Chem. Soc.* **2006**, *128*, 8150. (b) Farmer, J. L.; Hunter, H. N.; Organ, M. G. *J. Am. Chem. Soc.* **2012**, *134*, 17470. (c) Yang, Y.; Buchwald, S. L. *J. Am. Chem. Soc.* **2013**, *135*, 10642.
- (18) Ding, J.; Rybak, T.; Hall, D. G., *Nat. Commun.* **2014**, *5*, 5474.
- (19) Rybak, T.; Hall, D. G. *Org. Lett.* **2015**, *17*, 4156.

- (20) Potter, B.; Edelstein, E. K.; Morken, J. P. *Org. Lett.* **2016**, *18*, 3286.
- (21) Rubial, B.; Collins, B. S.; Bigler, R.; Aichhorn, S.; Noble, A.; Aggarwal, V. K. *Angew. Chem., Int. Ed.* **2019**, *58*, 1366.
- (22) Sandrock, D. L.; Jean-Gerard, L.; Chen, C.-Y.; Dreher, S. D.; Molander, G. A. *J. Am. Chem. Soc.* **2010**, *132*, 17108.
- (23) Hoang, G. L.; Yang, Z. D.; Smith, S. M.; Pal, R.; Miska, J. L.; Pérez, D. E.; Takacs, J. M. *Org. Lett.* **2015**, *17*, 940.
- (24) Hoang, G. L.; Takacs, J. M. *Chem. Sci.* **2017**, *8*, 4511.
- (25) Ohmura, T.; Miwa, K.; Awano, T.; Suginome, M. *Chem. - Asian J.* **2018**, *13*, 2414.
- (26) Daini, M.; Suginome, M. *J. Am. Chem. Soc.* **2011**, *133*, 4758.
- (27) Blaisdell, T. P.; Morken, J. P. *J. Am. Chem. Soc.* **2015**, *137*, 8712.
- (28) Willems, S.; Toupalas, G.; Reisenbauer, J. C.; Morandi, B. *Chem. Commun.* **2021**, *57*, 3909.
- (29) LaPorte, A. J.; Shi, Y.; Hein, J. E.; Burke, M. D. *ACS Catal.* **2022**, *12*, 10905.
- (30) Molander, G. A.; Wisniewski, S. R. *J. Am. Chem. Soc.* **2012**, *134*, 16856.
- (31) Laitar, D. S.; Tsui, E. Y.; Sadighi, J. P. *J. Am. Chem. Soc.* **2006**, *128*, 11036.

- (32) Kurahayashi, K.; Hanaya, K.; Sugai, T.; Hirai, G.; Higashibayashi, S.
Chem. - Eur. J., **2023**, *29*, e2022203376.
- (33) Lee, J. C. H.; McDonald, R.; Hall, D. G. *Nat. Chem.* **2011**, *3*, 894.
- (34) Feng, X.; Jeon, H.; Yun, J. *Angew. Chem., Int. Ed.* **2013**, *52*, 3989.
- (35) Sun, C.; Potter, B.; Morken, J. P. *J. Am. Chem. Soc.* **2014**, *136*, 6534.
- (36) Potter, B.; Szymaniak, A. A.; Edelstein, E. K.; Morken, J. P. *J. Am. Chem. Soc.* **2014**, *136*, 17918.
- (37) Li, L.; Zhao, S.; Joshi-Pangu, A.; Diane, M.; Biscoe, M. R. *J. Am. Chem. Soc.* **2014**, *136*, 14027.
- (38) Zhao, S.; Gensch, T.; Murray, B.; Niemeyer, Z. L.; Sigman, M. S.; Biscoe, M. R. *Science* **2018**, *362*, 670.
- (39) Lehmann, J. W.; Crouch, I. T.; Blair, D. J.; Trobe, M.; Wang, P.; Li, J.; Burke, M. D. *Nat. Commun.* **2019**, *10*, 1263.

CHAPTER 5

Stereospecific Acylative Suzuki-Miyaura Cross-Coupling Reaction

This chapter has been adapted with permission from:

Roh, B.; Farah, A. O.; Kim, B.; Feoktistova, T.; Moeller, F.; Kim, K. D.;
Cheong, P. H.-Y.*; Lee, H. G.* *J. Am. Chem. Soc.* **2023**, *145*, 7075–7083.

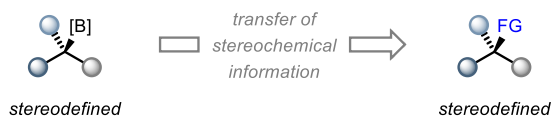
© 2023 American Chemical Society

5.1. Introduction

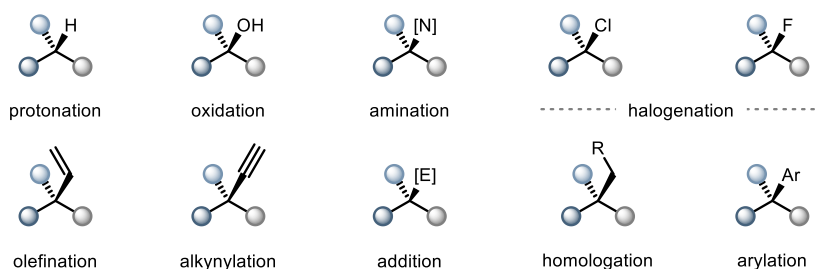
The stereospecific transformations of enantioenriched alkylboron compounds are highly powerful methods enabling precisely the introduction of stereogenic centers into molecular architectures (Figure 5.1A). In fact, we could readily transform the carbon-boron bonds of optically active alkylboron reagents to potentially accessible all types of functional groups, such as hydroxyl, amine, halogen, and diverse carbon-based groups, by utilizing the stereospecific strategies that have been reported until recently (Figure 5.1B).¹ At this stage, we were focused on stereospecific approaches utilizing chiral boronates for the synthesis of chiral carbonyl compounds. Despite the biomedical significance of chiral carbonyl moieties,² most of the existing synthetic strategies have been severely limited by either harsh conditions such as the necessity of alkyllithium reagents or multistep synthetic sequences (Figure 5.1C).³

In this context, we envisioned that Pd-catalyzed stereospecific Suzuki-Miyaura cross-coupling could enable the direct synthesis of chiral carbonyl groups from easily accessible carboxylic acid derivatives. As discussed in Chapter 4, a wide variety of chiral boronates have been utilized in stereospecific Suzuki reactions, allowing the precise transfer of stereochemical information into the complex molecules.⁴ Interestingly, most of the electrophilic coupling partners that participated in the protocols have been limited to aryl- and vinyl halides.

A. Stereospecific functionalization and transformation



B. Accessible functional groups from chiral boronates



C. Construction of chiral carbonyl compounds

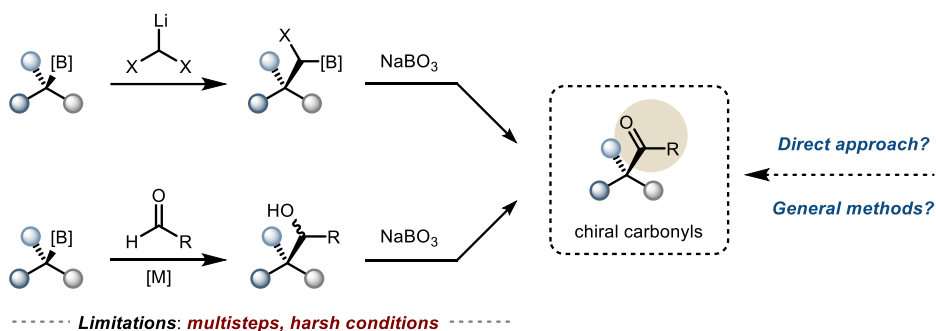
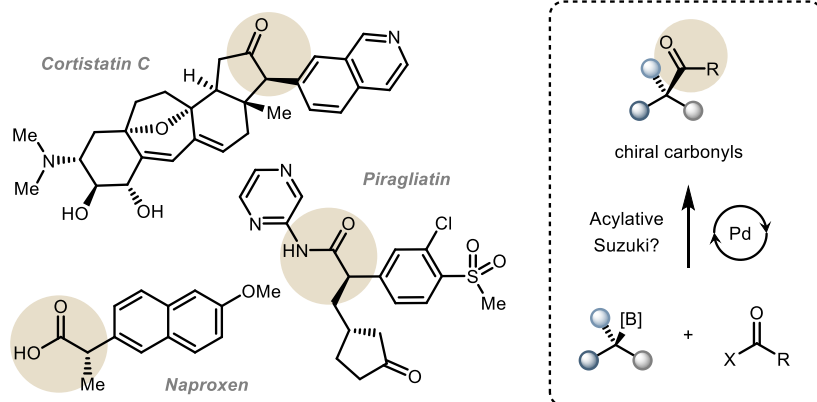


Figure 5.1. Stereospecific transformation utilizing chiral boronates and current synthetic strategies for access chiral carbonyl groups

We recognized that Pd-catalyzed stereospecific Suzuki-Miyaura cross-coupling could be extended to the acylative variant, efficiently providing enantioenriched carbonyl compounds which are an important class of structural motifs that are ubiquitously found in bioactive compounds (Figure 5.2A).⁵ In particular, we expected that the development of stereospecific acylation could be an ideal alternative method to the wide variety of existing

stereoselective approaches, whose performance of chiral catalysts can often be perturbed by numerous reaction parameters, for instance, the existing stereochemical information of the reaction partners and/or functional groups that can influence stereoselectivity. The utilization of enantioenriched, preformed organometallic reagents could, in principle, enable highly precise transfer of stereochemical information into the target structure, without depending on other complicating factors.⁴ Indeed, Biscoe and colleagues disclosed this possibility by enabling the preparation of optically active ketones from chiral alkyl stannanes (Figure 5.2B).⁶ Nevertheless, a wider application of the strategy has been hindered by the inherent limitations associated with the preparation and utilization of organotin reagents, both in terms of safety and practicality. In addition, the limited reactivity of organometallic reagents is not sufficient to provide generality for synthesizing chiral carbonyl compounds, particularly carboxylic acid derivatives. At this point, we believed that these crucial synthetic issues could be solved by the development of stereospecific Pd-catalysis utilizing enantioenriched organoboron (Figure 5.1C). Specifically, the rapidly developing borylation techniques⁷ can expand the system's synthetic applicability to allow facile access to a wider range of chiral carbonyl compounds.⁸

A. Biomedical significance of chiral carbonyls



B. Inspiring works

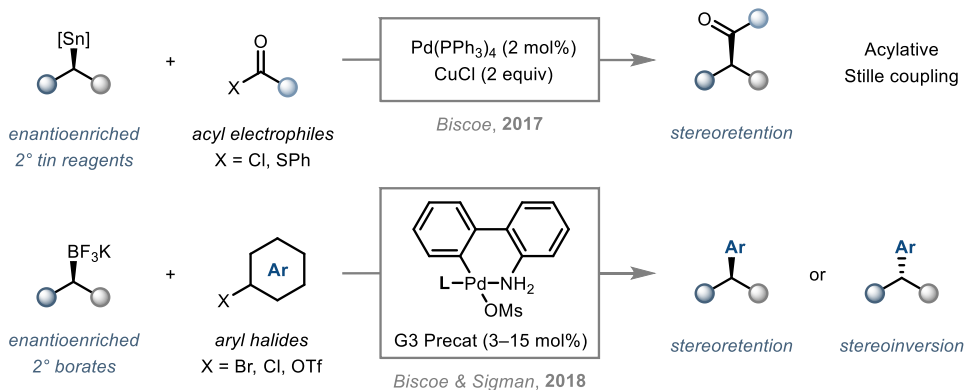


Figure 5.2. Significance of chiral carbonyl compounds and inspiring works

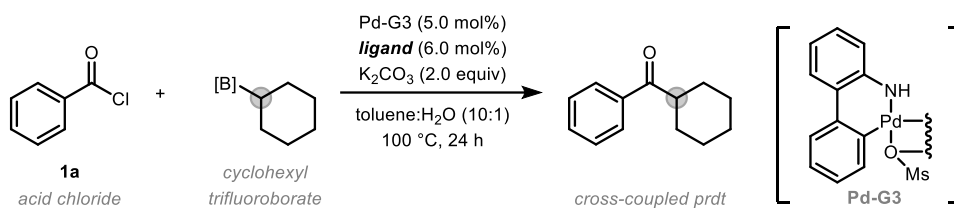
Herein, we disclosed an unprecedented stereospecific Pd-catalyzed acylative Suzuki-Miyaura reactions of chiral alkylboron compounds, delivering potentially accessible all types of chiral α -aryl carbonyl compounds.^{9–11} The developed protocol generally exhibits an high stereospecificity, which enables the complete transfer of stereochemical information from the starting materials, an enantioenriched organoboron reagent, to the reaction center of the targeted chiral carbonyl compounds.

5.2. Results and Discussion

5.2.1. Optimization of the Protocol

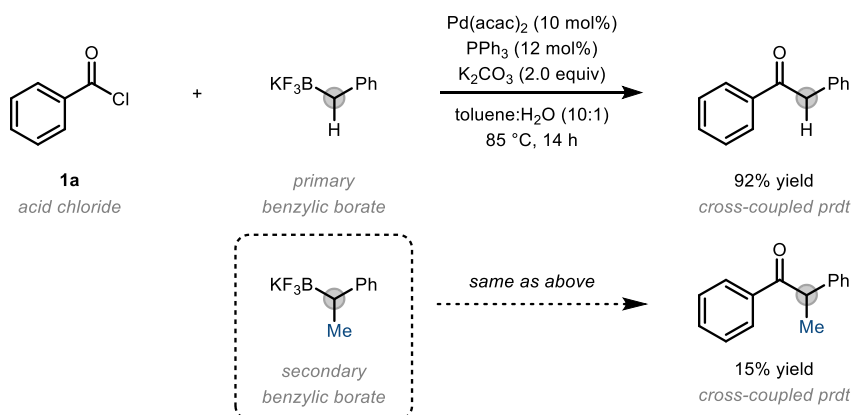
We commenced our initial investigation by examining the cross-coupling reaction between benzoyl chloride (**1a**) and cyclohexyl trifluoroborates to confirm the reactivity of unactivated secondary trifluoroborates for acylative cross-coupling. Inspired by Biscoe's pioneering work¹² on stereospecific arylation of unactivated secondary trifluoroborates, we applied comparable reaction conditions using a third-generation (G3) Buchwald precatalyst to an acylative variant (Table 5.1). Despite a wide range of ligand evaluations, neither the desired product nor side product formation was observed (entries 1–11). In addition, under Deng's reaction conditions¹⁰ that enabled acylative coupling between cyclopropyl boronic acids and acid chlorides, the cross-coupled product was not formed (entries 12–14). We next paid attention to the use of more reactive benzylic trifluoroborates to solve the issue of the low reactivity of unactivated trifluoroborates. When utilizing primary benzylic trifluoroborates, the desired cross-coupled ketone products were formed with excellent yield under the reaction conditions that we found on the basis of comprehensive evaluation of the reaction parameters (Scheme 5.1). However, when the secondary benzylic trifluoroborates were used as nucleophilic coupling partners, the reactivity was dramatically decreased, implying the need for different reaction conditions for the achievement of cross-coupling of secondary benzylic nucleophiles.

Table 5.1. Initial investigation for the development of acylative Suzuki coupling using unactivated secondary trifluoroborates



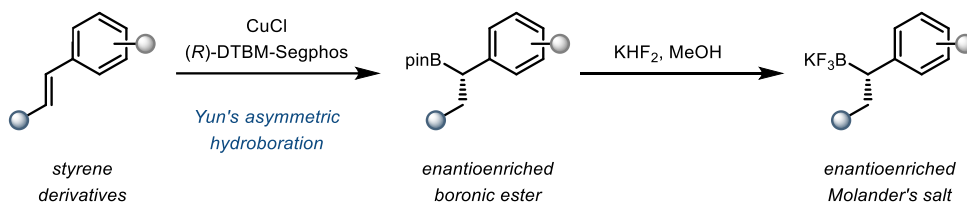
entry	ligand	[B]	note	yield (%) ^a
1	DavePhos	BF ₃ K	-	n.d. ^b
2	tBuDavePhos	BF ₃ K	-	n.d.
3	PhDavePhos	BF ₃ K	-	n.d.
4	XPhos	BF ₃ K	-	n.d.
5	tBuXPhos	BF ₃ K	-	n.d.
6	MePhos	BF ₃ K	-	n.d.
7	tBuMePhos	BF ₃ K	-	n.d.
8	JohnPhos	BF ₃ K	-	n.d.
9	CyJohnPhos	BF ₃ K	-	n.d.
10	RuPhos	BF ₃ K	-	n.d.
11	RuPhos-Pd-G3	BF ₃ K	-	n.d.
12		B(OH ₂)		n.d.
13	Pd(dppf)Cl ₂ /Ag ₂ O/K ₂ CO ₃	Bpin	<i>Deng's condition</i>	n.d.
14		BF ₃ K		n.d.

^aDetermined by ¹H NMR using 1,1,2,2-tetrachloroethane as an internal standard. ^bn.d. indicates not detected



Scheme 5.1. Early results of Pd-catalyzed acylative Suzuki-Miyaura cross-coupling with benzylic trifluoroborates

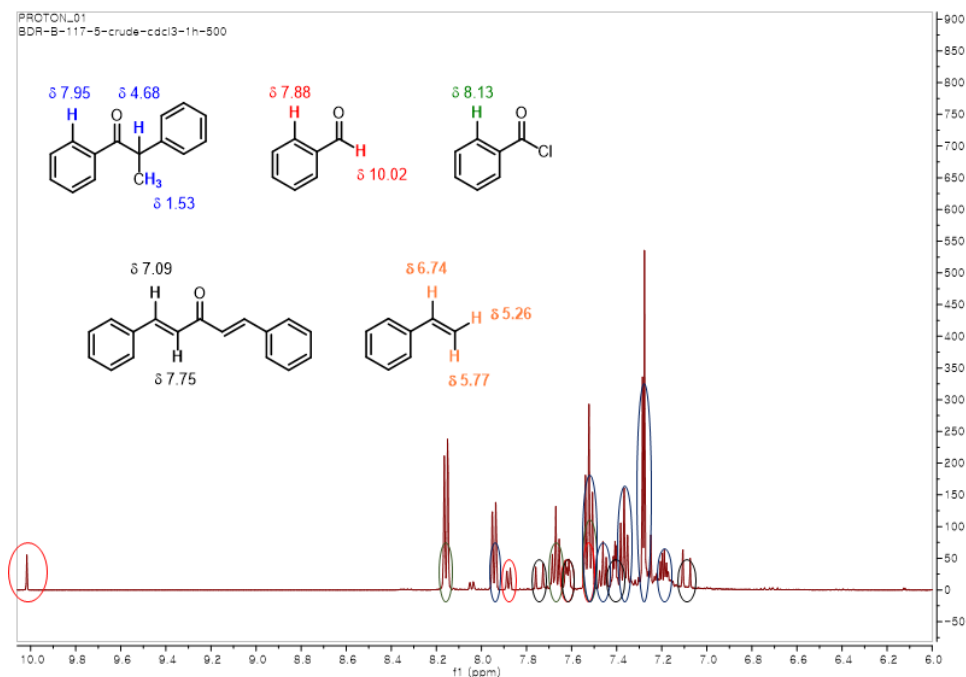
Next, we began our investigation for the development of acylative Suzuki-Miyaura cross-coupling of optically active secondary benzylic nucleophiles with the cross-coupling reaction between benzoyl chloride (**1a**) and an enantioenriched benzylic trifluoroborate (**2b**) as model substrates (Table 5.2).^{7b, 13} The enantioenriched secondary benzylic trifluoroborates were readily prepared through a two-step sequence of Yun's hydroboration¹⁴ of styrene derivatives and the subsequent precipitation into Molander's salts (Scheme 5.2).



Scheme 5.2. Preparation of enantioenriched benzylic trifluoroborates

After a wide variety of evaluation of reaction parameters, the use of Pd_2dba_3 as the $\text{Pd}(0)$ source and Na_2CO_3 as the base was demonstrated to be optimal. Notably, the catalytic system showed the best performance in rigorously anhydrous 1,2-dichloroethane (DCE) solvent, suggesting the unique participation of trifluoroborate salt in its native form (*vide infra*).¹⁵ Another crucial factor for successful transformation is the identity of the supporting ligand. Regardless of the types of supporting ligands, five chemical species were commonly formed, which were observed through ^1H NMR investigations of the crude mixtures: an excess amount of acid chlorides,

dibenzylideneacetone (dba) derived from Pd₂dba₃, the desired cross-coupled product, and aldehyde and styrene generated due to the unproductive side pathway that is the β -hydride elimination/reductive elimination sequence (Scheme 5.3). Most bidentate (**L2–L5**), which are well known to prevent β -hydride elimination by occupation of vacant sites, were not effective providing similar amounts of both the desired product and side product. Also, the use of Buchwald-type ligands (**L7–L9**), that is dialkylbiarylphosphine ligands, did not improve the reactivity.

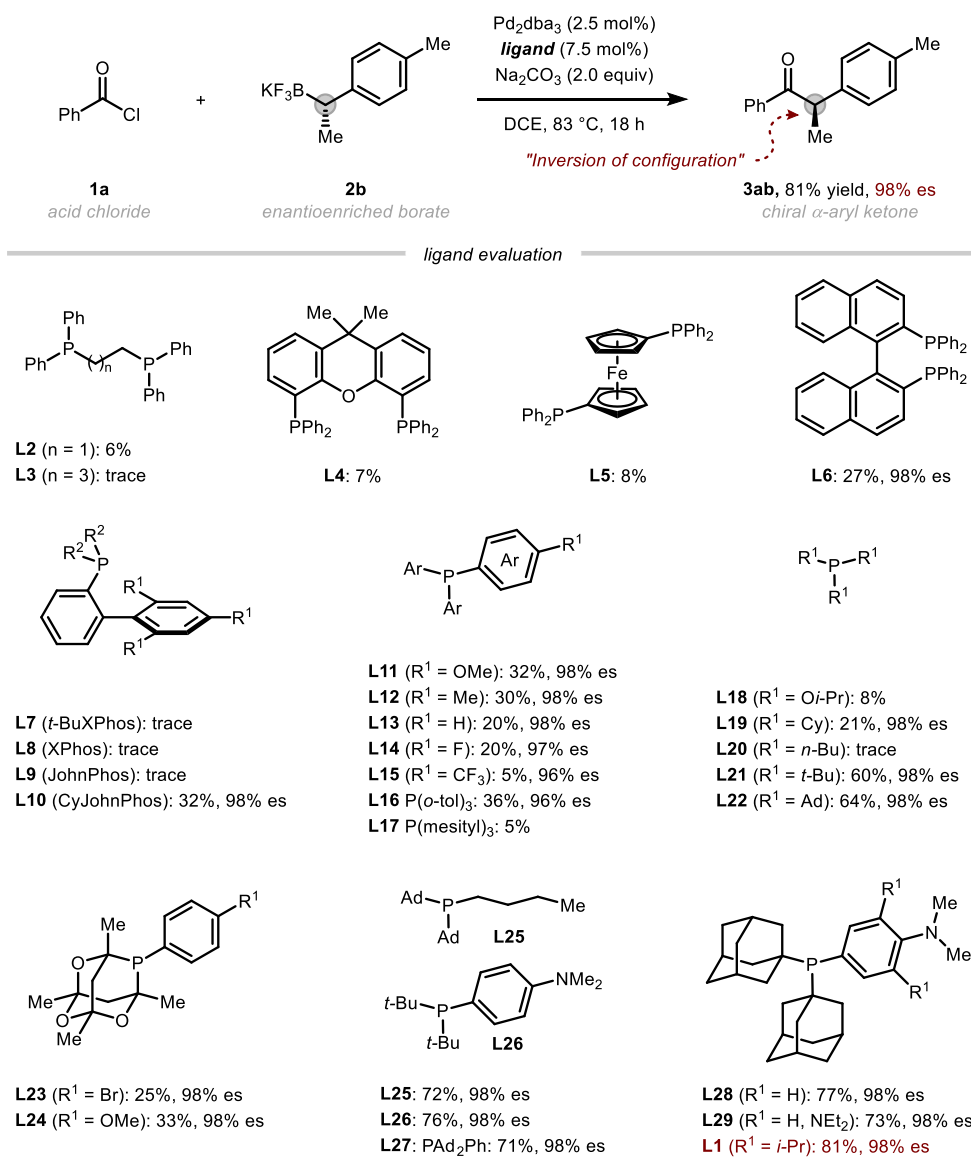


Scheme 5.3. ¹H NMR investigations of crude reaction mixtures

Among them, BINAP (**L6**) and CyJohnPhos (**L10**) only exhibited slightly increased reactivity in terms of desired product formation. In contrast, it was found that monodentate triaryl (**L11–L16**) and trialkyl phosphines (**L19–L22**)

improved the reactivity to a noticeable level. Of note, more efficient formation of the target product was achieved with bulkier and more electron-rich phosphine ligand (**L21** and **L22**). The further optimization of the ligand structure resulted in the phosphine ligand, which is installed with two bulky alkyl groups and one arene ring, effectively facilitating the transformation with great yield. (**L23–L29**). Eventually, diadamantyl phosphine bearing a highly electron-rich arene was identified as the optimal ligand (**L1**).¹⁶ Overall, the variations in the ligand structure hardly affected the stereochemical outcome. Throughout the evaluation of the supporting ligand, a high level of enantiospecificity was obtained generally, and the stereochemical information of the starting materials was delivered at the reaction center of the product in stereoinvertive manner.

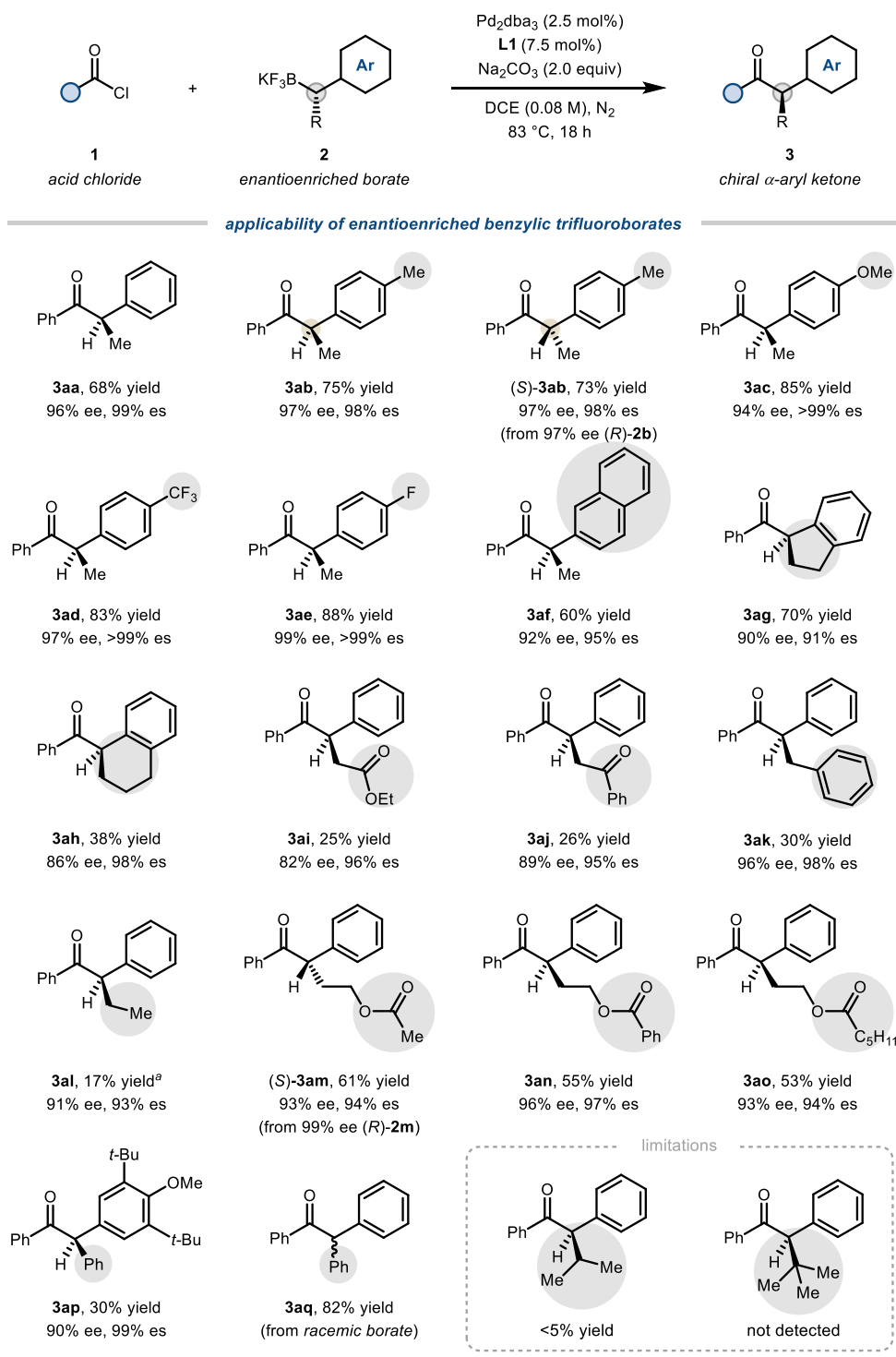
Table 5.2. Evaluation of the supporting ligands



5.2.2. Applicability of the Protocol

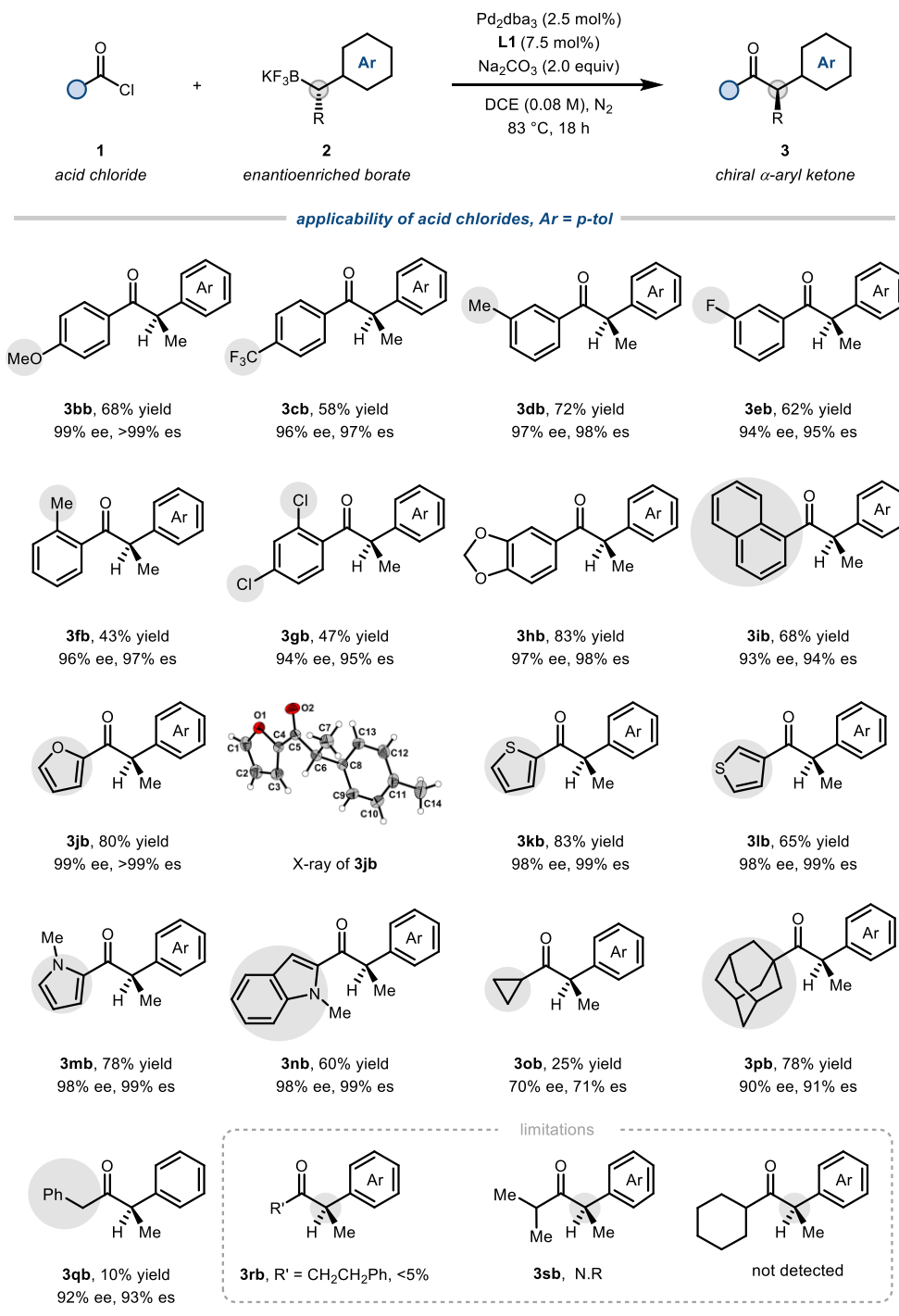
With the established optimal conditions in hand, the applicability of the protocol with respect to both enantioenriched alkylboron reagents and acyl donors was investigated by forming optically pure α -aryl ketones (**Table 5.3**). First, benzylic trifluoroborates bearing a wide variety of arene substituents, with different electronic and steric properties, were tolerated, affording the desired chiral ketones in good yields with excellent enantiospecificity (**3aa–3ah**). The enantioenriched trifluoroborates including either an electron-rich arene (**3aa–3ac**) or an electron-deficient arene (**3ad** and **3ae**) underwent the protocol equally with high efficiency. An extended π system or a bicyclic unit-containing trifluoroborates were also competent coupling partners (**3af–3ah**). Of note, trifluoroborates bearing variously functionalized alkyl chains could participate in the reactions as nucleophilic counterparts (**3ai–3ao**). Considering the limited reactivity of the related benzylic organometallic reagents,¹⁷ the demonstrated examples within the protocols represent significant advances in the progress of the developed protocol. Furthermore, the method could be utilized to construct an α,α -diarylated ketone in an enantiopure form (**3ap**). The observed lower reactivity in this case is presumably due to the steric hinderance derived from the bulkier aryl group existing in trifluoroborates. Importantly, stereochemical outcome was simply controlled by utilizing a reaction partner with alternative stereochemistry (**(S)-3ab** and **(S)-3am**).

Table 5.3. Evaluation of chiral secondary benzylic trifluoroborates



^aAPhos (7.5 mol%) was used instead of **L1** with Ag_2CO_3 (1.0 equiv) additive.

Table 5.4. Evaluation of acid chlorides



Afterward, the reactivity of the acyl donor was investigated (**Table 5.4**). The introduction of various substituents, exhibiting diverse electronic properties, onto the arene ring of the acyl donor was well tolerated (**3bb–3ib**). Moreover, acid chlorides having chloroarene ring proved to be suitable for product formation, underscoring the mildness of the reaction conditions (**3gb**). Also, sterically encumbered substrates could readily participate in this protocol, providing the corresponding products in useful synthetic yields (**3fb** and **3ib**). Remarkably, the incorporation of medicinally important heterocycles into the product successfully enabled the construction of pharmaceutically relevant structural motifs (**3jb–3nb**).¹⁸ Furthermore, aliphatic acid chlorides also exhibited the desired reactivity (**3ob–3qb**). Interestingly, sterically demanding acid chlorides exhibited even greater efficiency in terms of product formation (**3pb**) than substrates containing a smaller aliphatic alkyl group (**3ob** and **3qb**).

Next, to overcome the observed limited reactivity of specific substrates, such as aliphatic acid chlorides (**3rb** and **3sb**) and sterically hindered trifluoroborates (**3al**) as shown above, we further explored the various reaction parameters such as the supporting ligand, temperature and additives. The ethyl-substituted trifluoroborates **2b** gave the desired product under the slightly modified conditions utilizing Ag₂CO₃ as additional base and Apos as supporting ligand (**Table 5.5**). However, despite conducting a wide range of evaluations on various reaction parameters, the reactivity did not reach a

practical level of improvement. Of note, propylbenzene (**S3**), presumably generated due to the deborylation pathway, accounts for the majority of the side products, providing further evidence for the observed limited reactivity of bulkier trifluoroborates. On the other hands, during the reactions with aliphatic acid chloride as electrophiles, no noticeable side products were found, which could provide a clue for resolving the reactivity issue (**Table 5.6**).

Table 5.5. Further evaluation of reaction parameters for sterically encumbered trifluoroborates

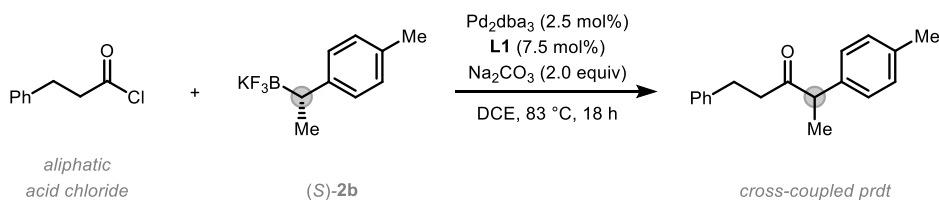
Ph-COCl (1a, 2.0 equiv) + $\text{KF}_3\text{B-Ph-Et}$ ((S)-2b, 0.1 mmol) $\xrightarrow[\text{DCE, 83 }^\circ\text{C, 18 h}]{\text{Pd}_2\text{dba}_3 (2.5 \text{ mol}\%), \text{APhos} (7.5 \text{ mol}\%), \text{Na}_2\text{CO}_3 (2.0 \text{ equiv}), \text{Ag}_2\text{CO}_3 (1.0 \text{ equiv})}$ Ph-CO-Ph-Et (cross-coupled prdt)

S1 **S2** **S3** **S4**

entry	variation	prdt (%) ^a	S1 (%) ^a	S2 (%) ^a	S3 (%) ^a	S4 (%) ^a
1	APhos	20	16	22	36	-
2	dppe	-	2	6	9	24
3	dppp	-	3	9	14	-
4	dppb	5	8	17	16	13
5	dpppe	-	1	3	9	34
6	dppf	-	1	3	9	21
7	dtbpf	2	2	9	21	7
8	dppBz	-	1	3	4	6
9	1.3-dppBz	-	1	-	5	8
10	DPEphos	-	1	-	11	30
11	XantPhos	-	-	31	14	1
12	BINAP	-	1	12	16	30
13	BIPHEP	-	1	8	10	3
14	48 h	19	19	25	45	-
15	Pd/L = 10/15	21	21	29	38	30
16	DCE = 0.7	17	12	19	25	4
17	DCE = 2.0	23	22	25	41	9
18	1 : 2 = 3.0 : 1.0	17	14	17	36	6
19	1 : 2 = 1.0 : 1.5	24	20	27	45	7

^aDetermined by ¹H NMR using 1,3,5-trimethoxybenzene as an internal standard.

Table 5.6. Further evaluation of reaction parameters for aliphatic acid chlorides



entry	deviation from standard conditions	solvent	yield (%) ^a
1	-	-	10
2	Li ₂ CO ₃	-	n.d. ^b
3	K ₂ CO ₃	-	5
4	Ag ₂ CO ₃	-	n.d.
5	Ag ₂ O	-	16
6	K ₃ PO ₄	-	n.d.
7	PCy ₃	-	5
8	P(<i>o</i> -tol) ₃	-	4
9	DavePhos	-	n.d.
10	-	toluene	2
11	-	1,4-dioxane	14
12	-	diisopropyl ether	trace
13	-	xylene	13
14	100 °C	1,4-dioxane	14
15	120 °C	1,4-dioxane	trace

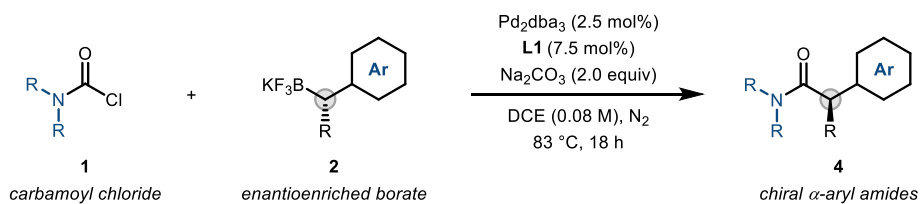
^aDetermined by ¹H NMR using 1,3,5-trimethoxybenzene as an internal standard. ^bn.d. indicates not detected

Subsequently, we applied the developed synthetic approach to synthesize carboxylic acid derivatives (**Table 5.7A**). By harnessing readily available carbamoyl chlorides, we successfully incorporated them into the catalytic carbamoylation process, enabled the formation of chiral α -aryl amides (**4a–4e**). It is worth noting that *N*-methoxy-*N*-methylcarbamoyl chloride proved to be an efficient carbamoyl donor under slightly modified conditions, leading to the generation of the corresponding Weinreb amide (**4f**)¹⁹. Furthermore, the scalability of the protocol was demonstrated, with no significant loss of reactivity observed even when the reaction scale was increased by tenfold. As a result, by utilizing the Weinreb amide as a pivotal intermediate, this

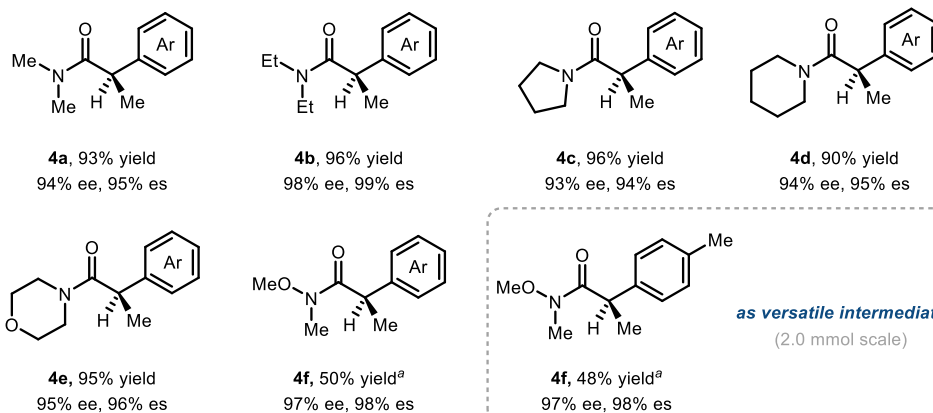
developed strategy can be extended to a general synthetic protocol for the preparation of valuable chiral α -aryl carbonyl compounds (**Table 5.7B**). Simple hydride addition or Fisher esterification could be employed to construct the corresponding chiral aldehyde or methyl ester (**5a** and **5b**). Moreover, we discovered that nucleophilic substitution with various carbon-based organometallic reagents allowed access to a range of challenging chiral ketones. For instance, a primary alkyl ketone (**5c**), which is difficult to obtain with the extension of the method (e.g., **Table 5.4, 3rb** and **3sb**), and α,β -unsaturated ketones (**5d** and **5e**), which are typically incompatible with a nucleophilic reaction partner, could now be synthesized. Finally, we achieved direct installation of a heterocycle, providing a pharmaceutically relevant carbonyl compound (**5f**), while preserving complete stereochemical integrity in all these cases.

Finally, to further demonstrate the robustness of this synthetic strategy, we attempted the direct functionalization of complex commercial pharmaceuticals (**3tb–3vb**) (**Table 5.8**). Acid chlorides derived from adapalene, probenecid, and febuxostat were successfully utilized, leading to the corresponding ketone products in synthetically useful yields with excellent stereochemical integrity. Throughout the transformation, the complex architecture of these bioactive molecules remained unaffected.

Table 5.7. Evaluation of carbamoyl chlorides and transformation of chiral Weinreb amide as versatile intermediate



A. applicability of carbamoyl chlorides, Ar = *p*-tol



^aPA₃ (7.5 mol%) was used instead of L1

B. Transformation of chiral Weinreb amide

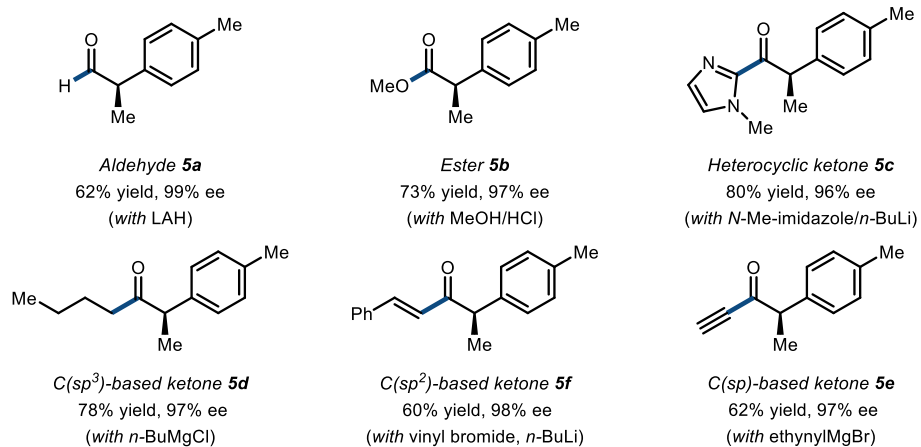
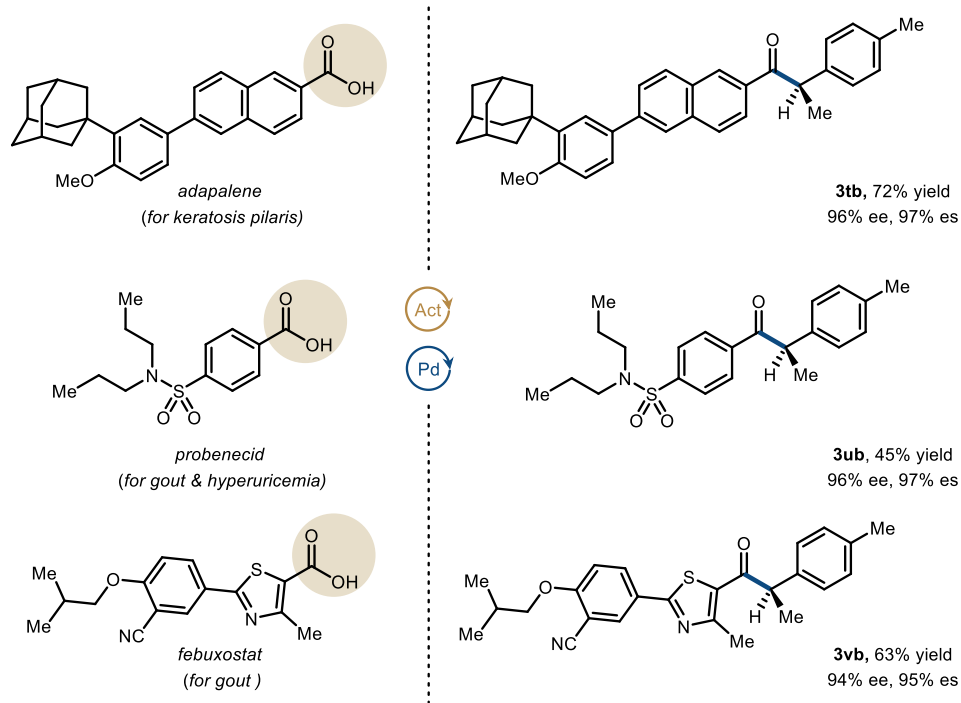
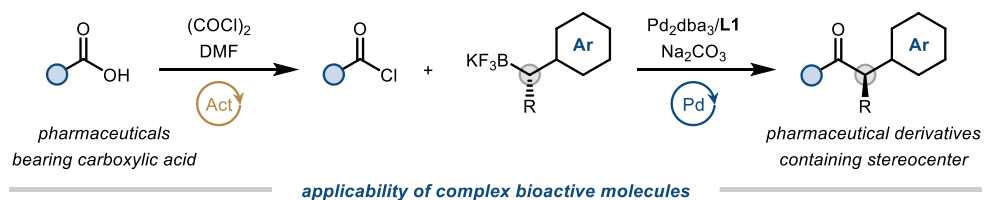


Table 5.8. Functionalization of complex commercial pharmaceuticals



5.2.3. DFT Computed Reaction Mechanism

The DFT computations were conducted by PHYC Research Lab (Oregon State University) (Abdikani Omar Farah, Taisiia Feoktistova and Prof. Paul Ha-Yeon Cheong)

We then explored the origin of the high stereospecificity of the catalytic system. In a stereospecific cross-coupling reaction of chiral organoboron reagents, the stereochemical outcome is governed by the mechanism over the course of transmetalation, which usually follows an S_E2 -type mechanism.⁶ A stereoretentive pathway is commonly observed, although several factors, including internal coordination by the substrate,²⁰ supporting ligand,²¹ steric nature of nucleophile²² or additives²³ are known to influence the process. To shed light on the robust stereoinvertive transmetalation of our system, we used density functional theory computations using Gaussian 16 with PBE-D3BJ/6-31G(d) and LANL2DZ. A solvent model based on density was employed for DCE at 83 °C.

The overall process (**Figure 5.3A**) begins with the coordination of carbonyl chloride **1a** to the bisligated palladium(0) species **I**, which undergoes oxidative addition with a barrier of 14.7 kcal/mol (**oxidative addition-TS-II**). The initially formed *cis*- oxidative addition complex (**Int-III**) isomerizes to the *trans*- complex (**Int-III'**). Then the dissociation of an APhos ligand from **Int-III'** to give the monoligated acylpalladium(II) species (**Int-IV**) sets the stage for the key transmetalation.^{24,25} An alternative pathway,

initiated by ligand dissociation from **I** followed by oxidative addition to a monoligated palladium(0), was calculated to be unfavorable (*See SI for details*). Finally, reductive elimination from transmetalation complex (**Int-VI**) completes the catalytic cycle (**reductive elimination-TS-VII**).

The selectivity of the overall cross-coupling process is determined in the transmetalation step, which can proceed either via inversion or retention of the stereochemistry (**Figure 5.3B**). The transition state leading to inversion (**inversion transmetalation-TS-V**) was found to be lower in energy than that of retention (**retention-transmetalation-TS-V**) by 2.3 kcal/mol (93% ee), which agrees well with the experimental selectivity of 2.7 (96% ee).²⁶ Interestingly, the Pd–C–B angle of the **inversion transmetalation-TS-V** deviates from the conventionally proposed 180° arrangement (135.6°), and the multiple metal-halogen interaction array of reaction partners coordinated to the potassium ion lowers the reaction barrier by 3.8 kcal/mol (*See SI for details*).²⁷ The metal-halogen interactions arise from the mitigation of developing negative charge on the unhydrolyzed trifluoroborate ion. This further underscores the importance of the anhydrous reaction medium (*vide supra*).^{15a-c, f} The potential formation of a cationic palladium species through the liberation of the chloride ligand was demonstrated to be energetically unfavorable. Presumably, the nonpolar nature of the reaction medium disfavors the commonly postulated prerequisite step for a facile transmetalation.^{15f}

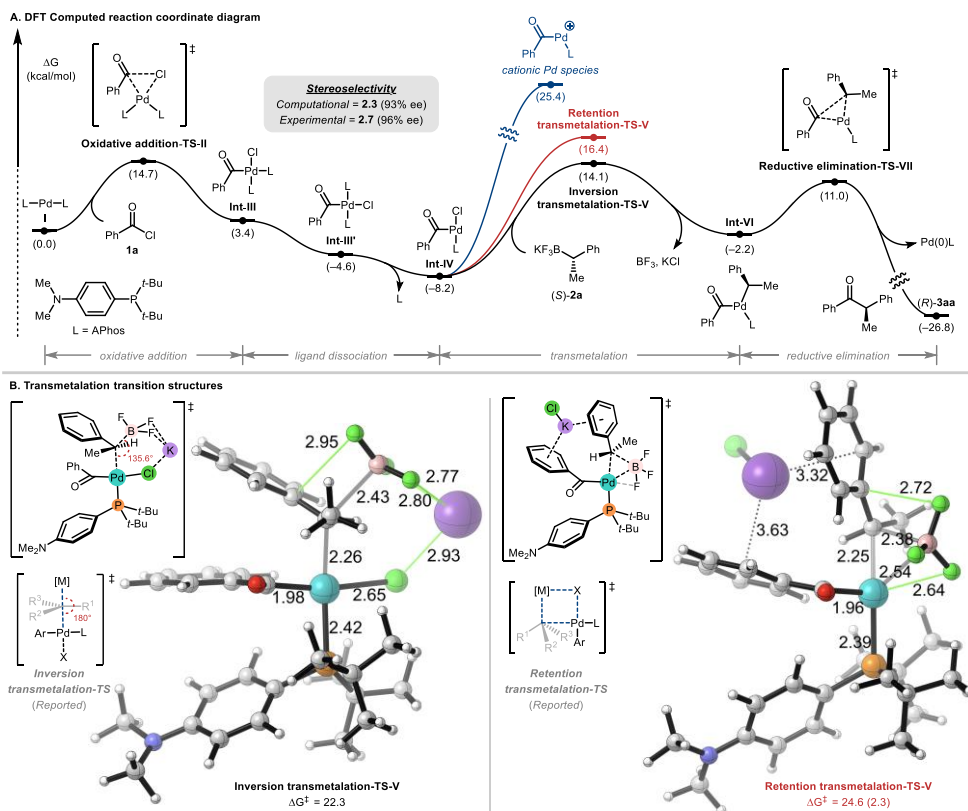


Figure 5.3. DFT computed reaction coordinate diagram (Top, A); Transmetalation transition structures, energies in kcal/mol, distances in Å (Bottom, B).

5.2.4. Mechanistic Investigations

The computationally identified mechanistic features of the reaction were further supported by experimental studies (**Figure 5.4**). First, the acylation experiment of acid chloride **1k** using a preformed oxidative addition complex **[Pd]-A** furnished both **3kb** and **3ab** in an enantiomerically pure form, indicating an active participation of the **[Pd]-A** as an intermediate of the catalytic cycle (**Figure 5.4A**).²⁸

Furthermore, the experiments using **[Pd]-A** as the Pd source with or without added ligand confirmed the importance of the bulky supporting ligand (**Figure 5.4B**). The desired level of reactivity was acquired only in the presence of **L1**, which presumably undergoes ligand exchange with the supporting ligand of **[Pd]-A**, to afford the monoligated acylpalladium (II) species (**Int-IV**).

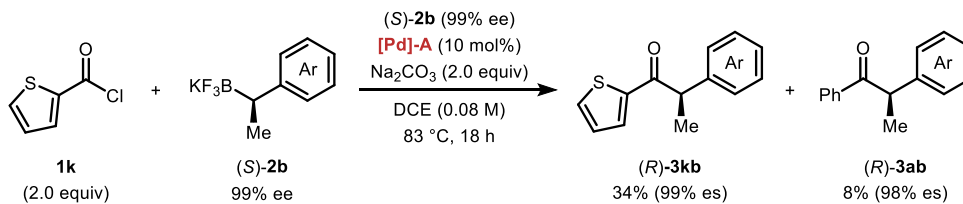
The crucial involvement of the potassium ion in the cyclic transition state of the stereo-invertive transmetalation was substantiated by a series of control experiments (**Figure 5.4C**). Incorporation of the potassium chelator, 18-crown-6, proportionally impeded product formation,²⁹ suggesting the importance of the potassium ion for product formation.³⁰ During the course, the stereospecificity remained virtually unchanged. Interestingly, smaller crown ethers, *i.e.*, 15-crown-5 and 12-crown-4, which are known to exhibit diminished specificity for potassium binding, were shown to be less efficient in obstructing product formation. In addition, the replacement of the counter

cation of the trifluoroborate had a paramount impact on the reaction outcome. The use of a larger counter cation (Cs), which induces a more relaxed interaction with halogen atoms, resulted in significantly reduced reactivity for the acylation.

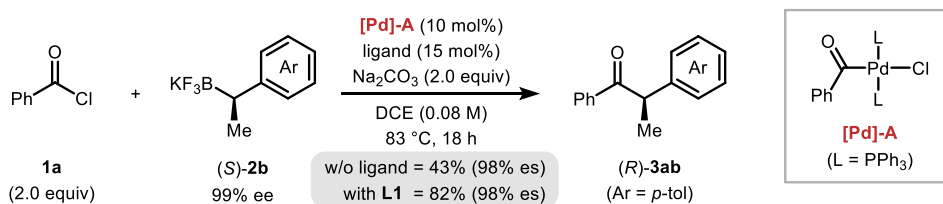
Ultimately, when the trifluoroborate is paired with a non-coordinating counter cation, tetra *n*-butyl ammonium, the reactivity was completely shut off. Taken together, these results support the essential potassium-halogen interaction for the stereospecific transmetalation step.

Figure 5.4. Mechanistic investigations

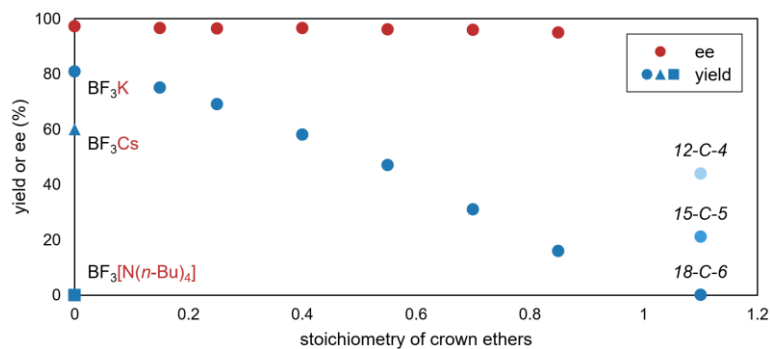
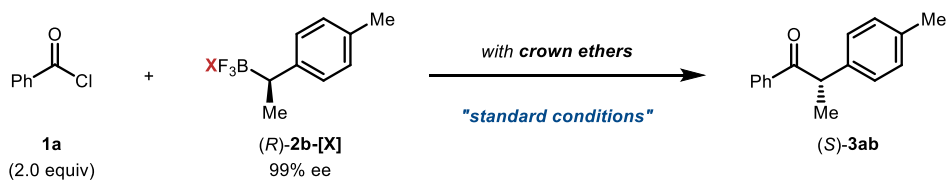
A. Control experiment with a preformed oxidative addition complex as the Pd source



B. Improved reactivity with L1



C. Impact of counteraction



5.3. Conclusion

In conclusion, we have developed a new Pd-catalyzed method for the preparation of valuable chiral α -aryl carbonyl compounds. The method exploits a direct use of activated acyl and carbamoyl donors that react with stereochemically enriched benzylic trifluoroborates in a highly stereospecific fashion. By utilizing the strategy, a wide range of α -arylated ketones and carboxylic acid derivatives were prepared with high stereochemical integrity. The process was successfully mediated by a catalyst system supported by a bulky and electron-rich monodentate dialkylaryl phosphine ligand. In addition, a unique metal-halogen interaction in the transition state was identified to facilitate a novel invertive transmetalation process at the sp^3 -hybridized reaction center. It is expected that the mechanistic insights attained from this study should extend the applicability of the $C(sp^3)$ -based organometallic compounds to a more general setting.

5.4. References

- (1) Sandford, C.; Aggarwal, V. K. *Chem. Commun.* **2017**, *53*, 5481.
- (2) (a) Hao, Y.-J.; Hu, X.-S.; Zhou, Y.; Zhou, J.; Yu, J.-S. *ACS Catal.* **2020**, *10*, 955. (b) Orlandi, M.; Escudero-Casao, M.; Licini, G. *Synthesis* **2021**, *53*, 4559.
- (3) (a) Matteson, D. S.; Man, H.-W.; Ho, O. C. *J. Am. Chem. Soc.* **1996**, *118*, 4560. (b) Ros, A.; Aggarwal, V. K. *Angew. Chem., Int. Ed.* **2009**, *48*, 6289. (c) Sonawane, R. P.; Jheengut, V.; Rabalakos, C.; Larouche-Gauthier, R.; Scott, H. K.; Aggarwal, V. K. *Angew. Chem., Int. Ed.* **2011**, *50*, 3760. (d) Fandrick, K. R.; Mulder, J. A.; Patel, N. D.; Gao, J.; Konrad, M.; Archer, E.; Buono, F. G.; Duran, A.; Schmid, R.; Daeubler, J.; Desrosiers, J.-N.; Zeng, X.; Rodriguez, S.; Ma, S.; Qu, B.; Li, Z.; Fandrick, D. R.; Grinberg, N.; Lee, H.; Bosanac, T.; Takahashi, H.; Chen, Z.; Bartolozzi, A.; Nemoto, P.; Busacca, C. A.; Song, J. J.; Yee, N. K.; Mahaney, P. E.; Senanayake, C. H. *J. Org. Chem.* **2015**, *80*, 1651.
- (4) For representative reviews on stereospecific cross-coupling, see: (a) Wang, C.-Y.; Derosa, J.; Biscoe, M. R. *Chem. Sci.* **2015**, *6*, 5105. (b) Leonori, D.; Aggarwal, V. K. *Angew. Chem., Int. Ed.* **2015**, *54*, 1082. (c) Cherney, A. H.; Kadunce, N. T.; Reisman, S. E. *Chem. Rev.* **2015**, *115*, 9587. (d) Rygus, J. P. G.; Crudden, C. M. *J. Am. Chem. Soc.* **2017**, *139*, 18124. (e) Ma, X.; Murray, B.; Biscoe, M. R. *Nat. Rev. Chem.* **2020**, *4*, 584.

- (5) (a) Sarabu, R.; Bizzarro, F. T.; Corbett, W. L.; Dvorožniak, M. T.; Geng, W.; Grippo, J. F.; Haynes, N.-E.; Hutchings, S.; Garofalo, L.; Guertin, K. R.; Hilliard, D. W.; Kabat, M.; Kester, R. F.; Ka, W.; Liang, Z.; Mahaney, P. E.; Marcus, L.; Matschinsky, F. M.; Moore, D.; Racha, J.; Radinov, R.; Ren, Y.; Qi, L.; Pignatello, M.; Spence, C. L.; Steele, T.; Teng, J.; Grimsby, J. *J. Med. Chem.* **2012**, *55*, 7021. (b) Harrington, P. J.; Lodewijk, E. *Org. Process Res. Dev.* **1997**, *1*, 72. (c) Aoki, S.; Watanabe, Y.; Sanagawa, M.; Setiawan, A.; Kotoku, N.; Kobayashi, M. *J. Am. Chem. Soc.* **2006**, *128*, 3148.
- (6) For selected examples on stereospecific Pd-catalyzed acylative Stille cross-coupling, see: (a) Ye, J.; Bhatt, R. K.; Falck, J. R. *J. Am. Chem. Soc.* **1994**, *116*, 1. (b) Kells, K. W.; Chong, J. M. *J. Am. Chem. Soc.* **2004**, *126*, 15666. (c) Wang, C.-Y.; Ralph, G.; Derosa, J.; Biscoe, M. R. *Angew. Chem., Int. Ed.* **2017**, *56*, 856. (d) Zhu, F.; Rodriguez, J.; O'Neill, S.; Walczak, M. A. *ACS Cent. Sci.* **2018**, *4*, 1652. (e) Ma, X.; Zhao, H.; Binayeva, M.; Ralph, G.; Diane, M.; Zhao, S.; Wang, C.-Y.; Biscoe, M. R. *Chem* **2020**, *6*, 781.
- (7) For representative reviews on borylation, see: (a) Leonori, D.; Aggarwal, V. K. *Acc. Chem. Res.* **2014**, *47*, 3174. (b) Collins, B. S. L.; Wilson, C. M.; Myers, E. L.; Aggarwal, V. K. *Angew. Chem., Int. Ed.* **2017**, *56*, 11700. (c) Friese, F. W.; Studer, A. *Chem. Sci.* **2019**, *10*, 8503. (d) Wang, M.; Shi, Z. *Chem. Rev.* **2020**, *120*, 7348. (e) Tian, Y.-M.; Guo, X.-N.;

Braunschweig, H.; Radius, U.; Marder, T. B. *Chem. Rev.* **2021**, *121*, 3561. (f) Hu, J.; Ferger, M.; Shi, Z.; Marder, T. B. *Chem. Soc. Rev.* **2021**, *50*, 13129.

- (8) For representative reviews on applications of organoboron compounds, see: (a) Miyaura, N.; Suzuki, A. *Chem. Rev.* **1995**, *95*, 2457. (b) Johansson Seechurn, C. C. C.; Kitching, M. O.; Colacot, T. J.; Snieckus, V. *Angew. Chem., Int. Ed.* **2012**, *51*, 5062. (c) Maluenda, I.; Navarro, O. *Molecules* **2015**, *20*, 7528. (d) Lennox, A.J.J.; Lloyd-Jones, G.C. *Chem. Soc. Rev.* **2014**, *43*, 412. (e) Defrancesco, H.; Dudley, J.; Coca, A. *ACS Symp. Ser.* **2016**, *1236*, 1. (f) Fyfe, J. W. B.; Watson, A. J. B. *Chem.* **2017**, *3*, 31. (g) Sandford, C.; Aggarwal, V. K. *Chem. Commun.* **2017**, *53*, 5481. (h) Beletskaya, I. P.; Alonso, F.; Tyurin, V. *Coord. Chem. Rev.* **2019**, *385*, 137. (i) Buchspies, J.; Szostak, M. *Catalysts* **2019**, *9*, 53. (j) El-Maiss, J.; Mohy El Dine, T.; Lu, C.-S.; Karame, I.; Kanj, A.; Polychronopoulou, K.; Shaya, J. *Catalysts* **2020**, *10*, 296.
- (9) For examples of non-stereoselective acylation of alkyl organoboron reagents, see: (a) Amani, J.; Sodagar, E.; Molander, G. A. *Org. Lett.* **2016**, *18*, 732. (b) Amani, J.; Molander, G. A. *J. Org. Chem.* **2017**, *82*, 1856. (c) Amani, J.; Alam, R.; Badir, S.; Molander, G. *Org. Lett.* **2017**, *19*, 2426. (d) Amani, J.; Molander, G. A. *Org. Lett.* **2017**, *19*, 3612. (e) Masson-Makdissi, J.; Vandavasi, J.; Newman, S. *Org. Lett.* **2018**, *20*, 4094. (f) Chatupheeraphat, A.; Liao, H.-H.; Srimontree, W.; Guo, L.;

Minenkov, Y.; Poater, A.; Cavallo, L.; Rueping, M. *J. Am. Chem. Soc.* **2018**, *140*, 3724. (g) Liu, X.; Hsiao, C.; Guo, L.; Rueping, M. *Org. Lett.* **2018**, *20*, 2976. (h) Shi, W.; Zou, G. *Molecules* **2018**, *23*, 2412. (i) Meng, G.; Szostak, M. *Org. Lett.* **2018**, *20*, 6789. (j) Zheng, Y. L.; Xie, P. P.; Daneshfar, O.; Houk, K. N.; Hong, X.; Newman, S. G. *Angew. Chem., Int. Ed.* **2021**, *60*, 13476. (k) Huang, H.; Dai, Q.-S.; Leng, H.-J.; Li, Q.-Z.; Yang, S.-L.; Tao, Y.-M.; Zhang, X.; Qi, T.; Li, J.-L. *Chem. Sci.* **2022**, *13*, 2584.

(10) For diastereoselective acylative coupling of alkyl organoboron reagents, see: Chen, H.; Deng, M.-Z. *Org. Lett.* **2000**, *2*, 1649.

(11) During the preparation of this manuscript, a Cu-catalyzed stereoretentive acylation of chiral alkylboron compounds has been reported by the Morken group, see: Xu, N; Liang, H; Morken, J. P. *J. Am. Chem. Soc.* **2022**, *144*, 11546.

(12) (a) Li, L.; Zhao, S.; Joshi-Pangu, A.; Diane, M.; Biscoe, M. R. *J. Am. Chem. Soc.* **2014**, *136*, 14027. (b) Zhao, S.; Gensch, T.; Murray, B.; Niemeyer, Z. L.; Sigman, M. S.; Biscoe, M. R. *Science* **2018**, *362*, 670.

(13) (a) Molander, G. A.; Bernardi, C. R. *J. Org. Chem.* **2002**, *67*, 8424. (b) Molander, G. A.; Ellis, N. *Acc. Chem. Res.* **2007**, *40*, 275. (c) Molander, G. A. *J. Org. Chem.* **2015**, *80*, 7837.

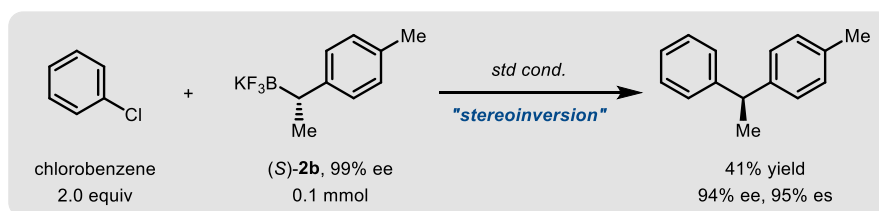
(14) Noh, D.; Yoon, S. K.; Won, J.; Lee, J. Y.; Yun, J. *Chem. - Asian J.* **2011**, *6*, 1967.

- (15) For selected examples on cross-coupling reactions of organoboron reagents under strictly non-aqueous or non-protic conditions, see: (a) Adonin, N. Y.; Babushkin, D. E.; Parmon, V. N.; Bardin, V. V.; Kostin, G. A.; Mashukov, V. I.; Frohn, H.-J. *Tetrahedron* **2008**, *64*, 5920. (b) Wang, B.; Sun, H.-X.; Sun, Z.-H. *Eur. J. Org. Chem.* **2009**, *2009*, 3688. (c) Shabalin, A. Y.; Adonin, N. Y.; Bardin, V. V.; Parmon, V. N. *Tetrahedron* **2014**, *70*, 3720. (d) Delaney, C. P.; Kassel, V. M.; Denmark, S. E. *ACS Catal.* **2020**, *10*, 73. (e) Kassel, V. M.; Hanneman, C. P.; Delaney, C. P.; Denmark, S. E. *J. Am. Chem. Soc.* **2021**, *143*, 13845. (f) Niwa, T.; Uetake, Y.; Isoda, M.; Takimoto, T.; Nakaoka, M.; Hashizume, D.; Sakurai, H.; Hosoya, T. *Nat. Catal.* **2021**, *4*, 1080. (g) Delaney, C. P.; Marron, D. P.; Shved, A. S.; Zar, R. N.; Waymouth, R. M.; Denmark, S. E. *J. Am. Chem. Soc.* **2022**, *144*, 4345.
- (16) Sinai, Á.; Simkó, D. C.; Szabó, F.; Paczal, A.; Gáti, T.; Bényei, A.; Novák, Z.; Kotschy, A. *Eur. J. Org. Chem.* **2020**, *2020*, 1122.
- (17) For selected recent examples on limited reactivity of related benzylic organometallic compounds, see: (a) Xiao, L.-J.; Fu, X.-N.; Zhou, M.-J.; Xie, J.-H.; Wang, L.-X.; Xu, X.-F.; Zhou, Q.-L. *J. Am. Chem. Soc.* **2016**, *138*, 2957. (b) Xiao, L.-J.; Cheng, L.; Feng, W.-M.; Li, M.-L.; Xie, J.-H.; Zhou, Q.-L. *Angew. Chem., Int. Ed.* **2018**, *57*, 461. (c) Zhou, Y.; Engl, O. D.; Bandar, J. S.; Chant, E. D.; Buchwald, S. L. *Angew. Chem., Int. Ed.* **2018**, *57*, 6672. (d) Chen, Y.-G.; Shuai, B.; Xu, X.-T.; Li, Y.-Q.; Yang,

- Q.-L.; Qiu, H.; Zhang, K.; Fang, P.; Mei, T.-S. *J. Am. Chem. Soc.* **2019**, *141*, 3395. (e) Liu, J.; Gong, H.; Zhu, S. *Angew. Chem., Int. Ed.* **2021**, *60*, 4060. (f) Slocumb, H. S.; Nie, S.; Dong, V. M.; Yang, X.-H. *J. Am. Chem. Soc.* **2022**, *144*, 18246.
- (18) (a) Fraga, B. M. *Nat. Prod. Rep.* **2013**, *30*, 1226. (b) Tharra, P.; Baire, B. *J. Org. Chem.* **2015**, *80*, 8314.
- (19) (a) Nahm, S.; Weinreb, S. M. *Tetrahedron Lett.* **1981**, *22*, 3815. (b) Senatore, R.; Ielo, L.; Monticelli, S.; Castoldi, L.; Pace, V. *Synthesis* **2019**, *51*, 2792.
- (20) (a) Ohmura, T.; Awano, T.; Suginome, M. *J. Am. Chem. Soc.* **2010**, *132*, 13191. (b) Sandrock, D. L.; Jean-Gérard, L.; Chen, C.-y; Dreher, S. D.; Molander, G. A. *J. Am. Chem. Soc.* **2010**, *132*, 17108. (c) Lee, J. C. H.; McDonald, R.; Hall, D. G. *Nat. Chem.* **2011**, *3*, 894. (d) Molander, G. A.; Wisniewski, S. R. *J. Am. Chem. Soc.* **2012**, *134*, 16856.
- (21) (a) Zhao, S.; Gensch, T.; Murray, B.; Niemeyer, Z. L.; Sigman, M. S.; Biscoe, M. R. *Science* **2018**, *362*, 670. (b) Lehmann, J. W.; Crouch, I. T.; Blair, D. J.; Trobe, M.; Wang, P.; Li, J.; Burke, M. D. *Nat. Commun.* **2019**, *10*, 1263.
- (22) (a) Li, L.; Zhao, S.; Joshi-Pangu, A.; Diane, M.; Biscoe, M. R. *J. Am. Chem. Soc.* **2014**, *136*, 14027. (b) Murray, B.; Zhao, S.; Aramini, J. M.; Wang, H.; Biscoe, M. R. *ACS Catal.* **2021**, *11*, 2504.

- (23) (a) Awano, T.; Ohmura, T.; Suginome, M. *J. Am. Chem. Soc.* **2011**, *133*, 20738. (b) Lou, Y.; Cao, P.; Jia, T.; Zhang, Y.; Wang, M.; Liao, J. *Angew. Chem., Int. Ed.* **2015**, *54*, 12134. (c) Ohmura, T.; Miwa, K.; Awano, T.; Suginome, M. *Chem. Asian J.* **2018**, *13*, 2414.
- (24) For selected examples on the involvement of monoligated Pd-complexes in transmetalation, see: (a) Barrios-Landeros, F.; Hartwig, J. F. *J. Am. Chem. Soc.* **2005**, *127*, 6944. (b) Ariafard, A.; Yates, B. F. *J. Am. Chem. Soc.* **2009**, *131*, 13981. (c) McMullin, C. L.; Fey, N.; Harvey, J. N. *Dalt. Trans.* **2014**, *43*, 13545. (d) Zheng, Q.; Liu, Y.; Chen, Q.; Hu, M.; Helmy, R.; Sherer, E. C.; Welch, C. J.; Chen, H. *J. Am. Chem. Soc.* **2015**, *137*, 14035. (e) Lyngvi, E.; Sanhueza, I. A.; Schoenebeck, F. *Organometallics* **2015**, *34*, 805. (f) Quesnel, J. S.; Moncho, S.; Ylijoki, K. E. O.; Torres, G. M.; Brothers, E. N.; Bengali, A. A.; Arndtsen, B. A. *Chem. Eur. J.* **2016**, *22*, 15107. (g) Niemeyer, Z. L.; Milo, A.; Hickey, D. P.; Sigman, M. S. *Nat. Chem.* **2016**, *8*, 610. (h) Sperger, T.; Fisher, H. C.; Schoenebeck, F. *Wiley Interdiscip. Rev. Comput. Mol. Sci.* **2016**, *6*, 226. (i) Firsan, S. J.; Sivakumar, V.; Colacot, T. J. *Chem. Rev.* **2022**, *122*, 16983.
- (25) Computational studies have demonstrated that the ligand dissociation process is unfavorable when relatively smaller ligands, such as PPh₃ or PMe₃, were used. This is likely due to the high stability of the bis-ligated palladium complex (*see SI for details*).

(26) The reaction with an aryl chloride also exhibited inversion of configuration, suggesting the generality of this type of mechanism.



(27) A related interaction has been reported for a ground state Pd complex, see: Wolfe, M. M. W.; Shanahan, J. P.; Kampf, J. W.; Szymczak, N. K. *J. Am. Chem. Soc.* **2020**, *142*, 18698.

(28) Unfortunately, the acyl Pd complex with **L1** could not be prepared, presumably due to the reduced stability of the complex. For the preparation of **[Pd]-A**, see: Zhou, T.; Xie, P.-P.; Ji, C.-L.; Hong, X.; Szostak, M. *Org. Lett.* **2020**, *22*, 6434.

(29) (a) Toutov, A. A.; Liu, W. B.; Betz, K. N.; Fedorov, A.; Stoltz, B. M.; Grubbs, R. H. *Nature* **2015**, *518*, 80. (b) Banerjee, S.; Yang, Y. F.; Jenkins, I. D.; Liang, Y.; Toutov, A. A.; Liu, W. B.; Schuman, D. P.; Grubbs, R. H.; Stoltz, B. M.; Krenske, E. H.; Houk, K. N.; Zare, R. N. *J. Am. Chem. Soc.* **2017**, *139*, 6880.

(30) A related role of potassium ion for the transmetalation of C(sp²)-based organoboron reagents has been proposed. (a) Zhang, H.; Kwong, F. Y.; Tian, Y.; Chan, K. S. *J. Org. Chem.* **1998**, *63*, 6886. (b) Mutoh, Y.; Yamamoto, K.; Saito, S. *ACS Catal.* **2020**, *10*, 352.

5.5. Experimental Section

5.5.1. General Information

All reagents were purchased from commercial suppliers including Sigma-Aldrich (Merck), Thermo-Fisher Scientific (for Acros Organics and Alfa Aesar), TCI and Strem, and used without further purification unless otherwise stated. Di-1-adamantylphosphine was purchased from Angene chemical. Dry tetrahydrofuran (THF) and dichloromethane (DCM) were obtained by passing through an activated alumina column of solvent purification system. Other solvents for reactions such as toluene and 1,2-dichloroethane (DCE) were used as anhydrous grade from commercial vendors. All indicated yields represent isolated yield of chromatographically homogeneous product or/and ^1H NMR yield using 1,3,5-trimethoxybenzene (TMB) as an internal standard. All reactions were monitored by thin-layers chromatography (TLC) with 0.25 mm E. Merck silica gel plates (60F-254) using UV light or staining solution including potassium permanganate, *p*-anisaldehyde and phosphomolybdic Acid (PMA) for visualization. NMR spectra were recorded on an Agilent 400-MR DD2 Magnetic Resonance System, Varian/Oxford As-500 instrument and Bruker 500MHz NMR spectrometer and calibrated using residual undeuterated solvent (CHCl_3 at $\delta 7.26$ ppm for ^1H NMR and $\delta 77.16$ ppm for ^{13}C NMR as internal reference. $\text{BF}_3\cdot\text{OEt}_2$ (15% w/w in CDCl_3) and H_3PO_4 (85% w/w in H_2O) solution were used as external standards for obtaining ^{11}B and ^{31}P NMR spectra respectively. For ^{19}F NMR spectra, fluorobenzene was

used as an external standard (-113.15 ppm). Chemical shifts (δ) are reported in parts per million (ppm) and coupling constants (J) are reported in hertz (Hz). The following abbreviations were used to explain multiplicities of NMR spectra: s = singlet, d = doublet, t = triplet, q = quartet, m = multiplet, br = broad. Enantiomeric excess (ee) were determined by employing High-Performance Liquid Chromatography (HPLC) with columns containing chiral stationary phase and HPLC grade solvent (*n*-hexane and isopropanol) as eluents. HPLC equipment was C196-E061W (Shimadzu, degassing unit: DGU-20A5R, pump: LC-20AD, auto sampler: SIL-20A, communication bus module: CBM-20A, UV/Vis detector: SPD-20A, and column oven: CTO-20A). Optical rotations were recorded on JASCO P1030 polarimeter (D line of sodium vapor lamp) with a cylindrical glass cell from the same company. High-resolution mass spectra (HRMS) were recorded on HRMS-ESI Q-TOF 5600 spectrometer of National Instrumentation Center for Environmental Management (NICEM) at Seoul National University and ThermoFisher Scientific Orbitrap Exploris 120 of Core Faculty for Chemical Research, Department of Chemistry at Seoul National University. The crystal structure was solved and refined using the Bruker SHELXTL Software Package at the National Research Facilities and Equipment Center (NanoBioEnergy Materials Center) at Ewha Womans University.

5.5.2. Optimization in Details

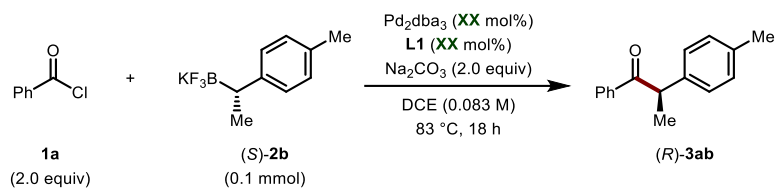
Table S5.1. Effect of Pd source as precatalyst on the reactions

Reaction scheme: Benzoyl chloride (**1a**, 2.0 equiv) reacts with (S)-2b (0.1 mmol) in the presence of Pd_2dba_3 (2.5 mol%), L1 (7.5 mol%), and Na_2CO_3 (2.0 equiv) in DCE (0.083 M) at 83 °C for 18 h to yield (R)-3ab.

entry ^a	deviation from standard conditions	3ab (%) ^b
1	none	81
2	$\text{Pd}(\text{dba})_2$	71
3	$\text{Pd}(\text{PPh}_3)_4$	68
4	$\text{Pd}(\text{COD})(\text{CH}_2\text{TMS})_2$	73
5	$\text{Pd}(\text{OAc})_2$	60
6	$\text{Pd}(\text{acac})_2$	33
7	PdCl_2	31
8	PdBr_2	21
9	PdI_2	6
10	$\text{Pd}(\text{PhCN})_2\text{Cl}_2$	64
11	$\text{Pd}(\text{dppf})\text{Cl}_2$	50
12	$\text{Pd}(\text{dppf})\text{Cl}_2\text{-DCM}$	50

^a**Reaction conditions:** benzoyl chloride **1a** (2.0 equiv), chiral potassium trifluoroborate (*S*)-**2b** (0.1 mmol, 1.0 equiv), Pd source (2.5 mol%), **L1** (7.5 mol%) and Na_2CO_3 (2.0 equiv) in 1.2 mL of DCE, 83 °C, 18 h. ^bYields were determined by ¹H NMR using 1,3,5-trimethoxybenzene as an internal standard.

Table S5.2. Effect of loading of Pd-precatalyst and Pd to **L1** ratio on the reactions

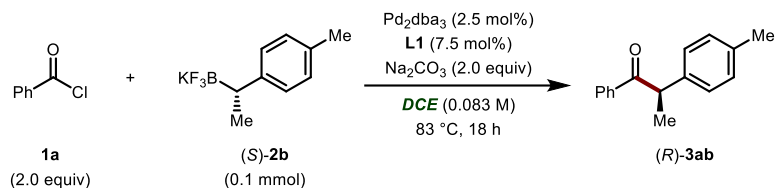


entry ^a	Pd ₂ dba ₃ (mol%)	[Pd] (mol%)	ligand (mol%)	Pd/L	3ab (%) ^b
1	2.5	5.0	5.0	1.0 : 1.0	59
2	2.5	5.0	6.25	1.0 : 1.25	72
3	2.5	5.0	7.5	1.0 : 1.5	81
4	2.5	5.0	10.0	1.0 : 2.0	82

5	0.5	1.25	2.0	1.0 : 1.5	56
6	1.25	2.5	3.75	1.0 : 1.5	70
3	2.5	5.0	7.5	1.0 : 1.5	81
7	3.75	7.5	11.25	1.0 : 1.5	83
8	5.0	10.0	15	1.0 : 1.5	80
9	7.5	15.0	22.5	1.0 : 1.5	77

^a**Reaction conditions:** benzoyl chloride **1a** (2.0 equiv), chiral potassium trifluoroborate (*S*)-**2b** (0.1 mmol, 1.0 equiv), Pd₂dba₃, **L1**, and Na₂CO₃ (2.0 equiv) in 1.2 mL of DCE, 83 °C, 18 h. ^bYields were determined by ¹H NMR using 1,3,5-trimethoxybenzene as an internal standard.

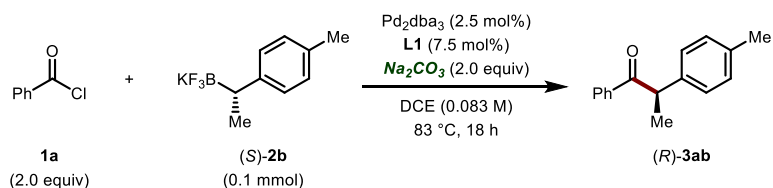
Table S5.3. Effect of solvent identity and the concentration of (*S*)-**2b** on the reactions



entry ^a	deviation from standard conditions	concentration (M)	3ab (%) ^b
1	none	0.33	75
2	none	0.167	75
3	none	0.111	77
4	none	0.083	81
5	none	0.05	80
6	DMF	0.083	N.D
7	DMA	0.083	N.D
8	DMSO	0.083	N.D
9	THF	0.083	41
10	toluene	0.083	58
11	1,4-dioxane	0.083	40
12	1,2-dimethoxyethane	0.083	30
13	Diisopropyl ether	0.083	54

^a**Reaction conditions:** benzoyl chloride **1a** (2.0 equiv), chiral potassium trifluoroborate (*S*)-**2b** (0.1 mmol, 1.0 equiv), Pd_2dba_3 (2.5 mol%), **L1** (7.5 mol%) and Na_2CO_3 (2.0 equiv) in solvent, 83 °C, 18 h. ^bYields were determined by ^1H NMR using 1,3,5-trimethoxybenzene as an internal standard.

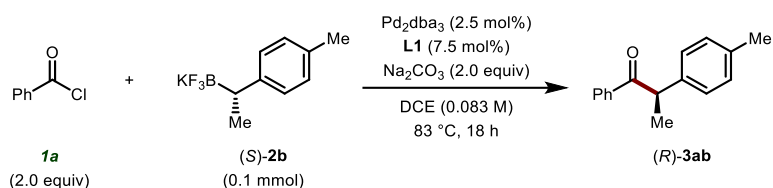
Table S5.4. Effect of additives on the reactions



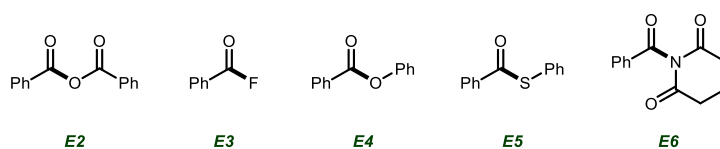
entry ^a	deviation from standard conditions	additives	3ab (%) ^b	es (%)	ee (%) ^c
1	none	-	81	98	97
2	w/o Na_2CO_3	-	5	-	-
3	Li_2CO_3	-	37	98	97
4	K_2CO_3	-	44	98	97
5	Cs_2CO_3	-	trace	-	-
6	Ag_2O	-	56	98	97
7	K_3PO_4	-	23	98	97
8	LiOMe	-	10	88	87
9	NaOt-Bu	-	11	87	86
10	KOt-Bu	-	N.D	-	-
11	none	1.0 equiv of H_2O	32	98	97
12	none	10 equiv of H_2O	15	98	97
13	none	67 equiv of H_2O	trace	-	-
14	set-up using schlenk line	-	51	98	97
15	under atmosphere	-	trace	-	-

^a**Reaction conditions:** benzoyl chloride **1a** (2.0 equiv), chiral potassium trifluoroborate (**(S)-2b**) (0.1 mmol, 1.0 equiv), Pd_2dba_3 (2.5 mol%), **L1** (7.5 mol%) and Na_2CO_3 (2.0 equiv) in 1.2 mL of DCE, 83 °C, 18 h. ^bYields were determined by ^1H NMR using 1,3,5-trimethoxybenzene as an internal standard. ^cThe enantiomeric excess were determined by HPLC analysis.

Table S5.5. Effect of electrophilic coupling partners on the reactions

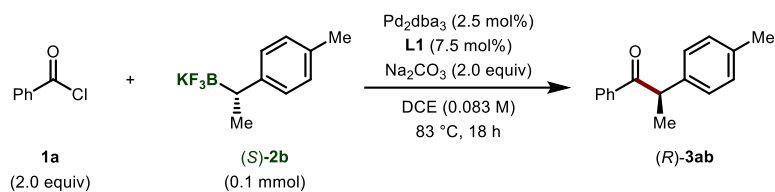


entry ^a	deviation from standard conditions	3ab (%) ^b
1	none	81
2	benzoic anhydride (E2)	15
3	benzoyl fluoride (E3)	N.R
4	phenyl benzoate (E4)	N.R
5	S-phenyl benzothioate (E5)	N.R
6	1-benzoylpiperidine-2,6-dione (E6)	N.R

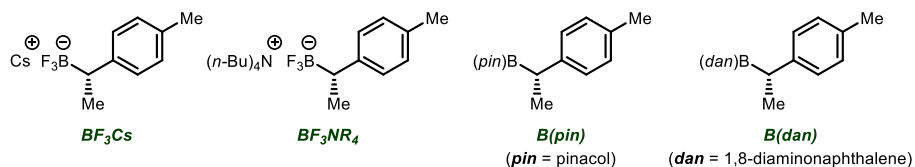


^a**Reaction conditions**: electrophiles (2.0 equiv), chiral potassium trifluoroborate (**S**)-**2b** (0.1 mmol, 1.0 equiv), Pd_2dba_3 (2.5 mol%), **L1** (7.5 mol%) and Na_2CO_3 (2.0 equiv) in 1.2 mL of DCE, 83 °C, 18 h. ^bYields were determined by ^1H NMR using 1,3,5-trimethoxybenzene as an internal standard.

Table S5.6. Effect of nucleophilic coupling partners on the reactions

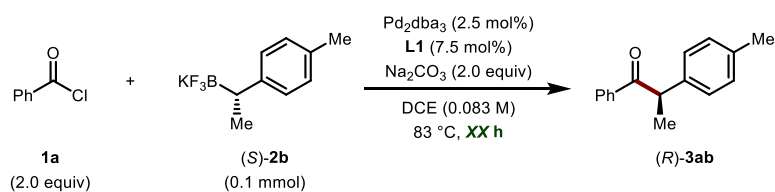


entry ^a	additives	deviation from standard conditions	3ab (%) ^b	es (%) ^b	ee (%) ^b
1	-	none	81	97	98
2	-	BF₃Cs	60	96	97
3	-	BF₃NR₄	N.D.	-	-
4	-	B(pin)	N.D.	-	-
5	-	B(dan)	N.D.	-	-
6	KHF ₂ (1.0 equiv)	B(pin)	trace	-	-

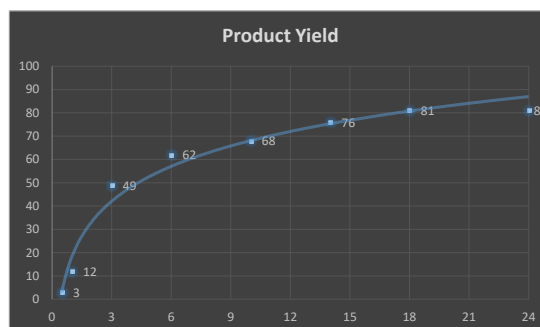


^a**Reaction conditions:** benzoyl chloride **1a** (2.0 equiv), enantioenriched nucleophiles (0.1 mmol, 1.0 equiv), Pd₂dba₃ (2.5 mol%), **L1** (7.5 mol%) and Na₂CO₃ (2.0 equiv) in 1.2 mL of DCE, 83 °C, 18 h. ^bYields were determined by ¹H NMR using 1,3,5-trimethoxybenzene as an internal standard. ^cThe enantiomeric excess were determined by HPLC analysis.

Table S5.7. Reaction profile over time

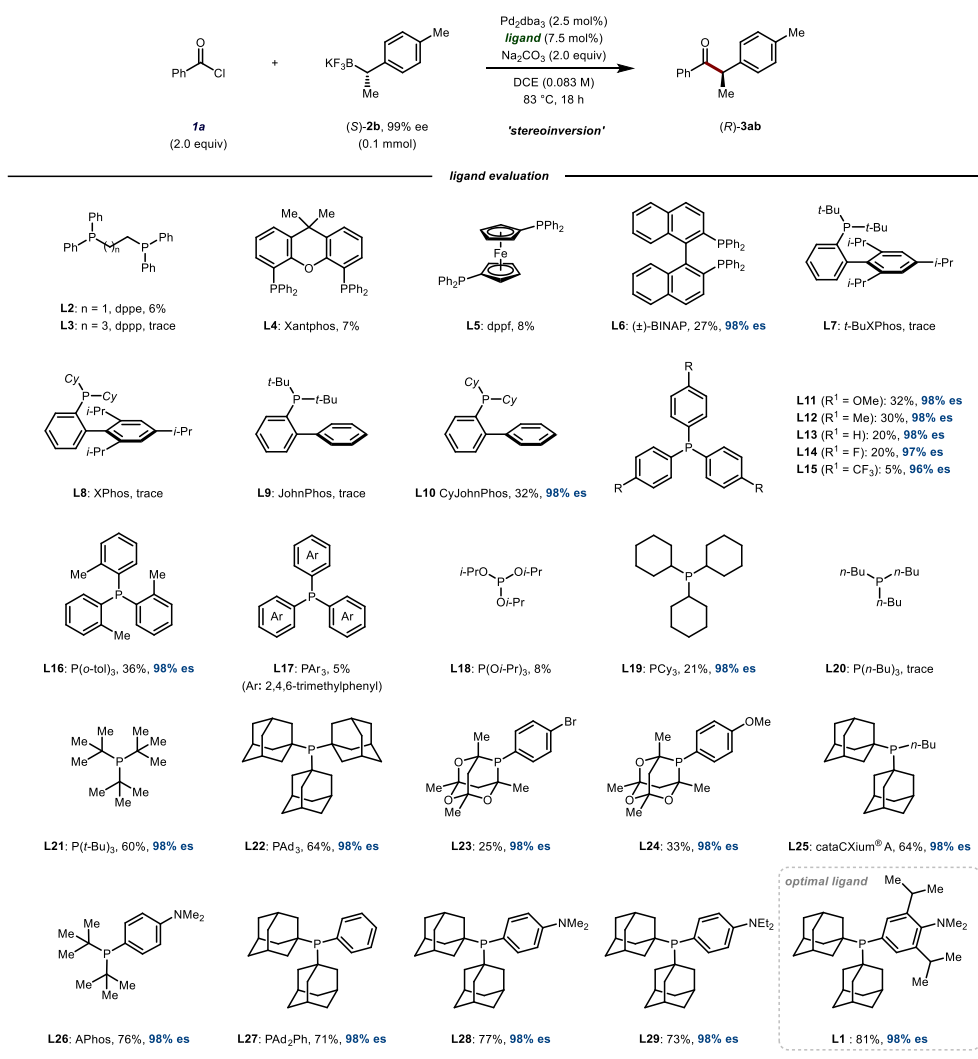


entry ^a	rxn time (h)	3ab (%) ^b
1	0.5	3
2	1.0	12
3	3.0	49
4	6.0	63
6	10.0	68
7	14.0	76
8	18.0	81
9	24.0	80



^a**Reaction conditions:** benzoyl chloride **1a** (2.0 equiv), chiral potassium trifluoroborate (*S*)-**2b** (0.1 mmol, 1.0 equiv), Pd₂dba₃ (2.5 mol%), **L1** (7.5 mol%) and Na₂CO₃ (2.0 equiv) in 1.2 mL of DCE, 83 °C. ^bYields were determined by ¹H NMR using 1,3,5-trimethoxybenzene as an internal standard.

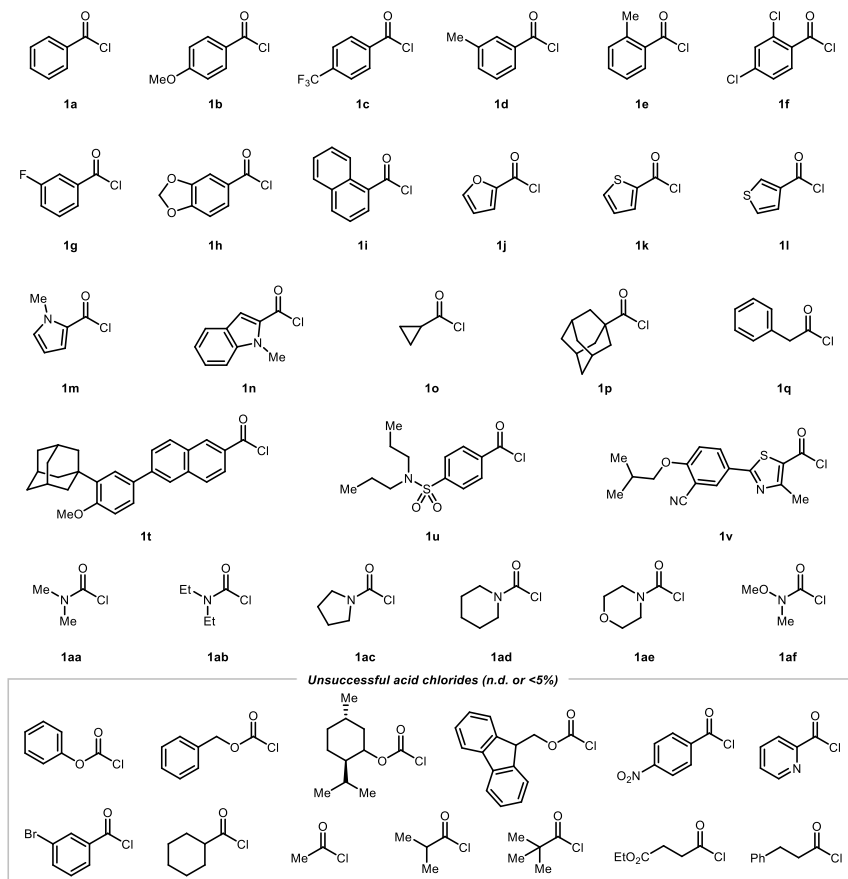
Table S5.8. Ligand evaluation^a



^a**Reaction conditions:** benzoyl chloride **1a** (2.0 equiv), chiral potassium trifluoroborate (*S*)-**2b** (0.1 mmol, 1.0 equiv), Pd₂dba₃ (2.5 mol%), *ligand* (7.5 mol%) and Na₂CO₃ (2.0 equiv) in 1.2 mL of DCE, 83 °C, 18 h. Yields were determined by ¹H NMR using 1,3,5-trimethoxybenzene as an internal standard. The enantiomeric excess was determined by HPLC analysis.

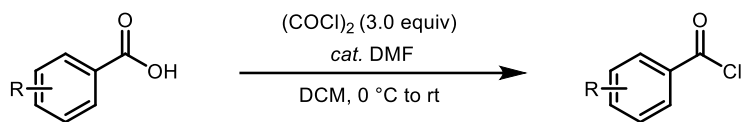
5.5.3. Procedure for the Preparation of Acid Chlorides and Borates

Table S5.9. Aryl and alkyl acid chlorides **1a–1u** and carbamoyl chlorides **1aa–1af**



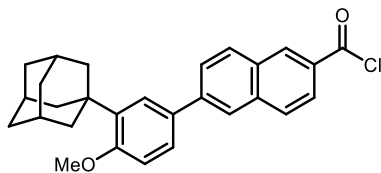
Compounds **1a**, **1b**, **1c**, **1d**, **1e**, **1f**, **1g**, **1h**, **1i**, **1j**, **1k**, **1l**, **1o**, **1p**, **1q**, **1aa**, **1ab**, **1ac**, **1ad**, **1ae** and **1af** were purchased from commercial sources. Acid chlorides **1m**, **1t**, **1u** and **1v** were prepared from the corresponding commercially available carboxylic acid according to *General Procedure A*. The corresponding carboxylic acid of **1n** were prepared according to literature procedure¹ and then **1n** was prepared according to *General Procedure A*

General Procedure A



A oven-dried 50 mL round-bottom flask (RBF) was charged with a magnetic stir bar and the corresponding carboxylic acid (1.0 mmol) and then, the flask was sealed with a rubber septum cap. The flask containing the carboxylic acid was placed under nitrogen atmosphere by three times of evacuating and nitrogen gas back-filling the flask through Schlenk line. Anhydrous dichloromethane (DCM, 0.167 M) was added to the flask via syringe and then, the resulting mixture was cooled to 0 °C under ice bath. After stirring for 10 min at 0 °C, Oxalyl chloride (3.0 equiv) was added dropwise to the reaction mixture. Sequentially, three drops of anhydrous DMF was added via 1 mL of syringe. The reaction mixture was allowed to warm to room temperature and then, stirred for overnight. After that time, the resulting mixture was concentrated under reduced pressure and then, dissolved in 100 mL of DCM/toluene mixture (v/v = 1:9) for azeotrope to remove remaining DMF. The reaction mixture was once more concentrated under reduced pressure and then, dried overnight under vacuum. The resulting product was used in the stereospecific acylative cross-coupling reaction without further purification.

6-(3-((3*r*,5*r*,7*r*)-adamantan-1-yl)-4-methoxyphenyl)-2-naphthoyl chloride (Table S5.9, **1t).**



Following *General Procedure A* from adapalene, the desired product was isolated quantitatively as a beige solid.

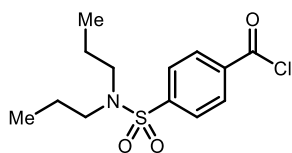
¹H NMR (500 MHz, CDCl₃) δ 8.75 (s, 1H), 8.09–8.00 (m, 3H), 7.94 (d, *J* = 8.7 Hz, 1H), 7.89–7.83 (m, 1H), 7.62 (d, *J* = 2.1 Hz, 1H), 7.59–7.53 (m, 1H), 7.01 (d, *J* = 8.4 Hz, 1H), 3.92 (s, 3H), 2.24–2.15 (m, 6H), 2.15–2.08 (m, 3H), 1.86–1.76 (m, 6H) ppm.

¹³C NMR (126 MHz, CDCl₃) δ 168.46, 159.36, 143.20, 139.27, 137.08, 134.78, 132.11, 131.12, 130.53, 129.88, 128.98, 127.31, 126.14, 125.98, 125.86, 124.75, 112.26, 55.32, 40.72, 37.37, 37.24, 29.22 ppm.

HRMS (ESI) calculated for [C₂₉H₃₀O₃+H]⁺: 427.2268, found: 427.2267.

(HRMS data for **1t** was observed in the form of the corresponding *methyl ester*)

4-(*N,N*-dipropylsulfamoyl)benzoyl chloride (Table S5.9, **1u).**



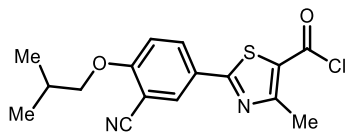
Following *General Procedure A* from probenecid, the desired product was isolated quantitatively as a beige solid.

¹H NMR (500 MHz, CDCl₃) δ 8.23 (d, *J* = 8.3 Hz, 2H), 7.94 (d, *J* = 8.4 Hz, 2H), 3.16–3.07 (m, 4H), 1.62–1.48 (m, 4H), 0.87 (t, *J* = 7.4 Hz, 6H) ppm.

¹³C NMR (126 MHz, CDCl₃) δ 167.57, 146.60, 136.16, 131.95, 127.56, 50.06, 22.07, 11.27 ppm.

HRMS (ESI) calculated for [C₁₄H₂₁NO₄S+H]⁺: 300.1264, found: 300.1261. (HRMS data for **1u** was observed in the form of the corresponding *methyl ester*)

2-(3-cyano-4-isobutoxyphenyl)-4-methylthiazole-5-carbonyl chloride
(Table S5.9, 1v).



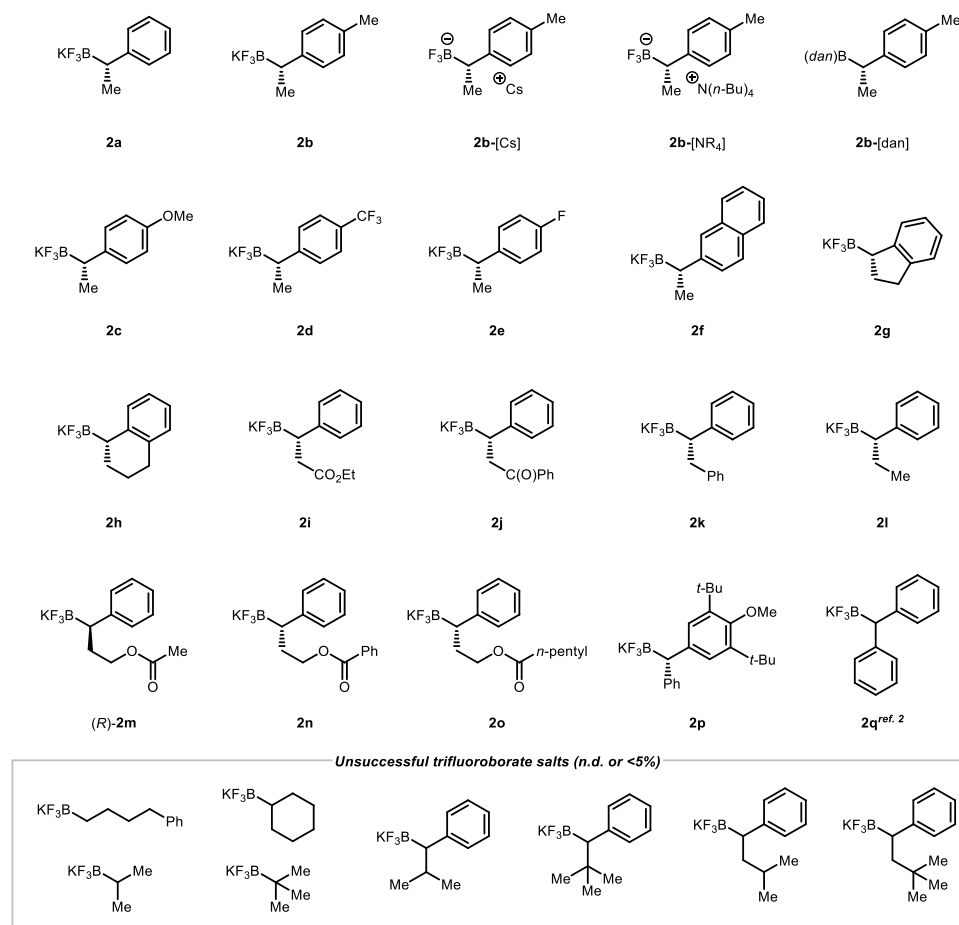
Following *General Procedure A* from febuxostat, the desired product was isolated quantitatively as a beige solid.

¹H NMR (500 MHz, CDCl₃) δ 8.21 (d, *J* = 2.1 Hz, 1H), 8.16–8.06 (m, 1H), 7.04 (d, *J* = 8.9 Hz, 1H), 3.92 (d, *J* = 6.5 Hz, 2H), 2.73 (s, 3H), 2.15–2.28 (m, 1H), 1.09 (d, *J* = 6.7 Hz, 6H) ppm.

¹³C NMR (126 MHz, CDCl₃) δ 171.09, 164.30, 163.30, 158.18, 132.94, 132.52, 127.54, 125.33, 115.23, 112.88, 103.39, 75.96, 28.27, 19.17, 18.61 ppm.

HRMS (ESI) calculated for [C₁₇H₁₈N₂O₃S+H]⁺: 331.1111, found: 331.1111.
(HRMS data for **1v** was observed in the form of the corresponding *methyl ester*)

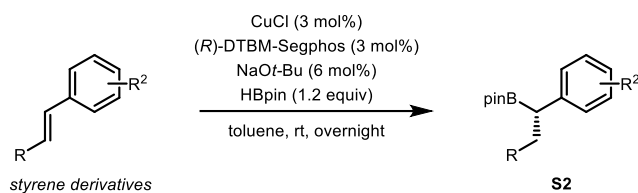
Table S5.10. Enantioenriched trifluoroborate salts **2a–2p**



The corresponding boronic acid pinacol esters **S2** for trifluoroborate salts were prepared according to literature procedures (*General Procedure B–E*). Potassium trifluoroborate salts were prepared from the corresponding boronic acid pinacol esters according to literature procedure (*General Procedure F*). Cesium or/and tetraalkylammonium trifluoroborate salt were prepared according to literature procedure (*General procedure G and H*). The 1,8-

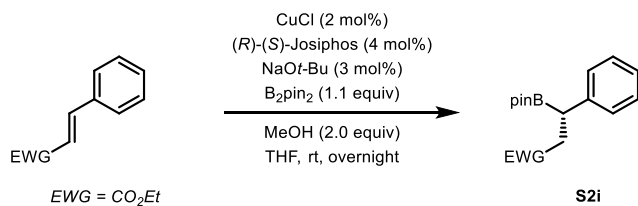
diaminonaphthalene (*dan*)-protected boronic acid was prepared according to literature procedure (*General procedure I*). The enantiomeric excess was analyzed using the corresponding oxidized alcohol originated from boronic acid pinacol ester according to literature procedure (*General procedure J*).

General Procedure B



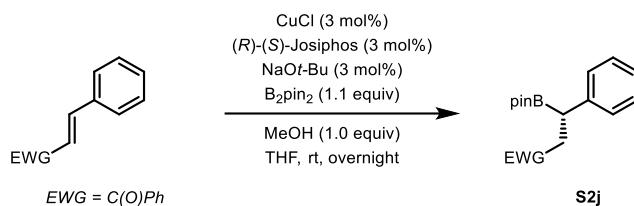
The boronic acid pinacol esters **2a**, **2b**, **2c**, **2d**, **2e**, **2f**, **2g**, **2h**, **2k**, **2l**, (*R*)-**2m**, **2n** and **2o** were prepared according to literature procedure of Prof. Dr. Yun.³

General Procedure C



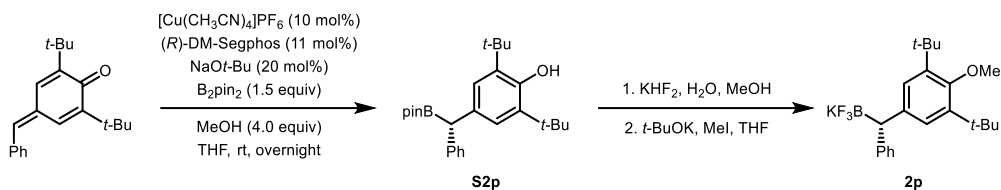
The boronic acid pinacol ester **2i** was prepared according to literature procedure of Prof. Dr. Yun.⁴

General Procedure D



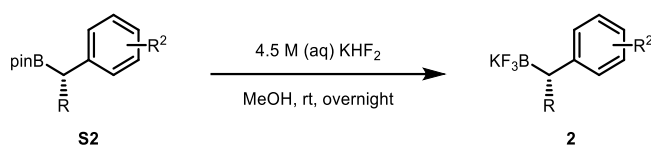
The boronic acid pinacol ester **2j** was prepared according to literature procedure of Prof. Dr. Yun.⁵

General Procedure E



The boronic acid pinacol ester **S2p** was prepared according to the literature procedure of Prof. Dr. Tortosa^{6a} and the trifluoroborate salts **2p** was prepared according to literature procedure of Prof. Dr. Liao.^{6b}

General Procedure F

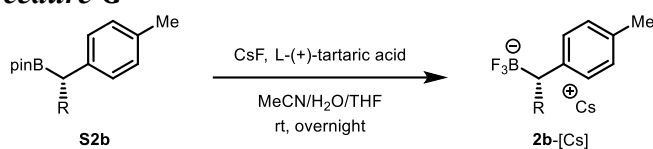


Potassium trifluoroborate salts were prepared according to a slightly modified literature procedure of Prof. Dr. Aggarwal.⁷

The corresponding boronic acid pinacol ester (5.0 mmol) and MeOH (30 mL) was added to a 100 mL plastic Erlenmeyer flask equipped with a magnetic stir bar. The flask was cooled to 0 °C and stirred for 10 min. An aqueous solution of potassium hydrogen fluoride (KHF₂, 4.5 M in H₂O, 22.5 mmol, 4.5 equiv) was slowly added to the flask. Upon completion of the addition, the flask was allowed to warm to room temperature and stirred overnight. The resulting mixture was transferred to a 500 mL round-bottom flask, and the mixture was diluted with toluene (100 mL) for azeotropic removal water. The biphasic mixture was concentrated under reduced pressure using rotary evaporation (20 mbar/40–50 °C). Subsequently, 120 mL of toluene/MeOH mixture (v/v = 10 : 1) were added to the resulting residue and concentrated under reduced pressure. This process was repeated four times. The resulting residue was dissolved in acetone (30 mL) and filtered to remove insoluble salts. The combined filtrate was diluted with toluene (100 mL) and concentrated under reduced pressure. This cycle was repeated two times. The flask was dried overnight under high vacuum on a Schlenk line to give the desired potassium trifluoroborates as white solid.

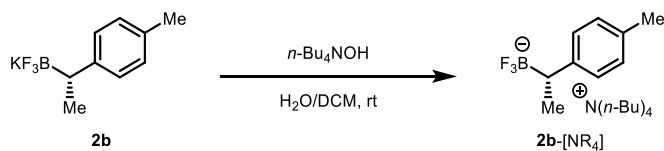
(*Note:* Stereospecific Pd-catalyzed acylative cross-coupling reaction are very sensitive to water. Therefore, it is crucial to remove the remaining water completely. Accordingly, the resulting products are dried overnight at 60 °C under high vacuum)

General Procedure G



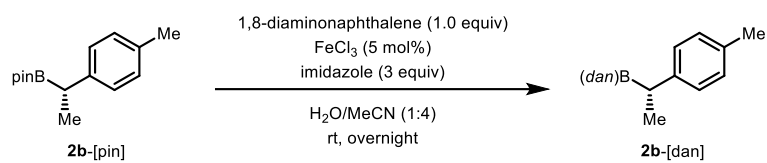
The cesium trifluoroborate salt **2b-[Cs]** was prepared according to literature procedure of *Prof. Dr. Takacs*.⁸

General Procedure H



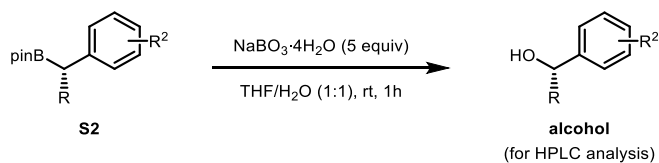
The tetrabutylammonium trifluoroborate salt **2b-[NR₄]** was prepared according to literature procedure of *Prof. Dr. Batrey*.⁹

General Procedure I



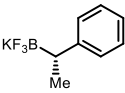
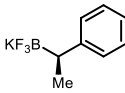
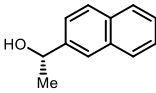
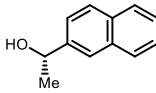
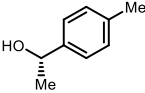
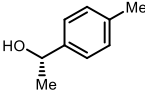
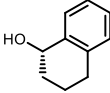
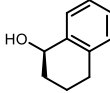
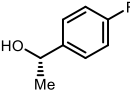
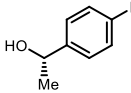
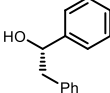
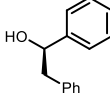
The 1,8-diaminonaphthalene (*dan*)-protected boronic acid **2b**-[dan] was prepared according to literature procedure of Prof. Dr. Saito.¹⁰

General Procedure J



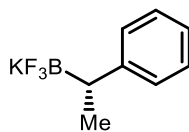
The corresponding alcohol was prepared according to literature procedure of Prof. Dr. Yun.³

Table S5.11. Comparison of value of the optical rotation

 <p>(<i>S</i>)-form $[\alpha]_D^{25} = -8.5$ (c = 1.00, MeCN)</p>	<p>Reported value (ref. 7)</p>  <p>(<i>R</i>)-form $[\alpha]_D^{25} = +4.5$ (c = 1.00, MeCN)</p>	 <p>(<i>S</i>)-form $[\alpha]_D^{25} = -21.2$ (c = 1.00, CHCl₃)</p>	<p>Reported value (ref. 11)</p>  <p>(<i>S</i>)-form $[\alpha]_D^{25} = -24.5$ (c = 0.67, CHCl₃)</p>
 <p>(<i>S</i>)-form $[\alpha]_D^{25} = -45.6$ (c = 1.00, CHCl₃)</p>	<p>Reported value (ref. 11)</p>  <p>(<i>S</i>)-form $[\alpha]_D^{25} = -43.9$ (c = 1.00, CHCl₃)</p>	 <p>(<i>S</i>)-form $[\alpha]_D^{25} = +25.1$ (c = 1.00, CHCl₃)</p>	<p>Reported value (ref. 12)</p>  <p>(<i>R</i>)-form $[\alpha]_D^{25} = -30.1$ (c = 0.55, CHCl₃)</p>
 <p>(<i>S</i>)-form $[\alpha]_D^{25} = -53.2$ (c = 1.00, CHCl₃)</p>	<p>Known compound</p>  <p>CAS: 101219-73-2 (Sigma) $[\alpha]_D^{25} = -49.0$ (c = 1.00, CHCl₃)</p>	 <p>(<i>S</i>)-form $[\alpha]_D^{25} = -32.5$ (c = 1.00, CHCl₃)</p>	<p>Reported value (ref. 12)</p>  <p>(<i>R</i>)-form $[\alpha]_D^{25} = +10.9$ (c = 1.00, CHCl₃)</p>

The absolute configuration for enantioenriched alkylboron compounds was determined by comparison with optical rotation of trifluoroborates **2a** or/and the corresponding alcohols of **2b**, **2e**, **2f**, **2h** and **2k** to literature value as shown above.

Potassium (*S*)-trifluoro(1-phenylethyl)borate (Table S5.10, 2a).



Following *General Procedure F* from corresponding boronic acid pinacol ester, trifluoroborate salt **2a** was isolated as a white solid. The enantiomeric excess (97% ee) was analyzed using the corresponding oxidized alcohol following *General Procedure J*.

¹H NMR (500 MHz, DMSO-*d*₆) δ 7.10–7.02 (m, 4H), 6.93– 6.85 (m, 1H), 1.65–1.55 (m, 1H), 1.05 (d, *J* = 7.3 Hz, 3H) ppm.

¹³C NMR (126 MHz, DMSO-*d*₆) δ 152.29, 127.55, 126.81, 122.22, 32.32, 17.33 ppm.

¹⁹F NMR (471 MHz, DMSO-*d*₆) δ –142.82 ppm.

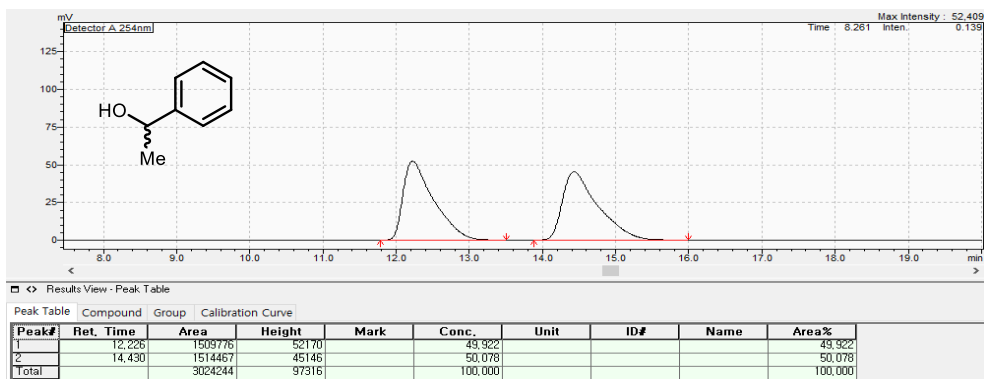
¹¹B NMR (161 MHz, DMSO-*d*₆) δ 4.25 ppm.

HRMS (ESI) calculated for [C₈H₉BF₃, M–K]: 173.0749, found: 173.0756.

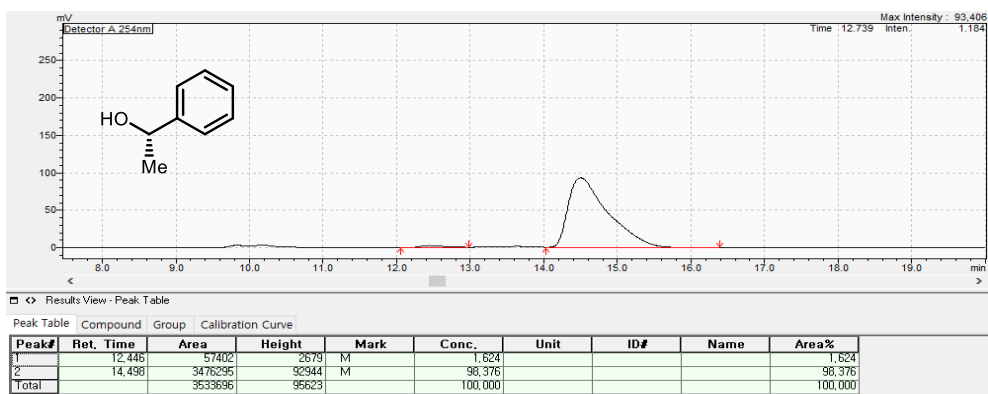
Optical rotation of 2a, [α]_D²² = –8.5 (c = 1.00, MeCN).

Enantiomeric excess, 97% ee was measured by HPLC (CHIRALCEL OD, *n*-hexane : *i*-PrOH = 97 : 3, 1.0 mL/min, wavelength = 254 nm, 28 °C); t_R = 14.498 min (major), t_R = 12.446 min (minor).

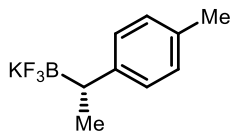
[Racemic alcohol for **2a**]



[Enantioenriched alcohol for **2a**]



Potassium (*S*)-trifluoro(1-(*p*-tolyl)ethyl)borate (Table S5.10, **2b).**



Following *General Procedure F* from corresponding boronic acid pinacol ester, trifluoroborate salt **2b** was isolated as a white solid. The enantiomeric excess (99% ee) was analyzed using the corresponding oxidized alcohol following *General Procedure J*.

¹H NMR (500 MHz, DMSO-*d*₆) δ 6.95 (d, *J* = 7.8 Hz, 2H), 6.87 (d, *J* = 7.8 Hz, 2H), 2.20 (s, 3H), 1.60–1.50 (m, 1H), 1.03 (d, *J* = 7.5 Hz, 3H) ppm.

¹³C NMR (126 MHz, DMSO-*d*₆) δ 149.05, 130.37, 127.35, 127.33, 31.69, 20.49, 17.43 ppm.

¹⁹F NMR (471 MHz, DMSO-*d*₆) δ –142.93 ppm.

¹¹B NMR (161 MHz, DMSO-*d*₆) δ 4.33 ppm.

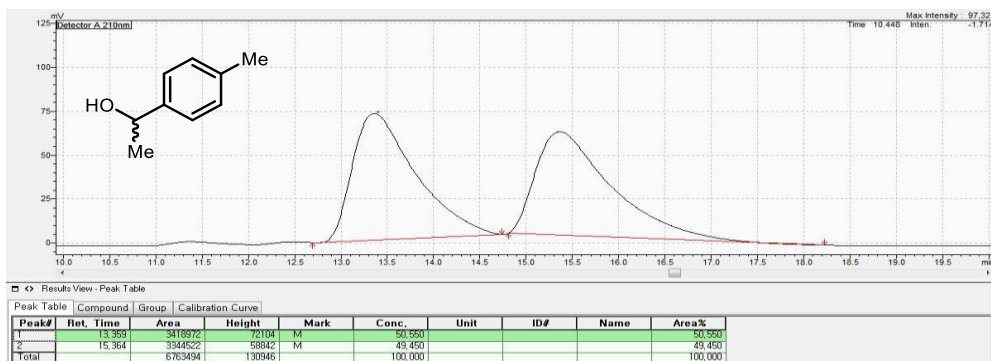
HRMS (ESI) calculated for [C₉H₁₁BF₃, M–K]: 187.0906, found: 187.0911.

Optical rotation of **2b**, [α]_D²² = –6.5 (c = 1.00, MeCN).

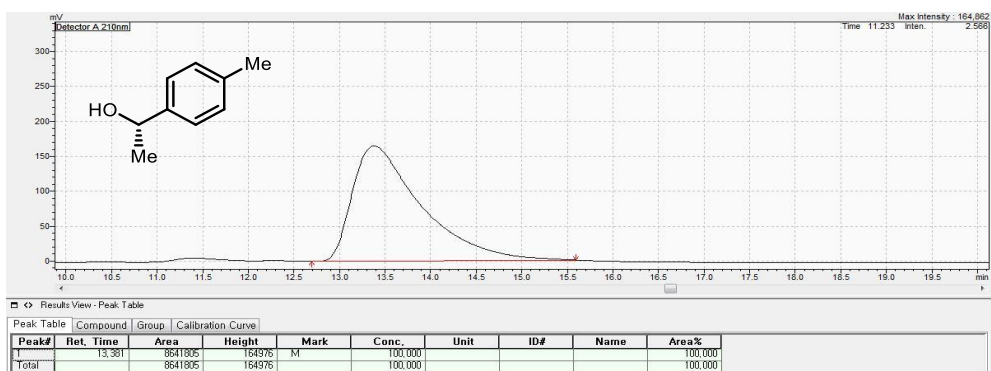
Optical rotation of alcohol, [α]_D²² = –45.6 (c = 1.00, CHCl₃).

Enantiomeric excess, 99% ee was measured by HPLC (CHIRALCEL OJ-H, *n*-hexane : *i*-PrOH = 97 : 3, 1.0 mL/min, wavelength = 210 nm, 28 °C); t_R = 13.381 min (major), t_R = 15.364 min (minor).

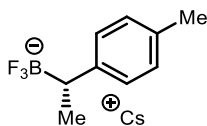
[Racemic alcohol for **2b**]



[Enantioenriched alcohol for **2b**]



Cesium (*S*)-trifluoro(1-(*p*-tolyl)ethyl)borate (Table S5.10, **2b-[Cs]).**



Following *General Procedure G* from corresponding boronic acid pinacol ester, cesium trifluoroborate salt **2b**-[Cs] was isolated as a white solid.

¹H NMR (500 MHz, Acetone-*d*₆) δ 7.05 (d, *J* = 7.8 Hz, 2H), 6.96 (d, *J* = 7.8 Hz, 2H), 2.23 (s, 3H), 1.72 (br s, 1H), 1.13 (d, *J* = 7.3 Hz, 3H) ppm.

¹³C NMR (126 MHz, Acetone-*d*₆) δ 149.12, 131.63, 128.02, 127.83, 31.70, 20.08, 16.07 ppm.

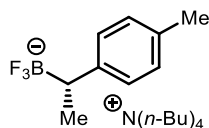
¹⁹F NMR (376 MHz, Acetone-*d*₆) δ -139.40 ppm.

¹¹B NMR (128 MHz, Acetone-*d*₆) δ 4.69 ppm.

HRMS (ESI) calculated for [C₉H₁₁BF₃, M-Cs]: 187.0911, found: 187.0922

Optical rotation of **2b-[Cs]**, [α]_D²² = -4.7 (c = 1.00, MeOH).

Tetra-*n*-butylammonium (S)-trifluoro(1-(*p*-tolyl)ethyl)borate (*Table S5.10*, **2b**-[NR₄]).



Following *General Procedure H* from corresponding potassium trifluoroborate **2b**, ammonium trifluoroborate salt **2b**-[NR₄] was isolated as a white solid.

¹H NMR (500 MHz, Acetone-*d*₆) δ 7.07 (d, *J* = 7.7 Hz, 2H), 6.85 (d, *J* = 7.6 Hz, 2H), 3.41–3.32 (m, 8H), 2.20 (s, 3H), 1.81–1.71 (m, 8H), 1.70 (br s, 1H), 1.47–1.36 (m, 8H), 1.14 (d, *J* = 7.2 Hz, 3H), 0.97 (t, *J* = 7.4 Hz, 12H) ppm.

¹³C NMR (126 MHz, Acetone-*d*₆) δ 151.58, 131.09, 128.88, 128.23, 59.27, 24.51, 21.12, 20.43, 18.38, 13.98 ppm.

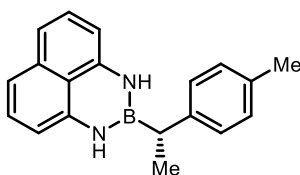
¹⁹F NMR (376 MHz, Acetone-*d*₆) δ –145.89 (m) ppm.

¹¹B NMR (128 MHz, Acetone-*d*₆) δ 4.23 (m) ppm.

HRMS (ESI) calculated for [C₉H₁₁BF₃, M–NR₄]: 187.0906, found: 187.0922

Optical rotation of 2b-[NR₄], [α]_D²² = –4.4 (c = 1.00, MeOH).

(S)-2-(1-(*p*-tolyl)ethyl)-2,3-dihydro-1H-naphtho[1,8-de][1,3,2]diazaborinine (Table S5.10, **2b-[dan]).**



Following *General Procedure I* from corresponding boronic acid pinacol ester, 1,8-diaminonaphthalene (*dan*)-protected boronic acid **2b**-[dan] was isolated as a brown syrup.

¹H NMR (400 MHz, CDCl₃) δ 7.16–7.06 (m, 4H), 7.02 (d, *J* = 8.2 Hz, 2H), 6.90 (d, *J* = 8.5 Hz, 2H), 6.27 (d, *J* = 7.3 Hz, 2H), 5.49 (s, 2H), 3.83 (s, 3H), 2.47 (q, *J* = 7.6 Hz, 1H), 1.41 (d, *J* = 7.6 Hz, 3H) ppm.

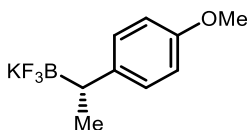
¹³C NMR (126 MHz, CDCl₃) δ 157.59, 141.13, 137.65, 136.38, 128.63, 127.64, 119.58, 117.67, 114.29, 105.83, 55.41, 27.04, 17.26 ppm.

¹¹B NMR (128 MHz, CDCl₃) δ 32.13 ppm.

HRMS (ESI) calculated for [C₁₉H₂₀BN₂O, M+OH]⁻: 303.1674, found: 303.1664.

Optical rotation of **2b-[dan]**, [α]_D²² = +40.6 (c = 0.5, CH₂Cl₂).

Potassium (*S*)-trifluoro(1-(4-methoxyphenyl)ethyl)borate (Table S5.10, 2c).



Following *General Procedure F* from corresponding boronic acid pinacol ester, trifluoroborate salt **2c** was isolated as a white solid. The enantiomeric excess (94% ee) was analyzed using the corresponding oxidized alcohol following *General Procedure J*.

¹H NMR (500 MHz, DMSO-*d*₆) δ 6.96 (d, *J* = 8.5 Hz, 2H), 6.65 (d, *J* = 8.5 Hz, 2H), 3.66 (s, 3H), 1.56–1.46 (m, 1H), 1.01 (d, *J* = 7.4 Hz, 3H) ppm.

¹³C NMR (126 MHz, DMSO-*d*₆) δ 155.21, 144.24, 128.10, 112.46, 54.85, 31.07, 17.78 ppm.

¹⁹F NMR (471 MHz, DMSO-*d*₆) δ -142.90 ppm.

¹¹B NMR (161 MHz, DMSO-*d*₆) δ 4.36 ppm.

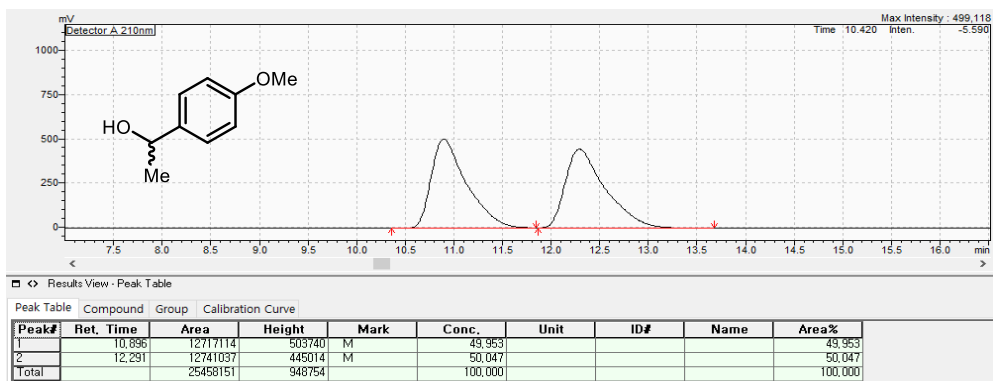
HRMS (ESI) calculated for [C₉H₁₁BF₃O, M–K]: 203.0855, found: 203.0861.

Optical rotation, $[\alpha]_{\text{D}}^{22} = -7.1$ (*c* = 1.00, MeCN).

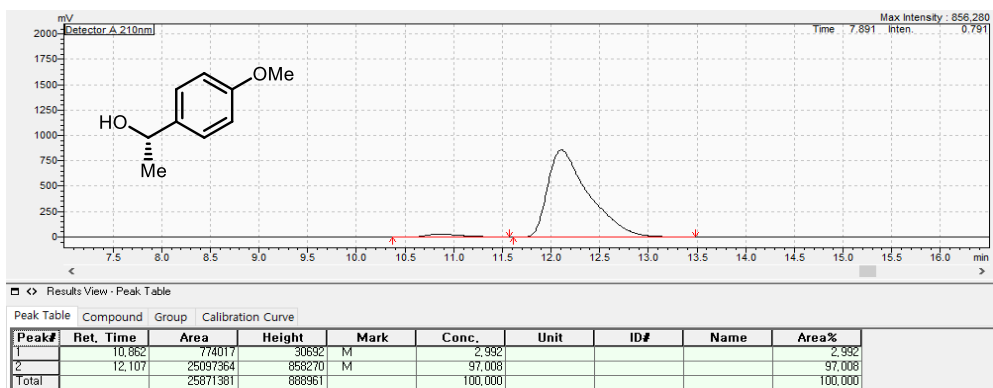
Optical rotation of alcohol, $[\alpha]_{\text{D}}^{22} = -91.5$ (*c* = 1.00, CHCl₃).

Enantiomeric excess, 94% ee was measured by HPLC (CHIRALCEL OD-H, *n*-hexane : *i*-PrOH = 95 : 5, 1.0 mL/min, wavelength = 210 nm, 30 °C); *t*_R = 12.107 min (major), *t*_R = 10.862 min (minor).

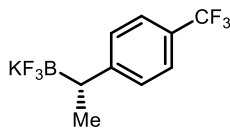
[Racemic alcohol for 2c]



[Enantioenriched alcohol for 2c]



Potassium (*S*)-trifluoro(1-(4-(trifluoromethyl)phenyl)ethyl)borate (Table S5.10, **2d).**



Following *General Procedure F* from corresponding boronic acid pinacol ester, trifluoroborate salt **2d** was isolated as a white solid. The enantiomeric excess (97% ee) was analyzed using the corresponding oxidized alcohol following *General Procedure J*.

¹H NMR (500 MHz, DMSO-*d*₆) δ 7.40 (d, *J* = 8.0 Hz, 2H), 7.22 (d, *J* = 8.0 Hz, 2H), 1.80–1.66 (m, 1H), 1.09 (d, *J* = 7.3 Hz, 3H) ppm.

¹³C NMR (126 MHz, DMSO-*d*₆) δ 157.79, 127.73, 125.16 (q, *J* = 271.0 Hz), 123.53 (q, *J* = 3.8 Hz), 123.05 (q, *J* = 31.2 Hz), 33.06, 16.54 ppm.

¹⁹F NMR (471 MHz, DMSO-*d*₆) δ –60.01, –143.38 ppm.

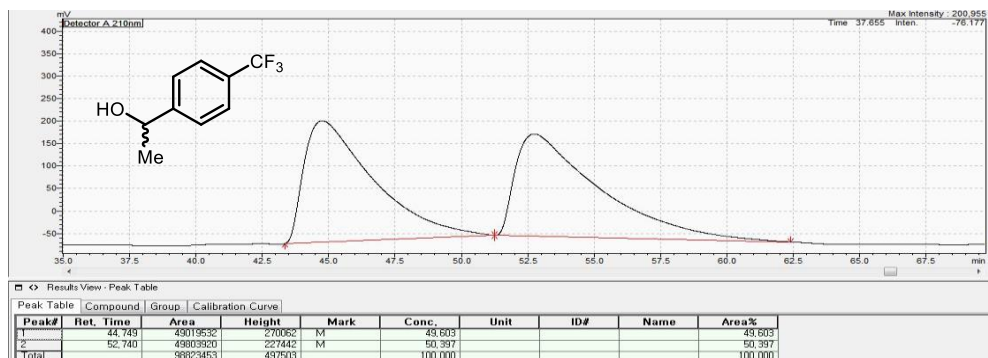
¹¹B NMR (161 MHz, DMSO-*d*₆) δ 4.01 ppm.

HRMS (ESI) calculated for [C₉H₈BF₆, M–K]: 241.0623, found: 241.0627.

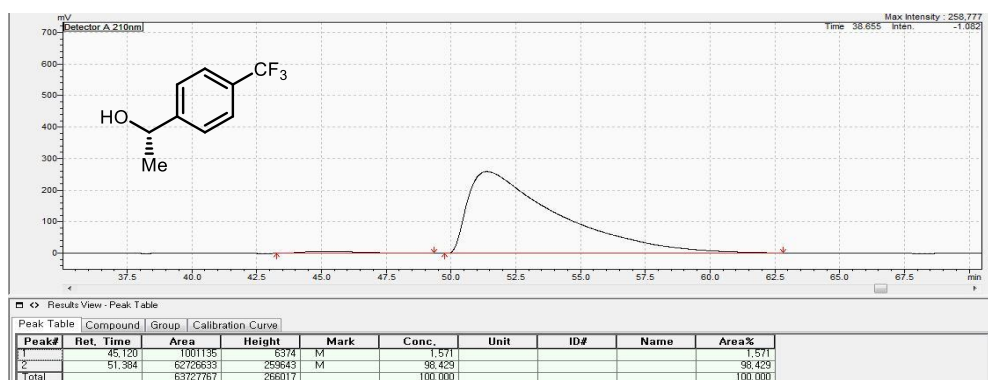
Optical rotation, [α]_D²² = –8.9 (c = 1.05, MeCN).

Enantiomeric excess, 97% ee was measured by HPLC (CHIRALCEL OJ-H, *n*-hexane : *i*-PrOH = 99.8 : 0.2, 1.0 mL/min, wavelength = 210 nm, 28 °C); t_R = 51.384 min (major), t_R = 45.120 min (minor).

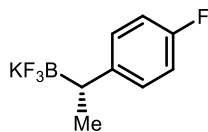
[Racemic alcohol for 2d]



[Enantioenriched alcohol for 2d]



Potassium (*S*)-trifluoro(1-(4-fluorophenyl)ethyl)borate (Table S5.10, 2e).



Following *General Procedure F* from corresponding boronic acid pinacol ester, trifluoroborate salt **2e** was isolated as a white solid. The enantiomeric excess (99% ee) was analyzed using the corresponding oxidized alcohol following *General Procedure J*.

¹H NMR (500 MHz, DMSO-*d*₆) δ 7.09–6.99 (m, 1H), 6.89–6.79 (m, 1H), 1.65–1.51 (m, 1H), 1.03 (d, *J* = 7.4 Hz, 3H) ppm.

¹³C NMR (126 MHz, DMSO-*d*₆) δ 158.81 (d, *J* = 235.7 Hz), 148.16, 128.46 (d, *J* = 7.2 Hz), 113.04 (d, *J* = 20.3 Hz), 31.33, 17.42 ppm.

¹⁹F NMR (471 MHz, DMSO-*d*₆) δ –126.90, –147.43 ppm.

¹¹B NMR (161 MHz, DMSO-*d*₆) δ 4.15 ppm.

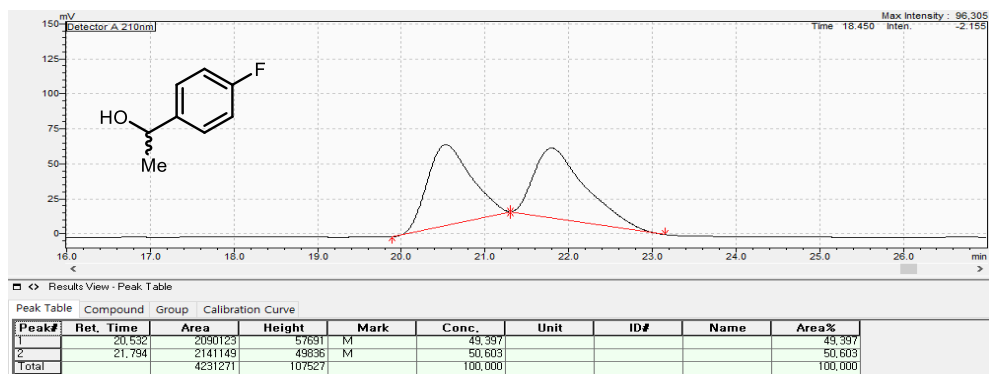
HRMS (ESI) calculated for [C₈H₈BF₄, M–K]: 191.0655, found: 191.0661.

Optical rotation, [α]_D²² = –8.5 (c = 1.00, MeCN).

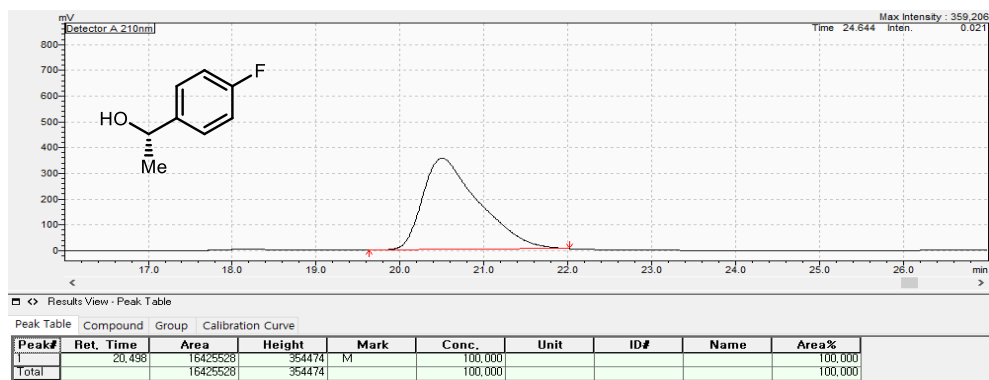
Optical rotation of alcohol, [α]_D²² = –53.2 (c = 1.00, CHCl₃).

Enantiomeric excess, 99% ee was measured by HPLC (CHIRALCEL OD-H, *n*-hexane : *i*-PrOH = 99 : 1, 1.0 mL/min, wavelength = 210 nm, 30 °C); t_R = 20.498 (major), t_R = 21.794 min (minor).

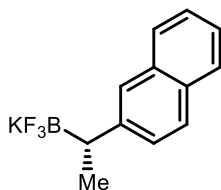
[Racemic alcohol for 2e]



[Enantioenriched alcohol for 2e]



Potassium (*S*)-trifluoro(1-(naphthalen-2-yl)ethyl)borate (Table S5.10, 2f).



Following *General Procedure F* from corresponding boronic acid pinacol ester, trifluoroborate salt **2f** was isolated as a white solid. The enantiomeric excess (97% ee) was analyzed using the corresponding oxidized alcohol following *General Procedure J*.

¹H NMR (500 MHz, DMSO-*d*₆) δ 7.78–7.68 (m, 2H), 7.62 (d, *J* = 8.5 Hz, 1H), 7.47 (s, 1H), 7.43–7.34 (m, 2H), 7.30 (t, *J* = 7.3 Hz, 1H), 1.90–1.80 (m, 1H), 1.20 (d, *J* = 7.4 Hz, 3H) ppm.

¹³C NMR (126 MHz, DMSO-*d*₆) δ 150.40, 133.45, 130.41, 128.90, 127.12, 126.78, 125.57, 124.90, 123.45, 123.30, 32.80, 17.14 ppm.

¹⁹F NMR (471 MHz, DMSO-*d*₆) δ –142.60 ppm.

¹¹B NMR (161 MHz, DMSO-*d*₆) δ 4.38 ppm.

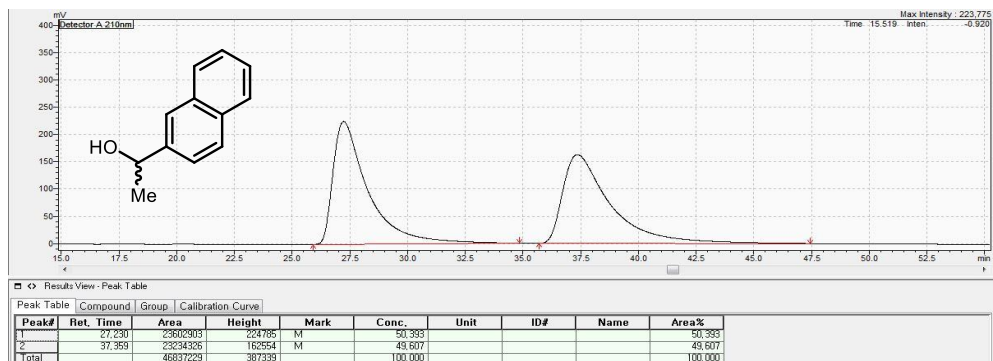
HRMS (ESI) calculated for [C₁₂H₁₁BF₃, M–K]: 223.0906, found: 223.0910.

Optical rotation, [α]_D²² = –19.6 (c = 1.00, MeCN).

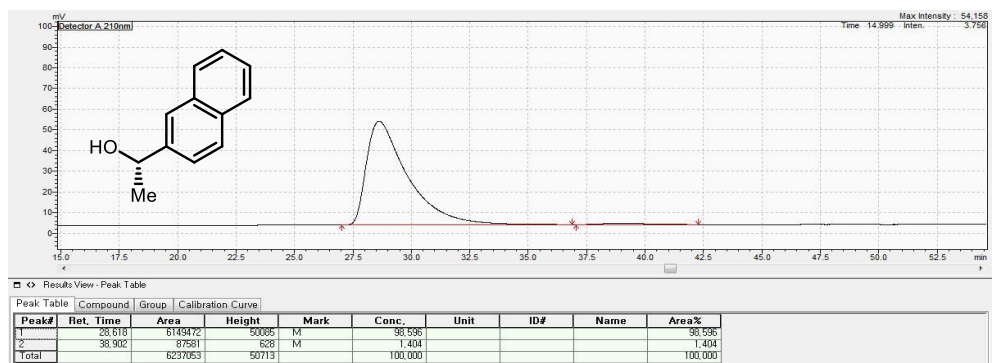
Optical rotation of alcohol, [α]_D²² = –21.2 (c = 1.00, CHCl₃).

Enantiomeric excess, 97% ee was measured by HPLC (CHIRALCEL OJ-H, *n*-hexane : *i*-PrOH = 96 : 4, 1.0 mL/min, wavelength = 210 nm, 28 °C); t_R = 28.618 min (major), t_R = 38.902 min (minor).

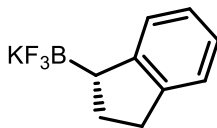
[Racemic alcohol for 2f]



[Enantioenriched alcohol for 2f]



Potassium (*S*)-(2,3-dihydro-1H-inden-1-yl)trifluoroborate (Table S5.10, 2g).



Following *General Procedure F* from corresponding boronic acid pinacol ester, trifluoroborate salt **2g** was isolated as a white solid. The enantiomeric excess (99% ee) was analyzed using the corresponding oxidized alcohol following *General Procedure J*.

¹H NMR (500 MHz, DMSO-*d*₆) δ 7.13 (d, *J* = 7.3 Hz, 1H), 7.02 (d, *J* = 7.3 Hz, 1H), 6.91 (t, *J* = 7.1 Hz, 1H), 6.84 (t, *J* = 7.1 Hz, 1H), 2.80–2.70 (m, 1H), 2.70–2.60 (m, 1H), 2.20–1.75 (m, 3H) ppm.

¹³C NMR (126 MHz, DMSO-*d*₆) δ 152.11, 143.85, 124.77, 124.20, 122.94, 122.88, 37.73, 32.92, 28.25. ppm.

¹⁹F NMR (471 MHz, DMSO-*d*₆) δ –141.28 ppm.

¹¹B NMR (161 MHz, DMSO-*d*₆) δ 4.62 ppm.

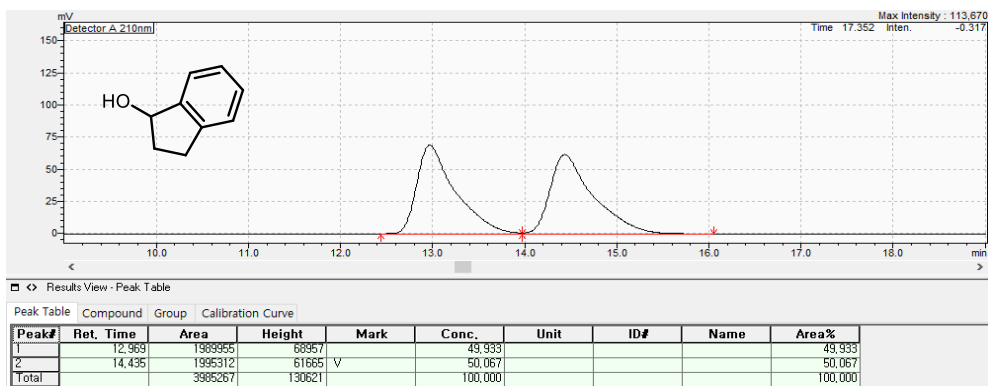
HRMS (ESI) calculated for [C₉H₉BF₃, M–K]: 185.0749, found: 185.0755.

Optical rotation, [α]_D²² = –9.2 (c = 1.00, MeCN).

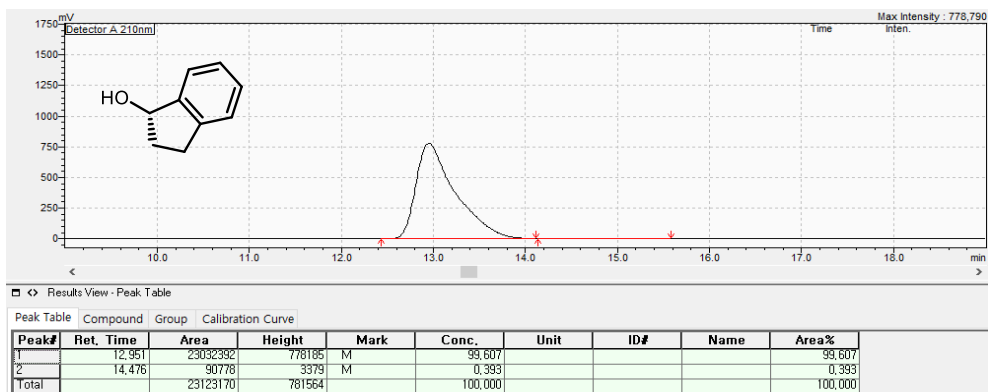
Optical rotation of alcohol, [α]_D²² = +6.9 (c = 1.00, CHCl₃).

Enantiomeric excess, 99% ee was measured by HPLC (CHIRALCEL OD, *n*-hexane : *i*-PrOH = 97 : 3, 1.0 mL/min, wavelength = 210 nm, 28 °C); t_R = 12.951 min (major), t_R = 14.476 min (minor).

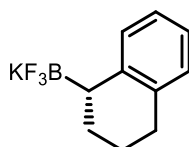
[Racemic alcohol for 2g]



[Enantioenriched alcohol for 2g]



Potassium (S)-trifluoro(1,2,3,4-tetrahydronaphthalen-1-yl)trifluoroborate
(Table S5.10, 2h).



Following *General Procedure F* from corresponding boronic acid pinacol ester, trifluoroborate salt **2h** was isolated as a white solid. The enantiomeric excess (88% ee) was analyzed using the corresponding oxidized alcohol following *General Procedure J*.

¹H NMR (400 MHz, DMSO-*d*₆) δ 7.17 (d, *J* = 7.4 Hz, 1H), 6.90–6.71 (m, 3H), 2.56 (t, *J* = 6.3 Hz, 2H), 1.95–1.82 (m, 1H), 1.76–1.61 (m, 2H), 1.61–1.50 (m, 1H), 1.49–1.36 (m, 1H) ppm.

¹³C NMR (126 MHz, DMSO-*d*₆) δ 145.19, 135.74, 129.46, 127.72, 123.89, 121.81, 30.31, 25.63, 21.96 ppm.

¹⁹F NMR (376 MHz, DMSO-*d*₆) δ –139.41 ppm.

¹¹B NMR (128 MHz, DMSO-*d*₆) δ 4.51 ppm.

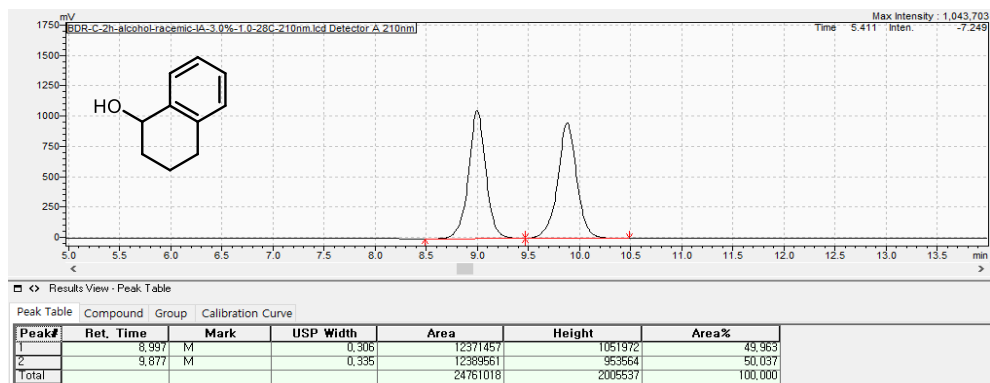
HRMS (ESI) calculated for [C₁₀H₁₁BF₃, M–K]: 199.0911, found: 199.0917.

Optical rotation, [α]_D²² = –9.2 (c = 1.00, MeCN).

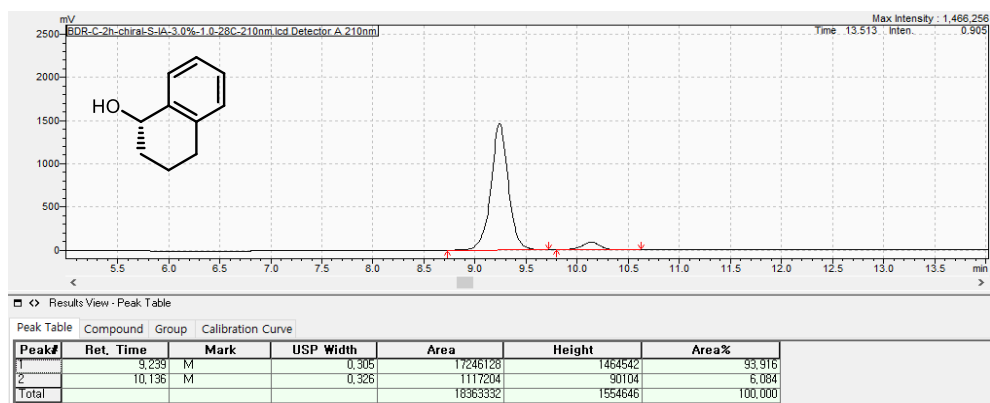
Optical rotation of alcohol, [α]_D²² = +25.1 (c = 1.00, CHCl₃).

Enantiomeric excess, 88% ee was measured by HPLC (CHIRALPAK IA, *n*-hexane : *i*-PrOH = 97 : 3, 1.0 mL/min, wavelength = 210 nm, 28 °C); t_R = 9.239 min (major), t_R = 10.136 min (minor).

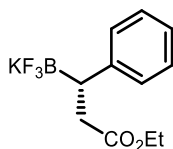
[Racemic alcohol for **2h**]



[Enantioenriched alcohol for **2h**]



Potassium (S)-(3-ethoxy-3-oxo-1-phenylpropyl)trifluoroborate (Table S5.10, 2i).



Following *General Procedure F* from corresponding boronic acid pinacol ester, trifluoroborate salt **2i** was isolated as a white solid. The enantiomeric excess (85% ee) was analyzed using the corresponding oxidized alcohol following *General Procedure J*.

¹H NMR (500 MHz, DMSO-*d*₆) δ 7.10–7.00 (m, 4H), 6.92–6.86 (m, 1H), 3.82 (q, *J* = 3.8 Hz, 1H), 2.53–2.47 (m, 1H), 2.44–2.35 (m, 1H), 2.00–1.91 (m, 1H), 0.97 (t, *J* = 7.1 Hz, 3H) ppm.

¹³C NMR (126 MHz, DMSO-*d*₆) δ 174.70, 148.55, 127.89, 126.82, 122.73, 58.66, 36.83, 35.66, 14.13 ppm.

¹⁹F NMR (471 MHz, DMSO-*d*₆) δ –143.04 ppm.

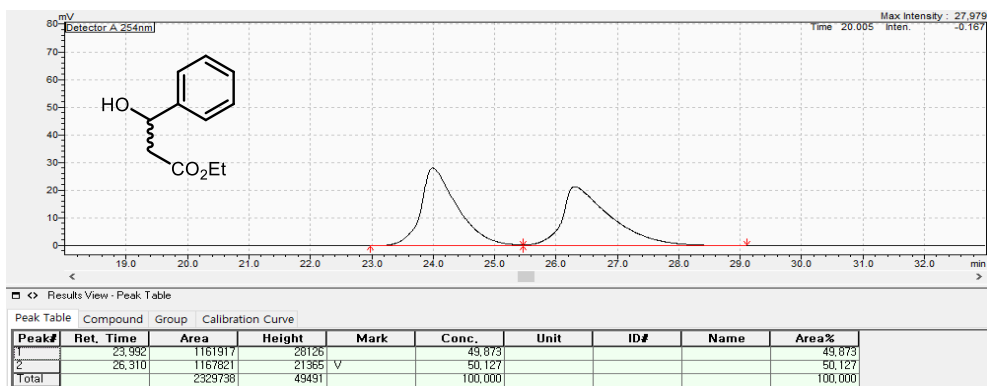
¹¹B NMR (161 MHz, DMSO-*d*₆) δ 3.81 ppm.

HRMS (ESI) calculated for [C₁₁H₁₃BF₃O₂, M–K]: 245.0961, found: 245.0965.

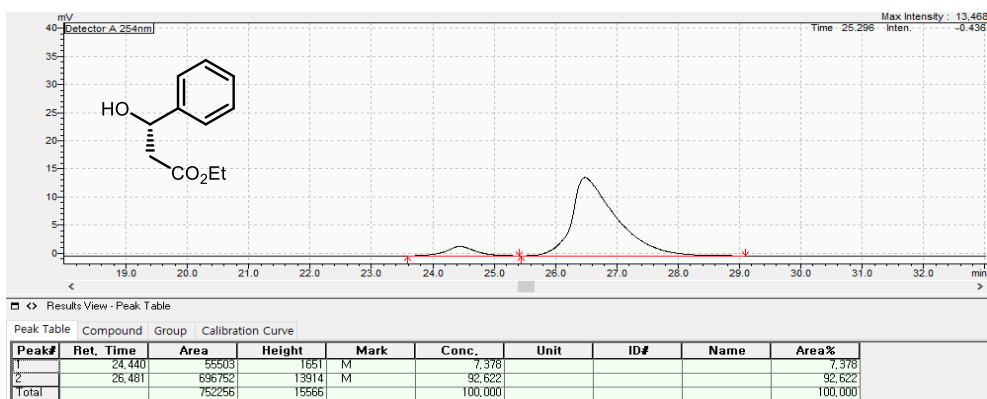
Optical rotation, [α]_D²² = +36.7 (c = 1.00, MeCN).

Enantiomeric excess, 85% ee was measured by HPLC (CHIRALPAK IA, *n*-hexane : *i*-PrOH = 99 : 1, 1.0 mL/min, wavelength = 254 nm, 28 °C); t_R = 26.481 min (major), t_R = 24.440 min (minor).

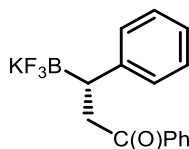
[Racemic alcohol for **2i**]



[Enantioenriched alcohol for **2i**]



Potassium (S)-(3-oxo-1,3-diphenylpropyl)trifluoroborate (Table S5.10, 2j).



Following *General Procedure F* from corresponding boronic acid pinacol ester, trifluoroborate salt **2j** was isolated as a white solid. The enantiomeric excess (94% ee) was analyzed using the corresponding oxidized alcohol following *General Procedure J*.

¹H NMR (400 MHz, DMSO-*d*₆) δ 7.83 (d, *J* = 7.6 Hz, 2H), 7.54 (t, *J* = 7.3 Hz, 1H), 7.45 (t, *J* = 7.6 Hz, 2H), 7.07–6.93 (m, 4H), 6.91–6.80 (m, 1H), 3.23 (dd, *J* = 15.5, 3.7 Hz, 1H), 3.06 (dd, *J* = 15.4, 11.0 Hz, 1H), 2.19–2.05 (m, 1H) ppm.

¹³C NMR (126 MHz, DMSO-*d*₆) δ 202.06, 148.78, 137.47, 132.19, 128.42, 127.98, 127.77, 126.77, 122.54, 41.27, 35.84 ppm.

¹⁹F NMR (376 MHz, DMSO-*d*₆) δ –142.64 ppm.

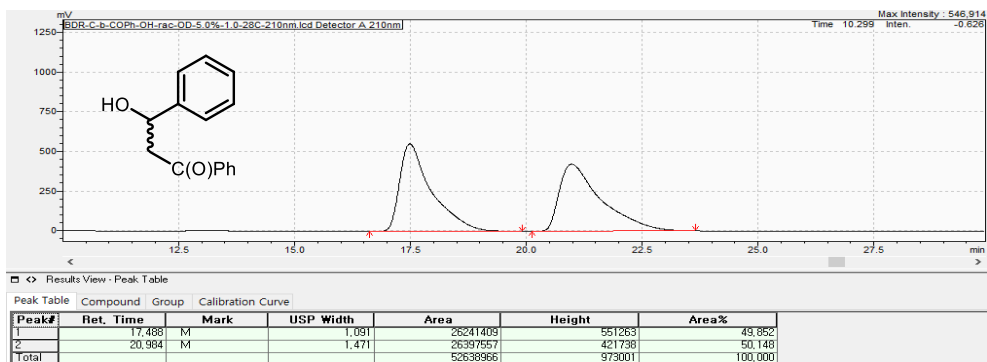
¹¹B NMR (128 MHz, DMSO-*d*₆) δ 4.50 ppm.

HRMS (ESI) calculated for [C₁₅H₁₃BF₃O, M–K]: 277.1017, found: 277.1012.

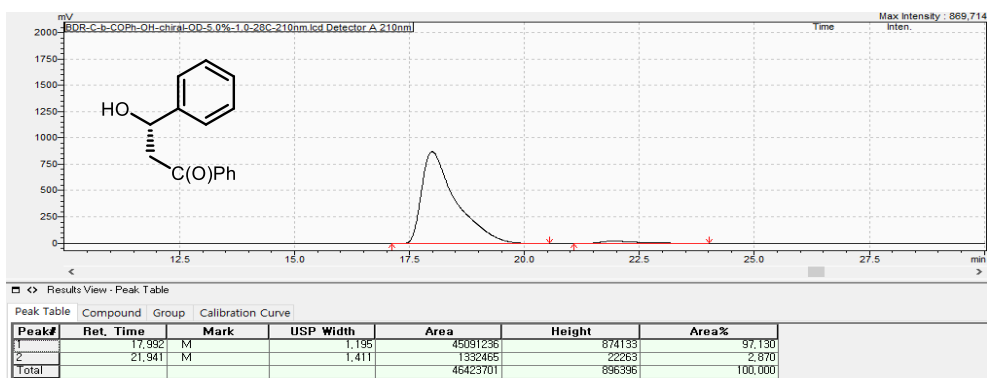
Optical rotation, $[\alpha]_{\text{D}}^{22} = +54.5$ (*c* = 1.00, MeOH).

Enantiomeric excess, 94% ee was measured by HPLC (CHIRALCEL OD, *n*-hexane : *i*-PrOH = 95 : 5, 1.0 mL/min, wavelength = 210 nm, 28 °C); *t*_R = 17.992 min (major), *t*_R = 21.941 min (minor).

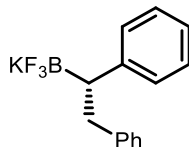
[Racemic alcohol for 2j]



[Enantioenriched alcohol for 2j]



Potassium (*S*)-(1,2-diphenylethyl)trifluoroborate (Table S5.10, 2k).



Following *General Procedure F* from corresponding boronic acid pinacol ester, trifluoroborate salt **2k** was isolated as a white solid. The enantiomeric excess (98% ee) was analyzed using the corresponding oxidized alcohol following *General Procedure J*.

¹H NMR (500 MHz, DMSO-*d*₆) δ 7.10–7.00 (m, 2H), 7.00–6.90 (m, 7H), 6.85–6.75 (m, 1H), 3.04–2.93 (m, 1H), 2.86–2.74 (m, 1H), 1.97–1.87 (m, 1H) ppm.

¹³C NMR (126 MHz, DMSO-*d*₆) δ 149.21, 145.21, 128.40, 128.38, 127.44, 126.63, 124.29, 122.18, 41.78, 37.19 ppm.

¹⁹F NMR (471 MHz, DMSO-*d*₆) δ –142.29 ppm.

¹¹B NMR (161 MHz, DMSO-*d*₆) δ 4.16 ppm.

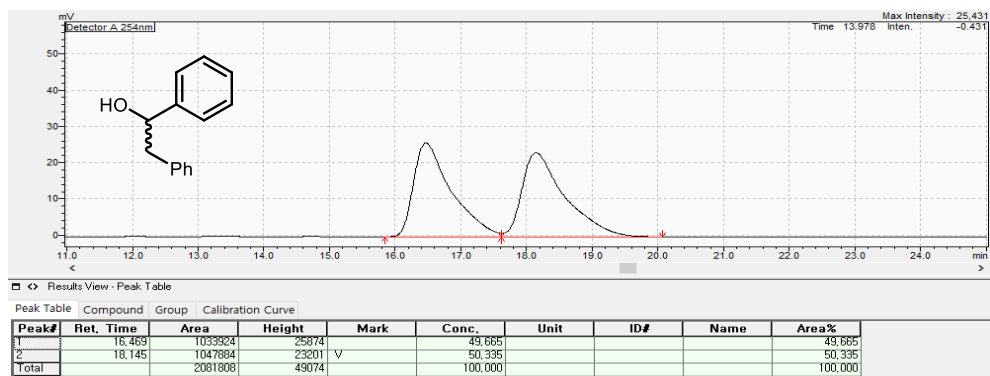
HRMS (ESI) calculated for [C₁₄H₁₃BF₃, M–K]: 249.1062, found: 249.1066.

Optical rotation, [α]_D²² = +95.7 (c = 1.05, MeCN).

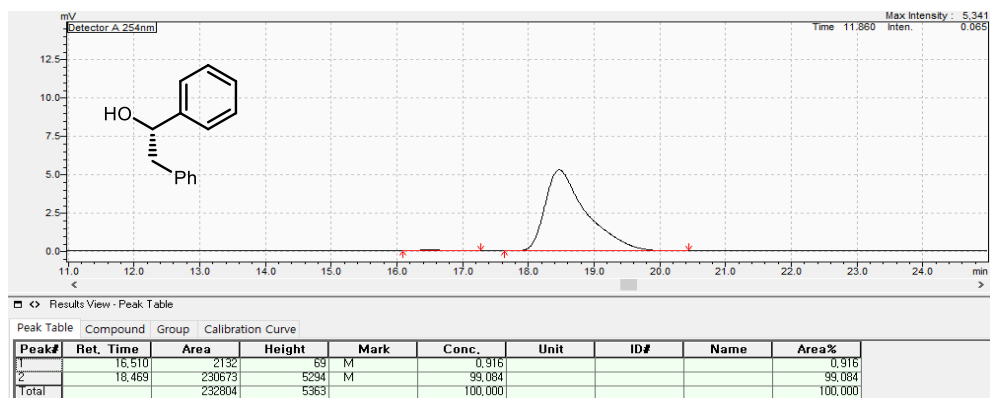
Optical rotation of alcohol, [α]_D²² = –32.5 (c = 1.00, CHCl₃).

Enantiomeric excess, 98% ee was measured by HPLC (CHIRALCEL OD, *n*-hexane : *i*-PrOH = 97 : 3, 1.0 mL/min, wavelength = 254 nm, 28 °C); t_R = 18.469 min (major), t_R = 16.510 min (minor).

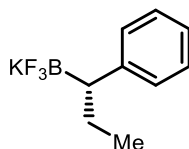
[Racemic alcohol for 2k]



[Enantioenriched alcohol for 2k]



Potassium (S)-(1-phenylpropyl)trifluoroborate (Table S5.10, 21).



Following *General Procedure F* from corresponding boronic acid pinacol ester, trifluoroborate salt **21** was isolated as a white solid. The enantiomeric excess (98% ee) was analyzed using the corresponding oxidized alcohol following *General Procedure J*.

¹H NMR (400 MHz, DMSO-*d*₆) δ 7.09–6.95 (m, 4H), 6.92–6.81(m, 1H), 1.76–1.57 (m, 1H), 1.53–1.38 (m, 1H), 1.37–1.25 (m, 1H), 0.66 (t, *J* = 7.2 Hz, 3H) ppm.

¹³C NMR (126 MHz, DMSO-*d*₆) δ 150.51, 128.30, 126.73, 122.14, 42.34, 24.37, 14.60 ppm.

¹⁹F NMR (376 MHz, DMSO-*d*₆) δ –141.26 ppm.

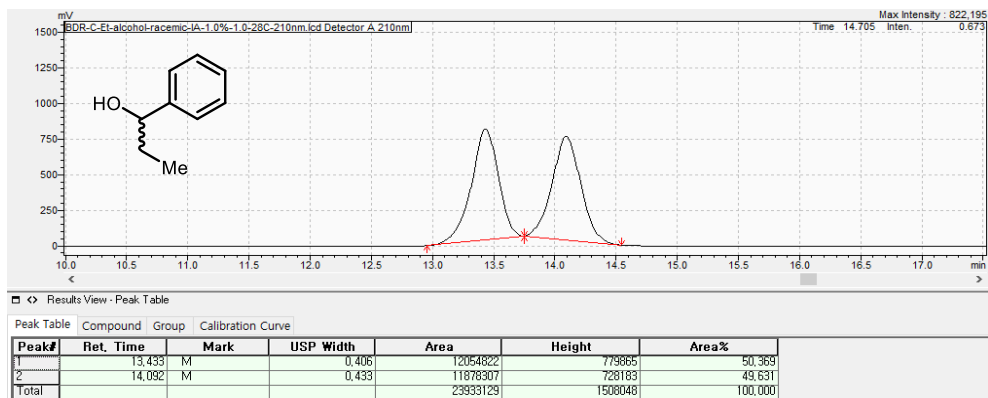
¹¹B NMR (128 MHz, DMSO-*d*₆) δ 3.85 ppm.

HRMS (ESI) calculated for [C₉H₁₁BF₃, M–K]: 187.0911, found: 187.0917

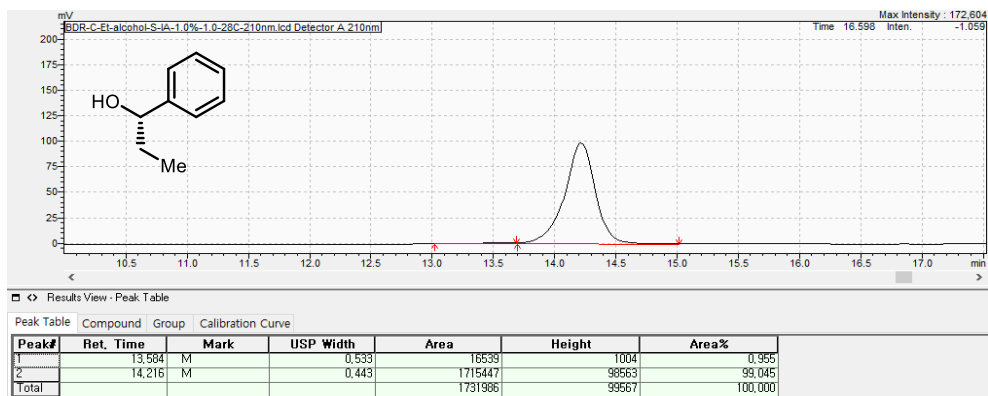
Optical rotation, [α]_D²² = +18.2 (c = 1.00, MeOH).

Enantiomeric excess, 98% ee was measured by HPLC (CHIRALPAK IA, *n*-hexane : *i*-PrOH = 99 : 1, 1.0 mL/min, wavelength = 210 nm, 28 °C); t_R = 14.216 min (major), t_R = 13.584 min (minor).

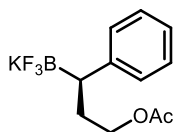
[Racemic alcohol for 21]



[Enantioenriched alcohol for 21]



Potassium (*R*)-(3-acetoxy-1-phenylpropyl)trifluoroborate (Table S5.10, (*R*)-2m).



Following *General Procedure F* from corresponding boronic acid pinacol ester, trifluoroborate salt (*R*)-2m was isolated as a white solid. The enantiomeric excess (99.5% ee) was analyzed using the corresponding oxidized alcohol following *General Procedure J*.

¹H NMR (500 MHz, DMSO-*d*₆) δ 7.12–6.97 (m, 4H), 6.95–6.86 (m, 1H), 3.78 (t, *J* = 7.6 Hz, 1H), 1.97–1.86 (m, 1H), 1.92 (s, 3H), 1.79–1.69 (m, 1H), 1.57–1.47 (m, 1H) ppm.

¹³C NMR (126 MHz, DMSO-*d*₆) δ 170.48, 149.50, 128.05, 127.01, 122.59, 65.16, 35.96, 30.65, 20.83 ppm.

¹⁹F NMR (471 MHz, DMSO-*d*₆) δ –141.95 ppm.

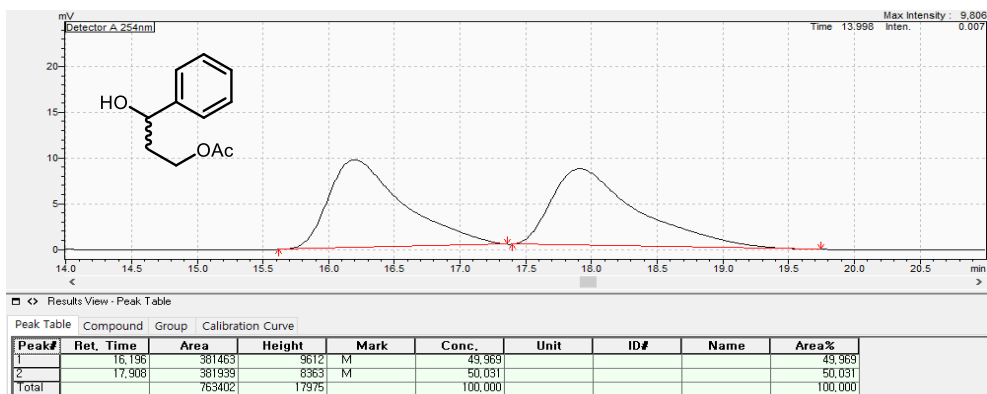
¹¹B NMR (161 MHz, DMSO-*d*₆) δ 3.94 ppm.

HRMS (ESI) calculated for [C₁₁H₁₃BF₃O₂, M–K]: 245.0961, found: 245.0964.

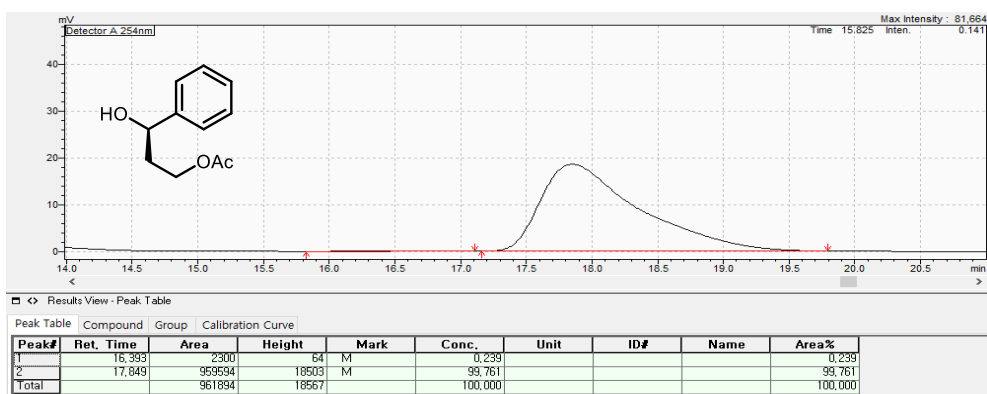
Optical rotation, [α]_D²² = –9.4 (c = 1.00, MeCN).

Enantiomeric excess, 99.5% ee was measured by HPLC (CHIRALCEL OD, *n*-hexane : *i*-PrOH = 95 : 5, 1.0 mL/min, wavelength = 254 nm, 28 °C); t_R = 17.849min (major), t_R = 16.393 min (minor).

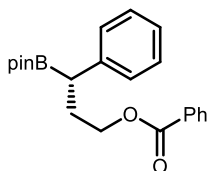
[Racemic alcohol for (R)-2m]



[Enantioenriched alcohol for (R)-2m]



(S)-3-phenyl-3-(4,4,5,5-tetramethyl-1,3,2-dioxaborolan-2-yl)propyl benzoate (S2n)



Following *General Procedure B* from corresponding styrene derivative, boronic acid pinacol ester **S2n** was isolated as a white solid. The enantiomeric excess (>99% ee) was analyzed using the corresponding oxidized alcohol following *General Procedure J*.

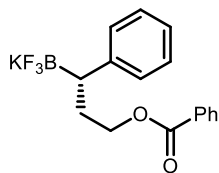
¹H NMR (400 MHz, CDCl₃) δ 8.02 (d, *J* = 7.6 Hz, 2H), 7.55 (t, *J* = 7.2 Hz, 1H), 7.43 (t, *J* = 7.5 Hz, 2H), 7.32–7.20 (m, 4H), 7.16 (t, *J* = 6.7 Hz, 1H), 4.35–4.17 (m, 2H), 2.55 (t, *J* = 7.8 Hz, 1H), 2.37–2.25 (m, 1H), 2.22–2.08 (m, 1H), 1.21 (d, *J* = 10.2 Hz, 12H) ppm.

¹³C NMR (126 MHz, CDCl₃) δ 166.71, 142.06, 132.90, 130.63, 129.72, 128.66, 128.58, 128.41, 125.70, 83.70, 64.35, 31.36, 24.78, 24.71 ppm.

¹¹B NMR (128 MHz, CDCl₃) δ 33.04.ppm.

HRMS (ESI) calculated for [C₂₂H₂₇BO₄+H]⁺: 367.2075, found: 367.2078.

Potassium (S)-3-(benzoyloxy)-1-phenylpropyltrifluoroborate (Table S5.10, 2n).



Following *General Procedure F* from corresponding boronic acid pinacol ester **S2n**, trifluoroborate salt **2n** was isolated as a white solid. The enantiomeric excess (>99% ee) was analyzed using the corresponding oxidized alcohol following *General Procedure J*.

¹H NMR (400 MHz, DMSO-*d*₆) δ 7.88 (d, *J* = 8.0 Hz, 2H), 7.62 (t, *J* = 7.1 Hz, 1H), 7.49 (t, *J* = 7.7 Hz, 2H), 7.12–7.02 (m, 4H), 6.96–6.86 (m, 1H), 4.13–3.97 (m, 2H), 2.13–2.01 (m, 1H), 1.94–1.80 (m, 1H), 1.68–1.56 (m, 1H) ppm.

¹³C NMR (126 MHz, DMSO-*d*₆) δ 165.80, 149.52, 132.96, 130.23, 128.97, 128.61, 128.07, 126.99, 122.55, 65.87, 35.72, 30.80 ppm.

¹⁹F NMR (376 MHz, DMSO-*d*₆) δ –142.01 ppm.

¹¹B NMR (128 MHz, DMSO-*d*₆) δ 4.32 ppm.

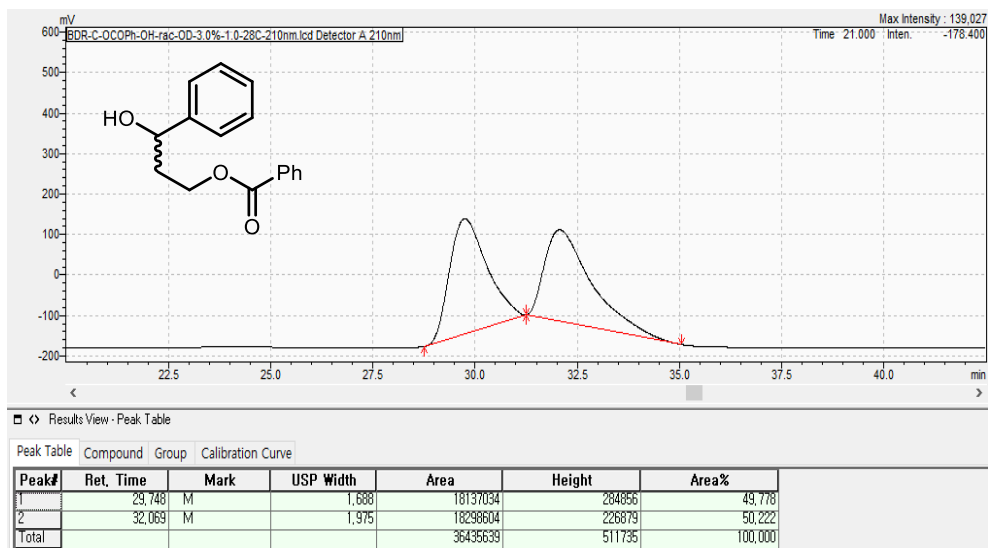
HRMS (ESI) calculated for [C₁₆H₁₅BF₃O₂, M–K]: 307.1123, found: 307.1135.

Optical rotation, [α]_D²² = +33.7 (c = 1.00, MeOH).

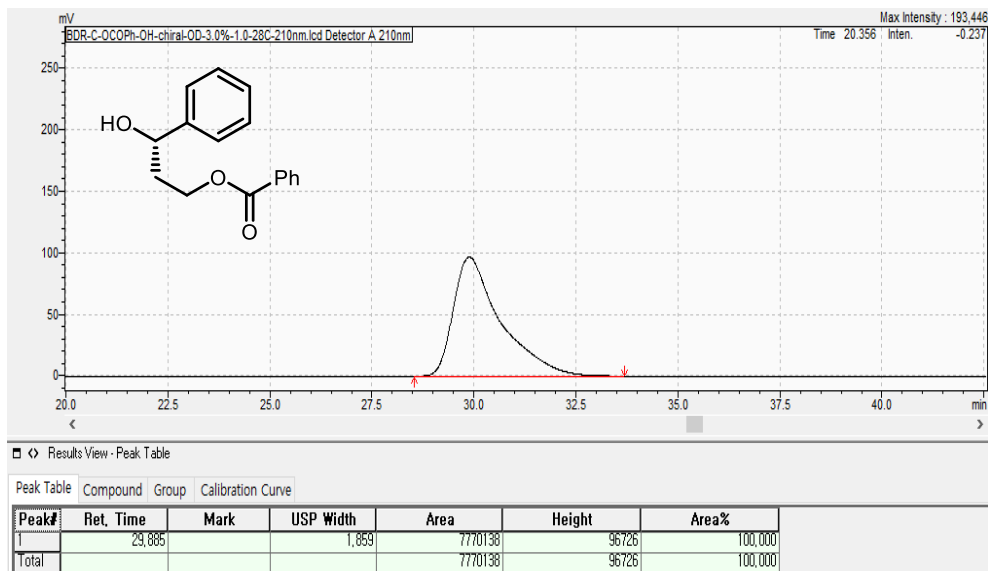
Optical rotation of alcohol, [α]_D²² = +11.1 (c = 1.00, CHCl₃).

Enantiomeric excess, >99% ee was measured by HPLC (CHIRALCEL OD, *n*-hexane : *i*-PrOH = 97 : 3, 1.0 mL/min, wavelength = 210 nm, 28 °C); t_R = 29.748 min (major), t_R = 32.069 min (minor).

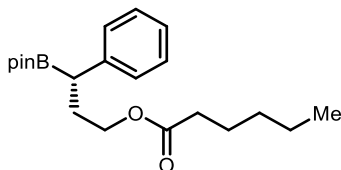
[Racemic alcohol for **2n**]



[Enantioenriched alcohol for **2n**]



Potassium (*S*)-(3-(benzoyloxy)-1-phenylpropyl)trifluoroborate (S2o**).**



Following *General Procedure B* from corresponding styrene derivative, boronic acid pinacol ester **S2o** was isolated as a colorless liquid. The enantiomeric excess (>99% ee) was analyzed using the corresponding oxidized alcohol following *General Procedure J*.

¹H NMR (400 MHz, DMSO-*d*₆) δ 7.88 (d, *J* = 8.0 Hz, 2H), 7.62 (t, *J* = 7.1 Hz, 1H), 7.49 (t, *J* = 7.7 Hz, 2H), 7.12–7.02 (m, 4H), 6.96–6.86 (m, 1H), 4.13–3.97 (m, 2H), 2.13–2.01 (m, 1H), 1.94–1.80 (m, 1H), 1.68–1.56 (m, 1H) ppm.

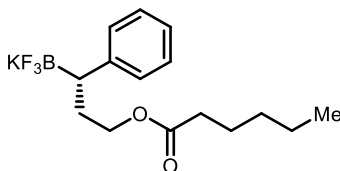
¹³C NMR (126 MHz, DMSO-*d*₆) δ 165.80, 149.52, 132.96, 130.23, 128.97, 128.61, 128.07, 126.99, 122.55, 65.87, 35.72, 30.80 ppm.

¹⁹F NMR (376 MHz, DMSO-*d*₆) δ –142.01 ppm.

¹¹B NMR (128 MHz, DMSO-*d*₆) δ 4.32 ppm.

HRMS (ESI) calculated for [C₂₁H₃₃BO₄+H]⁺: 361.2545, found: 361.2556.

Potassium (S)-(3-(hexanoyloxy)-1-phenylpropyl)trifluoroborate (Table S5.10, 2o).



Following *General Procedure F* from corresponding boronic acid pinacol ester **S2o**, trifluoroborate salt **2o** was isolated as a beige syrup. The enantiomeric excess (99% ee) was analyzed using the corresponding oxidized alcohol following *General Procedure J*.

¹H NMR (400 MHz, DMSO-*d*₆) δ 7.11–6.97 (m, 4H), 6.89 (t, *J* = 7.0 Hz, 1H), 3.78 (t, *J* = 7.4 Hz, 2H), 2.18 (t, *J* = 7.2 Hz, 2H), 1.98–1.83 (m, 1H), 1.80–1.63 (m, 1H), 1.55–1.41 (m, 3H), 1.33–1.12 (m, 4H), 0.85 (t, *J* = 6.6 Hz, 3H) ppm.

¹³C NMR (126 MHz, DMSO-*d*₆) δ 172.96, 149.54, 128.02, 126.93, 122.51, 64.92, 35.68, 33.57, 30.68, 30.66, 24.21, 21.77, 13.80 ppm.

¹⁹F NMR (376 MHz, DMSO-*d*₆) δ –142.05 ppm.

¹¹B NMR (128 MHz, DMSO-*d*₆) δ 4.22 ppm.

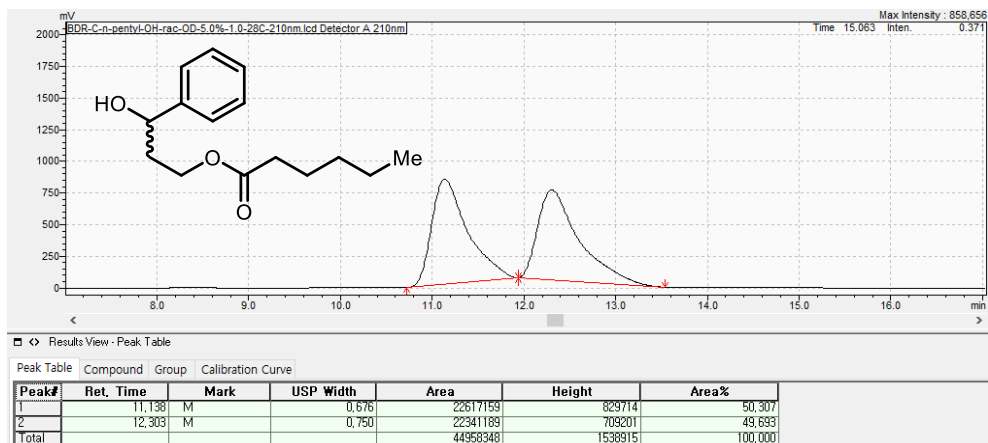
HRMS (ESI) calculated for [C₁₅H₂₁BF₃O₂, M–K]: 301.1592, found: 301.1595.

Optical rotation, [α]_D²² = +33.9 (c = 1.00, MeOH).

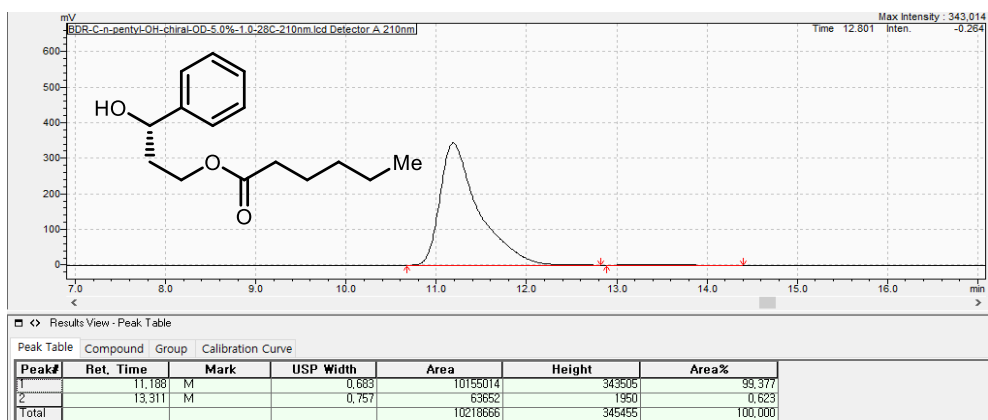
Optical rotation of alcohol, [α]_D²² = –5.9 (c = 1.00, CHCl₃).

Enantiomeric excess, 99% ee was measured by HPLC (CHIRALCEL OD, *n*-hexane : *i*-PrOH = 95 : 5, 1.0 mL/min, wavelength = 210 nm, 28 °C); t_R = 11.138 min (major), t_R = 12.303 min (minor).

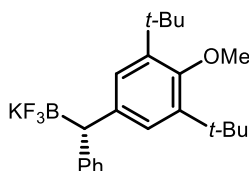
[Racemic alcohol for **2o**]



[Enantioenriched alcohol for **2o**]



Potassium (*S*)-((3,5-di-*tert*-butyl-4-methoxyphenyl)(phenyl)methyl)trifluoroborate (Table S5.10, 2p).

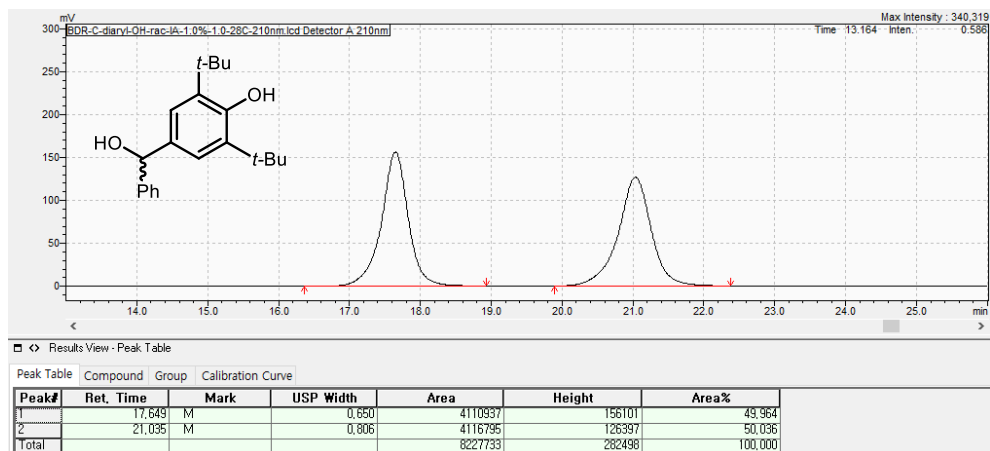


Following *General Procedure E* from corresponding boronic acid pinacol ester, trifluoroborate salt **2p** was isolated as a white solid. The enantiomeric excess (91% ee) was analyzed using the corresponding oxidized alcohol following *General Procedure J*. The spectral data are matched with literature data.^{6b}

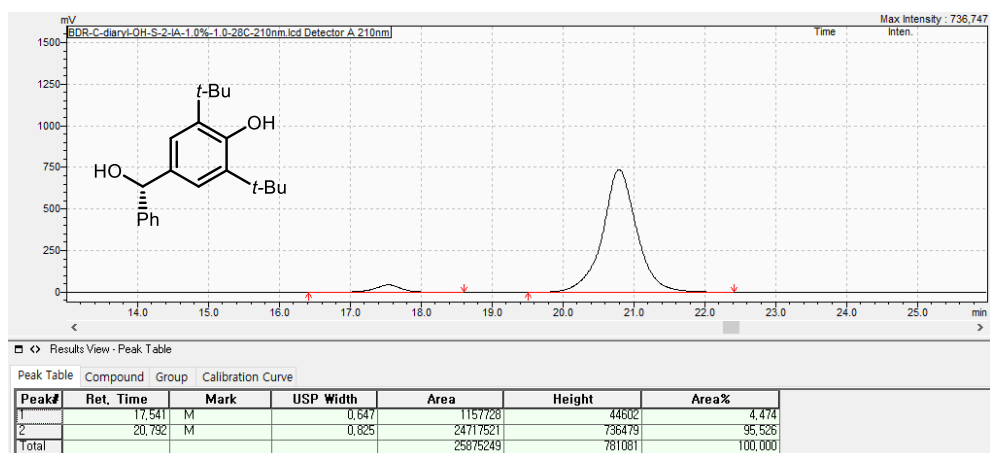
¹H NMR (400 MHz, DMSO-*d*₆) δ 7.18 (d, *J* = 7.6 Hz, 2H), 7.14 (s, 2H), 7.06 (t, *J* = 7.5 Hz, 2H), 6.90 (t, *J* = 7.3 Hz, 1H), 3.57 (s, 1H), 2.85 (m, 1H), 1.33 (s, 18H) ppm.

Enantiomeric excess, 91% ee was measured by HPLC (CHIRALPAK IA, *n*-hexane : *i*-PrOH = 99 : 1, 1.0 mL/min, wavelength = 210 nm, 28 °C); *t*_R = 17.541 min (major), *t*_R = 20.792 min (minor).

[Racemic alcohol for 2p]

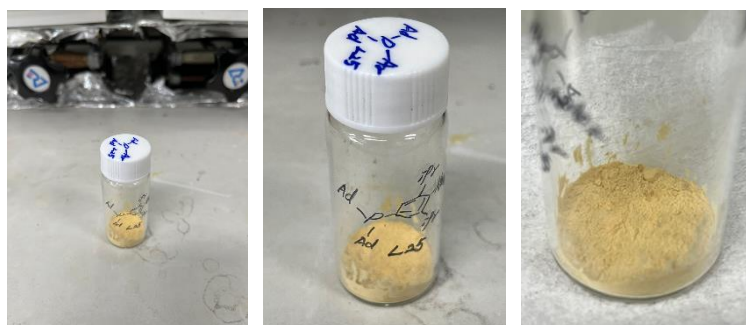
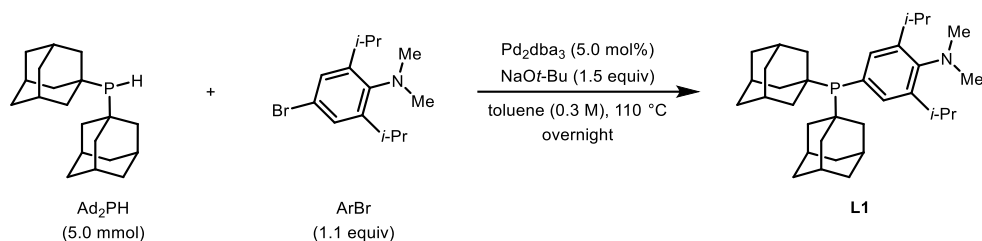


[Enantioenriched alcohol for 2p]



5.5.4. Procedure for the Preparation of Optimal Ligand L1

General Procedure K



4-(di((3*S*,5*S*,7*S*)-adamantan-1-yl)phosphaneyl)-2,6-diisopropyl-*N,N*-dimethylaniline (L1)

Aryl bromide (ArBr) as shown above was prepared according to literature procedure.⁶ Optimal ligand L1 was prepared according to a slightly modified literature procedure.¹³ In a nitrogen-filled glovebox, an oven-dried 50 mL round-bottom flask was charged with a magnetic stir bar, Pd₂dba₃ (0.25 mmol, 5.0 mol% which is 10.0 mol% based on Pd, 230 mg), sodium *tert*-butoxide (7.5 mmol, 1.5 equiv, 721 mg) and aryl bromide (ArBr) (5.5 mmol, 1.1 equiv, 1.56 g) and di-1-adamantylphosphine (5.0 mmol, 1.51 g). Subsequently, anhydrous toluene (0.3 M, 16.25 mL) was added to the mixture via a syringe. The reaction mixture was sealed with a rubber septum cap. The flask was

removed from the glovebox and the reaction mixture was stirred in a pre-heated oil bath (110 °C) overnight under nitrogen atmosphere. After that time, the resulting mixture was concentrated under reduced pressure and quenched with water, then extracted with DCM (three times). The combined organic layer was dried over Na₂SO₄, filtered and concentrated under reduced pressure. Subsequently, 100 mL of DCM/EtOH mixture (v/v = 1 : 20) were added to the resulting residue and concentrated under reduced pressure. During evaporation, orange solid was generated. The orange solid formed was filtered and washed with EtOH (100 mL). The ethanol filtrate was discarded. Then the remaining filter cake was washed with DCM (100 mL). At this point, an unidentified black solid was formed and removed as filter cake. The combined DCM filtrate was concentrated under reduced pressure. The resulting residue was filtered and washed with EtOH (100 mL). The resulting product was finally dried overnight under high vacuum to afford the desired product **L1** as yellowish beige solid as shown above (1.9 g, 75% yield).

¹H NMR (400 MHz, C₆D₆) δ 7.74 (d, *J* = 7.2 Hz, 2H), 3.49–3.34 (m, 2H), 2.71 (s, 6H), 2.25–2.06 (m, 12H), 1.87 (s, 6H), 1.68–1.57 (m, 12H), 1.36 (d, *J* = 5.3 Hz, 12H) ppm.

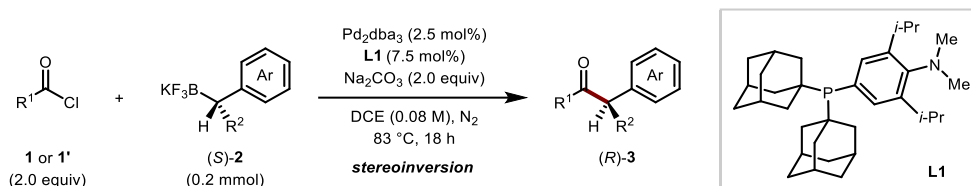
¹³C NMR (126 MHz, C₆D₆) δ 148.36, 132.84, 132.67, 128.35, 128.17, 127.97, 44.30, 42.34 (d, *J* = 12.5 Hz), 37.39, 36.97, 36.79, 29.34 (d, *J* = 8.3 Hz), 28.55, 24.80 ppm (observed complexity is due to C–P coupling).

³¹P NMR (162 MHz, C₆D₆) δ 40.70 ppm.

HRMS (ESI) calculated for [C₃₄H₅₂NP+H]⁺: 506.3910, found: 506.3911.

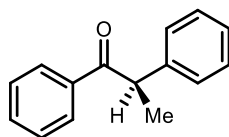
5.5.5. General Procedure for Pd-Catalyzed Stereospecific Couplings

General Procedure L



In a nitrogen-filled glovebox, an oven-dried 4 mL dram-vial (or screw capped reaction tube) was charged with a magnetic stir bar, Pd₂dba₃ (0.005 mmol, 2.5 mol% which is 5.0 mol% based on Pd, 4.58 mg), **L1** (0.015 mmol, 7.5 mol%, 7.59 mg), **(S)-2** (0.2 mmol) and Na₂CO₃ (0.4 mmol, 2.0 equiv, 42.4 mg). Subsequently, 2.4 mL of dichloroethane (DCE) and the corresponding carbonyl chloride **1** or carbamoyl chloride **1'** was added to the mixture via a syringe, in that order. The reaction mixture was sealed with screw cap. The vial (or reaction tube) was removed from the glovebox and the reaction mixture was stirred in a pre-heated oil bath for 18 hours. The crude mixture was then diluted with NH₄Cl (sat.) and extracted with ethyl acetate (three times). The combined organic layer was dried over Na₂SO₄, filtered and concentrated in vacuum. The crude product was purified by flash column chromatography using silica gel and diethyl ether/hexanes as eluents. The racemic product **3** was prepared using (\pm)-**2**. Enantiomeric excess was determined by HPLC analysis.

**5.5.6. Determination of the Yields, Optical Rotations and ee Values
(*R*)-1,2-diphenylpropan-1-one (Table 5.2, 3aa).**



3aa

Following *General Procedure L*, the crude product was purified by silica gel chromatography (gradient elution: full hexanes to 5% ether in hexanes) to provide **3aa** as a yellowish liquid (29 mg, 68%, 96% ee, 99% es). The spectral data are matched with literature data and the value of optical rotation is consistent with (*R*)-form based on literature.¹⁴

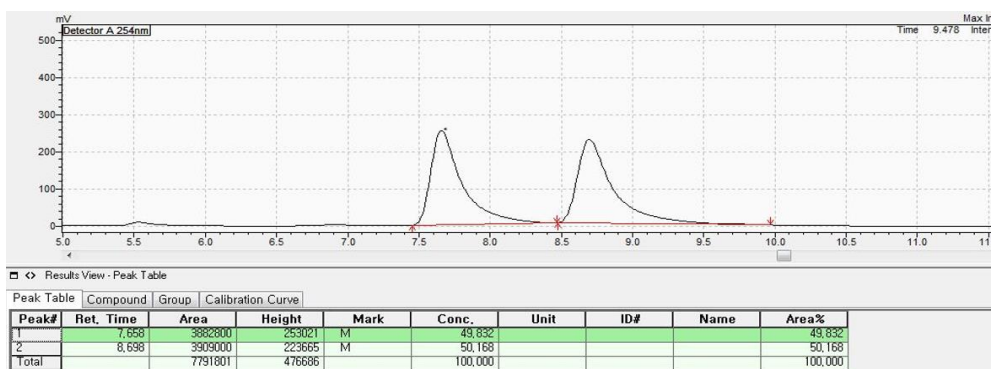
¹H NMR (500 MHz, CDCl₃) δ 8.00–7.92 (m, 2H), 7.50–7.44 (m, 1H), 7.38 (m, 2H), 7.30 (m, 4H), 7.21 (m, 1H), 4.70 (q, *J* = 6.8 Hz, 1H), 1.55 (d, *J* = 6.9 Hz, 2H) ppm.

¹³C NMR (126 MHz, CDCl₃) δ 200.41, 141.58, 136.59, 132.87, 129.08, 128.87, 128.58, 127.87, 126.99, 48.00, 19.62 ppm.

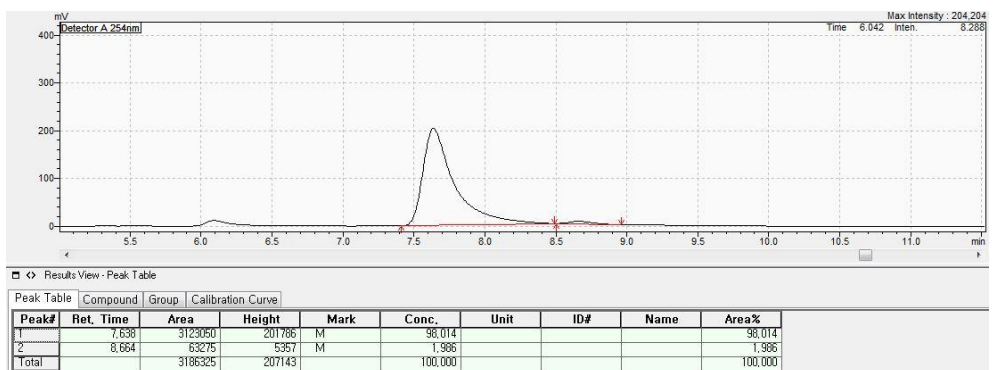
Optical rotation, $[\alpha]_{\text{D}}^{22} = -139.2$ (*c* = 1.05, CH₂Cl₂).

Enantiomeric excess, 96% ee was measured by HPLC (CHIRALPAK AD, *n*-hexane : *i*-PrOH = 98.5 : 1.5, 1.0 mL/min, wavelength = 254 nm, 24 °C); *t*_R = 7.638 min (major), *t*_R = 8.664 min (minor).

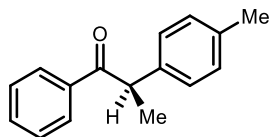
[Racemic 3aa]



[Enantioenriched 3aa]



(R)-1-phenyl-2-(p-tolyl)propan-1-one (Table 5.2, 3ab).



3ab

Following *General Procedure L*, the crude product was purified by silica gel chromatography (gradient elution: full hexanes to 5% ether in hexanes) to provide **3ab** as a colorless liquid (34 mg, 75%, 97% ee, 98% es). The spectral data are matched with literature data.¹⁴

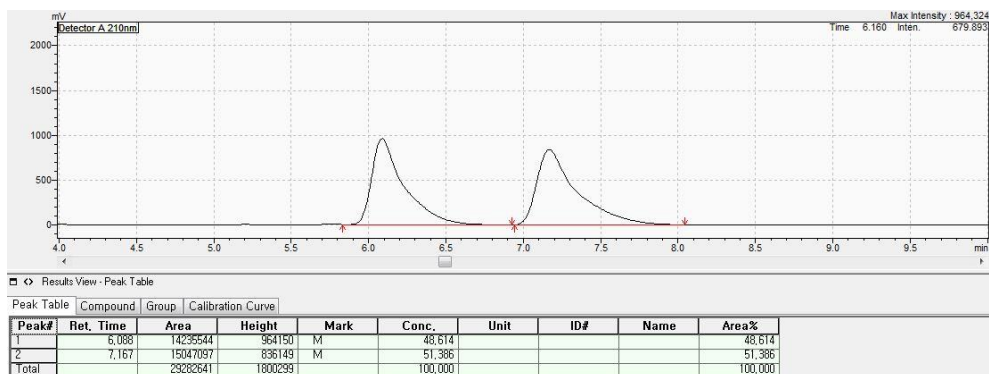
¹H NMR (500 MHz, CDCl₃) δ 7.97 (d, *J* = 7.5 Hz, 2H), 7.47 (t, *J* = 7.3 Hz, 1H), 7.38 (m, 2H), 7.19 (d, *J* = 7.9 Hz, 2H), 7.11 (d, *J* = 7.7 Hz, 2H), 4.67 (q, *J* = 6.8 Hz, 1H), 2.29 (s, 3H), 1.53 (d, *J* = 6.8 Hz, 3H) ppm.

¹³C NMR (126 MHz, CDCl₃) δ 200.55, 138.58, 136.64, 136.61, 132.81, 129.79, 128.88, 128.56, 127.74, 47.60, 21.13, 19.64 ppm.

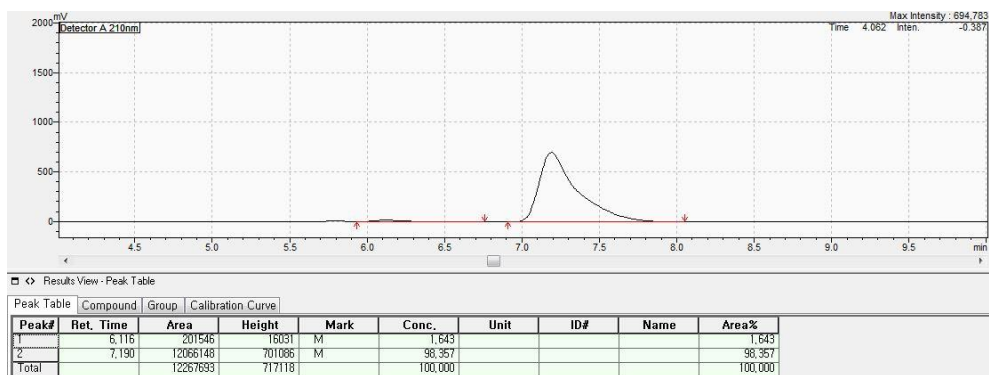
Optical rotation, $[\alpha]_{\text{D}}^{22} = -113.9$ (*c* = 1.35, CH₂Cl₂).

Enantiomeric excess, 97% ee was measured by HPLC (CHIRALCEL OD, *n*-hexane : *i*-PrOH = 99 : 1, 1.0 mL/min, wavelength = 210 nm, 28 °C); *t*_R = 7.190 min (major), *t*_R = 6.116 min (minor).

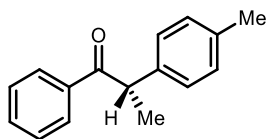
[Racemic **3ab**]



[Enantioenriched **3ab** from (*S*)-**2b**, 99% ee]



(R)-1-phenyl-2-(p-tolyl)propan-1-one (Table 5.2, (S)-3ab)



(S)-3ab

Following *General Procedure L*, the crude product was purified by silica gel chromatography (gradient elution: full hexanes to 5% ether in hexanes) to provide **(S)-3ab** as a colorless liquid (33 mg, 73%, 97% ee, 98% es). The spectral data are matched with literature data.¹⁴

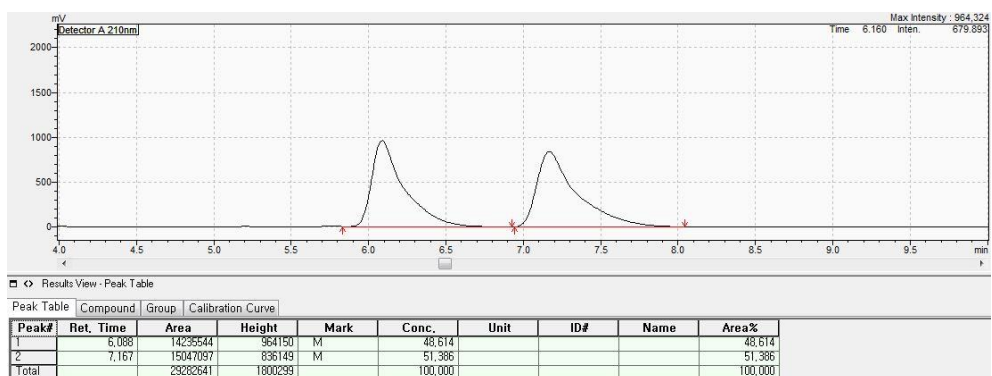
¹H NMR (400 MHz, CDCl₃) δ 7.99–7.90 (m, 2H), 7.47 (t, $J = 7.4$ Hz, 1H), 7.38 (m, 2H), 7.18 (d, $J = 7.9$ Hz, 2H), 7.11 (d, $J = 7.7$ Hz, 2H), 4.66 (q, $J = 6.7$ Hz, 1H), 2.29 (s, 3H), 1.52 (d, $J = 6.8$ Hz, 3H) ppm.

¹³C NMR (126 MHz, CDCl₃) δ 200.56, 138.58, 136.63, 136.62, 132.84, 129.81, 128.89, 128.58, 127.74, 47.61, 21.15, 19.65 ppm.

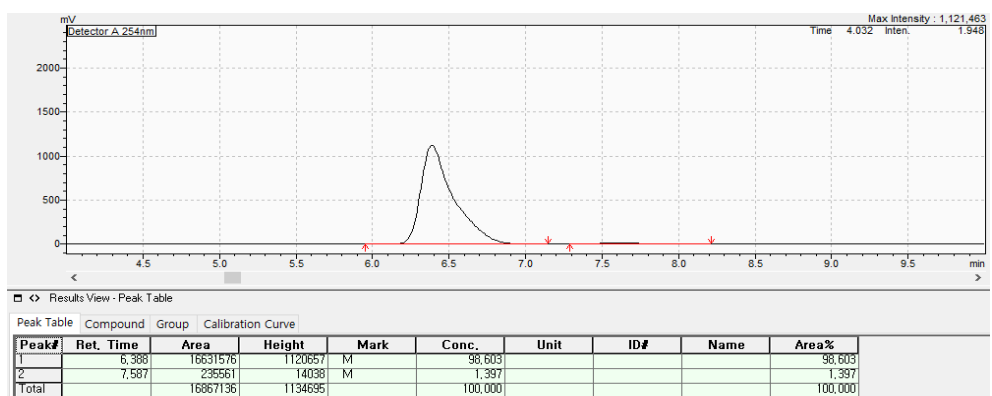
Optical rotation, $[\alpha]_{\text{D}}^{22} = +135.9$ ($c = 1.00$, CH₂Cl₂).

Enantiomeric excess, 97% ee was measured by HPLC (CHIRALCEL OD, *n*-hexane : *i*-PrOH = 99 : 1, 1.0 mL/min, wavelength = 210 nm, 28 °C); $t_{\text{R}} = 6.388$ min (major), $t_{\text{R}} = 7.587$ min (minor).

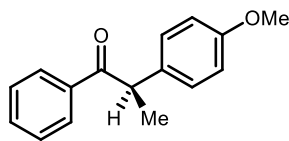
[Racemic **3ab**]



[Enantioenriched **3ab** from (*R*)-**2b**, 99% ee]



(R)-2-(4-methoxyphenyl)-1-phenylpropan-1-one (Table 5.2, 3ac).



3ac

Following *General Procedure L*, the crude product was purified by silica gel chromatography (gradient elution: full hexanes to 5% ether in hexanes) to provide **3ac** as a colorless liquid (40 mg, 85%, 94% ee, >99% es). The spectral data are matched with literature data.¹⁴

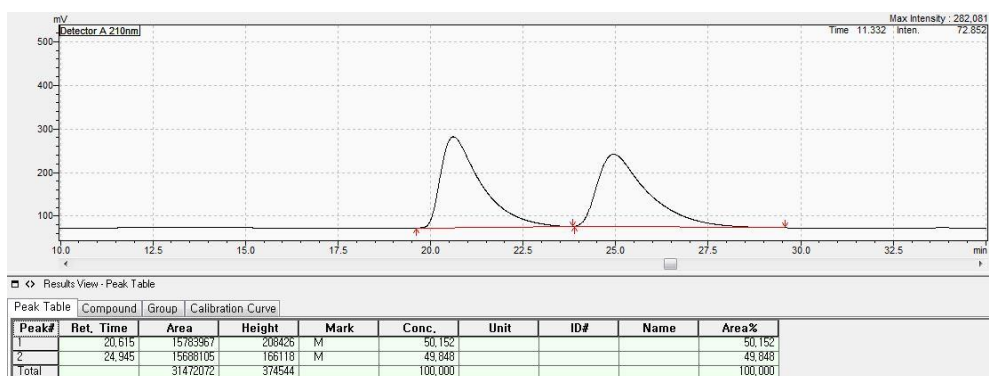
¹H NMR (500 MHz, CDCl₃) δ 7.95 (d, *J* = 7.2 Hz, 2H), 7.47 (t, *J* = 7.4 Hz, 1H), 7.38 (m, 2H), 7.20 (d, *J* = 8.7 Hz, 2H), 6.83 (d, *J* = 8.7 Hz, 2H), 4.64 (q, *J* = 6.8 Hz, 1H), 3.75 (s, 3H), 1.51 (d, *J* = 6.8 Hz, 3H) ppm.

¹³C NMR (126 MHz, CDCl₃) δ 200.67, 158.60, 136.65, 133.62, 132.83, 128.92, 128.88, 128.59, 114.51, 55.34, 47.11, 19.65 ppm.

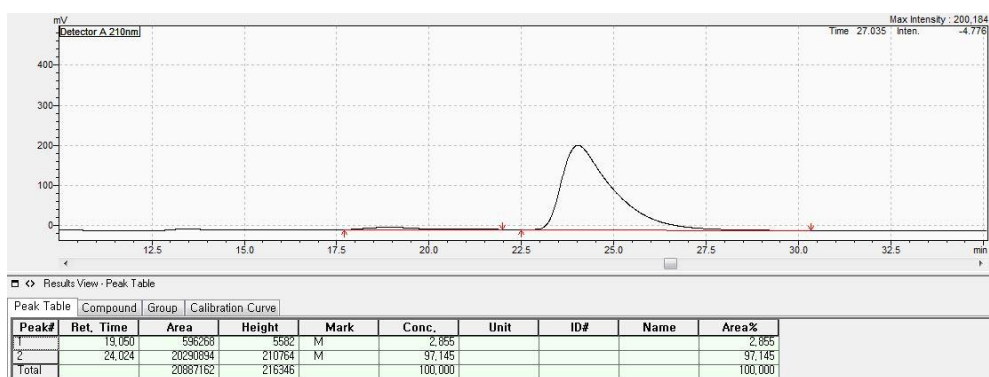
Optical rotation, $[\alpha]_D^{22} = -114.3$ (c = 1.30, CH₂Cl₂).

Enantiomeric excess, 94% ee was measured by HPLC (CHIRALCEL OJ, *n*-hexane : *i*-PrOH = 96 : 4, 1.0 mL/min, wavelength = 210 nm, 28 °C); *t*_R = 24.024 min (major), *t*_R = 19.050 min (minor).

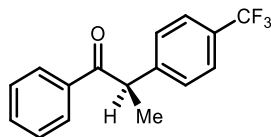
[Racemic 3ac]



[Enantioenriched 3ac]



(R)-1-phenyl-2-(4-(trifluoromethyl)phenyl)propan-1-one (Table 5.2, 3ad)



3ad

Following *General Procedure L*, the crude product was purified by silica gel chromatography (gradient elution: full hexanes to 5% ether in hexanes) to provide **3ad** as a yellowish liquid (46 mg, 83%, 97% ee, >99% es). The spectral data are matched with literature data and the value of optical rotation is opposite to the (*S*)-form based on literature.¹⁵

¹H NMR (500 MHz, CDCl₃) δ 7.95 (d, *J* = 7.5 Hz, 2H), 7.56 (d, *J* = 8.0 Hz, 2H), 7.51 (t, *J* = 7.3 Hz, 1H), 7.41 (m, 4H), 4.78 (q, *J* = 6.8 Hz, 1H), 1.56 (d, *J* = 6.9 Hz, 3H) ppm.

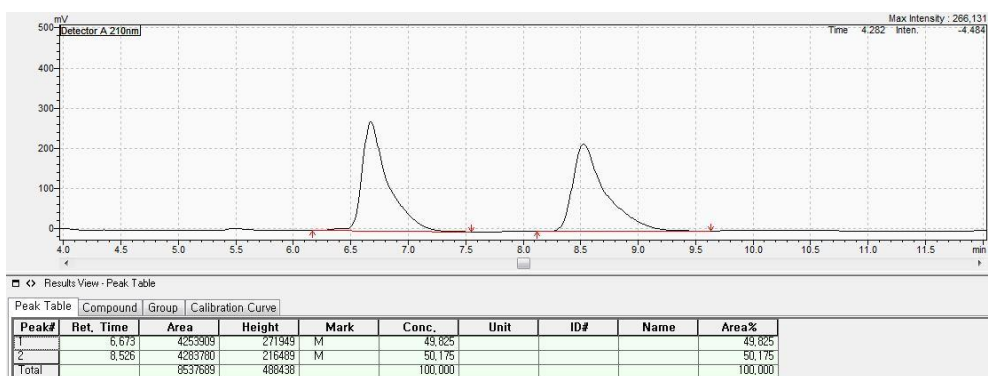
¹³C NMR (126 MHz, CDCl₃) δ 199.78, 145.49, 136.25, 133.32, 129.40 (q, *J* = 32.7 Hz), 128.86, 128.81, 128.31, 124.21 (q, *J* = 272.0 Hz), 126.06 (q, *J* = 3.7 Hz), 47.64, 19.56 ppm.

¹⁹F NMR (376 MHz, CDCl₃) δ -62.57 ppm.

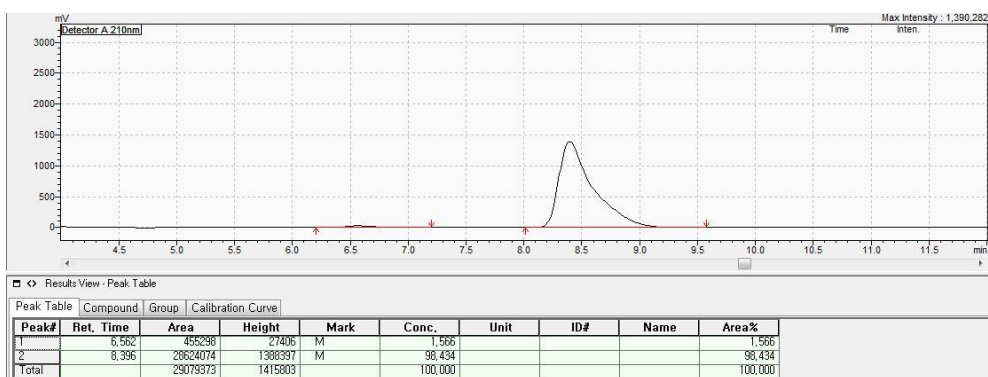
Optical rotation, $[\alpha]_{\text{D}}^{22} = -87.3$ (*c* = 1.00, CH₂Cl₂).

Enantiomeric excess, 97% ee was measured by HPLC (CHIRALCEL OD, *n*-hexane : *i*-PrOH = 99 : 1, 1.0 mL/min, wavelength = 210 nm, 28 °C); *t*_R = 8.396 min (major), *t*_R = 6.562 min (minor).

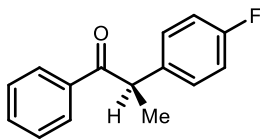
[Racemic 3ad]



[Enantioenriched 3ad]



(R)-2-(4-fluorophenyl)-1-phenylpropan-1-one (Table 5.2, 3ae)



3ae

Following *General Procedure L*, the crude product was purified by silica gel chromatography (gradient elution: full hexanes to 5% ether in hexanes) to provide **3ae** as a colorless liquid (40 mg, 88%, 99% ee, >99% es). The spectral data are matched with literature data.¹⁶

¹H NMR (500 MHz, CDCl₃) δ 7.94 (d, *J* = 7.6 Hz, 2H), 7.49 (t, *J* = 7.2 Hz, 1H), 7.39 (m, 2H), 7.26 (m, 2H), 6.98 (m, 2H), 4.69 (q, *J* = 6.7 Hz, 1H), 1.52 (d, *J* = 6.8 Hz, 3H) ppm.

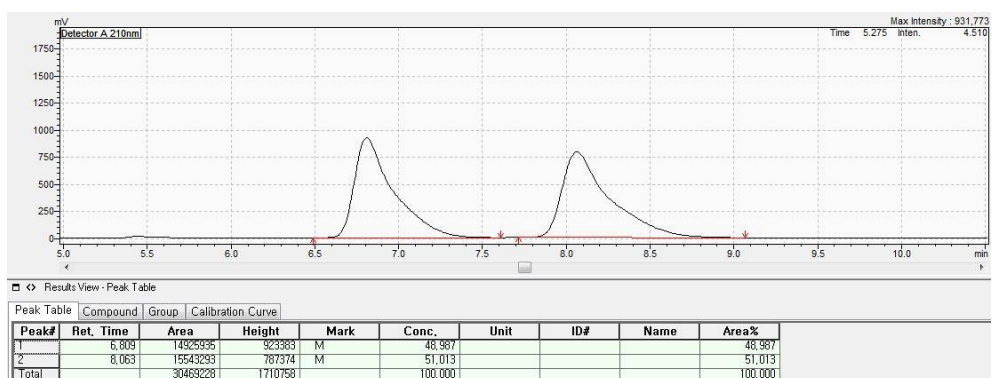
¹³C NMR (126 MHz, CDCl₃) δ 200.32, 161.86 (d, *J* = 245.5 Hz), 137.21 (d, *J* = 3.3 Hz), 136.38, 133.04, 129.40 (d, *J* = 8.0 Hz), 128.82, 128.66, 115.92 (d, *J* = 21.4 Hz), 47.04, 19.68 ppm.

¹⁹F NMR (376 MHz, CDCl₃) δ -115.84 ppm.

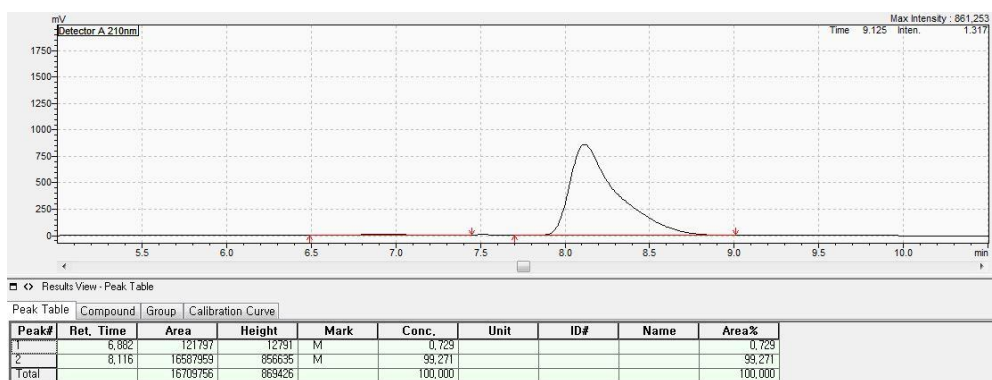
Optical rotation, [α]_D²² = -117.2 (c = 2.00, CH₂Cl₂).

Enantiomeric excess, 99% ee was measured by HPLC (CHIRALCEL OD, *n*-hexane : *i*-PrOH = 99 : 1, 1.0 mL/min, wavelength = 210 nm, 28 °C); t_R = 8.116 min (major), t_R = 6.882 min (minor).

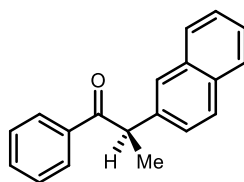
[Racemic 3ae]



[Enantioenriched 3ae]



(R)-2-(naphthalen-2-yl)-1-phenylpropan-1-one (Table 5.2, 3af)



3af

Following *General Procedure L*, the crude product was purified by silica gel chromatography (gradient elution: full hexanes to 5% ether in hexanes) to provide **3af** as white solid (31 mg, 60%, 92% ee, 95% es). The spectral data are matched with literature data.¹⁴

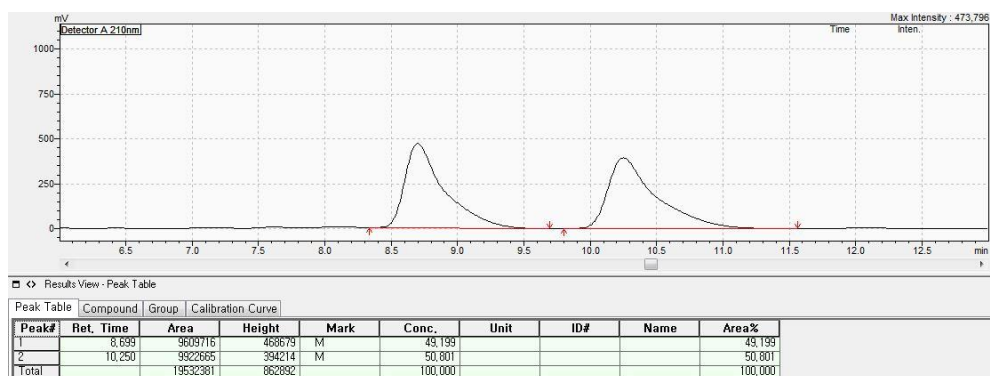
¹H NMR (500 MHz, CDCl₃) δ 8.00 (d, *J* = 7.5 Hz, 2H), 7.86–7.69 (m, 4H), 7.50–7.40 (m, 4H), 7.40–7.32 (m, 2H), 4.86 (q, *J* = 6.8 Hz, 1H), 1.62 (d, *J* = 6.7 Hz, 3H) ppm.

¹³C NMR (126 MHz, CDCl₃) δ 200.24, 138.99, 136.45, 133.66, 132.80, 132.35, 128.79, 128.48, 127.71, 127.61, 126.41, 126.16, 125.93, 125.77, 48.03, 19.54 ppm.

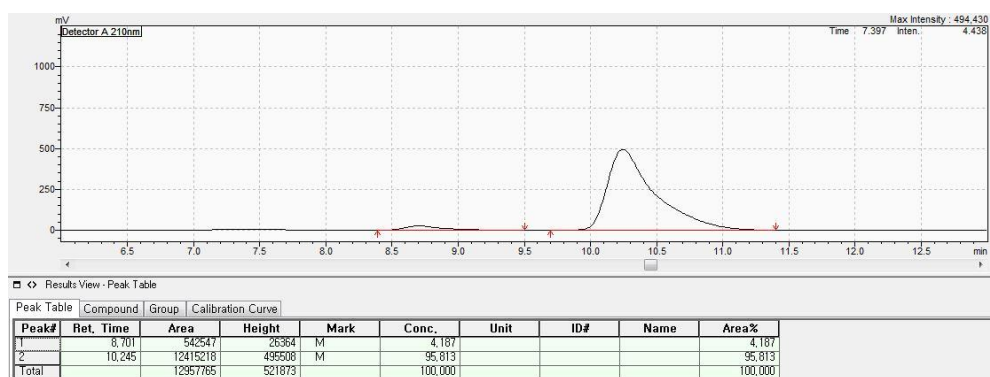
Optical rotation, $[\alpha]_{\text{D}}^{22} = -139.2$ (*c* = 1.30, CH₂Cl₂).

Enantiomeric excess, 92% ee was measured by HPLC (CHIRALCEL OD, *n*-hexane : *i*-PrOH = 99 : 1, 1.0 mL/min, wavelength = 210 nm, 28 °C); *t*_R = 10.245 min (major), *t*_R = 8.701 min (minor).

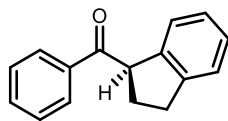
[Racemic 3af]



[Enantioenriched 3af]



(R)-(2,3-dihydro-1H-inden-1-yl)(phenyl)methanone (Table 5.2, 3ag)



3ag

Following *General Procedure L*, the crude product was purified by silica gel chromatography (gradient elution: full hexanes to 5% ether in hexanes) to provide **3ag** as a colorless liquid (31 mg, 70%, 90% ee, 91% es).

¹H NMR (500 MHz, CDCl₃) δ 8.07 (d, *J* = 7.4 Hz, 2H), 7.62 (t, *J* = 7.4 Hz, 1H), 7.57–7.49 (m, 2H), 7.32–7.27 (m, 1H), 7.20 (t, *J* = 7.3 Hz, 1H), 7.14–7.03 (m, 2H), 5.06 (t, *J* = 7.5 Hz, 1H), 3.25–3.11 (m, 1H), 3.09–2.97 (m, 1H), 2.61–2.37 (m, 2H) ppm.

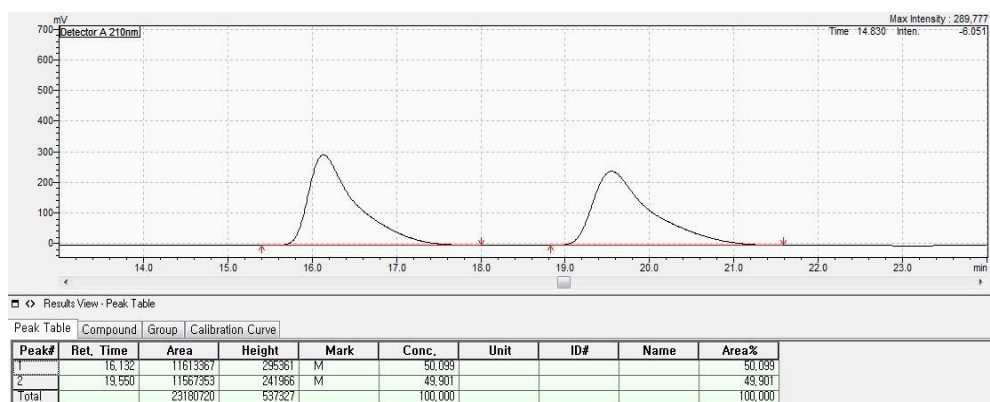
¹³C NMR (126 MHz, CDCl₃) δ 200.42, 144.63, 141.45, 137.04, 133.13, 128.90, 128.72, 127.30, 126.29, 125.01, 124.80, 52.50, 31.99, 29.61 ppm.

HRMS (ESI) calculated for [C₁₆H₁₄O+H]⁺: 223.1117, found: 223.1117.

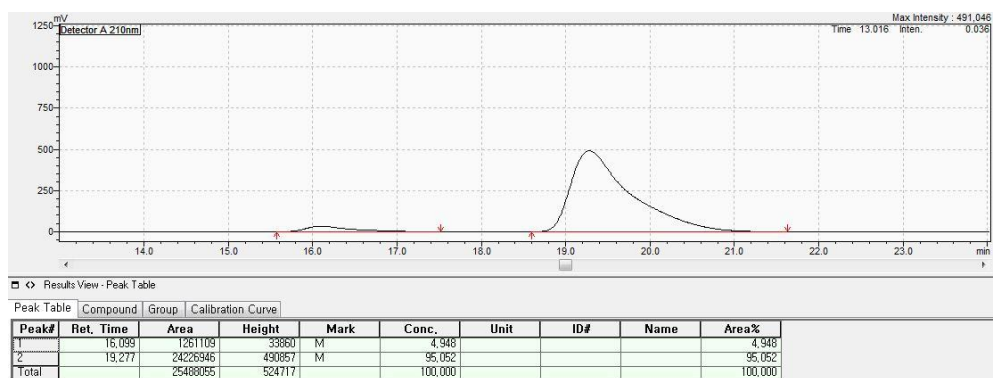
Optical rotation, [α]_D²² = +42.1 (c = 1.30, CH₂Cl₂).

Enantiomeric excess, 90% ee was measured by HPLC (CHIRALCEL OD, *n*-hexane : *i*-PrOH = 99 : 1, 1.0 mL/min, wavelength = 210 nm, 28 °C); t_R = 19.277 min (major), t_R = 16.099 min (minor).

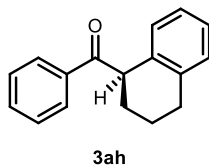
[Racemic 3ag]



[Enantioenriched 3ag]



(*R*)-phenyl(1,2,3,4-tetrahydronaphthalen-1-yl)methanone (Table 5.2, 3ah)



Following *General Procedure L*, the crude product was purified by silica gel chromatography (gradient elution: full hexanes to 5% ether in hexanes) to provide **3ah** as a colorless liquid (18 mg, 38%, 86% ee, 98% es). The spectral data are matched with literature data.¹⁷

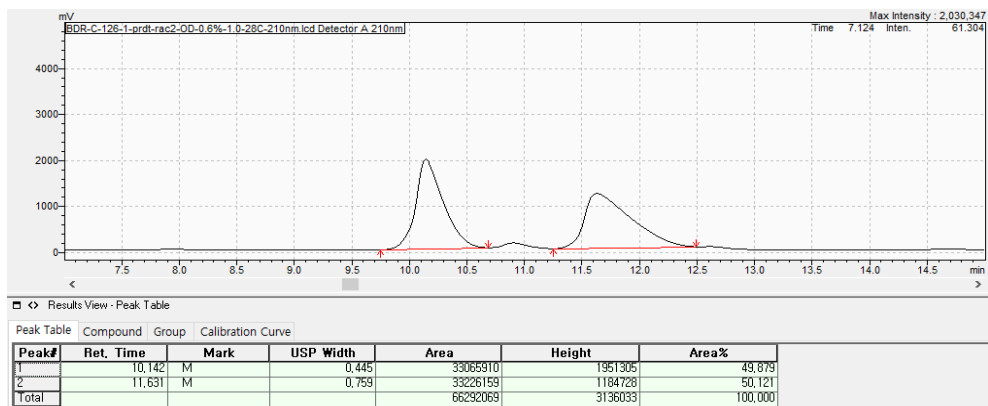
¹H NMR (500 MHz, CDCl₃) δ 8.01 (d, *J* = 7.9 Hz, 2H), 7.59 (t, *J* = 7.4 Hz, 1H), 7.49 (t, *J* = 7.6 Hz, 2H), 7.19–7.14 (m, 2H), 7.12–7.05 (m, 1H), 6.92 (d, *J* = 7.6 Hz, 1H), 4.84 (t, *J* = 6.6 Hz, 1H), 2.97–2.88 (m, 1H), 2.87–2.78 (m, 1H), 2.22–2.13 (m, 1H), 2.13–2.03 (m, 1H), 2.01–1.89 (m, 1H), 1.87–1.74 (m, 1H) ppm.

¹³C NMR (126 MHz, CDCl₃) δ 202.62, 137.72, 136.64, 134.75, 133.00, 129.46, 129.41, 128.81, 128.72, 126.67, 125.89, 47.38, 29.30, 27.62, 20.70 ppm.

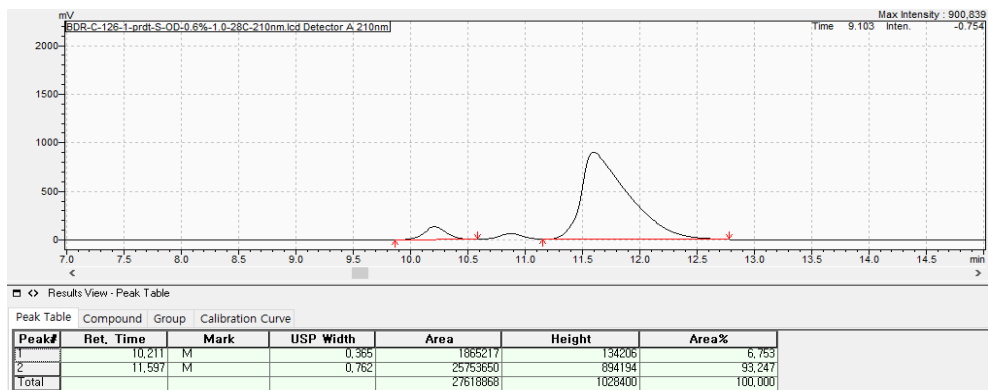
Optical rotation, [α]_D²² = +32.0 (*c* = 1.00, CHCl₃).

Enantiomeric excess, 86% ee was measured by HPLC (CHIRALCEL OD, *n*-hexane : *i*-PrOH = 99 : 1, 1.0 mL/min, wavelength = 210 nm, 28 °C); *t*_R = 11.597 min (major), *t*_R = 10.211 min (minor).

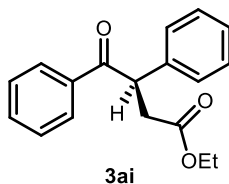
[Racemic 3ah]



[Enantioenriched 3ah]



Ethyl (*R*)-4-oxo-3,4-diphenylbutanoate (Table 5.2, 3ai)



Following *General Procedure L*, the crude product was purified by silica gel chromatography (gradient elution: full hexanes to 10% ether in hexanes) to provide **3ai** as a yellowish liquid (14 mg, 25%, 82% ee, 96% es).

¹H NMR (400 MHz, CDCl₃) δ 7.97 (d, *J* = 7.5 Hz, 2H), 7.47 (m, 1H), 7.40–7.35 (m, 2H), 7.33–7.24 (m, 5H), 5.09 (dd, *J* = 9.7, 5.0 Hz, 1H), 4.10 (q, *J* = 7.1 Hz, 1H), 3.37 (dd, *J* = 16.9, 9.8 Hz, 1H), 2.72 (dd, *J* = 16.9, 5.0 Hz, 1H), 1.19 (t, *J* = 7.1 Hz, 2H) ppm.

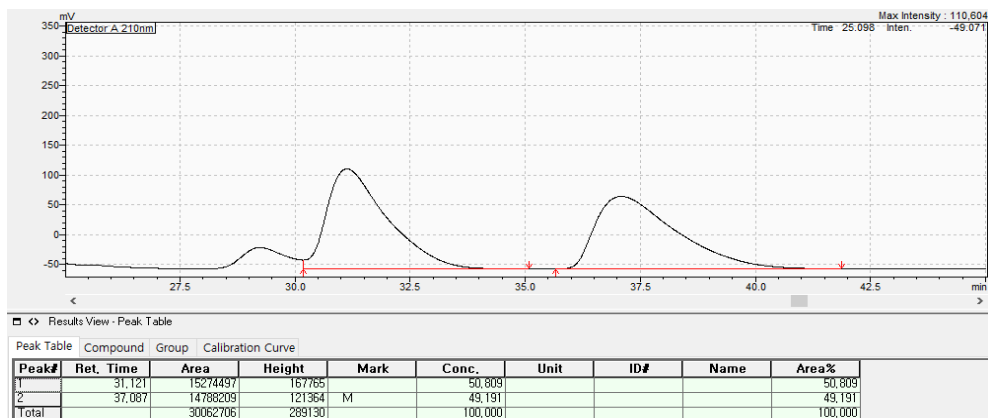
¹³C NMR (126 MHz, CDCl₃) δ 198.79, 172.17, 143.48, 138.23, 133.09, 129.29, 129.01, 128.63, 128.29, 127.59, 60.82, 49.66, 38.81, 14.25 ppm.

HRMS (ESI) calculated for [C₁₈H₁₈O+H]⁺: 283.1329, found: 283.1332.

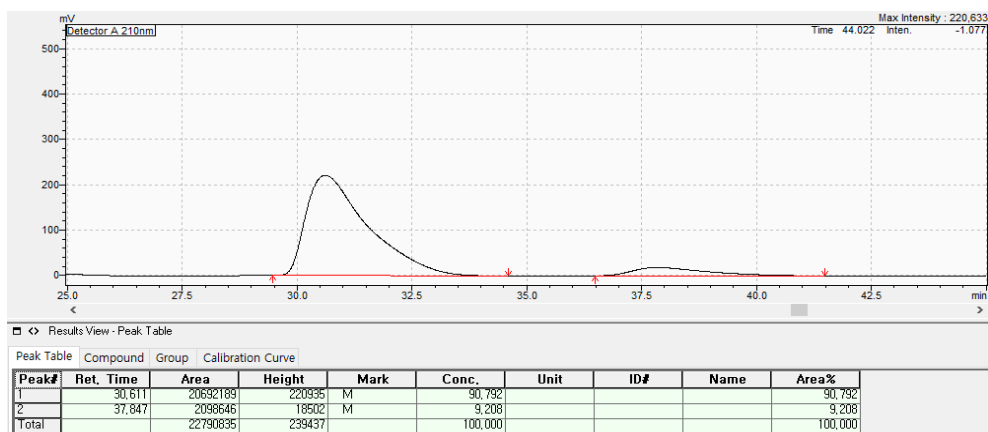
Optical rotation, [α]_D²² = −108.1 (c = 1.25, CH₂Cl₂).

Enantiomeric excess, 82% ee was measured by HPLC (CHIRALCEL OD, *n*-hexane : *i*-PrOH = 99 : 1, 1.0 mL/min, wavelength = 210 nm, 28 °C); t_R = 30.611 min (major), t_R = 37.847 min (minor).

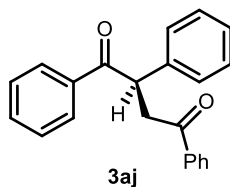
[Racemic 3ai]



[Enantioenriched 3ai]



(R)-1,2,4-triphenylbutane-1,4-dione (Table 5.2, 3aj)



Following *General Procedure L*, the crude product was purified by silica gel chromatography (gradient elution: full hexanes to 10% ethyl acetate in hexanes) to provide **3aj** as a yellowish liquid (23 mg, 26%, 89% ee, 95% es). The spectral data are matched with literature data.¹⁸

(*Note*: **3aj** and dba derived from Pd₂(dba)₃ are inseparable; the purified product has a ratio of **3aj** and dba of 2.5:1)

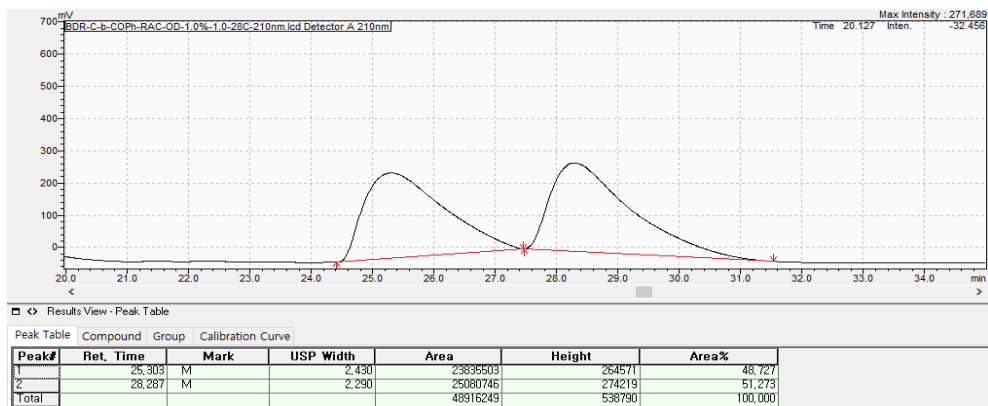
¹H NMR (400 MHz, CDCl₃) δ 8.06–7.96 (m, 4H), 7.56 (t, *J* = 7.4 Hz, 1H), 7.51–7.37 (m, 7H), 7.31 (t, *J* = 7.6 Hz, 2H), 7.26–7.19 (m, 1H), 5.33 (dd, *J* = 10.1, 3.7 Hz, 1H), 4.22 (dd, *J* = 18.0, 10.1 Hz, 1H), 3.31 (dd, *J* = 18.0, 3.7 Hz, 1H) ppm.

¹³C NMR (126 MHz, CDCl₃) δ 198.96, 198.11, 138.71, 136.53, 133.29, 132.93, 129.24, 129.02, 128.62, 128.54, 128.29, 128.21, 127.40, 48.77, 43.92 ppm.

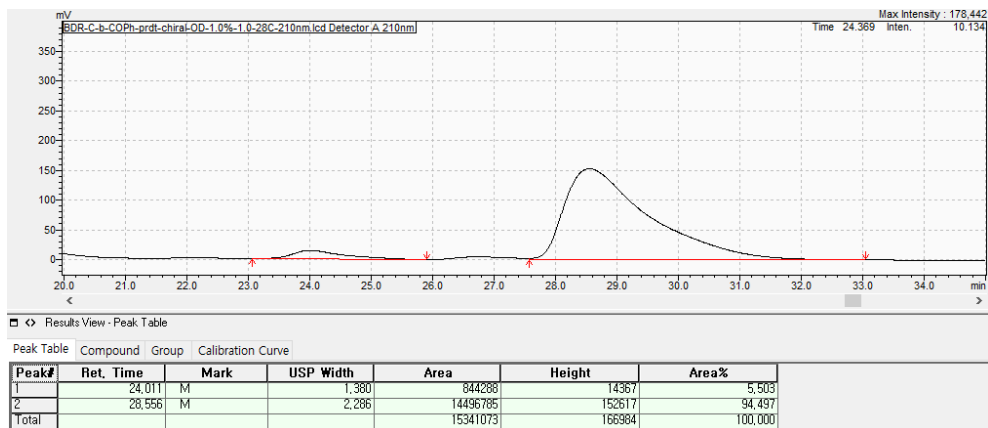
Optical rotation, $[\alpha]_{\text{D}}^{22} = -141.1$ (*c* = 0.5, CHCl₃).

Enantiomeric excess, 89% ee was measured by HPLC (CHIRALCEL OD, *n*-hexane : *i*-PrOH = 99 : 1, 1.0 mL/min, wavelength = 210 nm, 28 °C); *t*_R = 28.556 min (major), *t*_R = 24.011 min (minor).

[Racemic 3aj]



[Enantioenriched 3aj]



(R)-1,2,3-triphenylpropan-1-one (Table 5.2, 3ak)



Following *General Procedure L*, the crude product was purified by silica gel chromatography (gradient elution: full hexanes to 5% ether in hexanes) to provide **3ak** as a white solid (17 mg, 30%, 96% ee, 98% es). The spectral data are matched with literature data and the value of optical rotation is opposite to the (*S*)-form based on literature.¹⁶

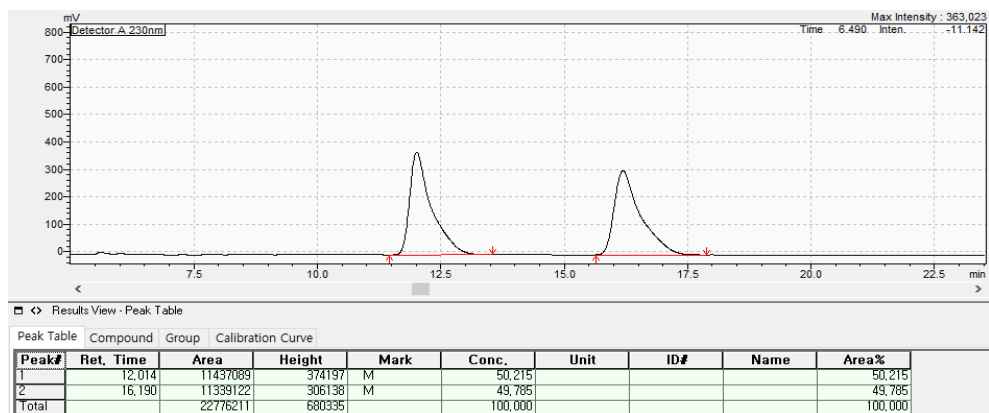
¹H NMR (500 MHz, CDCl₃) δ 7.91 (d, *J* = 7.4 Hz, 2H), 7.45 (t, *J* = 7.3 Hz, 1H), 7.38–7.31 (m, 2H), 7.29–7.23 (m, 4H), 7.23–7.17 (m, 3H), 7.16–7.12 (m, 1H), 7.09 (d, *J* = 7.1 Hz, 2H), 4.82 (t, *J* = 7.2 Hz, 1H), 3.58 (dd, *J* = 13.7, 7.5 Hz, 1H), 3.08 (dd, *J* = 13.7, 7.0 Hz, 1H) ppm.

¹³C NMR (126 MHz, CDCl₃) δ 199.33, 139.90, 139.20, 136.82, 132.98, 129.26, 129.02, 128.81, 128.60, 128.41, 128.35, 127.27, 126.25, 56.06, 56.03, 40.25 ppm.

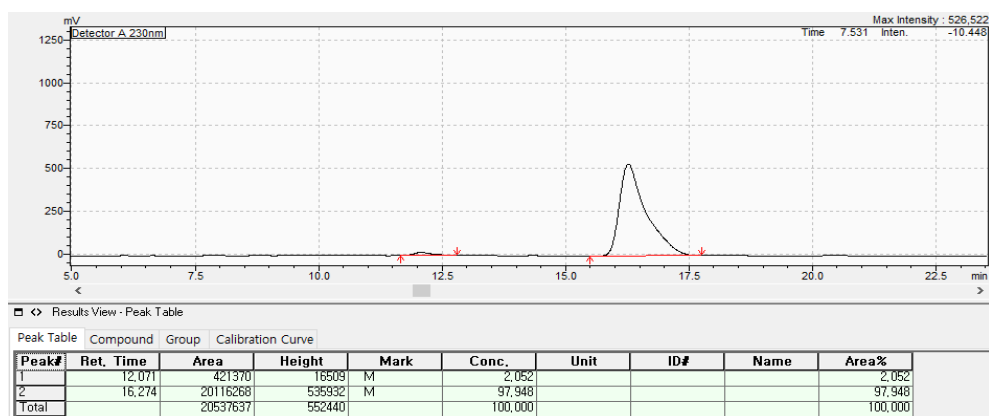
Optical rotation, $[\alpha]_{\text{D}}^{22} = -71.3$ (*c* = 1.00, CH₂Cl₂).

Enantiomeric excess, 96% ee was measured by HPLC (CHIRALCEL OD, *n*-hexane : *i*-PrOH = 99 : 1, 1.0 mL/min, wavelength = 230 nm, 28 °C); *t*_R = 16.274 min (major), *t*_R = 12.071 min (minor).

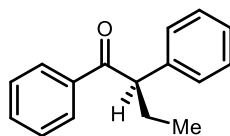
[Racemic 3ak]



[Enantioenriched 3ak]



(R)-1,2-diphenylbutan-1-one (Table 5.2, 3al)



3al

Following *General Procedure L* using APhos (7.5 mol%) as the supporting ligand and Ag₂CO₃ (1.0 equiv) as additional additives, the crude product was purified by silica gel chromatography (gradient elution: full hexanes to 5% ether in hexanes) to provide **3al** as a colorless liquid (8 mg, 17%, 91% ee, 93% es). The spectral data are matched with literature data.¹⁶

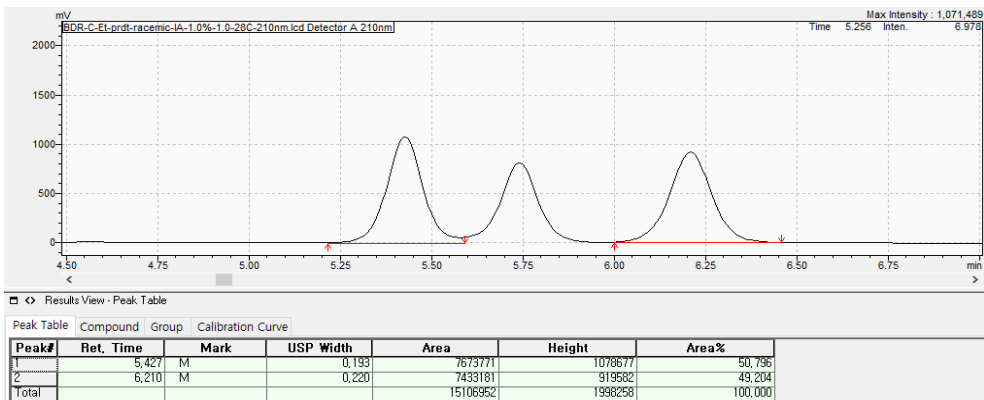
¹H NMR (400 MHz, CDCl₃) δ 7.96 (d, *J* = 7.4 Hz, 2H), 7.48 (t, *J* = 7.3 Hz, 1H), 7.39 (t, *J* = 7.8 Hz, 2H), 7.33–7.27 (m, 4H), 7.23–7.17 (m, 1H), 4.44 (t, *J* = 7.3 Hz, 1H), 2.28–2.13 (m, 1H), 1.92–1.79 (m, 1H), 0.91 (t, *J* = 7.4 Hz, 3H) ppm.

¹³C NMR (126 MHz, CDCl₃) δ 200.25, 139.78, 137.19, 132.91, 128.98, 128.79, 128.63, 128.41, 127.10, 55.61, 27.28, 12.45 ppm.

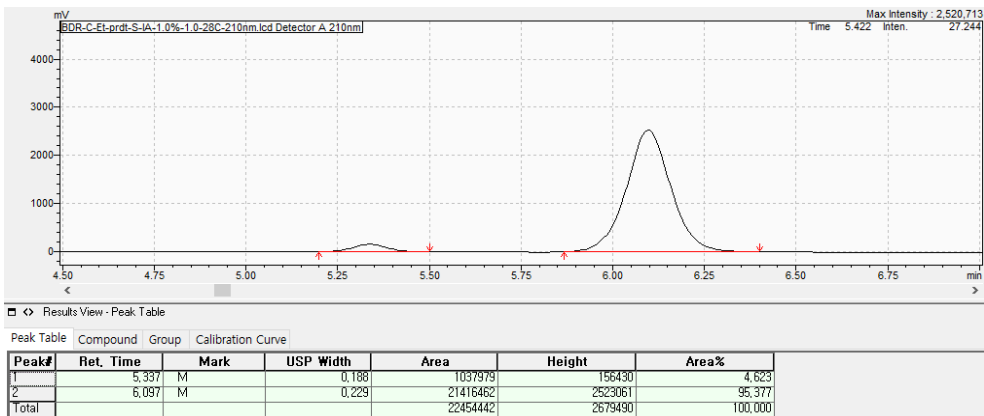
Optical rotation, $[\alpha]_{\text{D}}^{22} = -74.7$ (*c* = 1.00, CHCl₃).

Enantiomeric excess, 96% ee was measured by HPLC (CHIRALPAK IA, *n*-hexane : *i*-PrOH = 99 : 1, 1.0 mL/min, wavelength = 210 nm, 28 °C); *t*_R = 6.097 min (major), *t*_R = 5.337 min (minor).

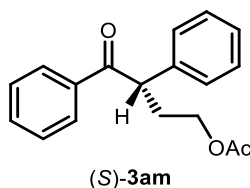
[Racemic 3a]



[Enantioenriched 3a]



(S)-4-oxo-3,4-diphenylbutyl acetate (Table 5.2, (S)-3am)



Following *General Procedure L*, the crude product was purified by silica gel chromatography (gradient elution: full hexanes to 20% ether in hexanes) to provide (S)-**3am** as a colorless liquid (35 mg, 61%, 93% ee, 94% es). The spectral data are matched with literature data and the value of optical rotation is consistent with (*R*)-form based on literature.¹⁵

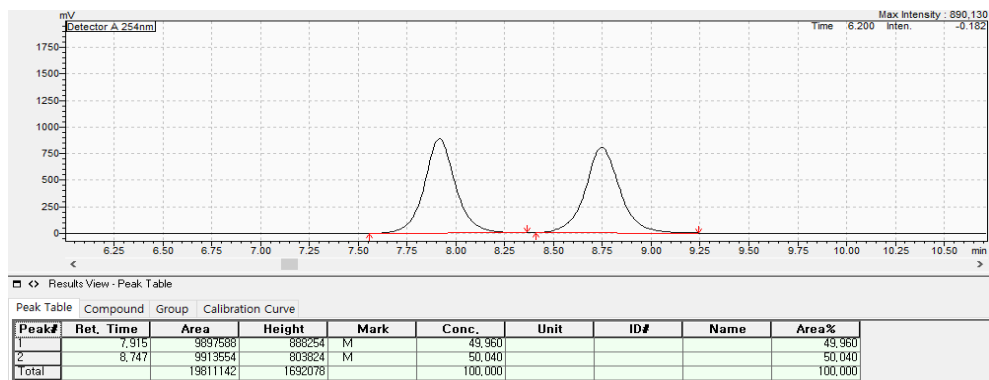
¹H NMR (400 MHz, CDCl₃) δ 8.00–7.91 (m, 2H), 7.52–7.45 (m, 1H), 7.43–7.34 (m, 2H), 7.24–7.18 (m, 4H), 7.24–7.18 (m, 1H), 4.70 (t, *J* = 7.3 Hz, 1H), 4.14–4.06 (m, 1H), 4.06–3.96 (m, 1H), 2.54 (td, *J* = 13.9, 7.2 Hz, 1H), 2.16 (td, *J* = 13.4, 6.0 Hz, 1H), 2.00 (s, 3H) ppm.

¹³C NMR (101 MHz, CDCl₃) δ 199.01, 171.04, 138.77, 136.60, 133.10, 129.25, 128.85, 128.67, 128.34, 127.47, 62.59, 50.36, 32.75, 21.03 ppm.

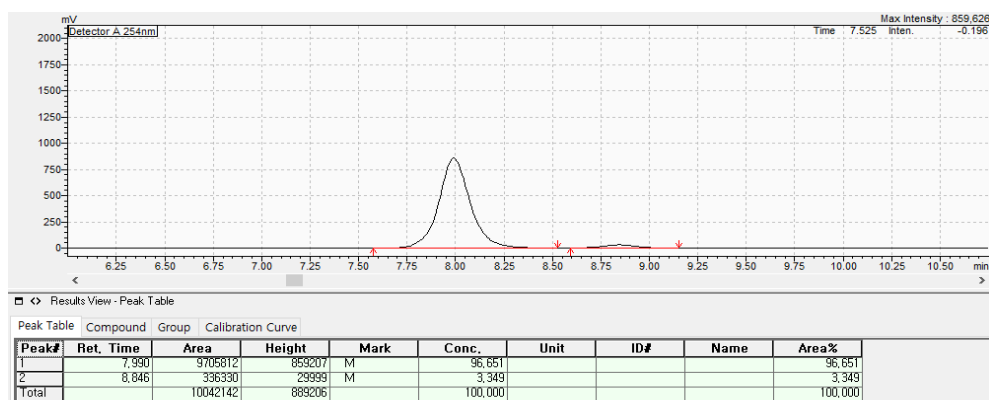
Optical rotation, $[\alpha]_{\text{D}}^{22} = +130.3$ (*c* = 1.00, CH₂Cl₂).

Enantiomeric excess, 93% ee was measured by HPLC (CHIRALPAK IA, *n*-hexane : *i*-PrOH = 97 : 3, 1.0 mL/min, wavelength = 254 nm, 28 °C); *t*_R = 7.990 min (major), *t*_R = 8.846 min (minor).

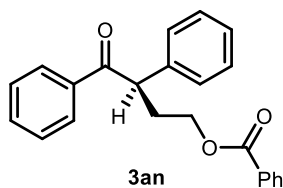
[Racemic **3am**]



[Enantioenriched **3am** from (*R*)-**2m**, 99% ee]



(R)-4-oxo-3,4-diphenylbutyl benzoate (Table 5.2, 3an)



Following *General Procedure L*, the crude product was purified by silica gel chromatography (gradient elution: full hexanes to 20% ethyl acetate in hexanes) to provide **3an** as a white solid (38 mg, 55%, 96% ee, 97% es).

¹H NMR (500 MHz, CDCl₃) δ 7.97 (dd, *J* = 12.1, 8.0 Hz, 4H), 7.59–7.52 (m, 1H), 7.50–7.45 (m, 1H), 7.43 (t, *J* = 7.5 Hz, 2H), 7.37 (t, *J* = 7.7 Hz, 2H), 7.34–7.27 (m, 4H), 7.24–7.18 (m, 1H), 4.80 (t, *J* = 7.2 Hz, 1H), 4.39–4.32 (m, 1H), 4.31–4.22 (m, 1H), 2.69 (td, *J* = 14.0, 7.1 Hz, 1H), 2.31 (td, *J* = 13.5, 5.9 Hz, 1H) ppm.

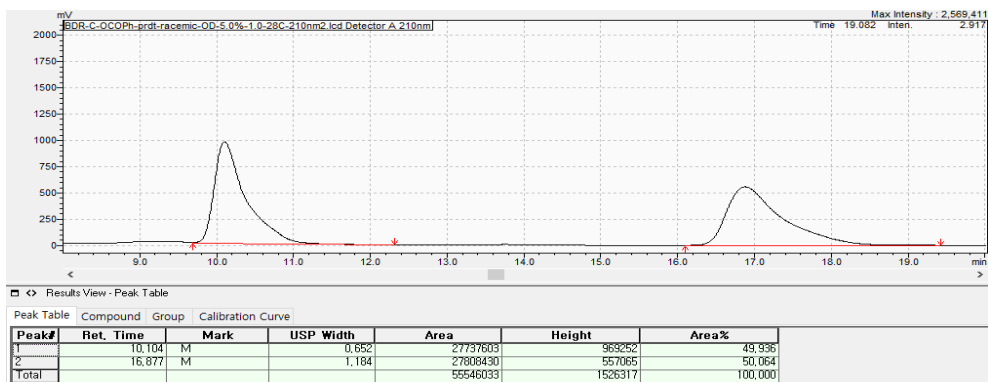
¹³C NMR (126 MHz, CDCl₃) δ 198.88, 166.44, 143.35, 138.66, 136.44, 133.02, 132.95, 129.56, 129.20, 128.79, 128.56, 128.37, 128.28, 127.39, 63.03, 50.41, 32.76 ppm.

HRMS (ESI) calculated for [C₂₃H₂₀O₃+H]⁺: 345.1485, found: 345.1486.

Optical rotation, [α]_D²² = -105.2 (*c* = 1.00, CHCl₃).

Enantiomeric excess, 96% ee was measured by HPLC (CHIRALCEL OD, *n*-hexane : *i*-PrOH = 95 : 5, 1.0 mL/min, wavelength = 210 nm, 28 °C); *t*_R = 10.160 min (major), *t*_R = 17.138 min (minor).

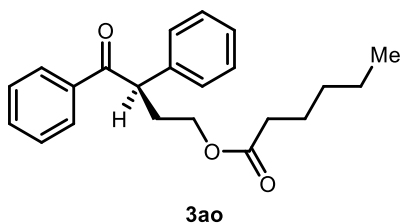
[Racemic 3an]



[Enantioenriched 3an]



(R)-4-oxo-3,4-diphenylbutyl hexanoate (Table 5.2, 3ao)



Following *General Procedure L*, the crude product was purified by silica gel chromatography (gradient elution: full hexanes to 20% ethyl acetate in hexanes) to provide **3ao** as a colorless liquid (36 mg, 53%, 93% ee, 94% es).

¹H NMR (400 MHz, CDCl₃) δ 7.96 (d, *J* = 8.1 Hz, 2H), 7.52–7.45 (m, 1H), 7.39 (t, *J* = 7.7 Hz, 2H), 7.32–7.27 (m, 4H), 7.25–7.18 (m, 1H), 4.71 (t, *J* = 7.2 Hz, 1H), 4.15–4.06 (m, 1H), 4.06–3.97 (m, 1H), 2.54 (td, *J* = 13.8, 6.9 Hz, 1H), 2.26 (t, *J* = 7.5 Hz, 2H), 2.16 (td, *J* = 13.5, 6.2 Hz, 1H), 1.66–1.52 (m, 2H), 1.37–1.22 (m, 4H), 0.89 (t, *J* = 6.7 Hz, 3H) ppm.

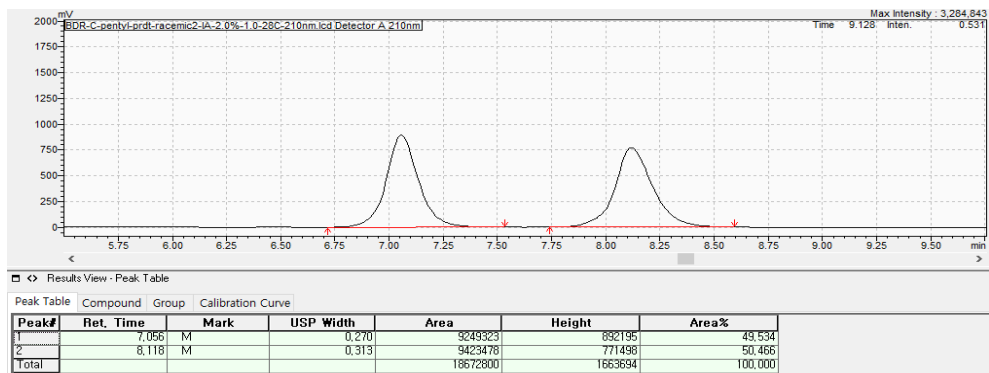
¹³C NMR (126 MHz, CDCl₃) δ 199.05, 173.84, 138.81, 136.64, 133.11, 129.25, 128.85, 128.67, 128.36, 127.46, 62.34, 50.33, 34.38, 32.83, 31.46, 24.79, 22.46, 14.04 ppm.

HRMS (ESI) calculated for [C₂₂H₂₆O₃+H]⁺: 339.1955, found: 339.1956.

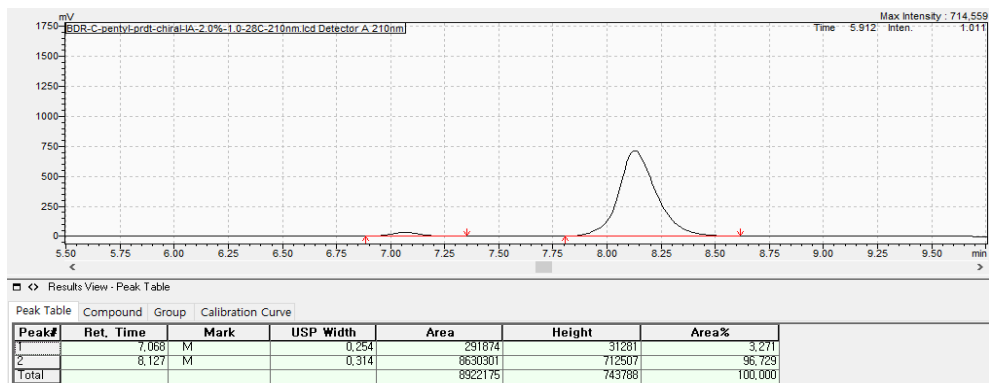
Optical rotation, [α]_D²² = -102.2 (c = 1.00, CHCl₃).

Enantiomeric excess, 93% ee was measured by HPLC (CHIRALPAK IA, *n*-hexane : *i*-PrOH = 98 : 2, 1.0 mL/min, wavelength = 210 nm, 28 °C); t_R = 8.127 min (major), t_R = 7.068 min (minor).

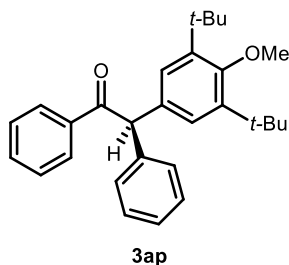
[Racemic 3ao]



[Enantioenriched 3ao]



(R)-2-(3,5-di-*tert*-butyl-4-methoxyphenyl)-1,2-diphenylethan-1-one
(Table 5.2, 3ap)



Following *General Procedure L*, the crude product was purified by silica gel chromatography (gradient elution: full hexanes to 10% ethyl acetate in hexanes) to provide **3ap** as a colorless liquid (25 mg, 30%, 88% ee, 97% es).

¹H NMR (400 MHz, CDCl₃) δ 8.01 (d, *J* = 7.4 Hz, 2H), 7.51 (t, *J* = 7.3 Hz, 1H), 7.42 (t, *J* = 7.7 Hz, 2H), 7.36–7.28 (m, 4H), 7.28–7.22 (m, 1H), 7.14 (s, 2H), 5.96 (s, 1H), 3.67 (s, 3H), 1.37 (s, 18H) ppm.

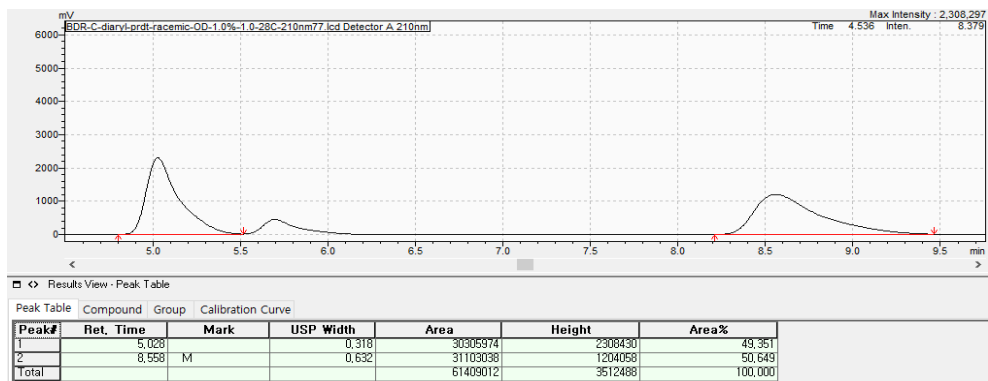
¹³C NMR (126 MHz, CDCl₃) δ 198.79, 158.61, 143.66, 139.65, 137.37, 132.95, 132.80, 129.24, 129.04, 128.77, 128.68, 127.64, 127.12, 64.27, 59.46, 35.92, 32.21 ppm.

HRMS (ESI) calculated for [C₂₉H₃₄O₂+H]⁺: 415.2632, found: 415.2629.

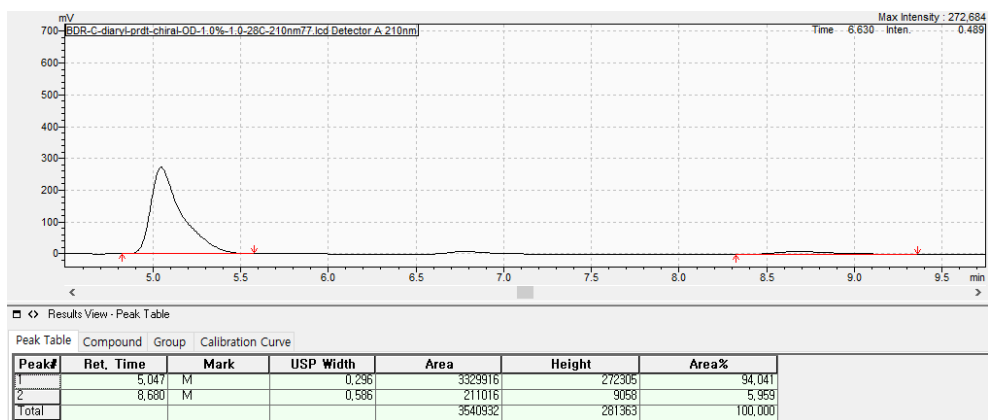
Optical rotation, [α]_D²² = -14.5 (c = 0.5, MeOH).

Enantiomeric excess, 88% ee was measured by HPLC (CHIRALCEL OD, *n*-hexane : *i*-PrOH = 99 : 1, 1.0 mL/min, wavelength = 210 nm, 28 °C); t_R = 5.047 min (major), t_R = 8.680 (minor).

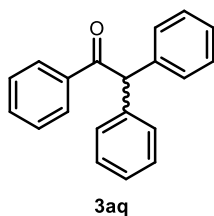
[Racemic 3ap]



[Enantioenriched 3ap]



1,2,2-triphenylethan-1-one (Table 5.2, 3aq)

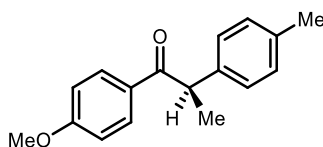


Following *General Procedure L*, the crude product was purified by silica gel chromatography (gradient elution: full hexanes to 10% ethyl acetate in hexanes) to provide **3aq** as a white solid (45 mg, 82%). The spectral data are matched with literature data.¹⁹

¹H NMR (400 MHz, CDCl₃) δ 8.01 (d, *J* = 7.4 Hz, 2H), 7.51 (t, *J* = 7.3 Hz, 1H), 7.42 (t, *J* = 7.7 Hz, 2H), 7.36–7.28 (m, 9H), 7.28–7.22 (m, 1H), 7.14 (s, 2H), 5.96 (s, 1H), 3.67 (s, 3H), 1.37 (s, 18H) ppm.

¹³C NMR (126 MHz, CDCl₃) δ 198.32, 139.23, 136.98, 133.17, 129.29, 129.11, 128.87, 128.76, 127.29, 59.57 ppm.

(R)-1-(4-methoxyphenyl)-2-(p-tolyl)propan-1-one (Table 5.2, 3bb)



3bb

Following *General Procedure L*, the crude product was purified by silica gel chromatography (gradient elution: full hexanes to 5% ether in hexanes) to provide **3bb** as a yellowish solid (35 mg, 68%, 99% ee, >99% es). The spectral data are matched with literature data.²⁰

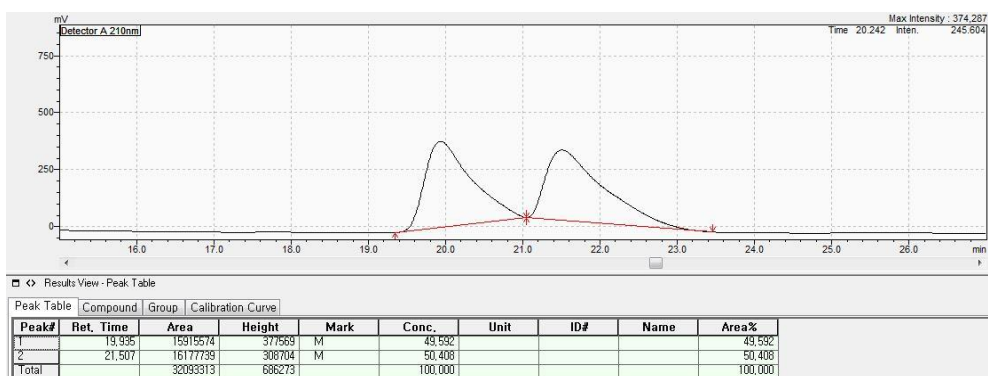
¹H NMR (400 MHz, CDCl₃) δ 7.95 (d, *J* = 8.8 Hz, 2H), 7.18 (d, *J* = 7.9 Hz, 2H), 7.10 (d, *J* = 7.8 Hz, 2H), 6.85 (d, *J* = 8.8 Hz, 2H), 4.61 (q, *J* = 6.8 Hz, 1H), 3.81 (s, 3H), 2.29 (s, 3H), 1.50 (d, *J* = 6.8 Hz, 3H).

¹³C NMR (101 MHz, CDCl₃) δ 199.11, 163.26, 139.05, 136.48, 131.16, 129.75, 129.62, 127.67, 113.74, 55.50, 47.25, 21.13, 19.68 ppm.

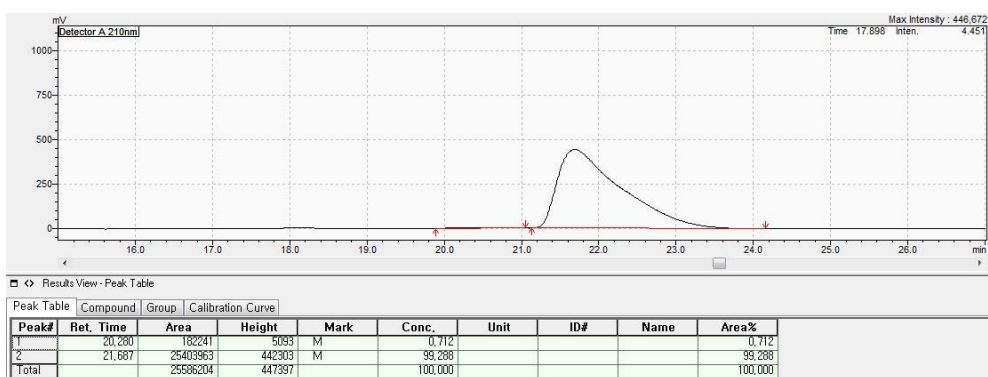
Optical rotation, $[\alpha]_D^{22} = -76.1$ (*c* = 1.10, CH₂Cl₂).

Enantiomeric excess, 99% ee was measured by HPLC (CHIRALCEL OD, *n*-hexane : *i*-PrOH = 99 : 1, 0.6 mL/min, wavelength = 210 nm, 28 °C); *t*_R = 21.687 min (major), *t*_R = 20.280 min (minor).

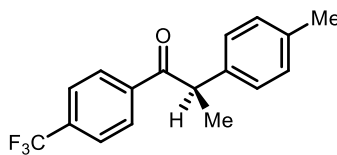
[Racemic 3bb]



[Enantioenriched 3bb]



(R)-2-(p-tolyl)-1-(4-(trifluoromethyl)phenyl)propan-1-one (Table 5.2, 3cb)



3cb

Following *General Procedure L*, the crude product was purified by silica gel chromatography (gradient elution: full hexanes to 5% ether in hexanes) to provide **3cb** as a colorless liquid (34 mg, 58%, 96% ee, 97% es).

¹H NMR (500 MHz, CDCl₃) δ 8.02 (d, *J* = 8.1 Hz, 2H), 7.63 (d, *J* = 8.2 Hz, 2H), 7.14 (d, *J* = 8.3 Hz, 2H), 7.11 (d, *J* = 8.2 Hz, 2H), 4.61 (q, *J* = 6.8 Hz, 1H), 2.29 (d, *J* = 8.0 Hz, 3H), 1.52 (d, *J* = 6.8 Hz, 3H) ppm.

¹³C NMR (126 MHz, CDCl₃) δ 199.48, 139.33, 137.90, 137.04, 134.04 (q, *J* = 32.6 Hz), 130.04, 129.20, 127.71, 125.65 (q, *J* = 3.7 Hz), 123.70 (q, *J* = 272.7 Hz), 48.25, 48.24, 21.15, 19.50 ppm.

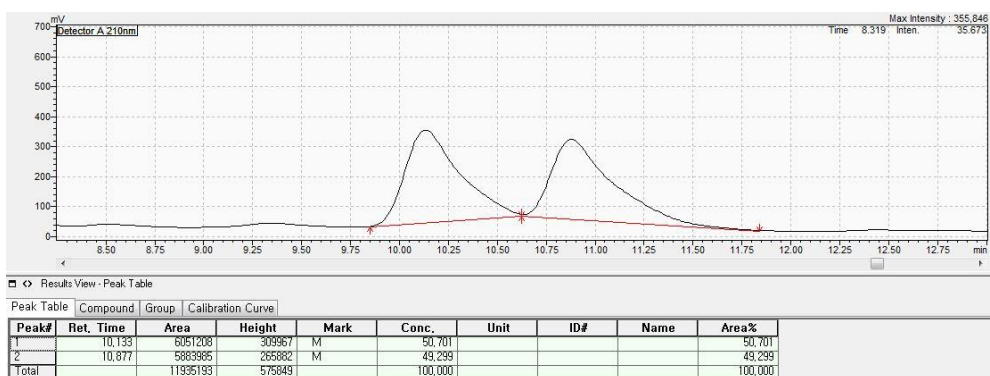
¹⁹F NMR (376 MHz, CDCl₃) δ -63.20 ppm.

HRMS (ESI) calculated for [C₁₇H₁₅F₃O+H]⁺: 293.1148, found: 293.1148.

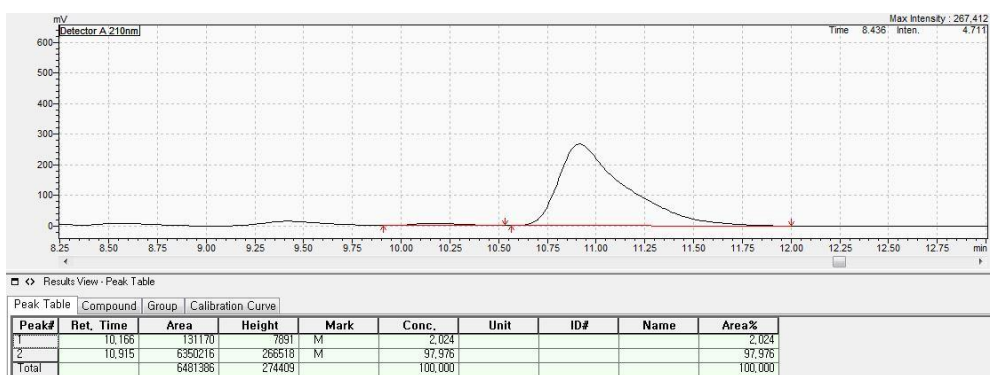
Optical rotation, [α]_D²² = +4.7 (c = 1.23, CH₂Cl₂).

Enantiomeric excess, 96% ee was measured by HPLC (CHIRALCEL OD, *n*-hexane : *i*-PrOH = 99 : 1, 0.5 mL/min, wavelength = 210 nm, 28 °C); t_R = 19.277 min (major), t_R = 16.099 min (minor).

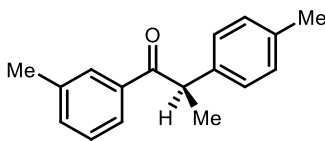
[Racemic 3cb]



[Enantioenriched 3cb]



(R)-1-(*m*-tolyl)-2-(*p*-tolyl)propan-1-one (Table 5.2, **3db).**



3db

Following *General Procedure L*, the crude product was purified by silica gel chromatography (gradient elution: full hexanes to 5% ether in hexanes) to provide **3db** as a colorless liquid (35 mg, 72%, 97% ee, 98% es).

¹H NMR (500 MHz, CDCl₃) δ 7.79 (s, 1H), 7.75 (d, *J* = 7.2 Hz, 1H), 7.31–7.23 (m, 2H), 7.19 (d, *J* = 7.9 Hz, 2H), 7.11 (d, *J* = 7.8 Hz, 2H), 4.66 (q, *J* = 6.8 Hz, 1H), 2.36 (s, 3H), 2.29 (s, 3H), 1.52 (d, *J* = 6.8 Hz, 3H) ppm.

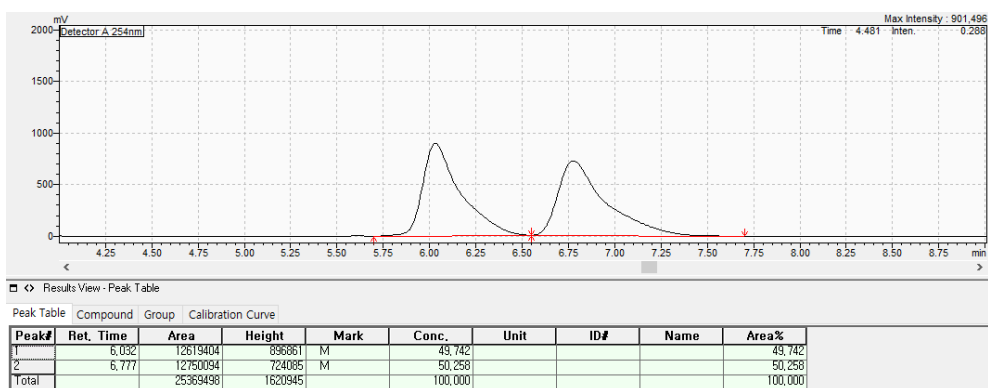
¹³C NMR (126 MHz, CDCl₃) δ 200.80, 138.63, 138.34, 136.66, 136.56, 133.63, 129.76, 129.37, 128.41, 127.73, 126.12, 47.52, 21.50, 21.14, 19.66 ppm.

HRMS (ESI) calculated for [C₁₇H₁₈O+H]⁺: 239.1430, found: 239.1430.

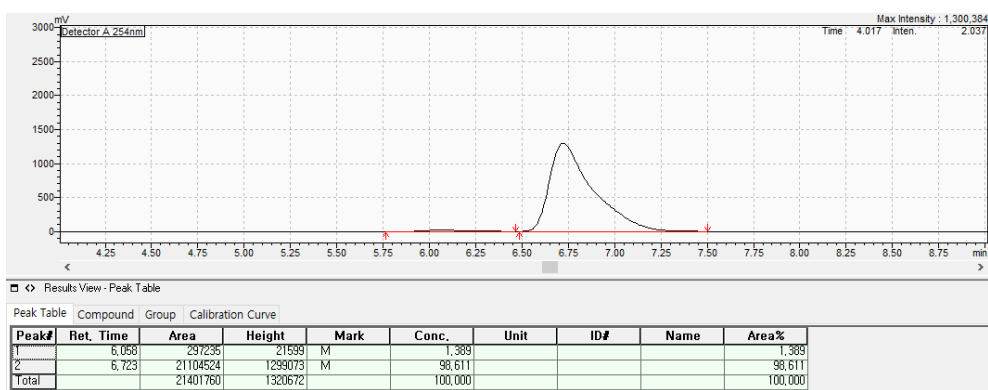
Optical rotation, [α]_D²² = –129.5 (c = 1.00, CH₂Cl₂).

Enantiomeric excess, 97% ee was measured by HPLC (CHIRALCEL OD, *n*-hexane : *i*-PrOH = 99 : 1, 1.0 mL/min, wavelength = 210 nm, 28 °C); t_R = 6.724 min (major), t_R = 6.058 min (minor).

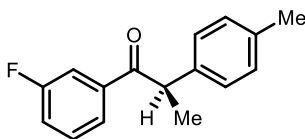
[Racemic 3db]



[Enantioenriched 3db]



(R)-1-(3-fluorophenyl)-2-(p-tolyl)propan-1-one (Table 5.2, 3eb).



3eb

Following *General Procedure L*, the crude product was purified by silica gel chromatography (gradient elution: full hexanes to 5% ether in hexanes) to provide **3eb** as a colorless liquid (30 mg, 62%, 94% ee, 95% es).

¹H NMR (400 MHz, CDCl₃) δ 7.72 (d, *J* = 7.6 Hz, 1H), 7.63 (d, *J* = 9.5 Hz, 1H), 7.40–7.29 (m, 1H), 7.21–7.06 (m, 5H), 4.59 (q, *J* = 6.7 Hz, 1H), 2.29 (s, 3H), 1.52 (d, *J* = 6.8 Hz, 3H) ppm.

¹³C NMR (101 MHz, CDCl₃) δ 199.25 (d, *J* = 2.0 Hz), 162.85 (d, *J* = 247.6 Hz), 138.75 (d, *J* = 6.2 Hz), 138.12, 136.87, 130.19 (d, *J* = 7.6 Hz), 129.93, 127.69, 124.62 (d, *J* = 3.0 Hz), 119.84 (d, *J* = 21.5 Hz), 115.63 (d, *J* = 22.4 Hz), 47.96, 21.15, 19.58 ppm.

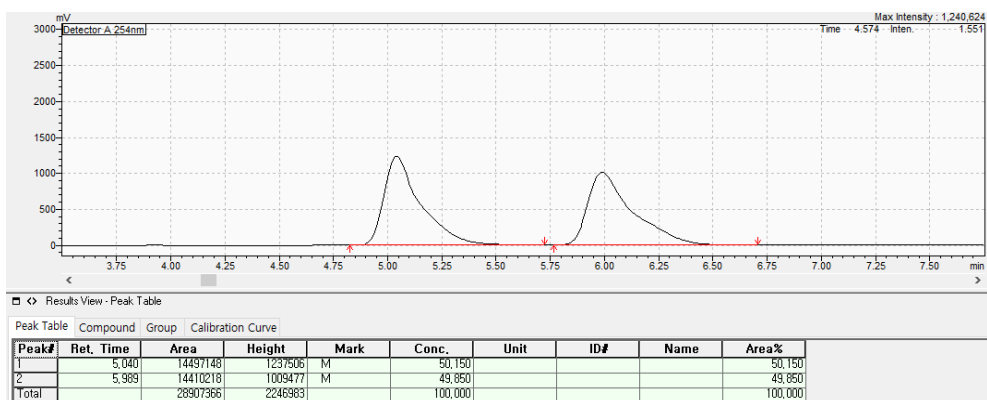
¹⁹F NMR (376 MHz, CDCl₃) δ –112.04 ppm.

HRMS (ESI) calculated for [C₁₆H₁₅FO+H]⁺: 243.1180, found: 243.1181.

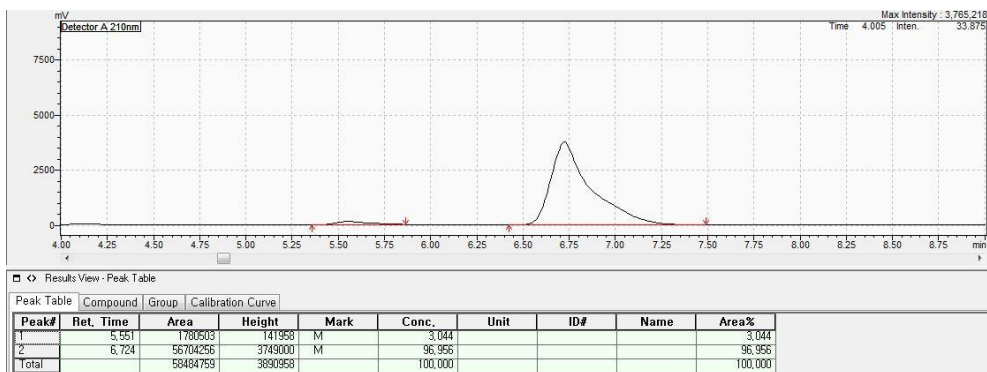
Optical rotation, [α]_D²² = –62.4 (c = 1.00, CH₂Cl₂).

Enantiomeric excess, 94% ee was measured by HPLC (CHIRALCEL OD, *n*-hexane : *i*-PrOH = 99 : 1, 1.0 mL/min, wavelength = 210 nm, 28 °C); t_R = 6.724 min (major), t_R = 5.551 min (minor).

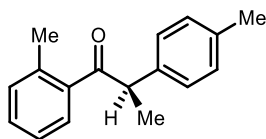
[Racemic 3eb]



[Enantioenriched 3eb]



(R)-1-(o-tolyl)-2-(p-tolyl)propan-1-one (Table 5.2, 3fb).



3fb

Following *General Procedure L*, the crude product was purified by silica gel chromatography (gradient elution: full hexanes to 5% ether in hexanes) to provide **3fb** as a yellowish liquid (20 mg, 43%, 96% ee, 97% es).

¹H NMR (400 MHz, CDCl₃) δ 7.52 (d, *J* = 7.6 Hz, 1H), 7.30–7.24 (m, 1H), 7.20–7.04 (m, 6H), 4.49 (q, *J* = 6.8 Hz, 1H), 2.33 (s, 3H), 2.28 (s, 3H), 1.52 (d, *J* = 6.9 Hz, 3H) ppm.

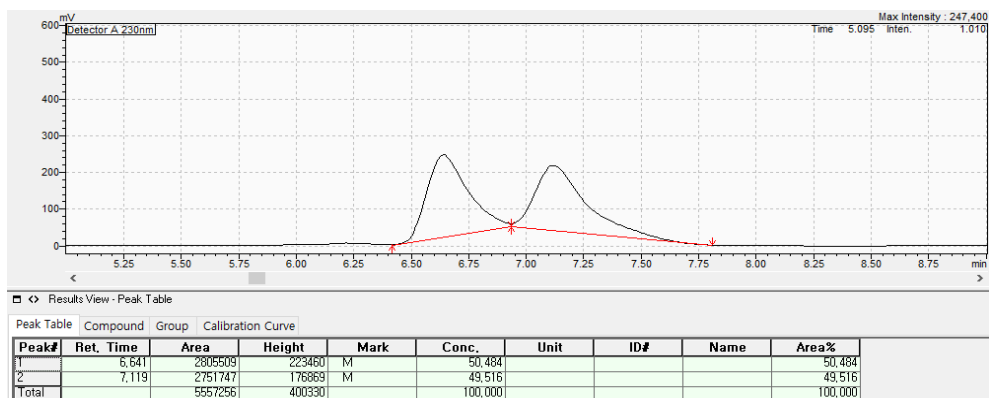
¹³C NMR (126 MHz, CDCl₃) δ 204.93, 140.11, 138.77, 137.97, 137.59, 136.66, 131.68, 130.76, 129.62, 127.95, 125.47, 50.46, 21.15, 20.92, 18.71 ppm.

HRMS (ESI) calculated for [C₁₇H₁₈O+H]⁺: 239.1430, found: 239.1431.

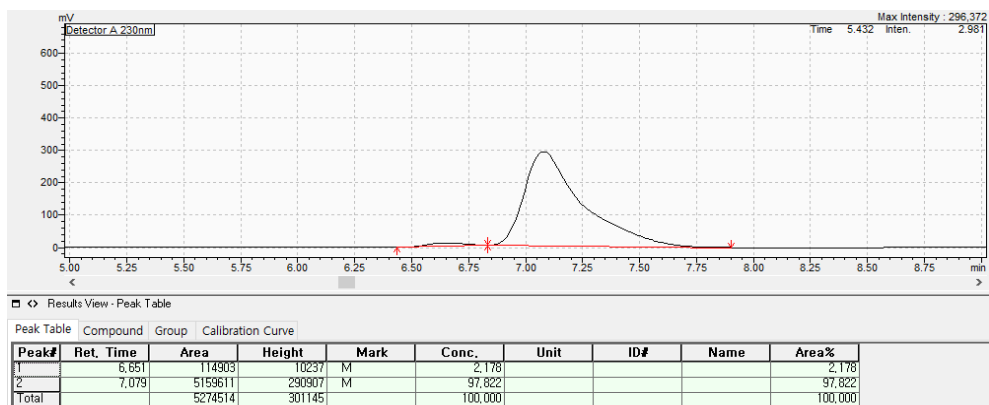
Optical rotation, [α]_D²² = –58.6 (c = 0.7, CH₂Cl₂).

Enantiomeric excess, 96% ee was measured by HPLC (CHIRALCEL OD, *n*-hexane : *i*-PrOH = 99 : 1, 1.0 mL/min, wavelength = 230 nm, 28 °C); t_R = 6.724 min (major), t_R = 5.551 min (minor).

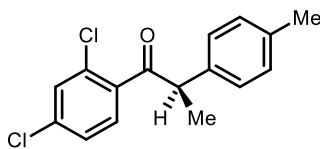
[Racemic 3fb]



[Enantioenriched 3fb]



(R)-1-(2,4-diphenyl)-2-(p-tolyl)propan-1-one (Table 5.2, 3gb).



3gb

Following *General Procedure L*, the crude product was purified by silica gel chromatography (gradient elution: full hexanes to 5% ether in hexanes) to provide **3gb** as a yellowish liquid (28 mg, 47%, 94% ee, 95% es).

¹H NMR (400 MHz, CDCl₃) δ 7.36 (d, *J* = 1.6 Hz, 1H), 7.17–7.11 (m, 1H), 7.10–7.00 (m, 5H), 4.44 (q, *J* = 6.9 Hz, 1H), 2.29 (s, 3H), 1.54 (d, *J* = 6.9 Hz, 3H) ppm.

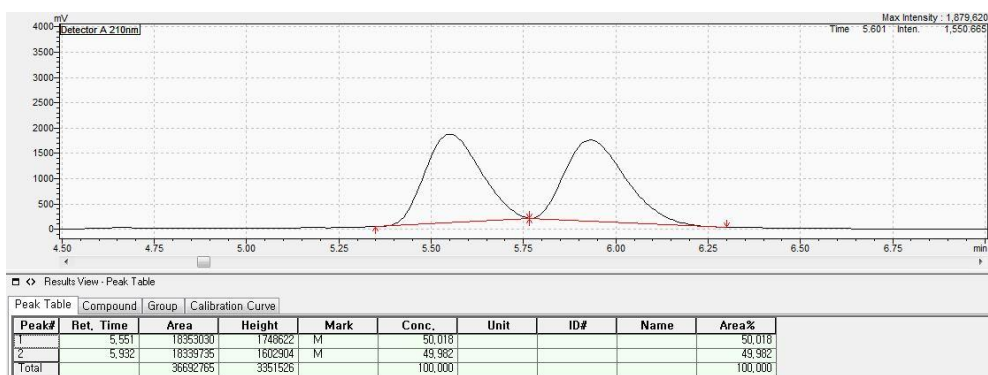
¹³C NMR (101 MHz, CDCl₃) δ 203.04, 138.11, 137.18, 136.57, 136.26, 131.58, 130.19, 129.97, 129.73, 128.17, 127.08, 51.81, 21.19, 17.89 ppm.

HRMS (ESI) calculated for [C₁₆H₁₄Cl₂O+H]⁺: 293.0495, found: 293.0492.

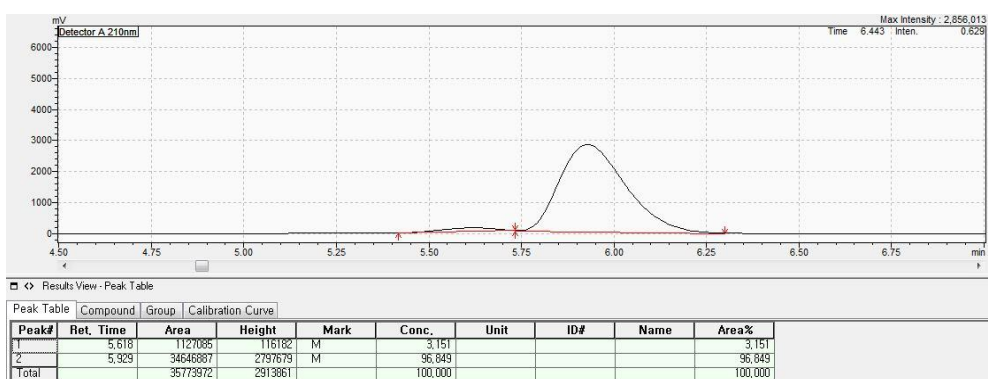
Optical rotation, [α]_D²² = -3.70 (c = 1.10, CH₂Cl₂).

Enantiomeric excess, 94% ee was measured by HPLC (CHIRALCEL OD-H, *n*-hexane : *i*-PrOH = 99 : 1, 1.0 mL/min, wavelength = 210 nm, 28 °C); t_R = 5.929 min (major), t_R = 5.618 min (minor).

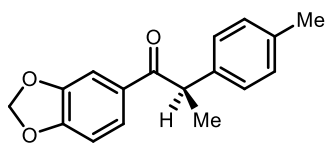
[Racemic 3gb]



[Enantioenriched 3gb]



(R)-1-(benzo[d][1,3]dioxol-5-yl)-2-(p-tolyl)propan-1-one (Table 5.2, 3hb).



3hb

Following *General Procedure L*, the crude product was purified by silica gel chromatography (gradient elution: full hexanes to 5% ether in hexanes) to provide **3hb** as a white solid (45 mg, 83%, 97% ee, 98% es).

¹H NMR (500 MHz, CDCl₃) δ 7.57 (d, *J* = 8.2 Hz, 1H), 7.43 (s, 1H), 7.15 (d, *J* = 7.9 Hz, 2H), 7.10 (d, *J* = 7.8 Hz, 2H), 6.76 (d, *J* = 8.2 Hz, 1H), 5.98 (s, 2H), 4.55 (q, *J* = 6.7 Hz, 1H), 2.29 (s, 3H), 1.48 (d, *J* = 6.8 Hz, 3H) ppm.

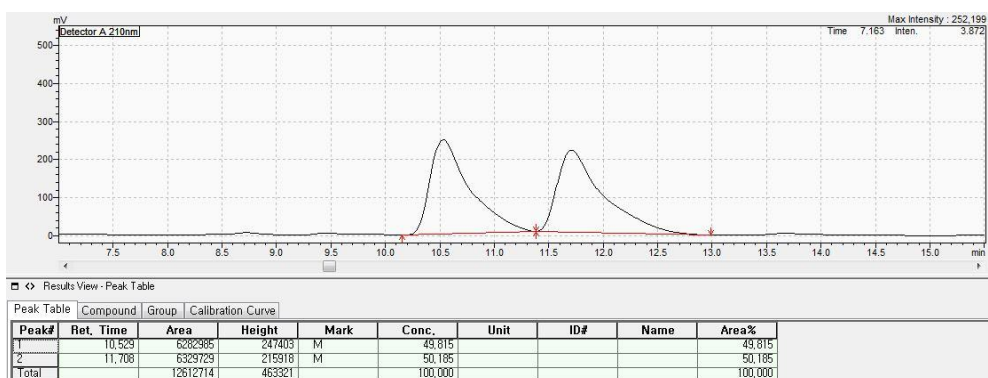
¹³C NMR (126 MHz, CDCl₃) δ 198.49, 151.40, 148.00, 138.76, 136.45, 131.28, 129.66, 127.48, 124.98, 108.63, 107.79, 101.71, 47.27, 21.00, 19.63 ppm.

HRMS (ESI) calculated for [C₁₇H₁₆O₃+H]⁺: 269.1172, found: 369.1173.

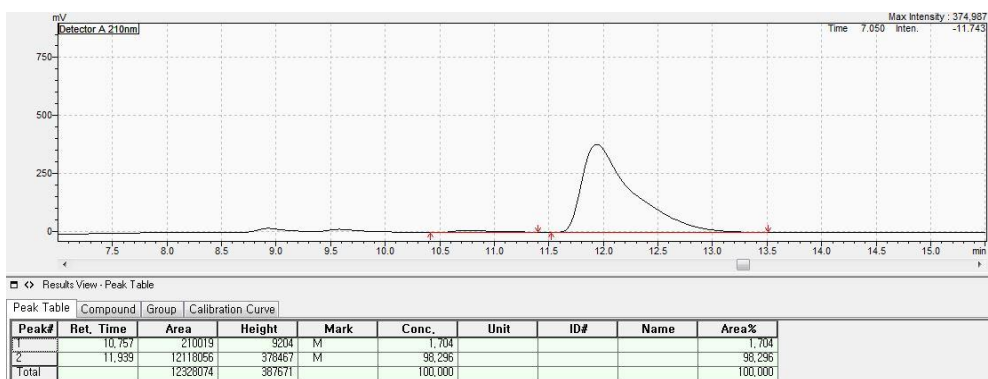
Optical rotation, [α]_D²² = -234.4 (c = 0.5, CH₂Cl₂).

Enantiomeric excess, 97% ee was measured by HPLC (CHIRALCEL OD, *n*-hexane : *i*-PrOH = 99 : 1, 1.0 mL/min, wavelength = 210 nm, 28 °C); t_R = 11.939 min (major), t_R = 10.757 min (minor).

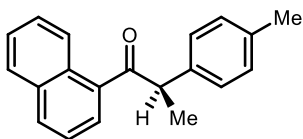
[Racemic **3hb**]



[Enantioenriched **3hb**]



(R)-1-(naphthalen-1-yl)-2-(p-tolyl)propan-1-one (Table 5.2, 3ib).



3ib

Following *General Procedure L*, the crude product was purified by silica gel chromatography (gradient elution: full hexanes to 5% ether in hexanes) to provide **3ib** as a yellowish liquid (37 mg, 68%, 93% ee, 94% es).

¹H NMR (400 MHz, CDCl₃) δ 8.35 (d, *J* = 8.3 Hz, 1H), 7.93–7.86 (m, 1H), 7.84–7.79 (m, 1H), 7.78–7.73 (m, 1H), 7.57–7.45 (m, 2H), 7.41 (t, *J* = 7.7 Hz, 1H), 7.18 (d, *J* = 7.9 Hz, 2H), 7.06 (d, *J* = 7.8 Hz, 2H), 4.67 (q, *J* = 6.8 Hz, 1H), 2.26 (s, 3H), 1.61 (d, *J* = 6.9 Hz, 3H) ppm.

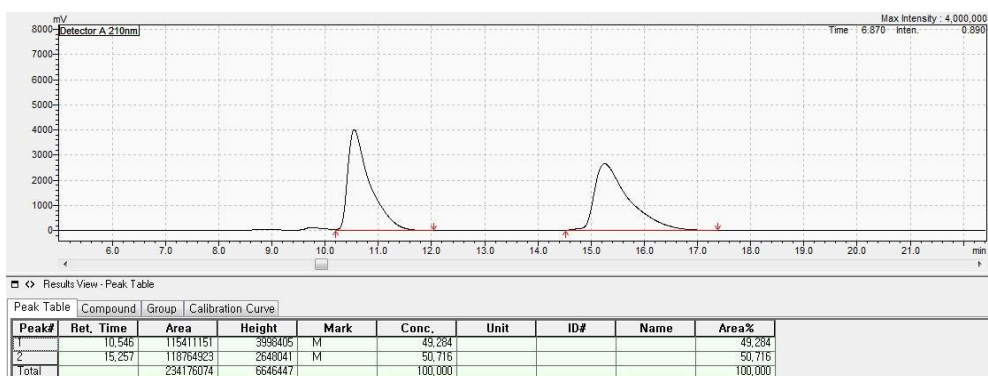
¹³C NMR (126 MHz, CDCl₃) δ 204.67, 137.61, 136.64, 136.55, 133.83, 131.93, 130.49, 129.54, 128.26, 127.74, 127.60, 126.77, 126.29, 125.69, 124.21, 50.89, 21.00, 18.95 ppm.

HRMS (ESI) calculated for [C₂₀H₁₈O+H]⁺: 275.1430, found: 275.1432.

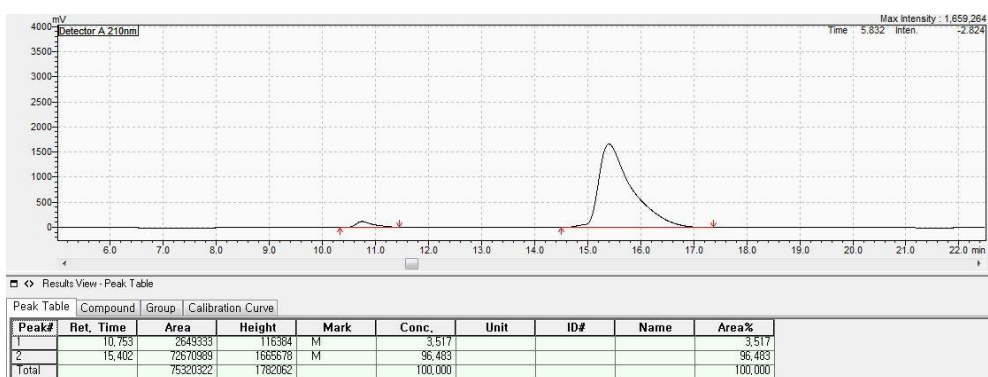
Optical rotation, [α]_D²² = -146.6 (c = 1.35, CH₂Cl₂).

Enantiomeric excess, 93% ee was measured by HPLC (CHIRALCEL OD, *n*-hexane : *i*-PrOH = 99 : 1, 1.0 mL/min, wavelength = 210 nm, 28 °C); t_R = 15.402 min (major), t_R = 10.753 min (minor).

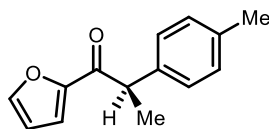
[Racemic 3ib]



[Enantioenriched 3ib]



(R)-1-(furan-2-yl)-2-(p-tolyl)propan-1-one (Table 5.2, 3jb)



3jb

Following *General Procedure L*, the crude product was purified by silica gel chromatography (gradient elution: full hexanes to 10% ether in hexanes) to provide **3jb** as a white solid (34 mg, 80%, 99% ee, >99% es).

^1H NMR (400 MHz, CDCl_3) δ 7.52 (d, $J = 0.8$ Hz, 1H), 7.24–7.18 (m, 2H), 7.15–7.08 (m, 3H), 6.45 (dd, $J = 3.5, 1.6$ Hz, 1H), 4.45 (q, $J = 7.0$ Hz, 1H), 2.30 (s, 3H), 1.50 (d, $J = 7.0$ Hz, 3H) ppm.

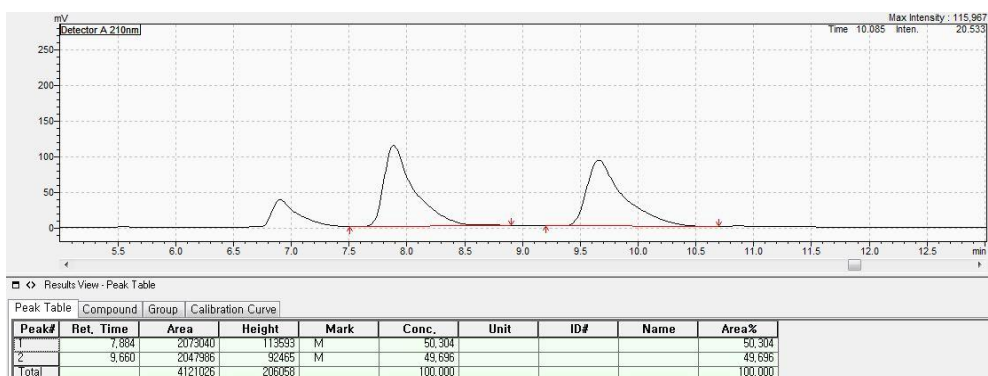
^{13}C NMR (101 MHz, CDCl_3) δ 189.70, 152.35, 146.37, 137.96, 136.80, 129.63, 127.88, 117.92, 112.27, 47.69, 21.17, 18.46 ppm.

HRMS (ESI) calculated for $[\text{C}_{20}\text{H}_{18}\text{O}+\text{H}]^+$: 215.1067, found: 215.1062.

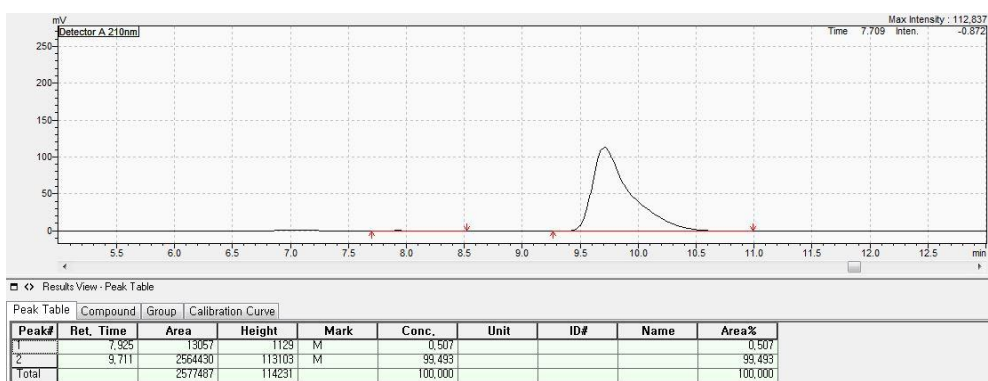
Optical rotation, $[\alpha]_{\text{D}}^{22} = -32.6$ ($c = 1.75$, CH_2Cl_2).

Enantiomeric excess, 99% ee was measured by HPLC (CHIRALCEL OD, *n*-hexane : *i*-PrOH = 99 : 1, 1.0 mL/min, wavelength = 210 nm, 28 °C); $t_{\text{R}} = 9.711$ min (major), $t_{\text{R}} = 7.925$ min (minor).

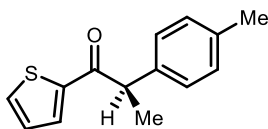
[Racemic 3jb]



[Enantioenriched 3jb]



(R)-1-(thiophen-2-yl)-2-(*p*-tolyl)propan-1-one (Table 5.2, 3kb)



3kb

Following *General Procedure L*, the crude product was purified by silica gel chromatography (gradient elution: full hexanes to 10% ether in hexanes) to provide **3kb** as a yellowish solid (38 mg, 83%, 98% ee, 99% es).

¹H NMR (500 MHz, CDCl₃) δ 7.67 (d, *J* = 3.7 Hz, 1H), 7.55 (d, *J* = 4.9 Hz, 1H), 7.22 (d, *J* = 7.9 Hz, 2H), 7.12 (d, *J* = 7.8 Hz, 2H), 7.06–7.00 (m, 1H), 4.48 (q, *J* = 6.8 Hz, 1H), 2.30 (s, 3H), 1.53 (d, *J* = 6.9 Hz, 3H) ppm.

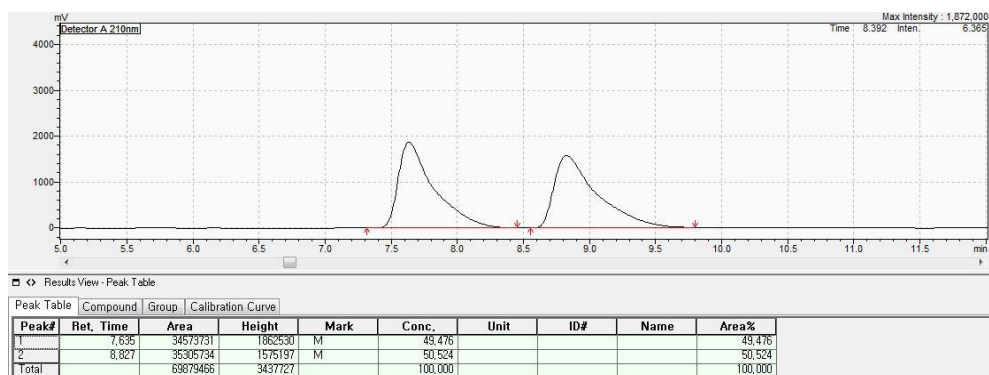
¹³C NMR (126 MHz, CDCl₃) δ 193.40, 143.73, 138.32, 136.71, 133.42, 132.35, 129.61, 127.99, 127.58, 48.95, 21.03, 19.17 ppm.

HRMS (ESI) calculated for [C₁₄H₁₄OS+H]⁺: 231.0838, found: 231.0838.

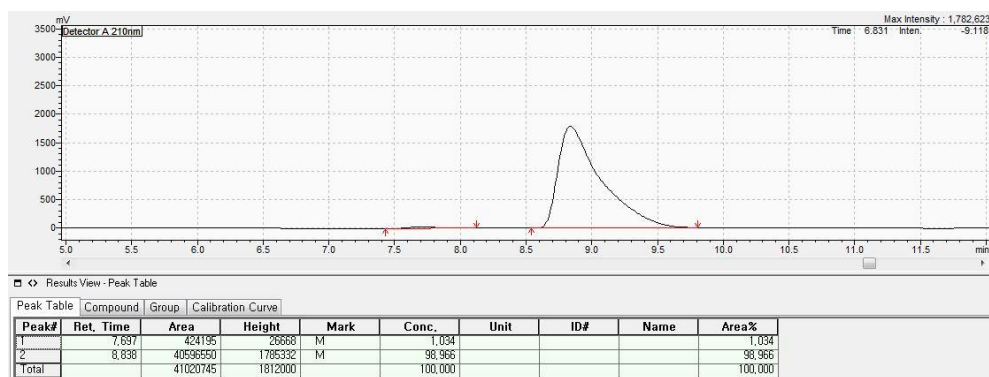
Optical rotation, [α]_D²² = −129.6 (c = 1.60, CH₂Cl₂).

Enantiomeric excess, 98% ee was measured by HPLC (CHIRALCEL OD, *n*-hexane : *i*-PrOH = 99 : 1, 1.0 mL/min, wavelength = 210 nm, 28 °C); t_R = 8.838 min (major), t_R = 7.697 min (minor).

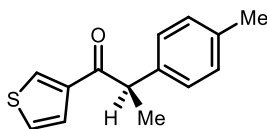
[Racemic 3kb]



[Enantioenriched 3kb]



(R)-1-(thiophen-3-yl)-2-(p-tolyl)propan-1-one (Table 5.2, 3b)



3b

Following *General Procedure L*, the crude product was purified by silica gel chromatography (gradient elution: full hexanes to 10% ether in hexanes) to provide **3b** as a colorless liquid (30 mg, 65%, 98% ee, 99% es).

¹H NMR (400 MHz, CDCl₃) δ 7.99 (m, 1H), 7.51 (d, *J* = 5.0 Hz, 1H), 7.22 (m, 1H), 7.18 (d, *J* = 8.0 Hz, 2H), 7.12 (d, *J* = 8.0 Hz, 2H), 4.44 (q, *J* = 6.9 Hz, 1H), 2.30 (s, 3H), 1.50 (d, *J* = 6.9 Hz, 3H) ppm.

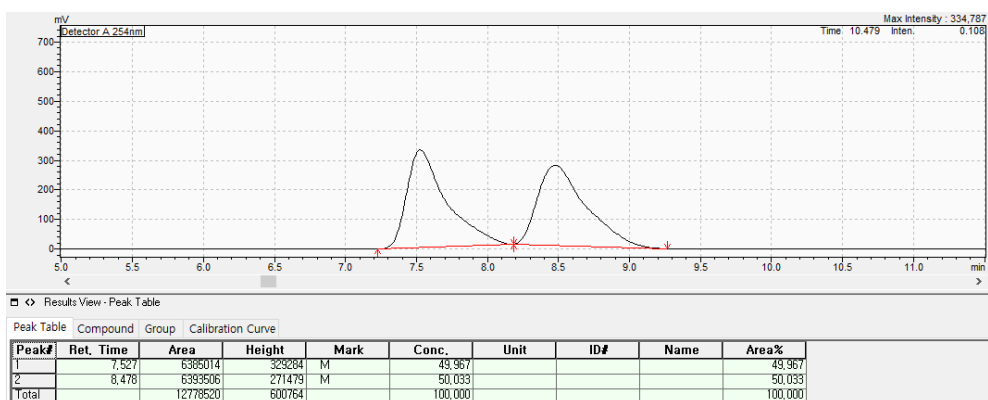
¹³C NMR (101 MHz, CDCl₃) δ 194.88, 141.74, 138.59, 136.75, 132.64, 129.82, 127.70, 127.67, 126.05, 49.45, 21.16, 19.30 ppm.

HRMS (ESI) calculated for [C₁₄H₁₄OS+H]⁺: 231.0838, found: 231.0841.

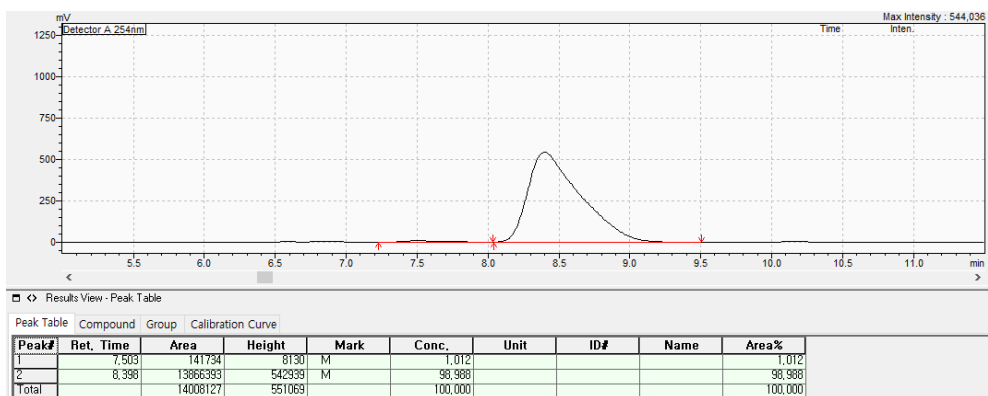
Optical rotation, [α]_D²² = -56.8 (c = 1.10, CH₂Cl₂).

Enantiomeric excess, 98% ee was measured by HPLC (CHIRALCEL OD, *n*-hexane : *i*-PrOH = 99 : 1, 1.0 mL/min, wavelength = 210 nm, 28 °C); t_R = 8.398 min (major), t_R = 7.503 min (minor).

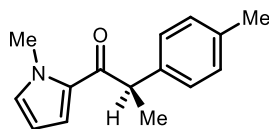
[Racemic 3**1b**]



[Enantioenriched 3**1b**]



(R)-1-(1-methyl-1H-pyrrol-2-yl)-2-(p-tolyl)propan-1-one (Table 5.2, 3mb)



3mb

Following *General Procedure L*, the crude product was purified by silica gel chromatography (gradient elution: full hexanes to 10% ether in hexanes) to provide **3mb** as a brown solid (36 mg, 78%, 98% ee, 99% es).

¹H NMR (400 MHz, CDCl₃) δ 7.23 (d, *J* = 7.8 Hz, 2H), 7.09 (d, *J* = 7.7 Hz, 2H), 7.01 (d, *J* = 3.7 Hz, 1H), 6.75 (s, 1H), 6.12–6.01 (m, 1H), 4.45 (q, *J* = 6.9 Hz, 1H), 3.90 (s, 1H), 2.28 (s, 2H), 1.48 (d, *J* = 6.9 Hz, 2H) ppm.

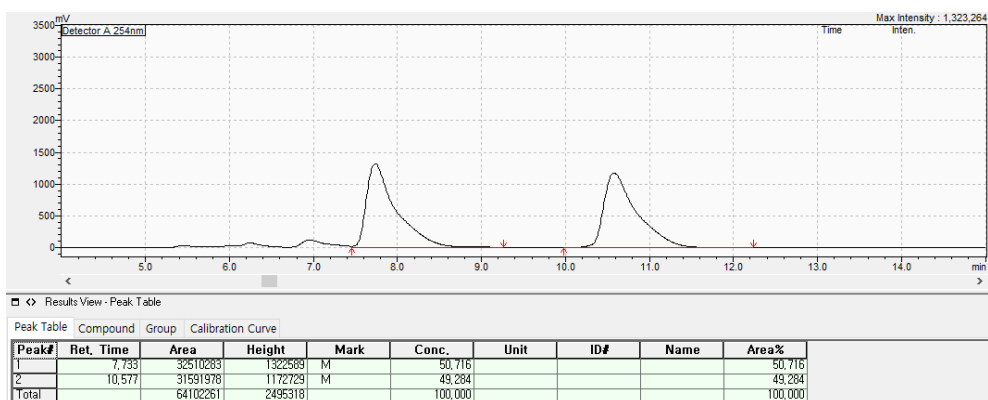
¹³C NMR (126 MHz, CDCl₃) δ 191.67, 139.31, 136.24, 131.24, 130.19, 129.35, 127.48, 119.52, 107.90, 47.59, 37.81, 21.03, 19.04 ppm.

HRMS (ESI) calculated for [C₁₅H₁₇NO+H]⁺: 228.1383, found: 228.1382.

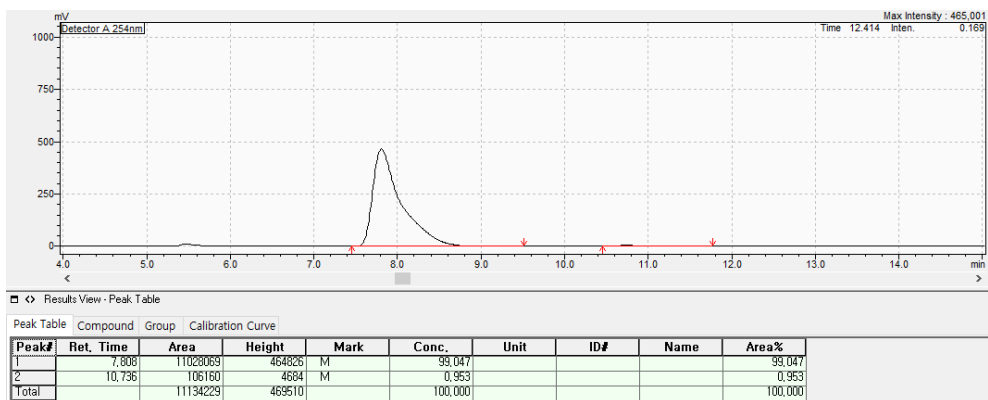
Optical rotation, [α]_D²² = -76.4 (c = 1.00, CH₂Cl₂).

Enantiomeric excess, 98% ee was measured by HPLC (CHIRALCEL OD, *n*-hexane : *i*-PrOH = 99 : 1, 1.0 mL/min, wavelength = 254 nm, 28 °C); t_R = 7.808 min (major), t_R = 10.736 min (minor).

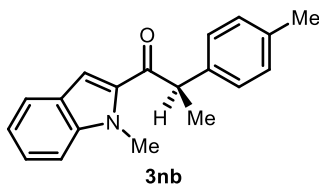
[Racemic 3mb]



[Enantioenriched 3mb]



(R)-1-(1-methyl-1H-indol-2-yl)-2-(p-tolyl)propan-1-one (Table 5.2, 3nb)



Following *General Procedure L*, the crude product was purified by silica gel chromatography (gradient elution: full hexanes to 15% ether in hexanes) to provide **3nb** as a brown solid (33 mg, 60%, 98% ee, 99% es).

¹H NMR (400 MHz, CDCl₃) δ 7.70–7.60 (m, 1H), 7.37–7.30 (m, 3H), 7.26 (d, *J* = 7.9 Hz, 2H), 7.15–7.05(m, 3H), 4.66 (q, *J* = 6.7 Hz, 1H), 4.04 (s, 3H), 2.28 (s, 3H), 1.55 (d, *J* = 6.9 Hz, 3H) ppm.

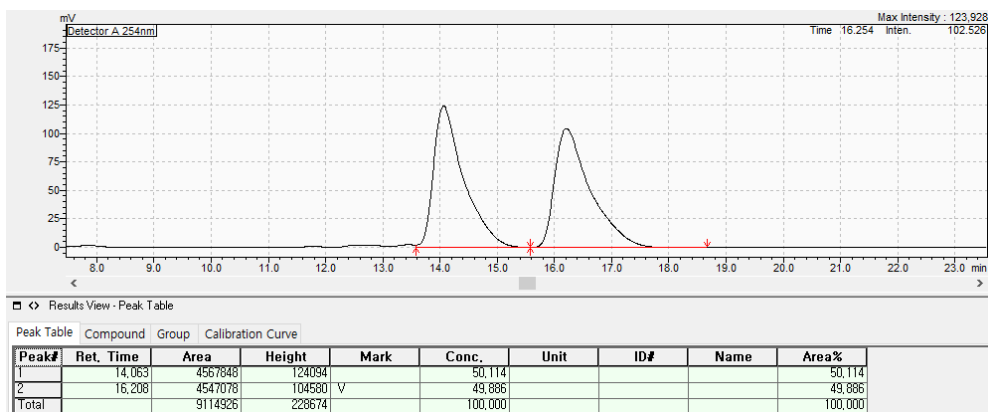
¹³C NMR (126 MHz, CDCl₃) δ 194.81, 140.25, 138.98, 136.60, 134.53, 129.64, 127.60, 125.93, 125.87, 123.04, 120.73, 111.83, 110.41, 48.70, 32.38, 21.13, 19.21 ppm.

HRMS (ESI) calculated for [C₁₉H₁₉NO+H]⁺: 278.1539, found: 278.1540.

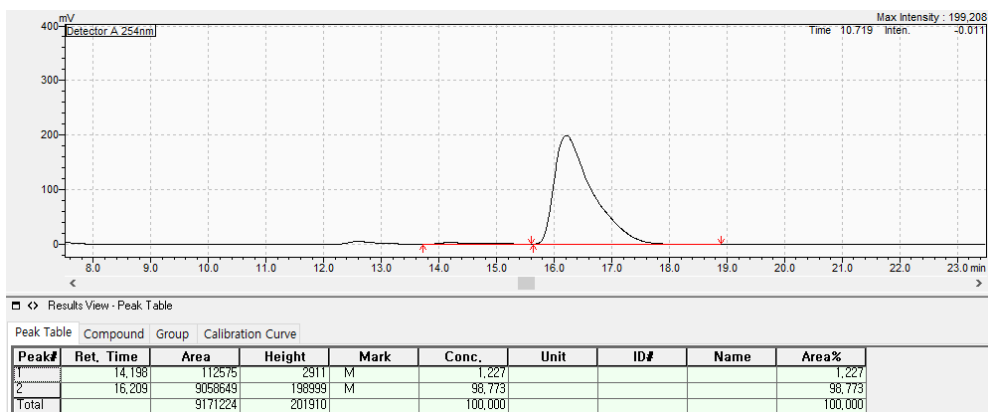
Optical rotation, [α]_D²² = +67.9 (c = 1.00, CH₂Cl₂).

Enantiomeric excess, 98% ee was measured by HPLC (CHIRALCEL OD, *n*-hexane : *i*-PrOH = 99 : 1, 1.0 mL/min, wavelength = 254nm, 28 °C); t_R = 16.209 min (major), t_R = 14.198 min (minor).

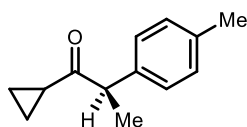
[Racemic 3nb]



[Enantioenriched 3nb]



(R)-1-cyclopropyl-2-(p-tolyl)propan-1-one (Table 5.2, 3ob)



3ob

Following *General Procedure L*, the crude product was purified by silica gel chromatography (gradient elution: full hexanes to 5% ether in hexanes) to provide **3ob** as a colorless liquid (33 mg, 25%, 70% ee, 71% es).

¹H NMR (400 MHz, CDCl₃) δ 7.19–7.08 (m, 4H), 3.87 (q, *J* = 6.9 Hz, 1H), 2.34 (s, 3H), 1.92–1.80 (m, 1H), 1.39 (d, *J* = 6.9 Hz, 3H), 1.02–0.92 (m, 2H), 0.82–0.65 (m, 2H).

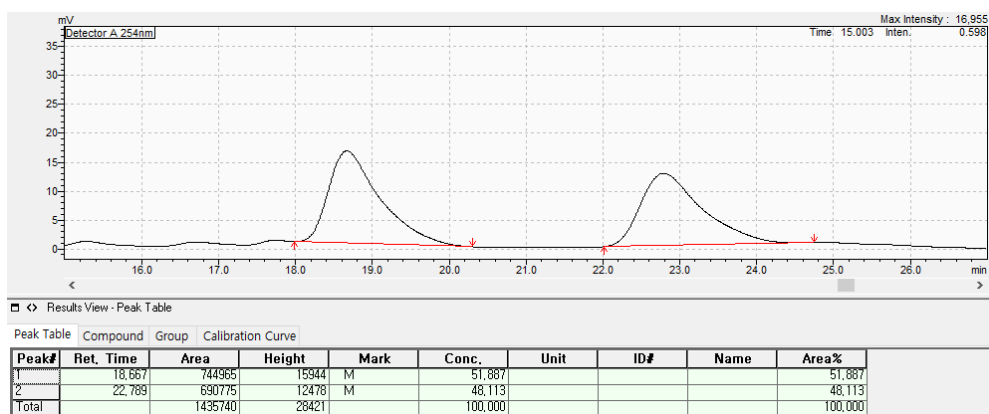
¹³C NMR (126 MHz, CDCl₃) δ 211.12, 138.06, 136.73, 129.68, 128.09, 53.47, 21.19, 19.76, 17.78, 11.42, 11.32 ppm.

HRMS (ESI) calculated for [C₁₃H₁₆O+H]⁺: 189.1274, found: 189.1270.

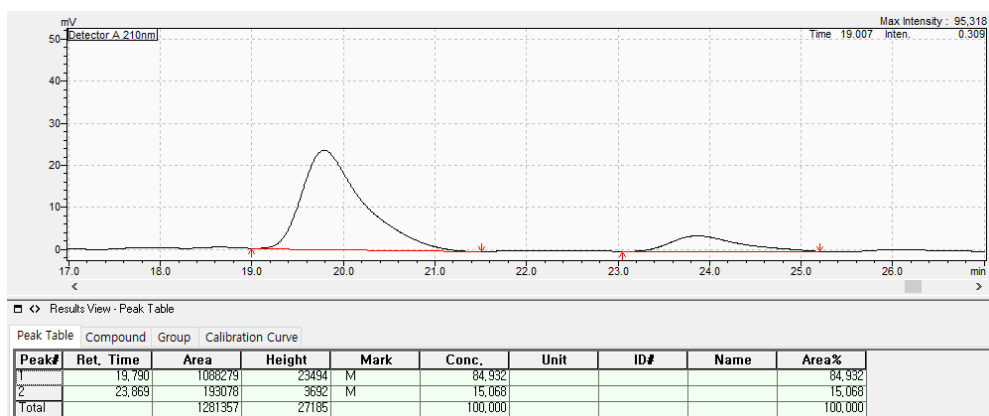
Optical rotation, [α]_D²² = +67.9 (c = 1.00, CH₂Cl₂).

Enantiomeric excess, 70% ee was measured by HPLC (CHIRALCEL OD, *n*-hexane : *i*-PrOH = 99 : 1, 1.0 mL/min, wavelength = 254 nm, 28 °C); t_R = 19.790 min (major), t_R = 23.869 min (minor).

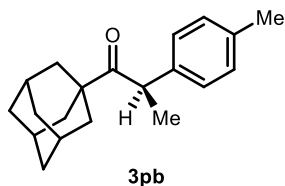
[Racemic 3ob]



[Enantioenriched 3ob]



(2R)-1-((1S,3S)-adamantan-1-yl)-2-(*p*-tolyl)propan-1-one (Table 5.2, 3pb)



Following *General Procedure L*, the crude product was purified by silica gel chromatography (gradient elution: full hexanes to 5% ether in hexanes) to provide **3pb** as a yellowish liquid (44 mg, 78%, 90% ee, 91% es).

¹H NMR (500 MHz, CDCl₃) δ 7.15 (d, *J* = 8.0 Hz, 2H), 7.22 (d, *J* = 7.9 Hz, 2H), 4.24 (q, *J* = 6.9 Hz, 1H), 2.31 (s, 3H), 2.03–1.94 (m, 3H), 1.79–1.73 (m, 6H), 1.73–1.67 (m, 3H), 1.67–1.60 (m, 3H), 1.32 (d, *J* = 6.9 Hz, 3H) ppm.

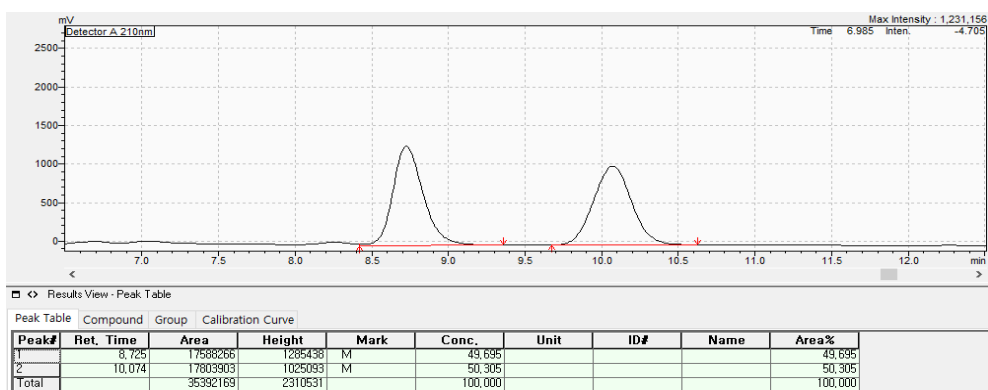
¹³C NMR (126 MHz, CDCl₃) δ 215.75, 138.42, 136.35, 129.41, 127.93, 47.48, 45.14, 38.33, 36.64, 28.01, 21.16, 21.00 ppm.

HRMS (ESI) calculated for [C₂₀H₂₆O+H]⁺: 283.2056, found: 283.2057.

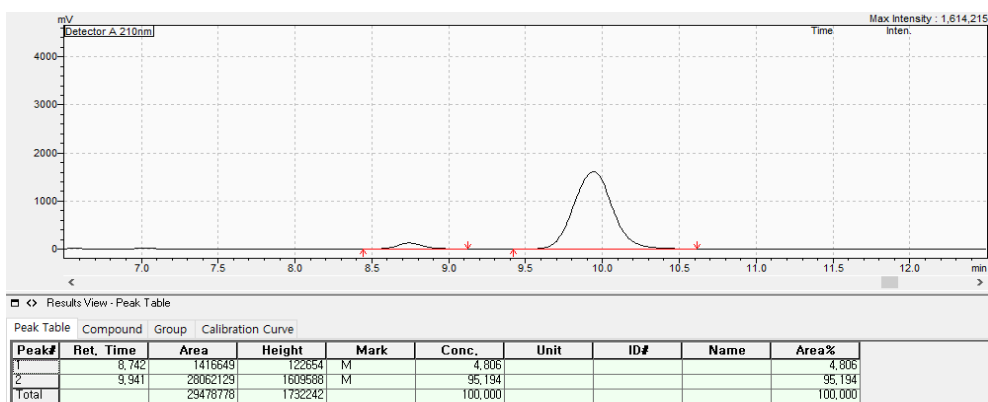
Optical rotation, [α]_D²² = –58.2 (c = 1.00, CH₂Cl₂).

Enantiomeric excess, 90% ee was measured by HPLC (CHIRALPAK IA, *n*-hexane : *i*-PrOH = 99 : 1, 0.5 mL/min, wavelength = 210 nm, 28 °C); t_R = 7.747 min (major), t_R = 7.309 min (minor).

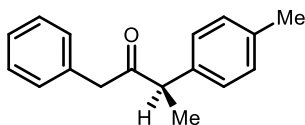
[Racemic 3pb]



[Enantioenriched 3pb]



(R)-1-phenyl-3-(p-tolyl)butan-2-one (Table 5.2, 3qb)



3qb

Following *General Procedure L*, the crude product was purified by silica gel chromatography (gradient elution: full hexanes to 5% ether in hexanes) to provide **3qb** as a colorless liquid (5 mg, 10%, 92% ee, 93% es).

¹H NMR (400 MHz, CDCl₃) δ 7.30–7.21 (m, 3H), 7.15 (d, *J* = 7.9 Hz, 2H), 7.11–7.03 (m, 4H), 3.81 (q, *J* = 6.9 Hz, 1H), 3.61 (s, 2H), 2.35 (s, 3H), 1.34 (d, *J* = 6.9 Hz, 3H) ppm.

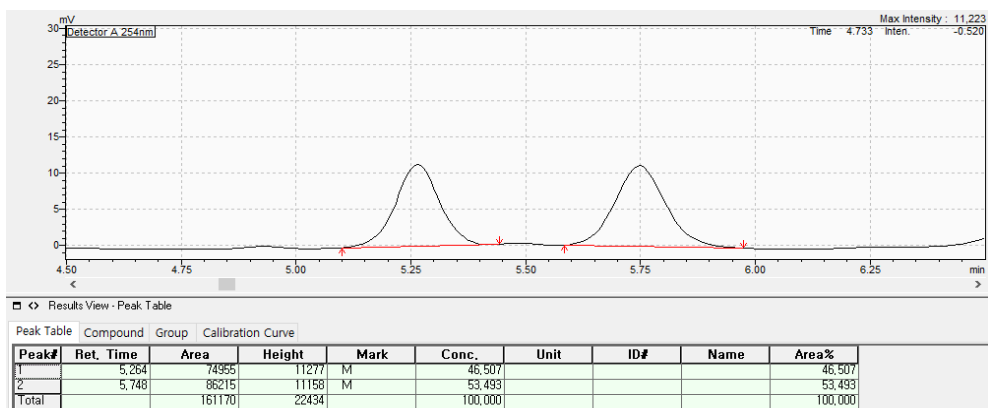
¹³C NMR (126 MHz, CDCl₃) δ 208.33, 137.51, 137.06, 134.58, 129.83, 129.59, 128.67, 128.07, 126.95, 51.79, 48.05, 21.21, 17.81 ppm.

HRMS (ESI) calculated for [C₁₇H₁₈O+H]⁺: 239.1430, found: 239.1434.

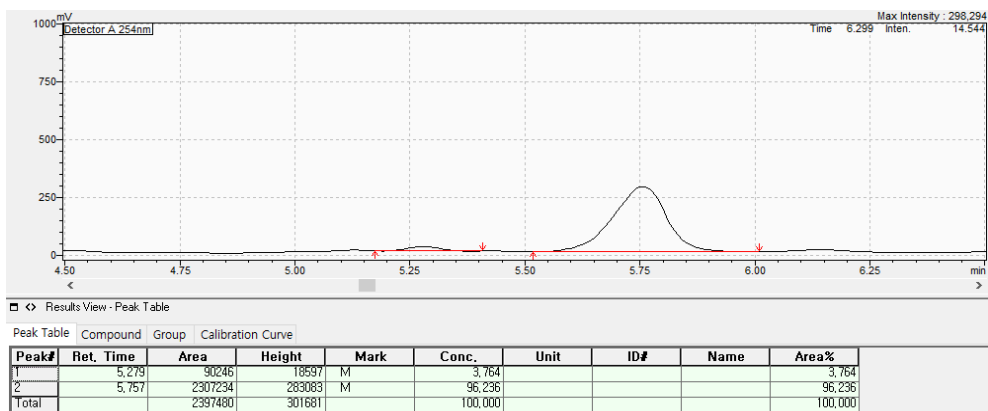
Optical rotation, [α]_D²² = -132.2 (c = 0.55, CH₂Cl₂).

Enantiomeric excess, 92% ee was measured by HPLC (CHIRALPAK IA, *n*-hexane : *i*-PrOH = 99 : 1, 1.0 mL/min, wavelength = 254 nm, 28 °C); t_R = 5.757 min (major), t_R = 5.279 min (minor).

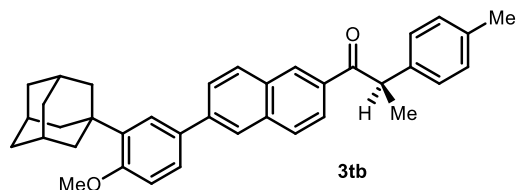
[Racemic 3qb]



[Enantioenriched 3qb]



(R)-1-(6-(3-((3R,5R,7R)-adamantan-1-yl)-4-methoxyphenyl)naphthalen-2-yl)-2-(p-tolyl)propan-1-one (Table 5.2, 3tb)



Following *General Procedure L*, the crude product was purified by silica gel chromatography (gradient elution: full hexanes to 5% ether in hexanes) to provide **3tb** as a white solid (74 mg, 72%, 96% ee, 97% es).

¹H NMR (500 MHz, CDCl₃) δ 8.50 (s, 1H), 8.04 (d, *J* = 8.4 Hz, 1H), 7.96 (s, 1H), 7.94 (d, *J* = 8.6 Hz, 1H), 7.86 (d, *J* = 8.6 Hz, 1H), 7.77 (d, *J* = 8.4 Hz, 1H), 7.60 (d, *J* = 1.3 Hz, 1H), 7.53 (d, *J* = 8.3 Hz, 1H), 7.27 (d, *J* = 7.8 Hz, 2H), 7.13 (d, *J* = 7.7 Hz, 2H), 6.99 (d, *J* = 8.4 Hz, 1H), 4.84 (q, *J* = 6.6 Hz, 1H), 3.90 (s, 3H), 2.29 (s, 3H), 2.23–2.17 (m, 6H), 2.16–2.09 (m, 3H), 1.86–1.78 (m, 6H), 1.60 (d, *J* = 6.7 Hz, 3H) ppm.

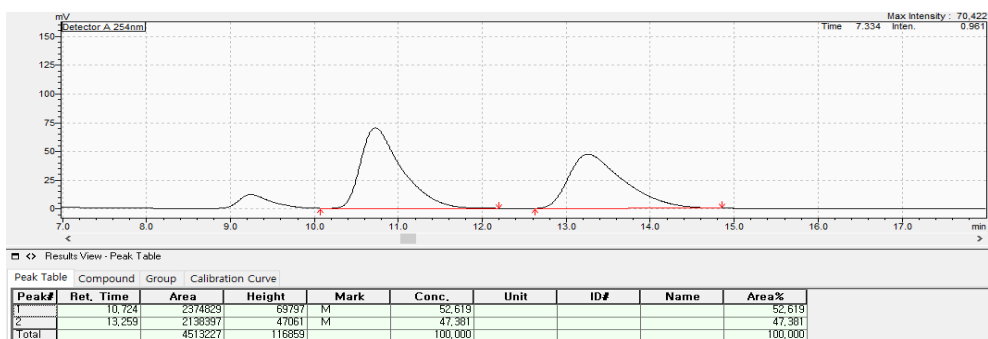
¹³C NMR (126 MHz, CDCl₃) δ 200.43, 159.04, 141.59, 139.10, 138.78, 136.60, 135.91, 133.55, 132.60, 131.30, 130.32, 130.09, 129.81, 128.45, 127.76, 126.50, 126.03, 125.83, 125.08, 124.72, 112.20, 55.26, 47.59, 40.71, 37.32, 37.24, 29.22, 21.13, 19.71 ppm.

HRMS (ESI) calculated for [C₃₇H₃₈O₂+H]⁺: 515.2945, found: 515.2944.

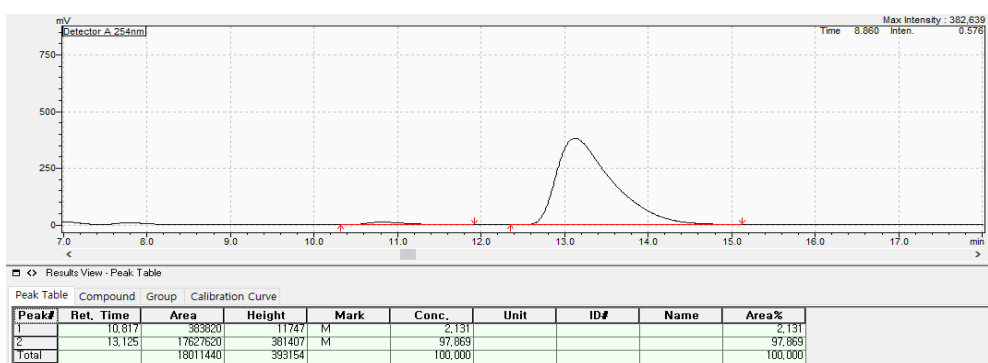
Optical rotation, [α]_D²² = +68.9 (c = 1.00, CH₂Cl₂).

Enantiomeric excess, 96% ee was measured by HPLC (CHIRALCEL OD, *n*-hexane : *i*-PrOH = 99 : 1, 1.0 mL/min, wavelength = 254 nm, 28 °C); t_R = 13.125 min (major), t_R = 10.817 min (minor).

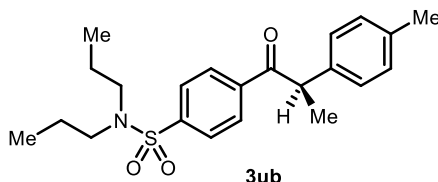
[Racemic 3tb]



[Enantioenriched 3tb]



(R)-N,N-diethyl-4-(2-(*p*-tolyl)propanoyl)benzenesulfonamide (Table 5.2, 3ub)



Following *General Procedure L*, the crude product was purified by silica gel chromatography (gradient elution: full hexanes to 5% ether in hexanes) to provide **3ub** as a colorless liquid (33 mg, 45%, 96% ee, 97% es).

¹H NMR (400 MHz, CDCl₃) δ 8.01 (d, *J* = 8.4 Hz, 2H), 7.78 (d, *J* = 8.4 Hz, 2H), 7.16–7.08 (m, 4H), 4.60 (q, *J* = 6.8 Hz, 1H), 3.09–2.99 (m, 4H), 2.29 (s, 3H), 1.58–1.46 (m, 7H), 0.84 (t, *J* = 7.4 Hz, 6H) ppm.

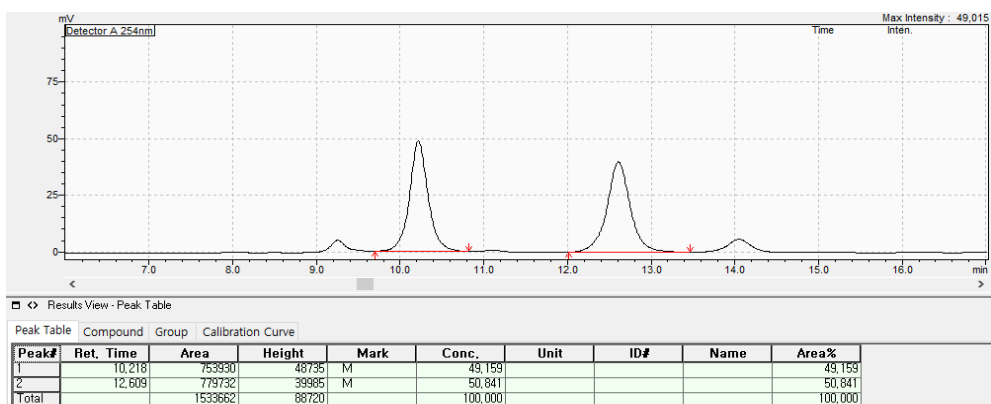
¹³C NMR (126 MHz, CDCl₃) δ 199.54, 143.80, 139.47, 137.77, 137.07, 130.03, 129.41, 127.74, 127.24, 50.13, 48.32, 22.15, 21.16, 19.51, 11.27 ppm.

HRMS (ESI) calculated for [C₂₂H₂₉NO₃S+H]⁺: 388.1941, found: 388.1941.

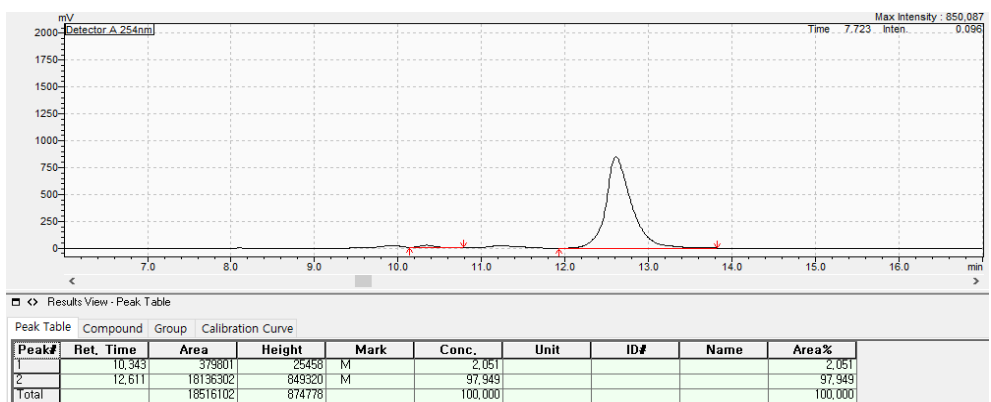
Optical rotation, [α]_D²² = -50.6 (c = 0.9, CH₂Cl₂).

Enantiomeric excess, 96% ee was measured by HPLC (CHIRALPAK IA, *n*-hexane : *i*-PrOH = 97 : 3, 1.0 mL/min, wavelength = 254 nm, 28 °C); t_R = 12.611 min (major), t_R = 10.343 min (minor).

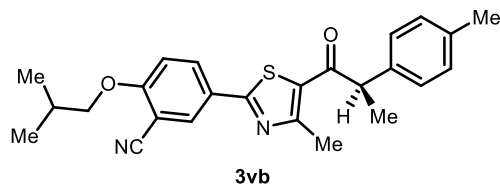
[Racemic 3ub]



[Enantioenriched 3ub]



(R)-2-isobutoxy-5-(4-methyl-5-(2-(*p*-tolyl)propanoyl)thiazol-2-yl)benzonitrile (Table 5.2, 3vb)



Following *General Procedure L*, the crude product was purified by silica gel chromatography (gradient elution: full hexanes to 25% ether in hexanes) to provide **3vb** as a colorless liquid (52 mg, 63%, 94% ee, 95% es).

¹H NMR (500 MHz, CDCl₃) δ 8.11–8.02 (m, 2H), 7.20 (d, *J* = 8.0 Hz, 2H), 7.14 (d, *J* = 8.0 Hz, 2H), 6.98 (d, *J* = 8.8 Hz, 1H), 4.21 (q, *J* = 6.7 Hz, 1H), 3.88 (d, *J* = 6.5 Hz, 2H), 2.75 (s, 3H), 2.31 (s, 3H), 2.26–2.12 (m, 1H), 1.51 (d, *J* = 6.8 Hz, 3H), 1.08 (d, *J* = 6.7 Hz, 6H) ppm.

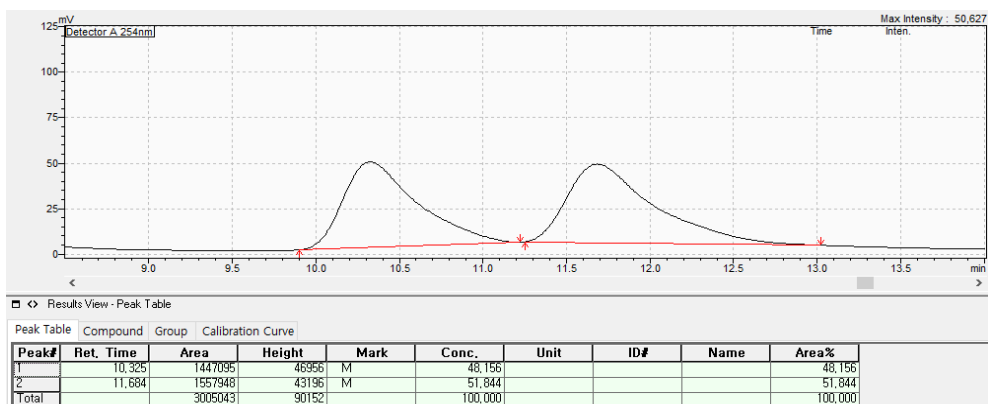
¹³C NMR (126 MHz, CDCl₃) δ 193.44, 166.40, 162.62, 161.52, 137.58, 137.28, 132.73, 132.30, 129.89, 129.16, 127.97, 125.95, 115.53, 112.68, 102.98, 75.79, 52.98, 28.27, 21.21, 19.48, 19.17, 18.67 ppm.

HRMS (ESI) calculated for [C₂₅H₂₆N₂O₂S+H]⁺: 419.1788, found: 419.1782.

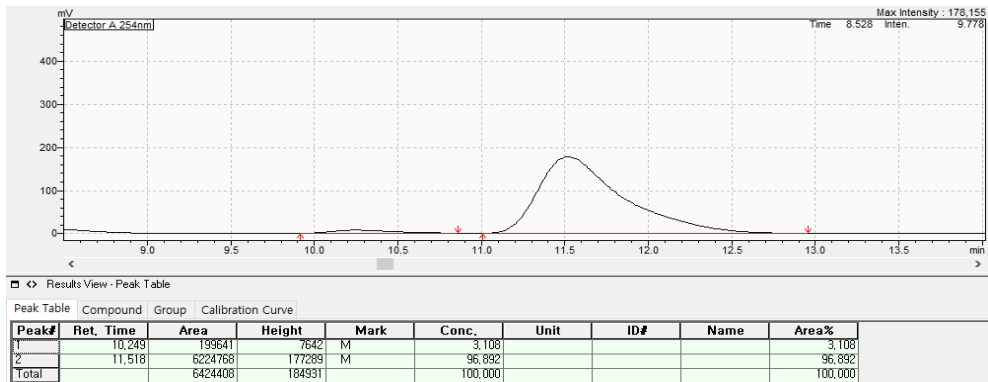
Optical rotation, [α]_D²² = +165.9 (c = 1.00, CH₂Cl₂).

Enantiomeric excess, 94% ee was measured by HPLC (CHIRALCEL OD, *n*-hexane : *i*-PrOH = 95 : 5, 1.0 mL/min, wavelength = 254 nm, 28 °C); t_R = 11.518 min (major), t_R = 10.249 min (minor).

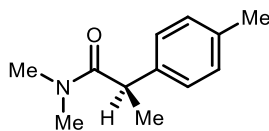
[Racemic 3vb]



[Enantioenriched 3vb]



(R)-N,N-dimethyl-2-(p-tolyl)propanamide (Table 5.3, 4a)



4a

Following *General Procedure L*, the crude product was purified by silica gel chromatography (gradient elution: full hexanes to 30% ethyl acetate in hexanes) to provide **4a** as a yellowish liquid (36 mg, 93%, 94% ee, 95% es). The spectral data are matched with literature data.²¹

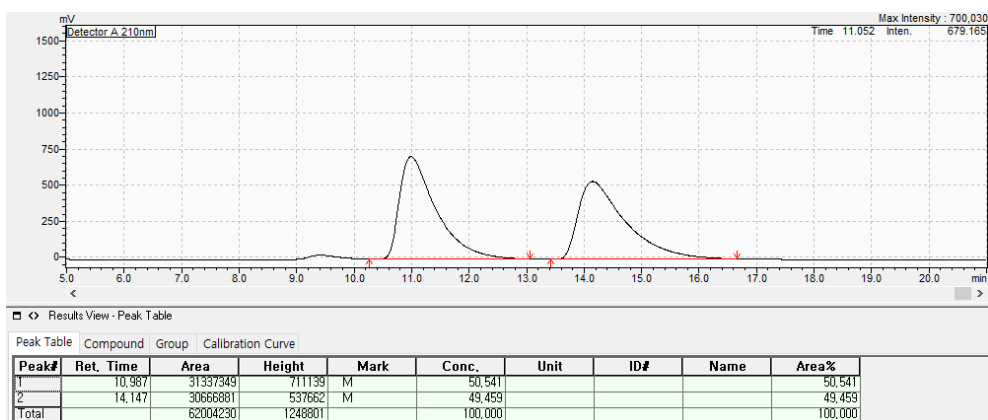
¹H NMR (500 MHz, CDCl₃) δ 7.15 (d, *J* = 7.9 Hz, 2H), 7.11 (d, *J* = 7.9 Hz, 2H), 3.84 (q, *J* = 6.9 Hz, 1H), 2.94 (s, 3H), 2.88 (s, 3H), 2.31 (s, 3H), 1.42 (d, *J* = 6.8 Hz, 3H) ppm.

¹³C NMR (126 MHz, CDCl₃) δ 173.95, 139.03, 136.40, 129.61, 127.31, 42.95, 37.26, 36.02, 21.13, 20.91 ppm.

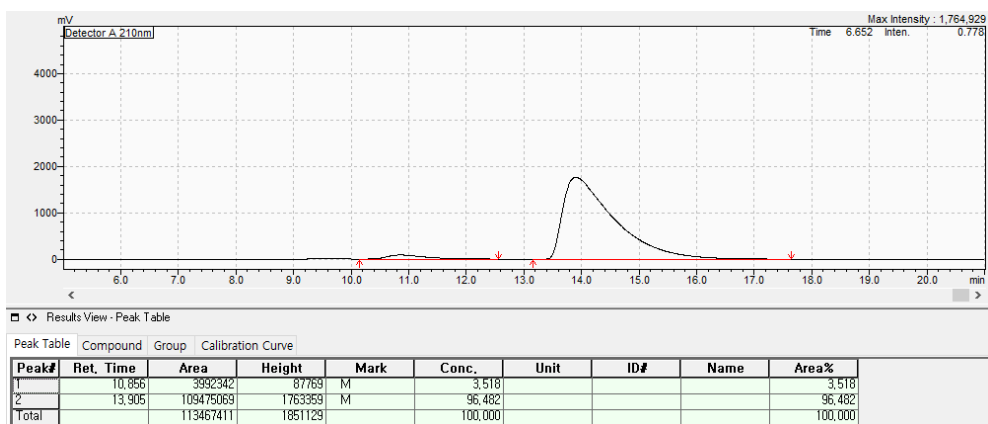
Optical rotation, $[\alpha]_D^{22} = -24.3$ (*c* = 0.25, CH₂Cl₂).

Enantiomeric excess, 94% ee was measured by HPLC (CHIRALCEL OJ-H, *n*-hexane : *i*-PrOH = 97 : 3, 1.0 mL/min, wavelength = 210 nm, 28 °C); *t*_R = 13.905 min (major), *t*_R = 10.856 min (minor).

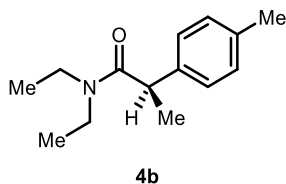
[Racemic 4a]



[Enantioenriched 4a]



(R)-N,N-diethyl-2-(p-tolyl)propanamide (Table 5.3, 4b)



Following *General Procedure L*, the crude product was purified by silica gel chromatography (gradient elution: full hexanes to 20% ethyl acetate in hexanes) to provide **4b** as a yellowish liquid (42 mg, 96%, 98% ee, 99% es).

¹H NMR (500 MHz, CDCl₃) δ 7.18 (d, *J* = 8.0 Hz, 2H), 7.12 (d, *J* = 7.9 Hz, 2H), 3.81 (q, *J* = 6.8 Hz, 1H), 3.52 (dq, *J* = 14.0, 7.1 Hz, 1H), 3.35 (dq, *J* = 14.3, 7.1 Hz, 1H), 3.27–3.17 (m, 1H), 3.12 (dq, *J* = 14.4, 7.1 Hz, 1H), 2.33 (s, 3H), 1.43 (d, *J* = 6.9 Hz, 3H), 1.10 (t, *J* = 7.1 Hz, 3H), 1.01 (t, *J* = 7.1 Hz, 3H) ppm.

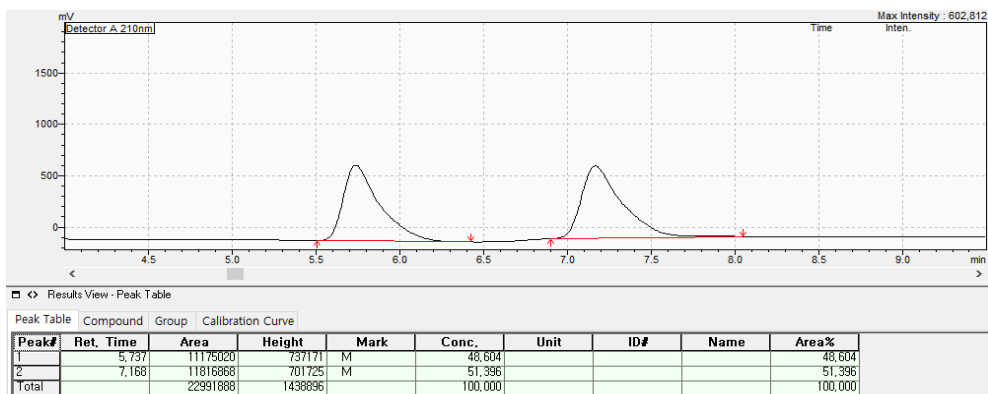
¹³C NMR (126 MHz, CDCl₃) δ 173.02, 139.62, 136.27, 129.53, 127.24, 42.82, 41.71, 40.36, 21.11, 21.09, 14.34, 12.93 ppm.

HRMS (ESI) calculated for [C₁₄H₂₁NO+H]⁺: 220.1696, found: 220.1692.

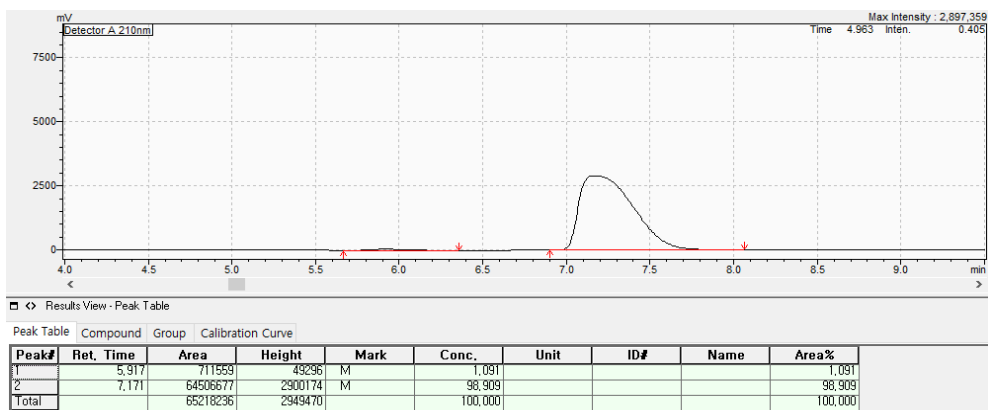
Optical rotation, [α]_D²² = -54.5 (c = 1.00, CH₂Cl₂).

Enantiomeric excess, 98% ee was measured by HPLC (CHIRALCEL OD-H, *n*-hexane : *i*-PrOH = 97 : 3, 1.0 mL/min, wavelength = 210 nm, 28 °C); t_R = 7.171 min (major), t_R = 5.917 min (minor).

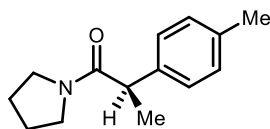
[Racemic **4b**]



[Enantioenriched **4b**]



(R)-1-(pyrrolidin-1-yl)-2-(*p*-tolyl)propan-1-one (Table 5.3, 4c)



4c

Following *General Procedure L*, the crude product was purified by silica gel chromatography (gradient elution: full hexanes to 30% ethyl acetate in hexanes) to provide **4c** as a yellowish liquid (42 mg, 96%, 93% ee, 94% es). The spectral data are matched with literature data.²²

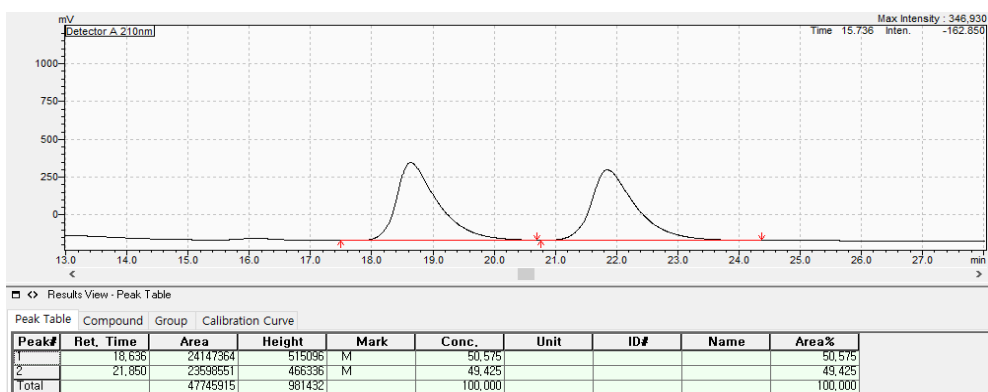
¹H NMR (500 MHz, CDCl₃) δ 7.18 (d, *J* = 8.0 Hz, 2H), 7.10 (d, *J* = 7.9 Hz, 2H), 7.22 (d, *J* = 7.9 Hz, 2H), 3.69 (q, *J* = 6.9 Hz, 1H), 3.57–3.48 (m, 1H), 3.47–3.36 (m, 2H), 3.20–3.11 (m, 2H), 2.31 (s, 3H), 1.93–1.82 (m, 1H), 1.81–1.69 (m, 3H), 1.42 (d, *J* = 6.8 Hz, 3H) ppm.

¹³C NMR (126 MHz, CDCl₃) δ 172.46, 138.85, 136.35, 129.49, 127.51, 46.31, 46.10, 44.67, 26.16, 24.25, 21.12, 20.45 ppm.

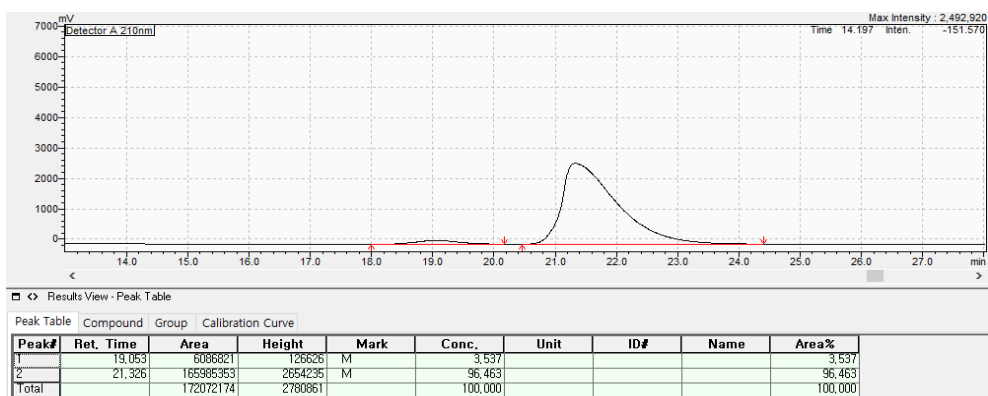
Optical rotation, $[\alpha]_D^{22} = -58.3$ (*c* = 1.00, CH₂Cl₂).

Enantiomeric excess, 93% ee was measured by HPLC (CHIRALPAK IA, *n*-hexane : *i*-PrOH = 97.5 : 2.5, 0.5 mL/min, wavelength = 210 nm, 28 °C); *t*_R = 21.326 min (major), *t*_R = 19.053 min (minor).

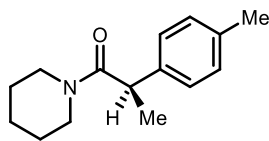
[Racemic 4c]



[Enantioenriched 4c]



(R)-1-(piperidin-1-yl)-2-(p-tolyl)propan-1-one (Table 5.3, 4d)



4d

Following *General Procedure L*, the crude product was purified by silica gel chromatography (gradient elution: full hexanes to 30% ethyl acetate in hexanes) to provide **4d** as a yellowish liquid (41 mg, 90%, 94% ee, 95% es). The spectral data are matched with literature data and the value of optical rotation is consistent with (*R*)-form based on literature.²³

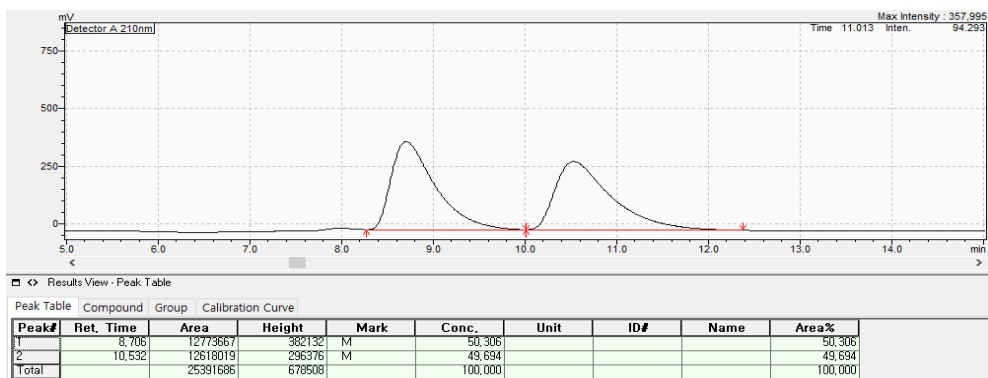
¹H NMR (500 MHz, CDCl₃) δ 7.18–7.05 (m, 4H), 3.84 (q, *J* = 6.8 Hz, 1H), 3.78–3.58 (m, 1H), 3.54–3.15 (m, 3H), 2.31 (s, 3H), 1.60–1.46 (m, 3H), 1.41 (d, *J* = 6.8 Hz, 3H), 1.46–1.25 (m, 3H) ppm.

¹³C NMR (126 MHz, CDCl₃) δ 172.06, 139.55, 136.26, 129.60, 127.25, 42.89, 31.09, 25.89, 24.68, 21.18, 21.01 ppm.

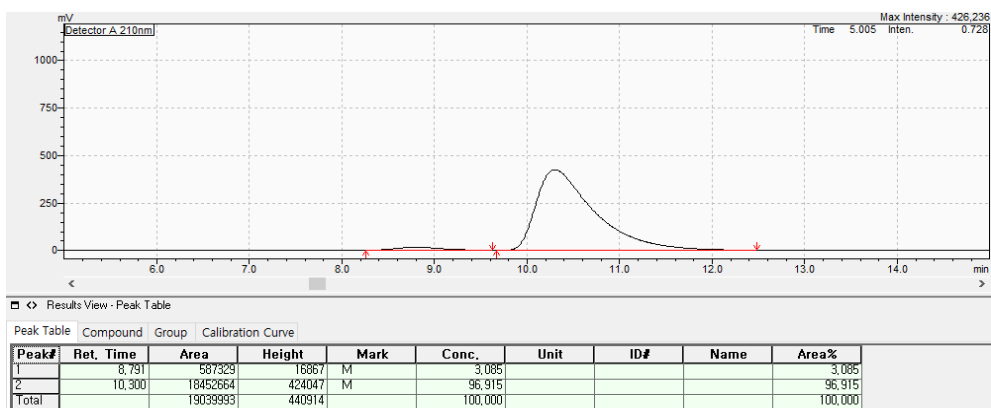
Optical rotation, $[\alpha]_D^{22} = -45.8$ (*c* = 0.25, CH₂Cl₂).

Enantiomeric excess, 94% ee was measured by HPLC (CHIRALCEL OJ-H, *n*-hexane : *i*-PrOH = 98 : 2, 1.0 mL/min, wavelength = 210 nm, 28 °C); *t*_R = 10.974 min (major), *t*_R = 8.989 min (minor).

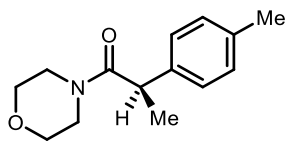
[Racemic 4d]



[Enantioenriched 4d]



(R)-1-morpholino-2-(*p*-tolyl)propan-1-one (Table 5.3, 4e)



4e

Following *General Procedure L*, the crude product was purified by silica gel chromatography (gradient elution: full hexanes to 30% ethyl acetate in hexanes) to provide **4e** as a yellowish liquid (44 mg, 95%, 95% ee, 96% es). The spectral data are matched with literature data.²⁴

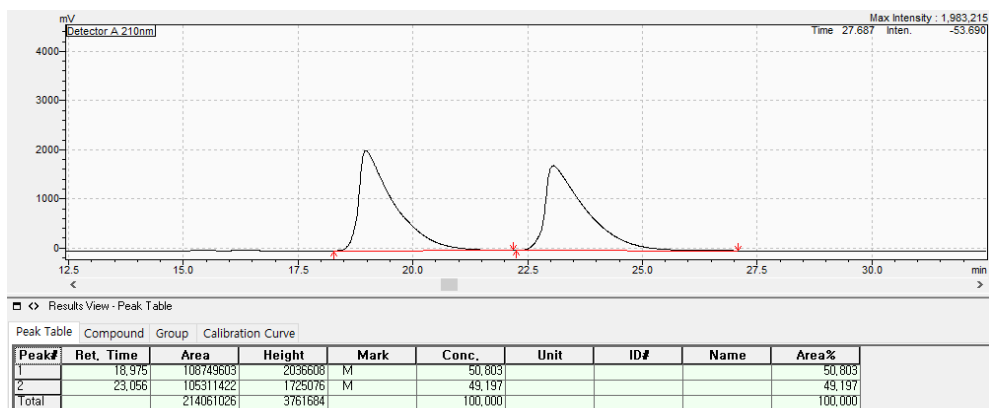
¹H NMR (500 MHz, CDCl₃) δ 7.16–7.08 (m, 4H), 3.84–3.71 (m, 2H), 3.69–3.59 (m, 1H), 3.57–3.42 (m, 3H), 3.42–3.33 (m, 1H), 3.33–3.24 (m, 1H), 3.17–3.06 (m, 1H), 2.31 (s, 3H), 1.42 (d, *J* = 7.0 Hz, 3H) ppm.

¹³C NMR (126 MHz, CDCl₃) δ 172.45, 138.89, 136.57, 129.76, 127.10, 66.88, 66.42, 46.08, 42.90, 42.44, 21.12, 20.78 ppm.

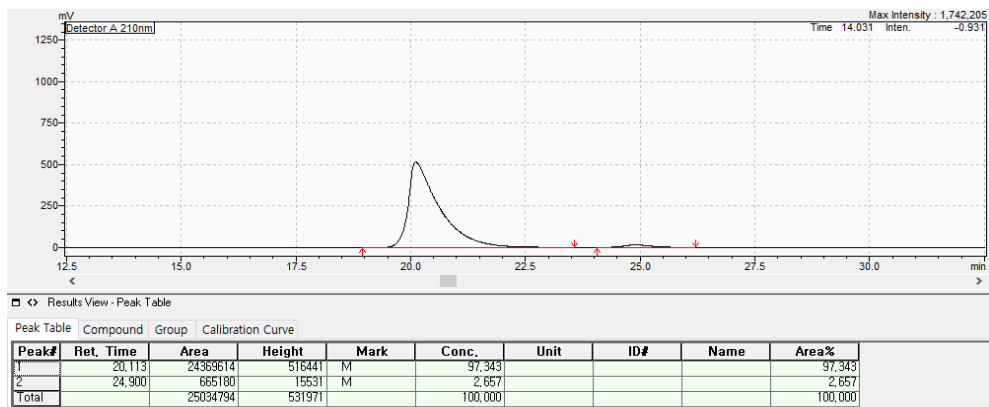
Optical rotation, $[\alpha]_{\text{D}}^{22} = -115.4$ (*c* = 1.00, CH₂Cl₂).

Enantiomeric excess, 95% ee was measured by HPLC (CHIRALPAK IA, *n*-hexane : *i*-PrOH = 99 : 1, 1.0 mL/min, wavelength = 210 nm, 28 °C); *t*_R = 20.113 min (major), *t*_R = 24.900 min (minor).

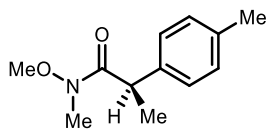
[Racemic 4e]



[Enantioenriched 4e]



(R)-2-(*p*-tolyl)heptan-3-one (Table 5.3, 4f)



4f

Following *General Procedure L* using PAd₃ (7.5 mol%) as the supporting ligand, the crude product was purified by silica gel chromatography (gradient elution: full hexanes to 30% ether in hexanes) to provide **4f** as a white solid (21 mg, 50%, 97% ee, 98% es).

¹H NMR (400 MHz, CDCl₃) δ 7.20 (d, *J* = 7.9 Hz, 2H), 7.11 (d, *J* = 7.8 Hz, 2H), 4.22–3.94 (m, 1H), 3.43 (s, 3H), 3.15 (s, 3H), 2.31 (s, 3H), 1.42 (d, *J* = 7.0 Hz, 3H) ppm.

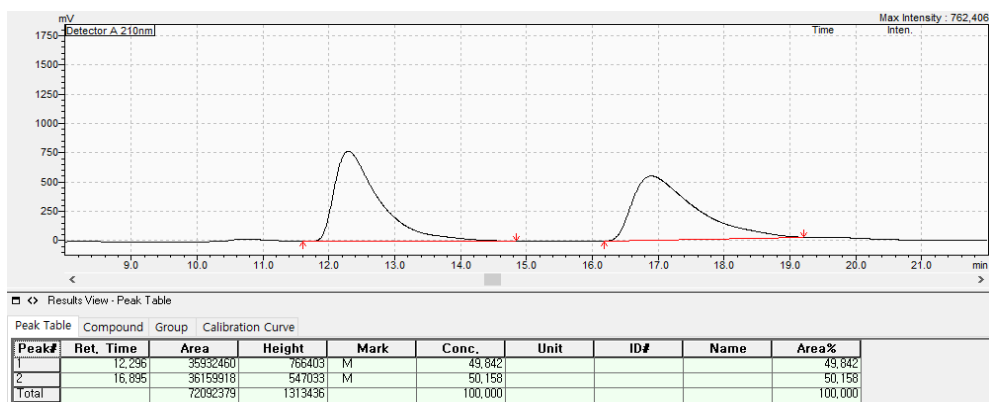
¹³C NMR (126 MHz, CDCl₃) δ 175.55, 138.96, 136.36, 129.34, 127.53, 61.21, 41.61, 32.43, 21.12, 19.73 ppm.

HRMS (ESI) calculated for [C₁₂H₁₇NO₂+H]⁺: 208.1332, found: 208.1328.

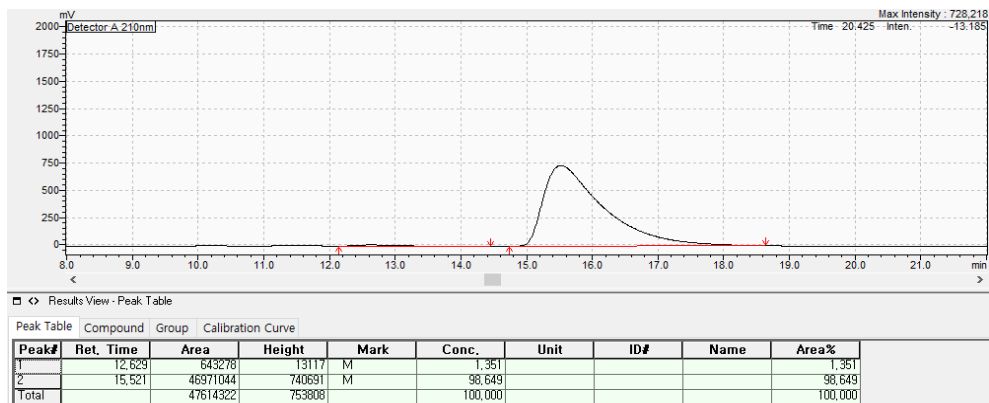
Optical rotation, [α]_D²² = −41.6 (c = 1.00, CH₂Cl₂).

Enantiomeric excess, 97% ee was measured by HPLC (CHIRALCEL OJ-H, *n*-hexane : *i*-PrOH = 97 : 3, 1.0 mL/min, wavelength = 210 nm, 28 °C); t_R = 15.521 min (major), t_R = 12.629 min (minor).

[Racemic 4f]

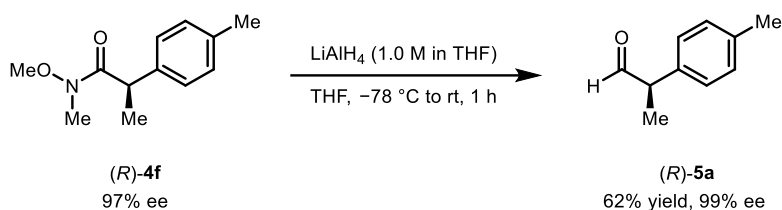


[Enantioenriched 4f]



5.5.7. Synthetic Applications

5.5.7.1. Hydride addition to access aldehyde



(R)-2-(*p*-tolyl)propanal (Table 5.3, 5a)

The solution of chiral Weinreb amide **(R)-4f** (0.2 mmol) in anhydrous THF (1 mL) was added to a flame-dried 25 mL round-bottom flask equipped with a magnetic stir bar under a nitrogen atmosphere. The flask was cooled to $-78\text{ }^{\circ}\text{C}$ for 10 min. Lithium aluminum hydride solution (0.1 mmol, 0.5 equiv, 1.0 M in THF) was slowly added to the mixture via a syringe, and the mixture was allowed to stir for 1 h at room temperature. The reaction mixture was quenched with aqueous saturated NH₄Cl solution (1 mL) at $-78\text{ }^{\circ}\text{C}$, and the flask was allowed to slowly warm to room temperature. The resulting mixture was separated into two phases. The aqueous layer was extracted with Et₂O (3 x 5 mL), and the combined organic layer was dried over anhydrous Na₂SO₄, filtered, and concentrated under reduced pressure using rotary evaporation (vacuum set: >400 mbar, the title compound is slightly volatile). The obtained crude product was purified by flash column chromatography on silica gel (gradient elution: 100/0 to 90/10 of hexanes/Et₂O) to afford the desired product **(R)-5a** as colorless liquid (18 mg, 62% yield, 99% ee). The spectral data are matched with literature data.²⁵

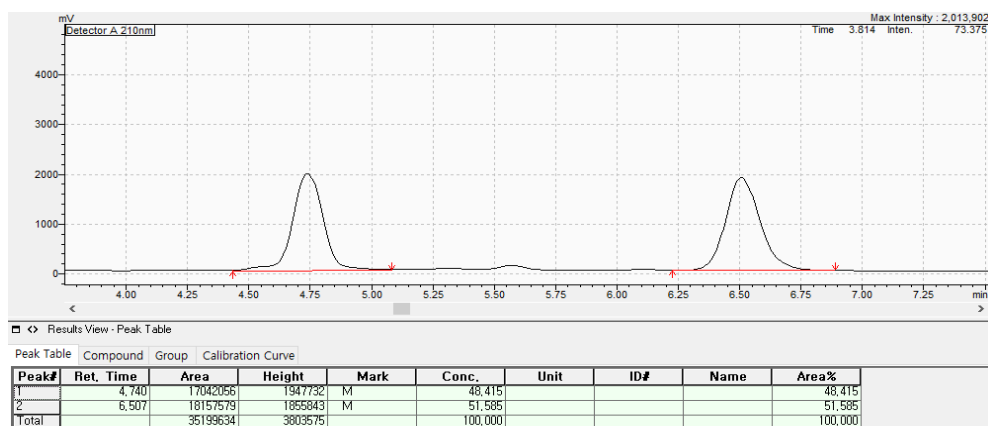
^1H NMR (400 MHz, CDCl_3) δ 9.67 (d, $J = 1.4$ Hz, 1H), 7.19 (d, $J = 7.8$ Hz, 2H), 7.10 (d, $J = 8.0$ Hz, 2H), 3.60 (q, $J = 7.0$ Hz, 1H), 2.35 (s, 3H), 1.43 (d, $J = 7.1$ Hz, 3H) ppm.

^{13}C NMR (126 MHz, CDCl_3) δ 201.39, 137.41, 134.77, 129.92, 128.35, 52.77, 21.19, 14.76 ppm.

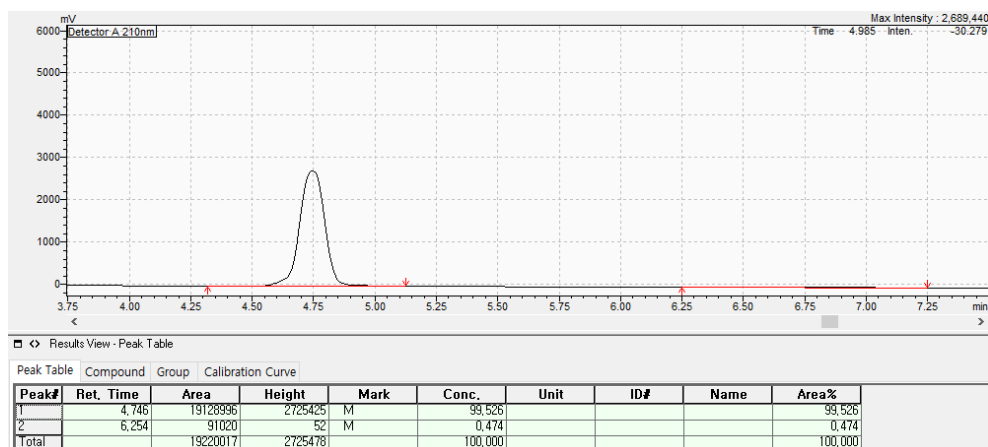
Optical rotation, $[\alpha]_D^{22} = -18.4$ ($c = 0.25$, CH_2Cl_2).

Enantiomeric excess, 99% ee was measured by HPLC (CHIRALPAK IA, *n*-hexane : *i*-PrOH = 99 : 1, 1.0 mL/min, wavelength = 210 nm, 28 °C); $t_R = 4.746$ min (major), $t_R = 6.254$ min (minor).

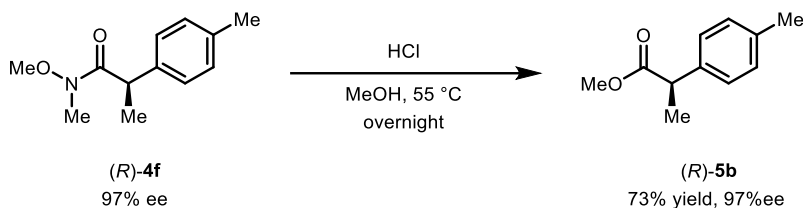
[Racemic **5a**]



[Enantioenriched **5a**]



5.5.7.2. Fisher esterification to access chiral ester



Methyl (*R*)-2-(*p*-tolyl)propanoate (Table 5.3, 5b)

The solution of chiral Weinreb amide (*R*)-**4f** (0.2 mmol) in MeOH (2 mL) was added to a flame-dried 25 mL round-bottom flask equipped with a magnetic stir bar under a nitrogen atmosphere. The flask was cooled to 0 °C for 10 min. Two drops of hydrochloric acid (36.5~38% w/w, aqueous solution) was added to the mixture via 1 mL of syringe, and the mixture was allowed to stir overnight at 55 °C. The reaction mixture was quenched with aqueous saturated NaCl solution (2 mL) and the resulting mixture was separated into two phases. The aqueous layer was extracted with EtOAc (3 x 5 mL), and the combined organic layer was dried over anhydrous Na₂SO₄, filtered, and concentrated under reduced pressure. The obtained crude product was purified by flash column chromatography on silica gel (gradient elution: 100/0 to 90/10 of hexanes/EtOAc) to afford the desired product (*R*)-**5c** as colorless liquid (36 mg, 73% yield, 97% ee).

¹H NMR (400 MHz, CDCl₃) δ 7.20 (d, *J* = 7.9 Hz, 2H), 7.11 (d, *J* = 7.8 Hz, 2H), 4.21–3.99 (m, 1H), 3.43 (s, 3H), 3.15 (s, 3H), 2.31 (s, 3H), 1.42 (d, *J* = 7.0 Hz, 3H) ppm.

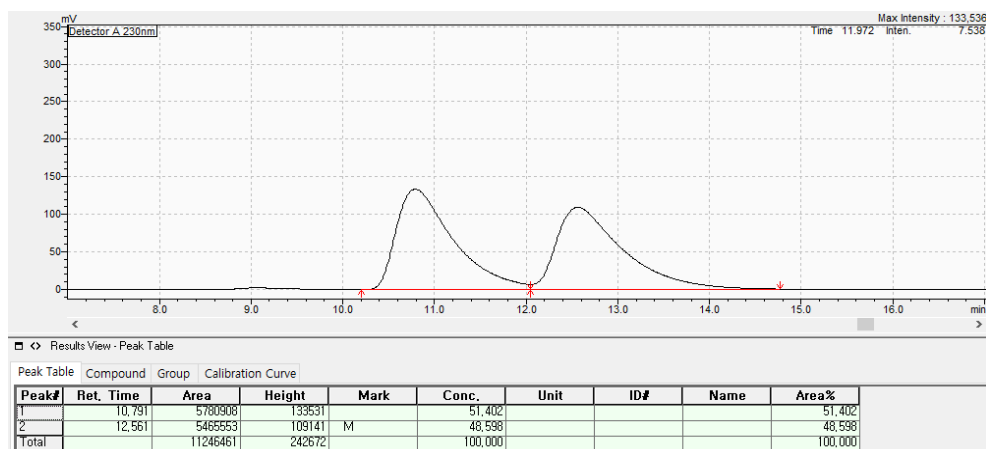
¹³C NMR (126 MHz, CDCl₃) δ 175.32, 137.74, 136.92, 129.47, 127.46, 52.13, 45.14, 21.18, 18.77 ppm.

HRMS (ESI) calculated for $[C_{11}H_{14}O_2+H]^+$: 179.1067, found: 179.1067.

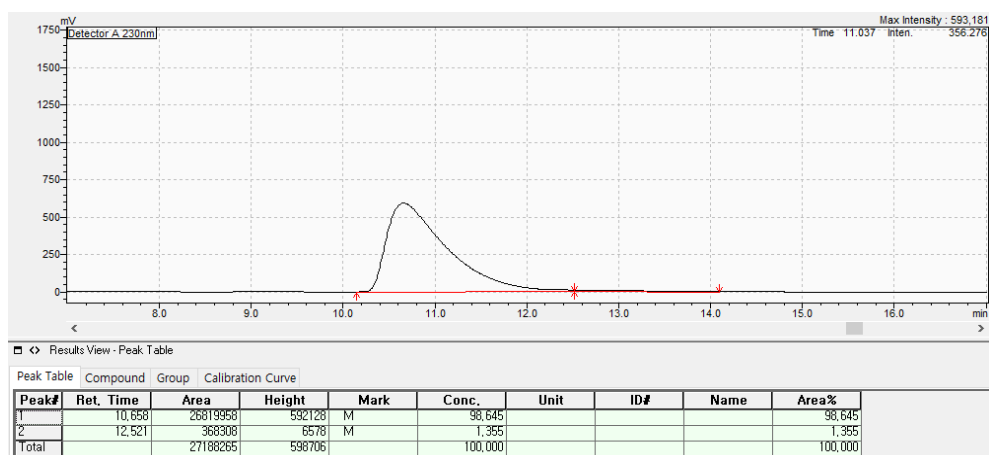
Optical rotation, $[\alpha]_D^{22} = -60.3$ ($c = 0.58$, CH_2Cl_2).

Enantiomeric excess, 97% ee was measured by HPLC (CHIRALCEL OJ-H, *n*-hexane : *i*-PrOH = 98 : 2, 1.0 mL/min, wavelength = 230 nm, 28 °C); $t_R = 10.658$ min (major), $t_R = 12.521$ min (minor).

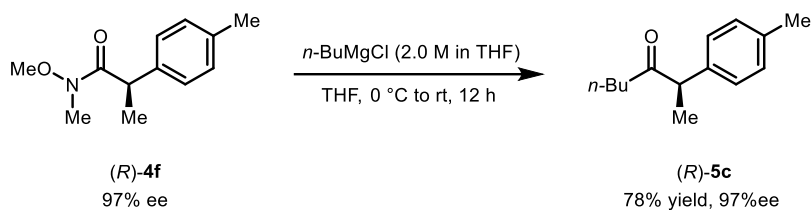
[Racemic **5b**]



[Enantioenriched **5b**]



5.5.7.3. Nucleophilic substitution to access chiral C(sp³)-containing ketone



(R)-2-(*p*-tolyl)heptan-3-one (Table 5.3, 5c)

The solution of chiral Weinreb amide (*R*)-**4f** (0.2 mmol) in anhydrous THF (1 mL) was added to a flame-dried 25 mL round-bottom flask equipped with a magnetic stir bar under a nitrogen atmosphere. The flask was cooled to 0 °C for 10 min. *n*-Butylmagnesium chloride solution (0.6 mmol, 3.0 equiv, 2.0 M in THF) was slowly added to the mixture via a syringe, and the mixture was stirred for 12 h at room temperature. The reaction mixture was quenched with aqueous saturated NH₄Cl solution (1 mL) and the resulting mixture was separated into two phases. The aqueous layer was extracted with EtOAc (3 x 5 mL), and the combined organic layer was dried over anhydrous Na₂SO₄, filtered, and concentrated under reduced pressure. The obtained crude product was purified by flash column chromatography on silica gel (gradient elution: 100/0 to 95/5 of hexanes/EtOAc) to afford the desired product (*R*)-**5c** as a colorless liquid (32 mg, 78% yield, 97% ee).

¹H NMR (500 MHz, CDCl₃) δ 7.13 (d, *J* = 7.9 Hz, 2H), 7.09 (d, *J* = 8.0 Hz, 2H), 3.71 (q, *J* = 6.9 Hz, 1H), 2.33 (s, 3H), 2.40–2.28 (m, 2H), 1.54–1.40 (m, 2H), 1.36 (d, *J* = 7.0 Hz, 3H), 1.24–1.12 (m, 2H), 0.81 (t, *J* = 7.3 Hz, 3H) ppm.

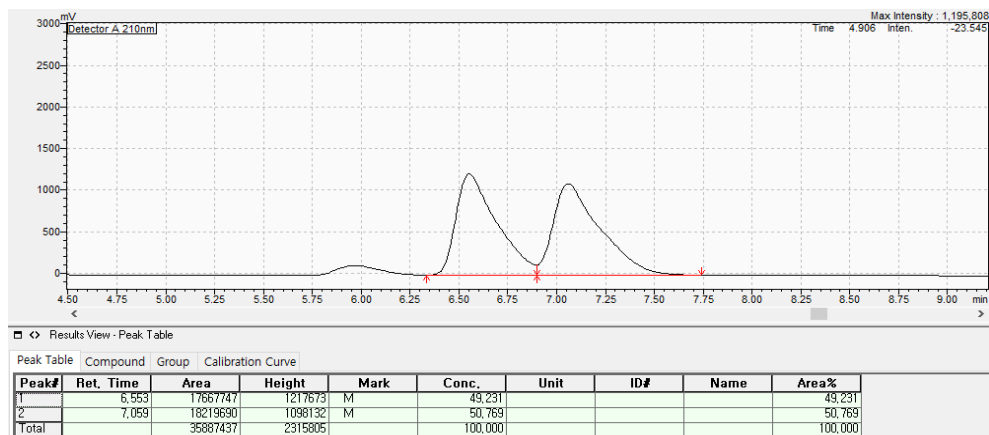
^{13}C NMR (126 MHz, CDCl_3) δ 211.23, 137.77, 136.66, 129.53, 127.71, 52.51, 40.68, 25.99, 22.20, 21.02, 17.50, 13.80 ppm.

HRMS (ESI) calculated for $[\text{C}_{14}\text{H}_{20}\text{O}+\text{H}]^+$: 205.1587, found: 205.1586.

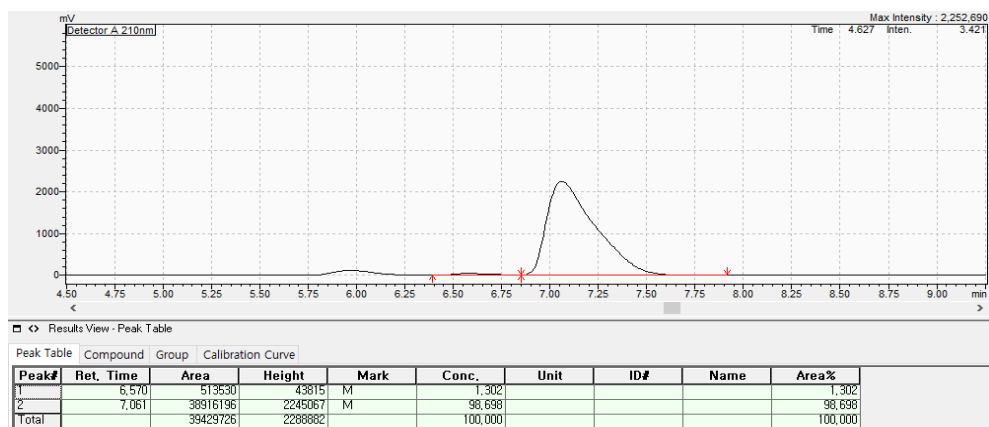
Optical rotation, $[\alpha]_D^{22} = -145.6$ ($c = 1.00$, CH_2Cl_2).

Enantiomeric excess, 97% ee was measured by HPLC (CHIRALCEL OD, n -hexane : i -PrOH = 99.4 : 0.6, 0.7 mL/min, wavelength = 210 nm, 28 °C); $t_{\text{R}} = 7.061$ min (major), $t_{\text{R}} = 6.570$ min (minor).

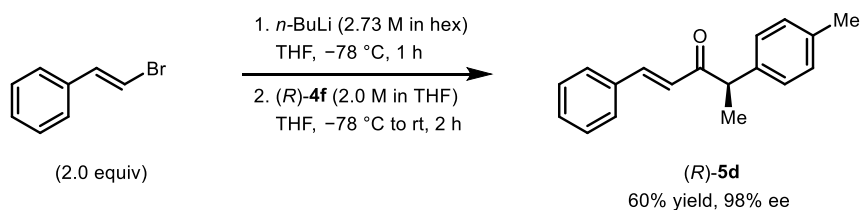
[Racemic 5c]



[Enantioenriched 5c]



5.5.7.4. Nucleophilic substitution to access chiral C(sp²)-containing ketone



(*R,E*)-1-phenyl-4-(*p*-tolyl)pent-1-en-3-one (Table 5.3, **5d**)

β-Bromostyrene (0.4 mmol, 2.0 equiv) and anhydrous THF (1 mL) was added to a flame-dried 25 mL round-bottom flask equipped with a magnetic stir bar under a nitrogen atmosphere. The flask was cooled to -78 °C for 10 min. *n*-Butyllithium solution (2.73 M in hexanes, 0.4 mmol, 2.0 equiv) was slowly added to the mixture via a syringe, and the mixture was allowed to stir for 1 h at -78 °C. After 1 h, the solution of chiral Weinreb amide (*R*)-**4f** (0.2 mmol) in THF (1 mL) was added dropwise to the flask. Upon completion of the addition, the reaction mixture was stirred for 2 hours at -78 °C. The reaction mixture was quenched with aqueous saturated NH₄Cl solution (1 mL) at -78 °C, and the flask was allowed to slowly warm to room temperature. The resulting mixture was separated into two phases. The aqueous layer was extracted with EtOAc (3 x 5 mL), and the combined organic layer was dried over anhydrous Na₂SO₄, filtered, and concentrated under reduced pressure. The obtained crude product was purified by flash column chromatography on silica gel (gradient elution: 100/0 to 90/10 of hexanes/EtOAc) to afford the desired product (*R*)-**5d** as a colorless liquid (27 mg, 60% yield, 98% ee). The spectral data are matched with literature data.²⁶

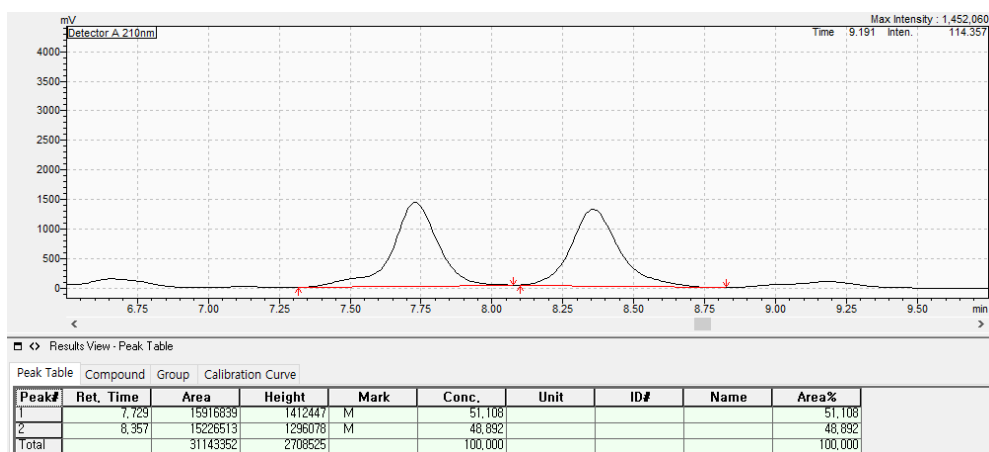
¹H NMR (500 MHz, CDCl₃) δ 7.61 (d, *J* = 15.8 Hz, 1H), 7.48–7.44 (m, 2H), 7.37–7.31 (m, 3H), 7.20–7.11 (m, 4H), 6.71 (d, *J* = 15.8 Hz, 1H), 3.99 (q, *J* = 6.9 Hz, 1H), 2.33 (s, 3H), 1.47 (d, *J* = 6.9 Hz, 3H) ppm

¹³C NMR (126 MHz, CDCl₃) δ 199.71, 142.56, 137.72, 136.91, 134.72, 130.43, 129.84, 128.82, 128.46, 128.07, 124.72, 51.70, 21.19, 17.99 ppm.

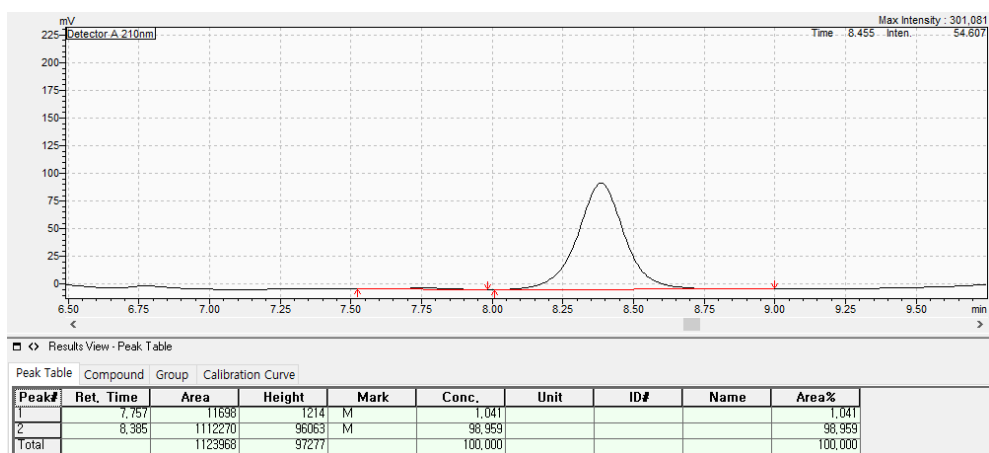
Optical rotation, $[\alpha]_D^{22} = -104.4$ (*c* = 1.00, CH₂Cl₂).

Enantiomeric excess, 98% ee was measured by HPLC (CHIRALPAK IA, *n*-hexane : *i*-PrOH = 98 : 2, 1.0 mL/min, wavelength = 210 nm, 28 °C); *t*_R = 8.385 min (major), *t*_R = 7.757 min (minor).

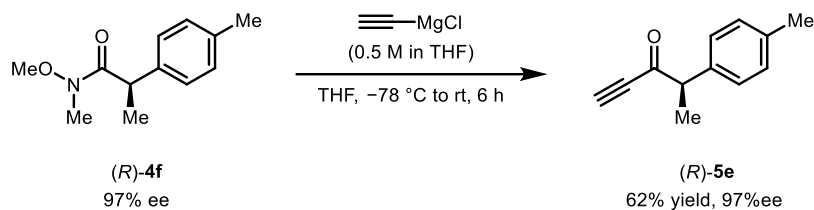
[Racemic 5d]



[Enantioenriched 5d]



5.5.7.5. Nucleophilic substitution to access chiral C(sp)-containing ketone



(*R,E*)-1-phenyl-4-(*p*-tolyl)pent-1-en-3-one (Table 5.3, 5e)

The solution of chiral Weinreb amide (*R*)-**4f** (0.2 mmol) in anhydrous THF (1 mL) was added to a flame-dried 25 mL round-bottom flask equipped with a magnetic stir bar under a nitrogen atmosphere. The flask was cooled to $-78\text{ }^{\circ}\text{C}$ for 10 min. Ethynylmagnesium bromide solution (0.4 mmol, 2.0 equiv, 0.5 M in THF) was slowly added to the mixture via a syringe, and the mixture was stirred for 6 h at room temperature. The reaction mixture was quenched with aqueous saturated NH_4Cl solution (1 mL) and the resulting mixture was separated into two phases. The aqueous layer was extracted with EtOAc (3 x 5 mL), and the combined organic layer was dried over anhydrous Na_2SO_4 , filtered, and concentrated under reduced pressure. The obtained crude product was purified by flash column chromatography on silica gel (gradient elution: 100/0 to 95/5 of hexanes/EtOAc) to afford the desired product (*R*)-**5c** as a colorless liquid (21 mg, 62% yield, 97% ee).

^1H NMR (400 MHz, CDCl_3) δ 7.21–7.10 (m, 4H), 3.84 (q, $J = 7.0$ Hz, 1H), 3.14 (s, 1H), 2.34 (s, 3H), 1.49 (d, $J = 7.0$ Hz, 3H).

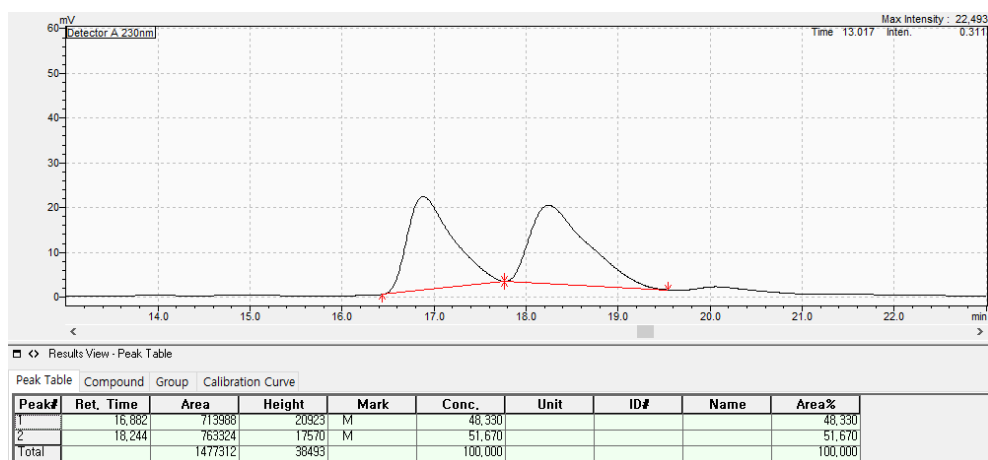
^{13}C NMR (126 MHz, CDCl_3) δ 187.73, 137.52, 135.55, 129.74, 128.25, 80.93, 80.20, 54.40, 21.25, 16.66 ppm.

HRMS (ESI) calculated for $[C_{12}H_{12}O+H]^+$: 173.0961, found: 173.0960.

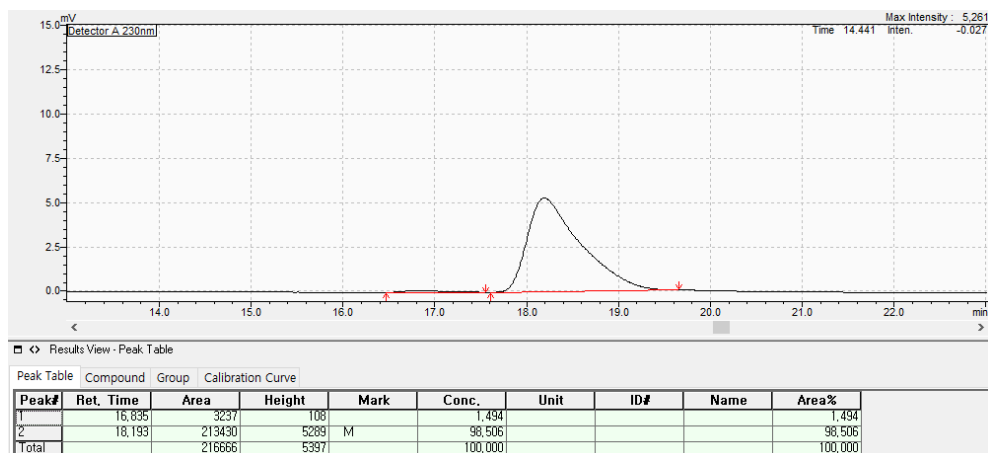
Optical rotation, $[\alpha]_D^{22} = -43.1$ ($c = 0.58$, CH_2Cl_2)

Enantiomeric excess, 97% ee was measured by HPLC (CHIRALCEL OD, *n*-hexane : *i*-PrOH = 99.6 : 0.4, 0.5 mL/min, wavelength = 230 nm, 28 °C); $t_R = 18.193$ min (major), $t_R = 16.835$ min (minor).

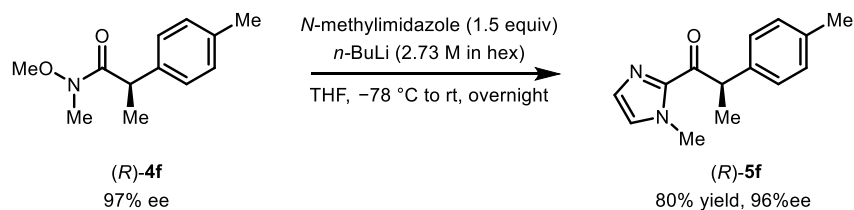
[Racemic 5e]



[Enantioenriched 5e]



5.5.7.6. Nucleophilic substitution to access heterocycle-containing ketone



(R)-1-(1-methyl-1H-imidazol-2-yl)-2-(p-tolyl)propan-1-one (Table 5.3, 5f)

N-methylimidazole (0.4 mmol, 2.0 equiv) and anhydrous THF (1 mL) was added to a flame-dried 25 mL round-bottom flask equipped with a magnetic stir bar under a nitrogen atmosphere. The flask was cooled to $-78\text{ }^\circ\text{C}$ for 10 min. *n*-Butyllithium solution (2.73 M in hexanes, 0.4 mmol, 2.0 equiv) was slowly added to the mixture via a syringe, and the mixture was allowed to stir for 1 h at $-78\text{ }^\circ\text{C}$. After 1 h, the solution of chiral Weinreb amide (*R*)-**4f** (0.2 mmol) in THF (1 mL) was added dropwise to the flask. Upon completion of the addition, the reaction mixture was warmed to room temperature and stirred overnight. The reaction mixture was quenched with aqueous saturated NH_4Cl solution (1 mL) at $-78\text{ }^\circ\text{C}$, and the flask was allowed to slowly warm to room temperature. The resulting mixture was separated into two phases. The aqueous layer was extracted with EtOAc (3 x 5 mL), and the combined organic layer was dried over anhydrous Na_2SO_4 , filtered, and concentrated under reduced pressure. The obtained crude product was purified by flash column chromatography on silica gel (gradient elution: 100/0 to 90/10 of hexanes/EtOAc) to afford the desired product (*R*)-**5f** as colorless liquid (33 mg, 80% yield, 96% ee).

^1H NMR (500 MHz, CDCl_3) δ 7.33 (d, $J = 8.0$ Hz, 2H), 7.13 (s, 1H), 7.10 (d, $J = 7.9$ Hz, 2H), 6.97 (s, 1H), 5.25 (q, $J = 7.0$ Hz, 1H), 3.93 (s, 1H), 2.29 (s, 1H), 1.53 (d, $J = 7.2$ Hz, 3H) ppm.

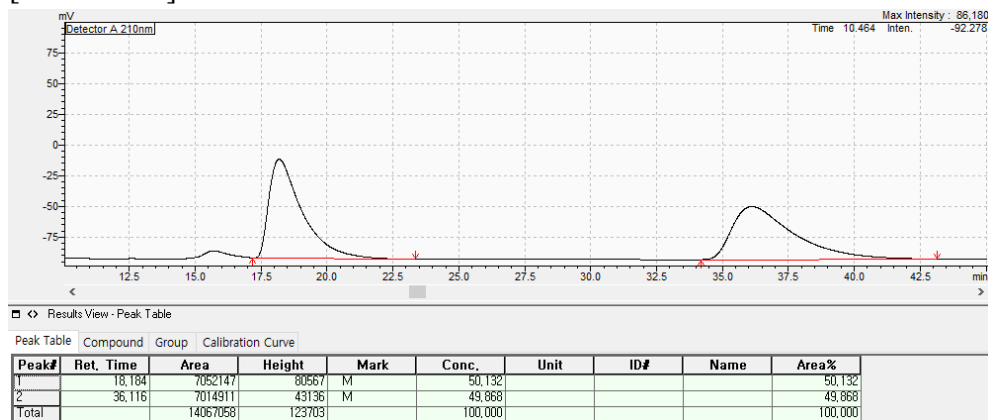
^{13}C NMR (126 MHz, CDCl_3) δ 193.46, 142.74, 137.93, 136.49, 129.33, 129.15, 128.27, 127.30, 46.43, 36.24, 21.09, 18.14 ppm.

HRMS (ESI) calculated for $[\text{C}_{14}\text{H}_{16}\text{N}_2\text{O}+\text{H}]^+$: 229.1335, found: 229.1332.

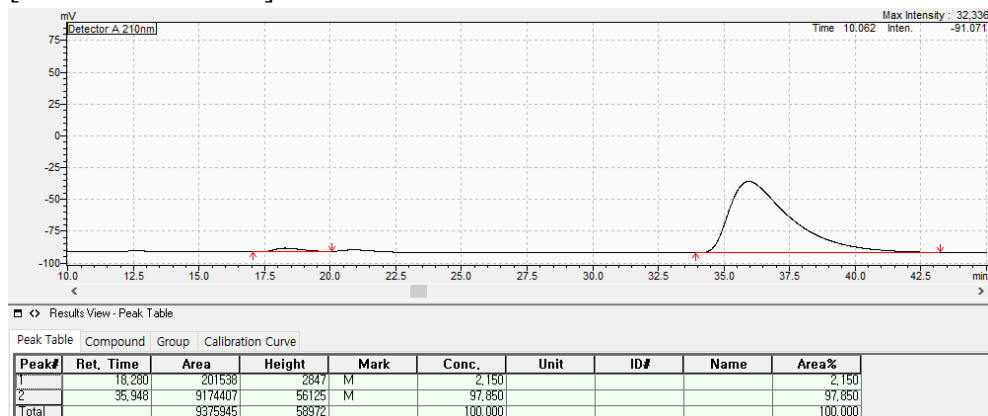
Optical rotation, $[\alpha]_{\text{D}}^{22} = -59.8$ ($c = 1.00$, CH_2Cl_2).

Enantiomeric excess, 96% ee was measured by HPLC (CHIRALCEL OJ-H, n -hexane : i -PrOH = 95 : 5, 1.0 mL/min, wavelength = 210 nm, 28 °C); $t_{\text{R}} = 35.948$ min (major), $t_{\text{R}} = 18.260$ min (minor).

[Racemic **5f**]

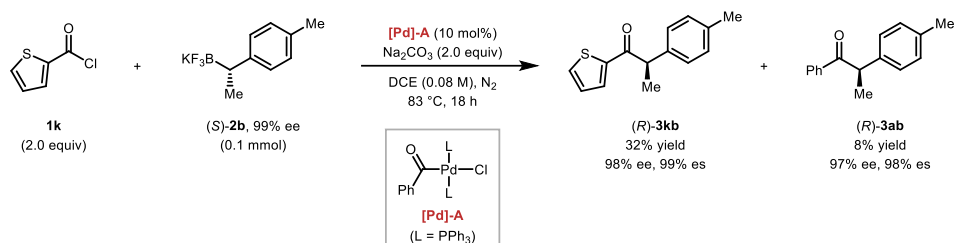


[Enantioenriched **5f**]



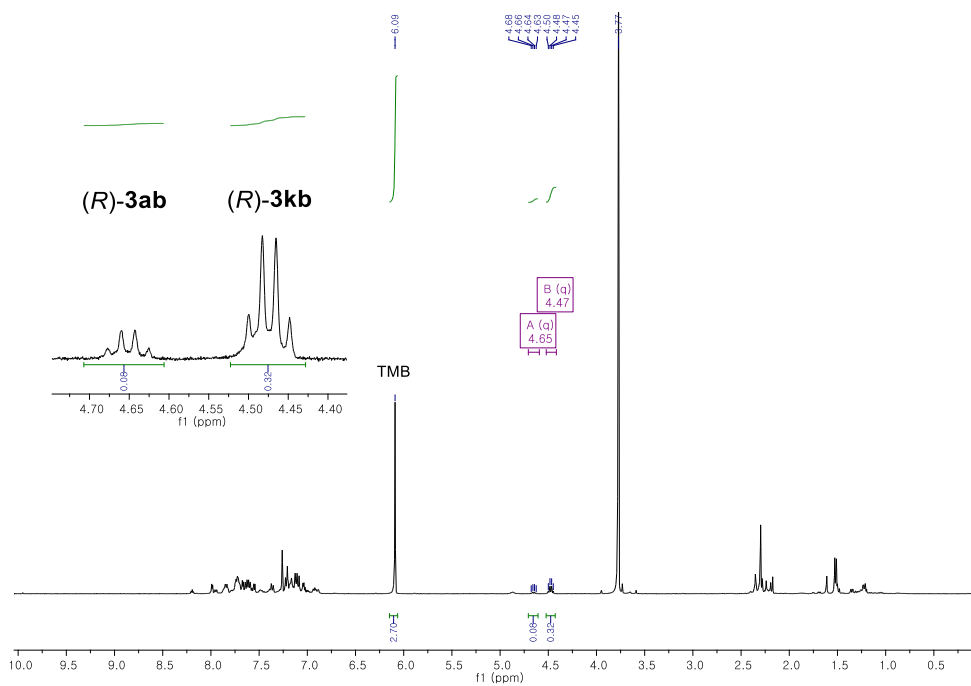
5.5.8. Mechanistic Investigations

5.5.8.1. Control experiment with [Pd]-A as the Pd source (Figure 5.3A).



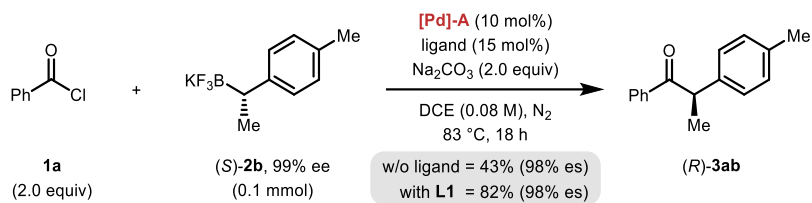
The pre-formed oxidative addition complex, [Pd]-A, as shown above was prepared according to literature procedure of Prof. Dr. Szostak.²⁷

In a nitrogen-filled glovebox, an oven-dried 4 mL dram-vial (or screw capped reaction tube) was charged with a magnetic stir bar, [Pd]-A (0.01 mmol, 10 mol%, 7.7 mg), (S)-**2b** (0.1 mmol) and Na₂CO₃ (0.2 mmol, 2.0 equiv, 22 mg). Subsequently, 1.2 mL of dichloroethane (DCE) and thiophene-2-carbonyl chloride **1k** (0.2 mmol, 2.0 equiv, 22 μL) was added to the mixture via a syringe, in that order. The reaction mixture was sealed with screw cap. The vial was removed from the glovebox and the reaction mixture was stirred in a pre-heated oil bath (83 °C) for 18 hours. The crude mixture was then diluted with ethyl acetate and filtered with celite. The combined organic layer was concentrated under reduced pressure. The yields were determined by ¹H NMR analysis with 1,3,5-trimethoxybenzene (0.09 mmol, 15.1 mg) as an internal standard and then, the crude product was purified via preparatory TLC with *n*-hexane/EtOAc = 95 : 5 for HPLC analysis.



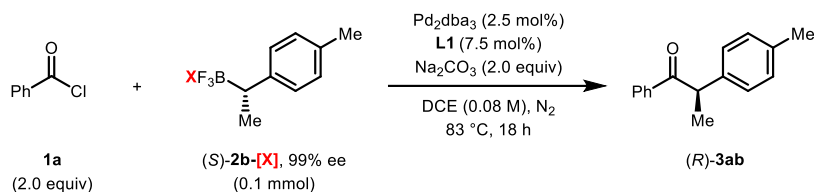
Scheme S5.1. ^1H NMR analysis of crude mixture for control experiment with **[Pd]-A** as catalyst.

5.5.8.2. Ligand exchange with L1 facilitating reaction (Figure 5.3B).



In a nitrogen-filled glovebox, an oven-dried 4 mL dram-vial (or screw capped reaction tube) was charged with a magnetic stir bar, **[Pd]-A** (0.01 mmol, 10 mol%, 7.7 mg), **L1** (0.015 mmol, 15 mol%, 7.6 mg), (*S*)-**2b** (0.1 mmol) and Na_2CO_3 (0.2 mmol, 2.0 equiv, 22 mg). Subsequently, 1.2 mL of dichloroethane (DCE) and benzoyl chloride **1a** (0.2 mmol, 2.0 equiv, 23 μL) was added to the mixture via a syringe, in that order. The reaction mixture was sealed with screw cap. The vial was removed from the glovebox and the reaction mixture was stirred in a pre-heated oil bath (83 °C) for 18 hours. The crude mixture was then diluted with ethyl acetate and filtered with celite. The combined organic layer was concentrated under reduced pressure. The yields were determined by ^1H NMR analysis with 1,3,5-trimethoxybenzene as an internal standard and then, the crude products were purified via preparatory TLC with *n*-hexane/EtOAc = 95 : 5 for HPLC analysis.

5.5.8.3. Effect of counter cations (Figure 5.3C).



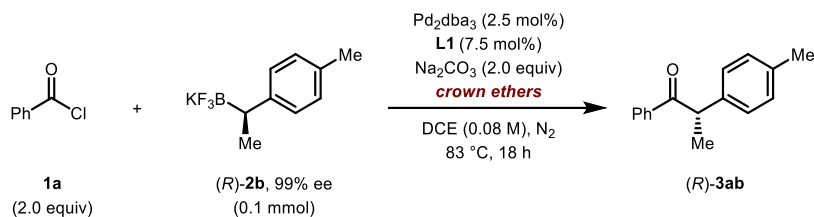
In a nitrogen-filled glovebox, an oven-dried 4 mL dram-vial (or screw capped reaction tube) was charged with a magnetic stir bar, Pd_2dba_3 (0.0025 mmol, 2.5 mol% which is 5.0 mol% based on Pd, 2.3 mg), **L1** (0.0075 mmol, 7.5 mol%, 3.8 mg), (*S*)-**2b**-[X] (0.1 mmol) and Na_2CO_3 (0.2 mmol, 2.0 equiv, 22 mg). Subsequently, 1.2 mL of dichloroethane (DCE) and benzoyl chloride **1a** (0.2 mmol, 2.0 equiv, 23 μL) was added to the mixture via a syringe, in that order. The reaction mixture was sealed with screw cap. The vial was removed from the glovebox and the reaction mixture was stirred in a pre-heated oil bath (83 °C) for 18 hours. The crude mixture was then diluted with ethyl acetate and filtered with celite. The combined organic layer was concentrated under reduced pressure. The yields were determined by ^1H NMR analysis with 1,3,5-trimethoxybenzene as an internal standard and then, the crude products were purified via preparatory TLC with *n*-hexane/EtOAc = 95 : 5 for HPLC analysis.

entry	trifluoroborate source, (<i>S</i>)- 2b -[X]	3ab (%) ^a	es (%)	ee (%) ^b
1	BF_3K	81	97	98
2	BF_3Cs	60	96	97
3	$\text{BF}_3[\text{N}(n\text{-Bu})_4]$	N.D	-	-

^aYields were determined by ^1H NMR using 1,3,5-trimethoxybenzene as an internal standard.

^bThe enantiomeric excess were determined by HPLC analysis.

5.5.8.4. Effect of crown ethers (Figure 5.3C).



In a nitrogen-filled glovebox, an oven-dried 4 mL dram-vial (or screw capped reaction tube) was charged with a magnetic stir bar, Pd₂dba₃ (0.0025 mmol, 2.5 mol% which is 5.0 mol% based on Pd, 2.3 mg), L1 (0.0075 mmol, 7.5 mol%, 3.8 mg), (R)-2b (0.1 mmol) and Na₂CO₃ (0.2 mmol, 2.0 equiv, 22 mg). Subsequently, 1.2 mL of dichloroethane (DCE) and benzoyl chloride 1a (0.2 mmol, 2.0 equiv, 23 μL) was added to the mixture via a syringe, in that order. Then, crown ethers (if solid, as solution in DCE; 18-crown-6 [0.54 M in DCE] and if liquid, as neat; 15-crown-5, 12-crown-4) were added to the vial. The reaction mixture was sealed with screw cap. The vial was removed from the glovebox and the reaction mixture was stirred in a pre-heated oil bath (83 °C) for 18 hours. The crude mixture was then diluted with ethyl acetate and filtered with celite. The combined organic layer was concentrated under reduced pressure. The yields were determined by ¹H NMR analysis with 1,3,5-trimethoxybenzene as an internal standard and then, the crude products were purified via preparatory TLC with *n*-hexane/EtOAc = 95 : 5 for HPLC analysis.

Table S5.12. Control experiments with *18-crown-6*

entry	additive	equiv	3ab (%)	es (%)	ee (%)
1	<i>none</i>	-	81	98.2	97.2
2	18-Crown-6	0.15	75	97.6	96.6
3	18-Crown-6	0.25	69	97.4	96.4
4	18-Crown-6	0.4	58	97.6	96.6
5	18-Crown-6	0.55	47	97.0	96.1
6	18-Crown-6	0.7	31	97.0	96.0
7	18-Crown-6	0.85	16	96.0	95.0
8	18-Crown-6	1.1	N.D	-	-

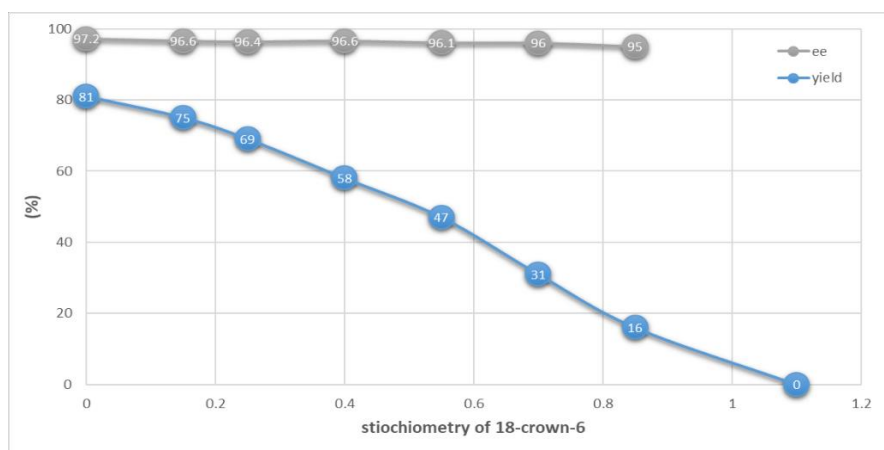
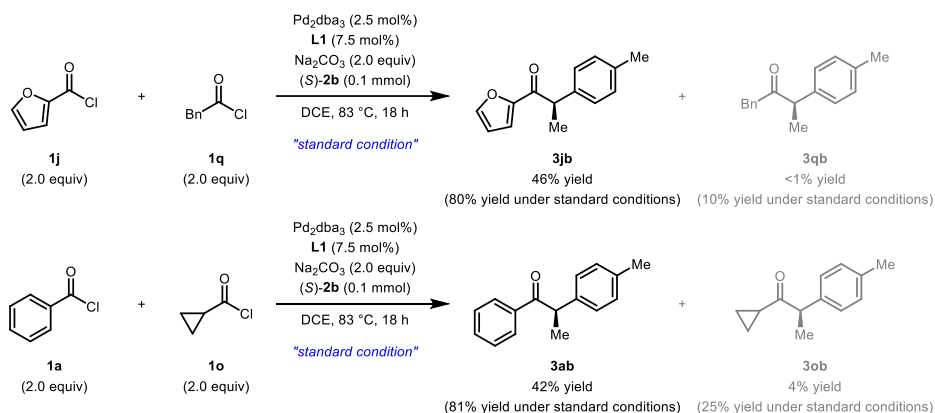


Table S5.13. Control experiments to compare the coordinating effect of crown ether

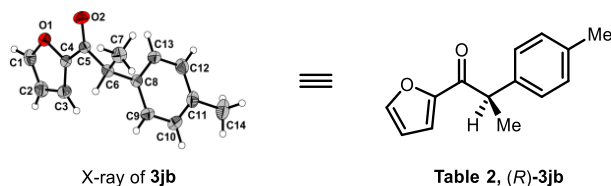
entry	additive	equiv	3ab (%)	es (%)	ee (%)
1	<i>none</i>	-	81	98.2	97.2
2	18-Crown-6	0.55	47	97.0	96.1
3	18-Crown-6	1.1	N.D	-	-
4	15-Crown-5	0.55	56	97.4	96.4
5	15-Crown-5	1.1	21	97.2	96.2
6	12-Crown-4	0.55	66	97.8	96.8
7	12-Crown-4	1.1	44	97.5	96.5

5.5.8.5. Unproductivity of aliphatic acid chlorides.



In a nitrogen-filled glovebox, an oven-dried 4 mL dram-vial was charged with a magnetic stir bar, Pd₂dba₃ (0.0025 mmol, 2.5 mol% which is 5.0 mol% based on Pd, 2.3 mg), **L1** (0.0075 mmol, 7.5 mol%, 3.8 mg), (**S**)-**2b** (0.1 mmol) and Na₂CO₃ (0.2 mmol, 2.0 equiv, 22 mg). Subsequently, 1.2 mL of dichloroethane (DCE), aryl chloride (**1j** or **1a**) and aliphatic acid chloride (**1q** or **1o**) were added to the mixture via a syringe, in that order. The reaction mixture was sealed with screw cap. The vial was removed from the glovebox and the reaction mixture was stirred in a pre-heated oil bath (83 °C) for 18 hours. The crude mixture was then diluted with ethyl acetate and filtered with celite. The combined organic layer was concentrated under reduced pressure. The yields were determined by ¹H NMR analysis with 1,3,5-trimethoxybenzene as an internal standard.

5.5.9. Assignment of Absolute Configuration



X-ray Crystallography

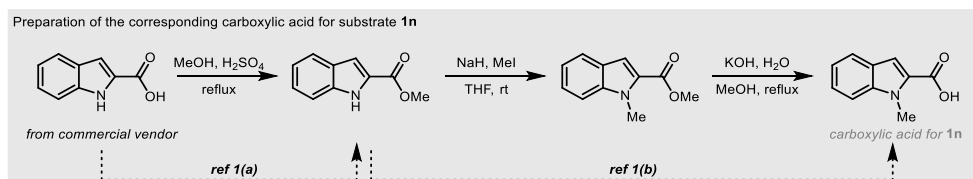
X-ray diffraction measurements were performed using a Bruker APEX-II Diffractometer equipped with a monochromator and a Mo K α ($\lambda = 0.71073$ Å) incident beam at the National Research Facilities and Equipment Center (NanoBio-Energy Materials Center) at Ewha Womans University. A crystal was mounted on a glass fibre. The CCD data were integrated and scaled using the Bruker-S SAINT software-2019.11 (Bruker, Karlsruhe, Germany) package, and the structure was solved and refined using SHELXTL-2018/3 (George Sheldrick, Georg-August Universität Göttingen, Göttingen, Germany). All hydrogen atoms were placed at the calculated positions. The crystallographic data, bond lengths and angles are listed in **Table S14**. Structural information was deposited at the Cambridge Crystallographic Data Centre. The CCDC reference number is 2180232.

Table S5.14. Crystal data and structure refinement for (*R*)-**3jb**.

Identification Code	3jb (CCDC 2180232)	
Empirical formula	C ₁₄ H ₁₄ O ₂	
Formula weight	214.25 g/mol	
Temperature	296(2) K	
Wavelength	0.71073 Å	
Crystal system	orthorhombic	
Space group	P 2 ₁ 2 ₁ 2 ₁	
Unit cell dimensions	a = 5.8273(8) Å b = 7.8697(11) Å c = 25.635(3) Å	α = 90° β = 90° γ = 90°
Volume	1175.6(3) Å ³	
Z	4	
Density (calculated)	1.211 g/cm ³	
Absorption coefficient	0.080 mm ⁻¹	
F(000)	456	
Crystal size	0.050 x 0.080 x 0.160 mm	
Theta range for data collection	2.71 to 28.50°	
Index ranges	-7 ≤ h ≤ 7, -10 ≤ k ≤ 10, - 34 ≤ l ≤ 34	
Reflections collected	54805	
Independent reflections	2957 [R(int) = 0.0805]	
Completeness to theta = 28.5°		
Absorption correction	Multi-Scan	
Max. and min. transmission	0.9960 and 0.9870	
Refinement method	Full-matrix least-squares on F ²	
Data / restraints / parameters	2957 / 0 / 147	
Goodness-of-fit on F²	1.081	
Final R indices [I > 2σ(I)]	R ₁ = 0.0540, wR ₂ = 0.1085	
R indices (all data)	R ₁ = 0.0758, wR ₂ = 0.1166	
Absolute structure parameter	0.4(5)	
Largest diff. peak and hole	0.134 and -0.106 eÅ ⁻³	

5.5.10. References in Experimental Section

- (1) (a) Ganton, M. D.; Kerr, M. A. *Org. Lett.* **2005**, *7*, 4777. (b) Mietke, T.; Cruchter, T.; Larionov, V. A.; Faber, T.; Harms, K.; Meggers, E. *Adv. Synth. Catal.* **2018**, *360*, 2093.



- (2) Go, S. Y.; Chung, H.; Shin, S. J.; Ahn, S.; Youn, J. H.; Im, T. Y.; Kim, J. Y.; Chung, T. D.; Lee, H. G. *J. Am. Chem. Soc.* **2022**, *144*, 9149.
- (3) Noh, D.; Yoon, S. K.; Won, J.; Lee, J. Y.; Yun, J. *Chem. - Asian J.* **2011**, *6*, 1967.
- (4) Lee, J. E.; Yun, J. *Angew. Chem., Int. Ed.* **2008**, *47*, 145.
- (5) Sim, H. S.; Feng, X.; Yun, J. *Chem. - Eur. J.* **2009**, *15*, 1939.
- (6) Jarava-Barrera, C.; Parra, A.; Lopez, A.; Cruz-Acosta, F.; Collado-Sanz, D.; Cardenas, D. J.; Tortosa, M. *ACS Catal.* **2016**, *6*, 442. (b) Lou, Y.-Z.; Cao, P.; Jia, T.; Zhang, Y.-L.; Wang, M.; Liao, J. *Angew. Chem., Int. Ed.* **2015**, *54*, 12134.
- (7) Bagutski, V.; Ros, A.; Aggarwal, V. K. *Tetrahedron* **2009**, *65*, 9956.
- (8) Hoang, G. L.; Takacs, J. M. *Chem. Sci.* **2017**, *8*, 4511.
- (9) Batey, R. A.; Quach, T. D. *Tetrahedron Lett.* **2001**, *42*, 9099.
- (10) Mutoh, Y.; Yamamoto, K.; Saito, S. *ACS Catal.* **2020**, *10*, 352.
- (11) Noh, D.; Chea, H.; Ju, J.; Yun, J. *Angew. Chem., Int. Ed.* **2009**, *48*, 6062.

- (12) Dong, X.; Weickgenannt, A.; Oestreich, M. *Nat. Commun.* **2017**, *8*, 15547.
- (13) Sinai, Á.; Simkó, D. C.; Szabó, F.; Paczal, A.; Gáti, T.; Bényei, A.; Novák, Z.; Kotschy, A. *Eur. J. Org. Chem.* **2020**, *2020*, 1122.
- (14) Cheon, C. H.; Kanno, O.; Toste, F. D. *J. Am. Chem. Soc.* **2011**, *133*, 13248.
- (15) Lou, S.; Fu, G. C. *J. Am. Chem. Soc.* **2010**, *132*, 1264.
- (16) Lundin, P. M.; Esquivias, J.; Fu, G. C. *Angew. Chem., Int. Ed.* **2009**, *48*, 154.
- (17) Li, L.; Cai, P.; Guo, Q.; Xue, S. *J. Org. Chem.* **2008**, *73*, 3516.
- (18) Cheng, Y.-Y.; Yu, J.-X.; Lei, T.; Hou, H.-Y.; Chen, B.; Tung, C.-H.; Wu, L.-Z. *Angew. Chem., Int. Ed.* **2021**, *60*, 26822.
- (19) Gu, Y.; Zhang, Z.; Wang, Y.-E.; Dai, Z.; Yuan, Y.; Xiong, D.; Li, J.; Walsh, P. J.; Mao, J. *J. Org. Chem.* **2022**, *87*, 406.
- (20) Ackermann, L.; Spatz, J. H.; Gschrei, C. J.; Born, R.; Althammer, A. *Angew. Chem., Int. Ed.* **2006**, *45*, 7627.
- (21) Zhou, X.; Zhang, G.; Gao, B.; Huang, H. *Org. Lett.* **2018**, *20*, 2208.
- (22) Sandoval, B. A.; Clayman, P. D.; Oblinsky, D. G.; Oh, S.; Nakano, Y.; Bird, M.; Scholes, G. D.; Hyster, T. K. *J. Am. Chem. Soc.* **2021**, *143*, 1735.
- (23) Yuan, Y.; Wu, F.-P.; Schünemann, C.; Holz, J.; Kamer, P. C. J.; Wu, X.-F. *Angew. Chem., Int. Ed.* **2020**, *59*, 22441.

- (24) Vasquez, A. M.; Gurak, J. A.; Joe, C. L.; Cherney, E. C.; Engle, K. M. *J. Am. Chem. Soc.* **2020**, *142*, 10477.
- (25) Geng, H. -Q.; Meyer, T.; Franke, R.; Wu, X. -F. *Chem. Sci.*, **2021**, *12*, 14937.
- (26) Trost, B. M.; Tracy, J. S.; Lin, E. Y. *ACS Catal.* **2019**, *9*, 11082.
- (27) Zhou, T.; Xie, P.-P.; Ji, C.-L.; Hong, X.; Szostak, M. *Org. Lett.* **2020**, *22*, 6434.

5.6. Computational Section

5.6.1. Complete Authorship of Gaussian 16

Gaussian 16, Revision A.03

M. J. Frisch, G. W. Trucks, H. B. Schlegel, G. E. Scuseria, M. A. Robb, J. R. Cheeseman, G. Scalmani, V. Barone, G. A. Petersson, H. Nakatsuji, X. Li, M. Caricato, A. V. Marenich, J. Bloino, B. G. Janesko, R. Gomperts, B. Mennucci, H. P. Hratchian, J. V. Ortiz, A. F. Izmaylov, J. L. Sonnenberg, D. Williams-Young, F. Ding, F. Lipparini, F. Egidi, J. Goings, B. Peng, A. Petrone, T. Henderson, D. Ranasinghe, V. G. Zakrzewski, J. Gao, N. Rega, G. Zheng, W. Liang, M. Hada, M. Ehara, K. Toyota, R. Fukuda, J. Hasegawa, M. Ishida, T. Nakajima, Y. Honda, O. Kitao, H. Nakai, T. Vreven, K. Throssell, J. A. Montgomery, Jr., J. E. Peralta, F. Ogliaro, M. J. Bearpark, J. J. Heyd, E. N. Brothers, K. N. Kudin, V. N. Staroverov, T. A. Keith, R. Kobayashi, J. Normand, K. Raghavachari, A. P. Rendell, J. C. Burant, S. S. Iyengar, J. Tomasi, M. Cossi, J. M. Millam, M. Klene, C. Adamo, R. Cammi, J. W. Ochterski, R. L. Martin, K. Morokuma, O. Farkas, J. B. Foresman, and D. J. Fox, Gaussian, Inc., Wallingford CT, 2016.

CYLview

Legault, C. Y. CYLview, 1.0.565 BETA; University of Sherbrooke, Québec,

Montreal, Canada, 2012. <https://www.cylview.org/>

GaussView, Version 6.0.16

Roy Dennington, Todd A. Keith, and John M. Millam, Semichem Inc., Shawnee Mission, KS, 2016.

Schrödinger Macromodel

Schrödinger Release 2019-4: MacroModel, Schrödinger, LLC, New York, NY, 2019.

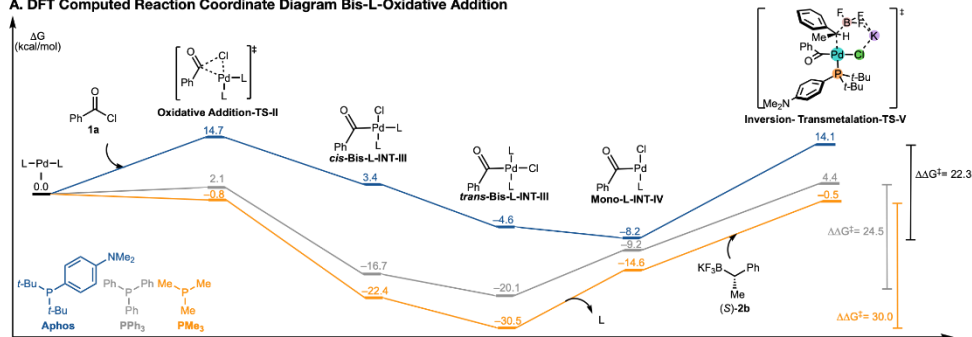
5.6.2. General Computational Procedure

Conformational searches were performed using Schrödinger Macromodel software package. All computations were performed using Density Functional Theory (DFT) with the Gaussian 16 software package. All reactants, intermediates, and products were optimized using PBE-D3BJ^{1,2} and LANL2DZ³ basis set for palladium and 6-31G(d)⁴ for all other atoms. Solvation model based on density (SMD)⁵ was used for dichloroethane at 1 atm and 356.15 K (83 °C). All reported energy values are free energies in kcal/mol and all distances are in Ångströms (Å).

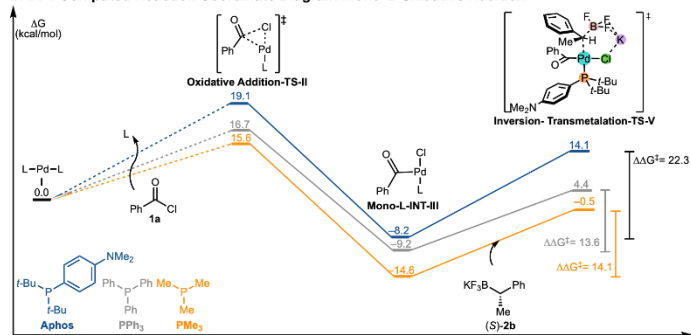
5.6.3. Ligand Comparison

The experimental observation that the reaction with smaller ligands result in diminished reactivity compared to bulky ligands was investigated (**Table S5.8**). The reaction coordinate diagram with smaller ligands ($L = \text{PPh}_3, \text{PMe}_3$) was computed (**Figure S5.1**). PPh_3 and APhos reaction profile comparison revealed that the transmetalation step is the rate-determining step compared to the oxidative addition (Bis-L) step (**Figure S5.1, A**).⁶ Then, the low yield obtained with the smaller ligands could be attributed to the high barrier of transmetalation. This is confirmed by model ligand PMe_3 which has the highest transmetalation barrier compared to APhos and PPh_3 . We believe this result stems from the stability of post-oxidative addition intermediates. Our results show that the *trans*-bis-ligated intermediate is the lowest ground state for small ligands and that the mono-ligated intermediate is the lowest ground state for bulky ligand. Therefore, the smaller ligands must overcome ligand dissociation barrier in order to reach mono-ligand intermediate in addition to the transmetalation barrier. In addition, mono-ligand oxidative addition route was considered for all three ligands (APhos, $\text{PPh}_3, \text{PMe}_3$) (**Figure S5.1, B**). In this mono-ligand path is hypothesized to proceed through ligands exchange with acylchloride. The results show that the mono-ligand oxidative addition transition state is higher in energy than the bis-ligand transition state.

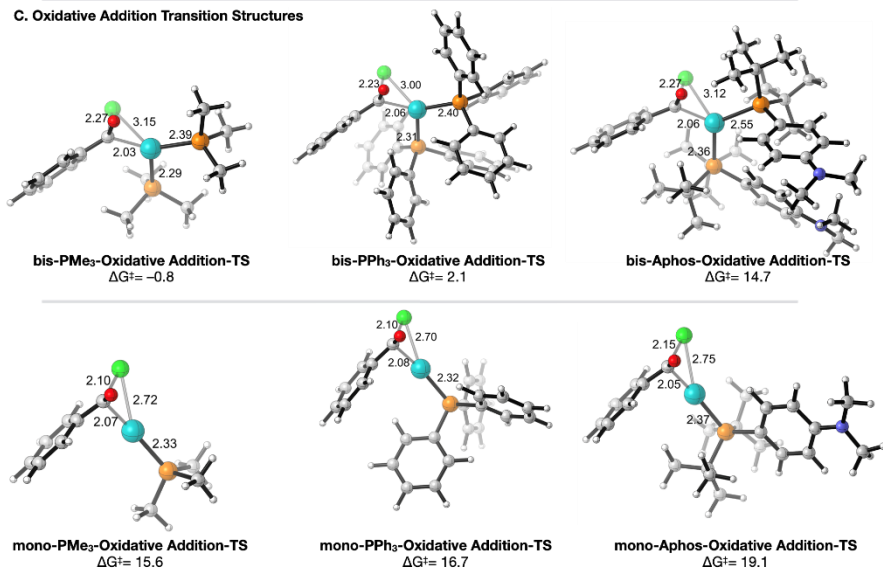
A. DFT Computed Reaction Coordinate Diagram Bis-L-Oxidative Addition



B. DFT Computed Reaction Coordinate Diagram Mono-L-Oxidative Addition



C. Oxidative Addition Transition Structures



D. Isomerization and ligand Dissociation

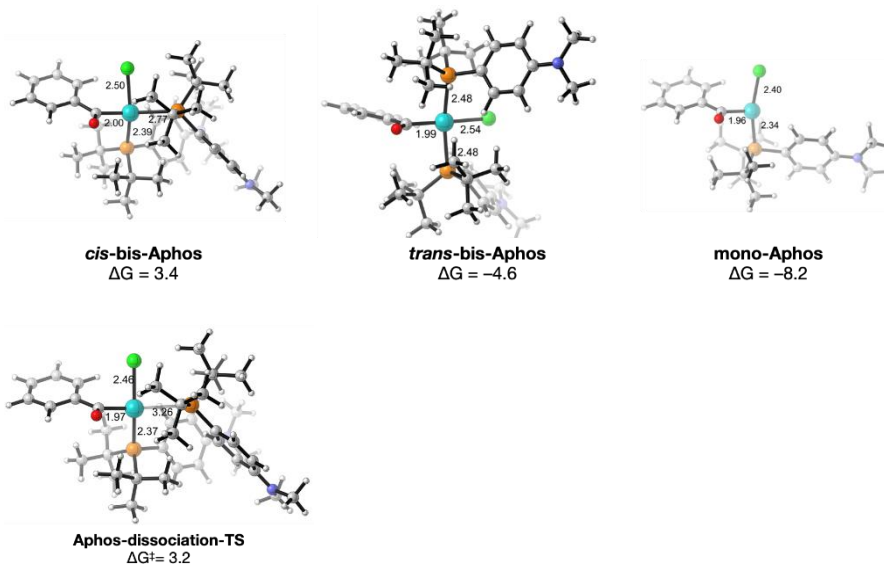


Figure S5.1. A. DFT computed reaction coordinate diagram of APPhos, PPh₃, and PMe₃ bis-oxidative addition and transmetalation steps, B. Mono-oxidative addition route to transmutation, C. DFT computed oxidative addition transition states, D. Isomerization and ligand dissociation (energies in kcal/mol, distances in Å)

5.6.4. Effect of KCl Coordination and Distortion-Interaction Analysis

Effect of KCl was explored by comparing transmetalation transition structures (TSs) with and without KCl. KCl has no effect on inversion vs retention selectivity. However, it does lower the overall barrier of the TSs (Figure S5.2). Distortion-interaction analysis revealed that the total distortions were higher by 8.7 kcal/mol, and therefore more destabilizing, for the favored **Inversion transmetalation-TS-V** (Figure S5.2, A). However, it is the greater interaction energy of the **Inversion transmetalation-TS-V** that overwhelms the distortion penalty and favors the inversion process over the retention (interaction energy greater by -11.1 kcal/mol compared to disfavored **Retention transmetalation-TS-V**).

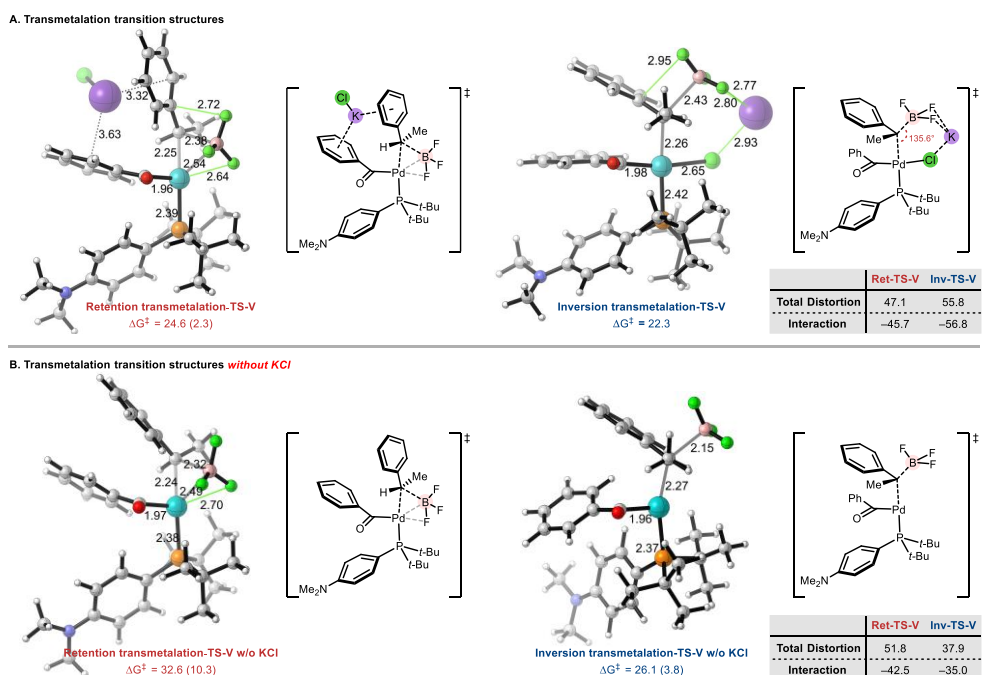


Figure S5.2. Transmetalation transition structures based on the presence (Top, A) or absence of KCl (Bottom, B).

5.6.5. Inversion and Retention Paths to Transmetalation

The crucial transmetalation of acylpalladium(II) species **Int-IV** to furnish the transmetalation complex **Int-VI** is initiated by forming an aggregate with the nucleophile (**[Int-IV+(S)-2a]**). From this intermediate, the corresponding transition states for both inversion and retention could be identified. While the former could be accessed directly from **Int-IV** and **(S)-2a**, the generation of the latter required the rearrangement of the chloride, triggered by the approach of the potassium ion to form (**[Int-IV+(S)-2a]'**).

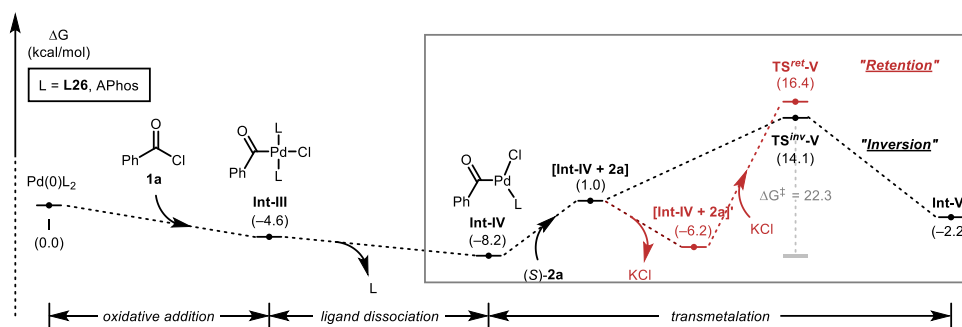
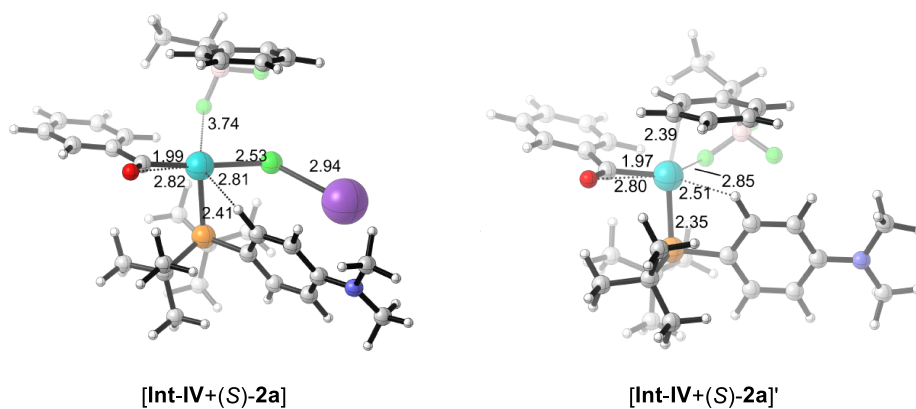


Figure S5.3. Paths leading to inversion and retention TS.



5.6.6. Ion Coordination

Analysis of ground states (GSs) for different ion coordinations in the solution revealed that 1) dissociation of fluoride from BF_3 is energetically disfavored; 2) post-transmetalation coordination of BF_3 and KCl to form KBF_3Cl complex is favored in energy by 10.6 kcal/mol.

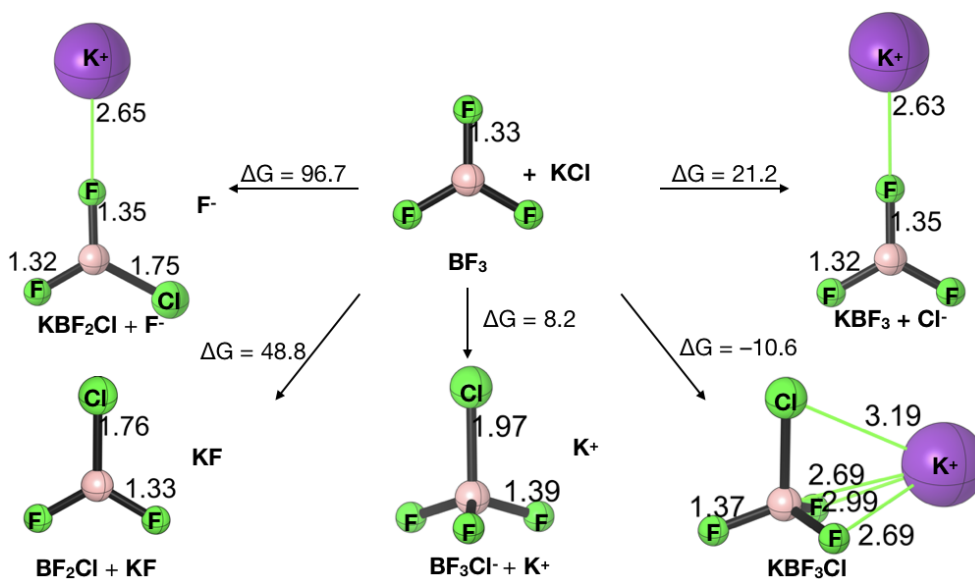


Figure S5.4. Model system analysis of possible ion coordination in solution.

5.6.7. References in Computational Section

- (1) Perdew, J. P.; Burke, K.; Ernzerhof, M. *Phys. Rev. Lett.* **1997**, *78*, 1396.
- (2) Perdew, J. P.; Burke, K.; Ernzerhof, M. *Phys. Rev. Lett.* **1996**, *77*, 3865.
- (3) (a) Hay, P. J.; Wadt, W. R. *J. Chem. Phys.* **1985**, *82*, 270. (b) Wadt, W. R.; Hay, P. J. *J. Chem. Phys.* **1985**, *82*, 284. (c) Hay, P. J.; Wadt, W. R. *J. Chem. Phys.* **1985**, *82*, 299.
- (4) Grimme, S.; Ehrlich, S.; Goerigk, L. *J. Comput. Chem.* **2011**, *32*, 1456.
- (5) Marenich, A. V.; Cramer, C. J.; Truhlar, D. G. *J. Phys. Chem. B.* **2009**, *113*, 6378.
- (6) (a) McMullin, C. L.; Fey, N.; Harvey, J. N. *Dalton Trans.* **2014**, *43*, 13545.
(b) Yang, C.; Zhang, L.; Lu, C.; Zhou, S.; Li, X.; Li, Y.; Yang, Y.; Li, Y.; Liu, Z.; Yang, J.; Houk, K. N.; Mo, F.; Guo, X. *Nat. Nanotechnol.* **2021**, *16*, 1214.

알킬붕소 화합물의 촉매적 비대칭 합성 및 입체특이적 변환

서울대학교 자연과학대학 화학부

노병도

새로운 탄소-탄소 결합 형성을 위한 방법론 개발은 유기화학 분야에서 핵심적인 주제로 간주된다. 지난 수십 년 동안, 전이금속 촉매를 활용한 교차-결합 반응은 복잡한 분자에 효율적인 접근을 가능케 하는 다재다능한 방법으로 인정받아왔다. 이러한 교차-결합 반응 중 스즈키-미야우라 교차-결합 반응은 친핵성으로 이용되는 유기붕소 화합물이 가지는 다양한 이점들, 예를 들면 낮은 독성, 환경 안전성, 온화한 반응 조건, 용이한 합성 등, 때문에 탄소-탄소 결합 형성에 있어 가장 매력적인 방법으로 평가되며, 전 세계적으로 활발히 연구되고 있다. 이에 따라 합성 유기화학 분야의 연구 공동체는 더욱 효율적인 유기붕소 화합물 합성 방법들을 지속적으로 요구하고 있으며, 또한 유기붕소 화합물을 유용한 합성 중간체로서 더 널리 활용하기 위해 많은 노력과 연구가 진행되고 있다. 그럼에도 불구하고 이러한 방법들의 대부분은 주로 sp^2 혼성탄소 기반의 유기붕소 화합물의 사용으로 제한되어 왔다. 이는 sp^3 혼성탄소 기반의 유기금속 화합물의 내재적인 낮은 반응성 및 생성된 알킬금속 반응

중간체로부터의 발생하는 부반응 경로 등 때문이다. 따라서, 이전에 미처 접근하지 못했던 3차원의 새로운 화학 공간으로 쉽게 접근 가능하게 하는 핵심 중간체로서 활용될 수 있는 sp^3 혼성탄소 기반의 유기붕소화합물의 효율적인 합성 및 활용에 대한 방법론의 개발은 여전히 도전적이며 해결해야 할 중요한 과제로 남아있다.

이러한 맥락으로, sp^3 혼성탄소 기반의 알킬붕소 화합물의 합성 및 기능화에 대해 더 효과적인 전략을 개발하고자 하였다. 제1장에서는 sp^3 혼성탄소 기반의 유기붕소 화합물의 합성과 기능화의 중요성을 간략히 소개하며, 그 다음 제2장에서는 알킬붕소 화합물의 합성을 위해 주로 같은자리-이붕소화합물의 활용법에 대해 논의한다. 이와 함께 선구적 연구들과 최근의 발전 사례를 강조하였다. 제3장에서는 새롭게 개발한 구리 촉매 기반의 같은자리-이붕소화합물의 α,β -불포화 이논으로의 비대칭 1,4-첨가반응을 설명하며, 이로써 복잡성이 더해진 새로운 구조의 카이랄성 알킬붕소 화합물을 합성할 수 있었다. 제4장에서는 알킬붕소 화합물의 입체특이적 기능화에 초점을 맞추고, 특히 카이랄성이 풍부한 sp^3 혼성탄소 기반의 유기붕소 화합물에 대한 입체특이적 스즈키-미야우라 교차-결합을 다룬다. 이어서 제5장에서는 매우 효율적인 입체화학적 전달을 보여주는 입체특이적 아실화 스즈키-미야우라 교차-결합에 대한 최근 개발 내용을 소개한다.

주요어: 유기붕소, 알킬붕소 화합물, 비대칭 촉매, 입체선택적 합성, 입체특이적 교차-결합, 카이랄성 카르보닐 화합물, 구리, 팔라듐

학 번: 2018-28460

To my beloved parents, 노영범 · 문연자 and my fiancé 김근영

&

"All Glory be to God, who has bestowed wisdom upon me"